TECHNISCHE UNIVERSITÄT MÜNCHEN

Wissenschaftszentrum Weihenstephan für Ernährung, Landnutzung und Umwelt

Lehrstuhl für biochemische Pflanzenpathologie

Nitrogen dioxide (NO_2) - induced signaling in *Arabidopsis thaliana*: NO_2 provides basal pathogen resistance or induces a hypersensitive response-like cell death

Dörte Mayer

Vollständiger Abdruck der von der Fakultät Wissenschaftszentrum Weihenstephan für Ernährung, Landnutzung und Umwelt der Technischen Universität München zur Erlangung des akademischen Grades eines

Doktors der Naturwissenschaften

genehmigten Dissertation.

Vorsitzender:	Prof. Dr. Erwin Grill
Prüfer der Dissertation:	1. Prof. Dr. Jörg Durner
	2. apl. Prof. Dr. Farhah Assaad-Gerbert

Die Dissertation wurde am 15.05.2018 bei der Technischen Universität München eingereicht und durch die Fakultät Wissenschaftszentrum Weihenstephan für Ernährung, Landnutzung und Umwelt am 21.08.2018 angenommen.

Publications related to this thesis:

D. Mayer, A Mithöfer, E. Glawischnig, E. Georgii, A. Ghirardo, J-P. Schnitzler, J. Durner, F. Gaupels, "Short-term exposure to NO_2 provides basal pathogen resistance in Arabidopsis", *Plant Phys*., pp-00704, **2018**.

D. Kasten, J. Durner, and F. Gaupels, "Gas Alert : The NO_2 Pitfall during NO Fumigation of Plants", *Front. Plant Sci.*, vol. 8, no. 2, pp. 8–11, **2017**.

D. Kasten, A. Mithöfer, E. Georgii, H. Lang, J. Durner, and F. Gaupels, "Nitrite is the driver, phytohormones are modulators while NO and H_2O_2 act as promoters of NO_2-induced cell death", *J. Exp. Bot.*, vol. 67, no. 22, pp. 6337–6349, **2016**.

D. Mayer, B. Kanawati, K. Kempkes, V. Kaever, D. Mackey, P. Schmitt-Kopplin, J. Durner, F. Gaupels, "Induction of cell death by NO_2 or the bacterial avirulence protein AvrRpm1 involves oxylipins, flavonoids and 2',3'-cyclic nucleotides as revealed by high-resolution metabolomics", (in preparation)

Table of Contents

Summary

Numerous studies concerning the anthropogenic air pollutant nitrogen dioxide (NO_2) have recognized that this reactive nitrogen species (RNS) provokes bifunctional, dose-dependent responses in plants. Exposure to high concentrations causes tissue damage, whereas low concentrations of NO_2 display beneficial growth- and yield-promoting effects. It has been shown that RNS play crucial roles during the biotic and abiotic stress response and pathogen defense. For instance, in cooperation with reactive oxygen species (ROS), nitric oxide (NO) and RNS trigger the hypersensitive response (HR) and programmed cell death (PCD) in tissues infected by avirulent pathogens. Moreover, RNS such as NO were demonstrated to be involved in the onset of pattern-triggered immunity (PTI) which conveys basal disease resistance by activating various defense mechanisms against a variety of pathogens**.** Nonetheless, little information is available to date about the molecular mechanisms that underlie these bifunctional effects of NO_2. Therefore, the aim of this work was to further characterize the effects of toxic and non-damaging concentrations of NO_2*.*

Fumigation of *Arabidopsis thaliana* with 20 and 30 parts per million (ppm) NO_2 for 1 h caused severe leaf damage and rapid cell death respectively, which correlated with a massive accumulation of nitrite (NO_2^-, disproportionation product of NO_2). Moreover, the NO_2-induced cell death was accompanied by significant increases in the S-nitrosylation (SNO) and tyrosine nitration of proteins, which are known to be involved in modifying protein activity. Histochemical quantification of H_2O_2 and NO further revealed an augmentation of these HR-PCD-inducing signaling molecules during the NO_2-induced cell death. Suppressing their accumulation by scavengers revealed that they are essential executers of the HR-PCD response. SNO, H_2O_2, and NO accumulated in a similar fashion when plants were infiltrated with cell death-inducing amounts of NO_2^-. This demonstrated that the concomitant increase of NO_2^- after NO_2 fumigation triggered the generation of ROS, RNS, and modified proteins, which ultimately led to the onset of cell death.

Contrarily, fumigation of Arabidopsis for 1 h with 10 ppm NO_2 did not cause any visible leaf damage, instead inducing transcriptional reprogramming related to pathogen resistance as determined via microarray analysis. Hormone measurements via LC-MS/MS revealed that NO_2 stimulated the accumulation of the defense hormone salicylic acid (SA), while simultaneously dampening the jasmonic acid (JA) response by promoting its catabolism. Moreover, NO_2-facilitated basal disease resistance against the necrotrophic fungus *Botrytis cinerea* and the hemibiotrophic bacterium *Pseudomonas syringae* resembling defense responses similar to PTI. Mutant analysis revealed that the NO_2-induced resistance against *B. cinerea* required functional JA- and SA-signaling pathways which were mediated by COI1 and NPR1, respectively.

Additionally, the resistance was dependent on functional PAD3 - the key enzyme during the synthesis of the antimicrobial indolic compound camalexin, even though no NO_2-induced alterations in camalexin levels were detected via HPLC. Mechanistically, the NO_2-induced resistance against *B. cinerea* and *P. syringae* was conveyed by an early enhanced deposition of callose, which is a common PTI-mediated defense that provides penetration resistance.

In summary, the toxicity of NO_2 is conveyed by the accumulation of NO_2^- that triggers a ROS and RNS burst which likely causes oxidative and nitrosative damage to the plant cells that ultimately can culminate in the death of the organism. However, non-damaging concentrations of NO_2 were demonstrated to benefit the plant by activating PTI-related defense responses that protected the plant from subsequent pathogen invasion. These results revealed a yet-unknown beneficial effect of NO_2 and encourages previous hypotheses of NO_2 being a potent signal inducer in plants.

Zusammenfassung

Zahlreiche Studien zum anthropogenen Luftschadstoff Stickstoffdioxid (NO_2) haben gezeigt, dass diese reaktive Stickstoffspezies (RNS) bifunktionelle, dosisabhängige Reaktionen in Pflanzen hervorruft. Die Exposition von Pflanzen mit hohen Konzentrationen verursacht Gewebeschäden, während niedrige Konzentrationen von NO_2 wachstums- und ertragsfördernde Effekte zeigen. Es hat sich gezeigt, dass RNS eine entscheidende Rolle bei der biotischen und abiotischen Stressreaktion und der Abwehr von Pathogenen spielt. So sind Stickstoffmonoxid (NO) und RNS zusammen mit reaktiven Sauerstoffspezies (ROS) an der hypersensitiven Reaktion (HR) und dem programmierten Zelltod (PCD) in Geweben beteiligt, die mit avirulenten Pathogenen infiziert sind. Darüber hinaus spielen RNS wie NO eine wichtige Rolle während der von Pathogen-assoziierten molekularen Mustern induzierten Immunität (*PAMP-triggered immunity*, PTI), die eine basale Resistenz vermittelt, indem sie verschiedene Abwehrmechanismen gegen eine Vielzahl von Pathogenen aktiviert. Dennoch gibt es bisher wenige Informationen über die molekularen Mechanismen, die diesen bifunktionellen Effekten von NO_2 zugrunde liegen. Daher war das Ziel dieser Arbeit, die Auswirkungen von toxischen und nicht schädlichen Konzentrationen von NO_2 zu charakterisieren.

Die Begasung von *Arabidopsis thaliana* mit 20 und 30 ppm NO_2 für 1 h verursachte schwere Blattschäden und Zelltod, was mit einer massiven Anreicherung von Nitrit (NO_2^-, Disproportionierungsprodukt von NO_2) korrelierte. Darüber hinaus wurden signifikante Erhöhungen der S-Nitrosylierung (SNO) und Tyrosin-Nitrierung von Proteinen gemessen, was bekanntlich zu Veränderungen der Proteinaktivität führen kann. Weiterhin ergab die histochemische Quantifizierung von H_2O_2 und NO, dass diese HR-PCD-induzierenden Signalmoleküle während des NO_2-induzierten Zelltods signifikant erhöht sind. Die Verhinderung ihrer Akkumulation durch *Scavenger*-Moleküle ergab, dass sie eine Schlüsselrolle im NO_2-induzierten Zelltod spielen. SNO, H_2O_2 und NO akkumulierten in ähnlicher Weise, wenn Pflanzen mit zelltod-induzierenden Mengen von NO_2^- infiltriert wurden. Dies zeigte, dass der Anstieg von NO_2^- nach NO_2-Begasung die Bildung von ROS, RNS und modifizierten Proteinen auslöst, was schließlich den Zelltod initiiert.

Im Gegensatz dazu verursachte die Begasung von Arabidopsis für 1 h mit 10 ppm NO_2 keine sichtbaren Blattschäden, sondern führte zu einer transkriptionellen Umprogrammierung, wie sie auch bei Pathogenresistenz beobachtet werden kann. Hormonmessungen via LC-MS/MS ergaben, dass NO_2 die Akkumulation des Abwehrhormons Salizylsäure (SA) stimuliert und gleichzeitig Jasmonsäure (JA)-induzierte Reaktionen durch Stimulation des JA-Abbaus dämpft. Infektionsstudien mit dem nekrotrophen Pilz *Botrytis cinerea* und dem hemibiotrophen Bakterium *Pseudomonas syringae* demonstrierten, dass NO_2 eine PTI-ähnliche Resistenz gegen diese

Pathogene stimuliert. Mutantenanalysen ergaben, dass die NO_2-induzierte Resistenz gegen *B. cinerea* funktionelle JA- und SA-Signalwege erfordert, die durch COI1, beziehungsweise NPR1 vermittelt werden. Darüber hinaus war die Resistenz abhängig von funktionellem PAD3 - dem Schlüsselenzym bei der Synthese der antimikrobiellen indolischen Verbindung Camalexin. Jedoch wurden mittels HPLC keine NO_2-induzierten Veränderungen von Camalexin-Konzentrationen in behandelten Arabidopsis Pflanzen nachgewiesen. Mechanistisch wurde die NO_2-induzierte Resistenz gegen *B. cinerea* und *P. syringae* durch eine frühzeitig verstärkte Ablagerung von Callose vermittelt. Diese Festigung zwischen Zellwand und Zellmembran am Infektionsort ist eine generalistische PTI-vermittelte Verteidigungsstrategie.

Zusammengefasst demonstriert diese Arbeit, dass die Toxizität von NO_2 durch die Akkumulation von NO_2^- vermittelt wird, was zu einem massiven Anstieg von ROS und RNS führt, der wahrscheinlich oxidative und nitrosative Schäden verursacht und letztendlich zum Tod der Pflanze führen können. Diese Arbeit verdeutlicht jedoch auch, dass nicht-schädliche Konzentrationen von NO_2 der Pflanze zugutekommen, indem PTI-ähnliche Abwehrmechanismen aktiviert werden, die die Pflanze vor einer späteren Pathogeninvasion schützen. Die Ergebnisse zeigen eine bisher unbekannte positive Wirkung von NO_2 und bekräftigen bestehende Hypothesen, dass NO_2 ein starker Signalinduktor in Pflanzen ist.

Abbreviations

2-DDG	2-deoxy-D-glucose
CAT	Catalase
CDPK	Ca^{2+}-dependent protein kinase
cPTIO	2-(4-carboxyphenyl)-4,4,5,5-tetramethylimidazoline-1-oxyl-3-oxide
DAB	diaminobenzidine tetrahydrochloride
DAF-FM DA	di-amino-fluorescein diacetate
DAMP	Damage-associated molecular pattern
ET	Ethylene
GO-term	Gene ontology term
HR	Hypersensitive response
JA	Jasmonic acid
JA-Ile	jasmonoyl-L-isoleucine
MAPK	Mitogen -activated protein kinase
NO	Nitric oxide
NO_2	Nitrogen dioxide
NO_2^-	Nitrite
NO_3^-	Nitrate
nTyr	Tyrosine nitration
O_2^-	Superoxide anion
$ONOO^-$	Peroxynitrite
PAMP	Pathogen-associated molecular pattern
PCD	Programmed cell death
ppm	Parts per million
PR1, 2, 3, 4, 5	PATHOGENESIS RELATED 1, 2, 3, 4, 5
PRR	Pattern recognition receptor
Pst	*Pseudomonas syringae* pv *tomato*
PTI	PAMP/pattern-triggered immunity
RNS	Reactive nitrogen species
ROS	Reactive oxygen species
SA	Salicylic acid
SD	Standard deviation
SEM	Standard error of the mean
SNO	S-nitrosylation
WT	Wild-type

List of Figures and Tables

Figures

Tables

1 Introduction

Over the last several years, small reactive nitrogen-containing compounds (reactive nitrogen species, RNS) such as NO or peroxynitrite (ONOO-) have emerged as crucial plant signaling mediators, for instance during cell death induction, plant biotic interactions, or abiotic stress responses [1]–[3]. Another highly reactive nitrogen species is the gaseous radical NO_2 which is renowned as an anthropogenic air pollutant. Multiple studies have addressed the question as to how NO_2 exposure affects the viability of plants. These studies revealed that NO_2 provokes dose-dependent responses which range from acute tissue damage and death at high NO_2 concentrations [4], [5] to growth- and yield-promoting effects caused by low-level exposure [6]–[8]. This dose-dependent bifunctionality leads to the hypothesis that NO_2 may be a modulator of plant signaling, as has been reported for NO. Therefore, this work is focused on the characterization of the NO_2-induced signaling in *Arabidopsis thaliana* which was exposed to varying concentrations of this gas. The following introductory chapters aim to provide an overview on the reactivity of NO_2 as well as the current knowledge with regards to the influence of NO_2 on plants.

1.1 Nitrogen dioxide – an anthropogenic air pollutant

The highly reactive free radical NO_2 is an atmospheric trace gas that is naturally formed via the oxidation of NO by atmospheric oxidants such as oxygen (O_2, Figure 1 (1)) or ozone (O_3, Figure 1 (2), [9], [10]). NO commonly originates from high-temperature combustions where atmospheric nitrogen (N_2) reacts with O_2 (Figure 1 (3), [11]). These reactions naturally occur during volcanic activity or lightning storms. Furthermore, NO_2 emission from soil, bacteria, or plants contribute to ambient atmospheric NO_2 concentrations ranging in the annual mean from 0.0002 to 0.005 parts per million (ppm) [10], [12], [13]. However, the anthropogenic combustion of fossil fuels in power plants or motor engines is constantly discharging massive amounts of nitrogen oxides (NO_x, sum of NO and NO_2). In 2000, the World Health Organization (WHO) reported that annual mean concentrations of NO_2 in urbanized areas ranged from 0.01 – 0.05 ppm. About twice a day, during rush-hour traffic in particular, these levels often even exceeded 0.5 ppm in their hourly average [10], [14]–[16]. This dramatic increase in ambient NO_2 levels can have detrimental effects on the environment and human health. The WHO summarized a multitude of studies in 2006 [10] which link NO_2 for instance to increased incidences of asthma and reduced lung function in children [17]–[20].

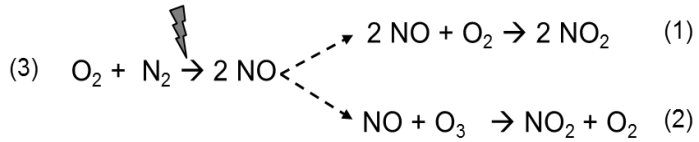

Figure 1: NO_2 formation during high-temperature combustion
NO can react with (1) oxygen (O_2) or (2) ozone (O_3) to give NO_2. Prior, NO is generated during the reaction of nitrogen (N_2) with O_2 (3) during high temperature combustion (bolt).

On a global scale, NO_2 promotes the progression of climate change, as it is the main source for tropospheric ozone when it reacts with volatile organic compounds (VOCs) [21], [22]. On an environmental scale, increasing nitrogen level due to man-made emissions of NO_x have detrimental effects on ecosystem functioning [23], [24]. For instance, alterations in plant species composition was found to be correlated with the proximity to highly frequented traffic routes [25]–[27]. Consequently, the WHO recommended critical NO_2 emission values of an annual mean of 0.02 ppm and a maximum hourly average of 0.1 ppm. These guidelines were manifested in 2008 in the directive 2008/50/EC (on ambient air quality and cleaner air for Europe) of the European Parliament. Nonetheless, 145 of 519 measuring stations within Germany have exceeded these critical values in 2016, with peak annual means of 0.04 ppm in Stuttgart and Munich (Deutsches Umweltbundesamt, last data update: 2017-09-08 [28]).

1.1.1 The multifaceted effects of NO_2 on plants

NO_2-inflicted damage on plants

Investigation and documentation into detrimental effects of NO_2 on a variety of plant species has been intensively conducted over the last 50 years. In 1979, Heck and Tingey categorized the various plant responses to phytotoxic levels of NO_2 into physiological, chronic, and acute injuries [29]. Occurrences of growth retardation as well as reduction in yields and photosynthesis were classified as physiological injuries. For instance, exposing Arabidopsis to 0.2 ppm NO_2 for 4 weeks led to a reduction of growth [30]. Moreover, a negative impact on chlorophyll content and photosynthesis efficiency was reported for Arabidopsis plants which were fumigated with 2 to 4.2 ppm NO_2 for 6 h per day for one week [31]. Heck and Tingey classified more severe symptoms such as chlorosis and increased defoliation as chronic injuries as they had been described for orange trees exposed to 0.25 to 1 ppm over 35 days [32]. Dramatic effects such as necrotic lesion formation and plant collapse were categorized as acute injuries and were observed in *Nicotiana glutinosa* after fumigation with 5 ppm NO_2 for 1 h or in pinto beans after a 4 h exposure to 10 ppm [4], [5]. Taken together, these

collected observations imply that the severity of NO_2-induced effects is highly variable and dependent on the applied dose of NO_2 (concentration and duration of exposure) and the utilized plant species [33].

Various studies have examined the events incited upon exposure to NO_2 in order to determine the cause of its detrimental influence upon plants. In aqueous environments, as found within plant cells, NO_2 exists in equilibrium with its dimer, dinitrogen tetroxide (N_2O_4), due to its low solubility in water (Figure 2-1). However, the dimers' water solubility is 100-fold higher and therefore disproportionates to nitrite (NO_2^-) and nitrate (NO_3^-) while releasing protons (H^+) [34], [35] (Figure 2-2). Within the plant, both nitrogen compounds are further converted to ammonia (NH_3) by the concerted action of the nitrate and nitrite reductases (NR, NiR, [36], [37], Figure 2-3). The conversion of NO_2^- and NO_3^- as well as the assimilation of NH_3 into the amino acid synthesis commonly consume the generated protons [38]. However, it has been reported that high doses of NO_2 acidify the leaf and therefore may cause severe injury [4], [38].

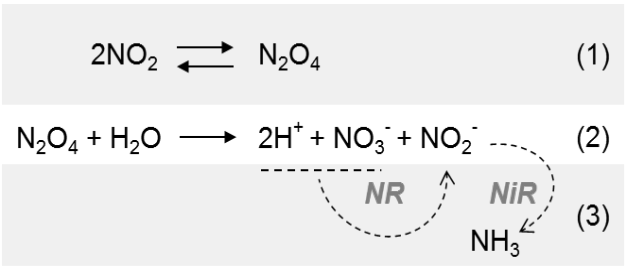

Figure 2: Disproportionation and assimilation of NO_2 within the cell
In aqueous environments NO_2 is in equilibrium with N_2O_4 (1) that can disproportionate in water to NO_3^- and NO_2^- (2). The assimilation of these products occurs via the enzymatic activity of the nitrate reductase (NR) that converts NO_3^- to NO_2^- and the nitrite reductase (NiR) which further converts NO_2^- to ammonia (NH_3) (3). NO_2 = nitrogen dioxide, N_2O_4 = dinitrogen tetroxide, NO_3^- = nitrate, NO_2^- = nitrite. Dashed arrows = enzymatic reaction, solid arrows = chemical reaction.

Other reports have linked NO_2-induced injuries to the accumulation of NO_2^- within the plant tissue [4], [39], [40]. NO_2^- is likely to react to nitric acid (HNO_3) within the aqueous cell and thereby causes acid burns [41]. Moreover, elevated NO_2^- levels lead to a shortage of NADP/NADPH due to its consumption during the reduction of NO_3^- and NO_2^- when it otherwise would be needed during the photosynthetic fixation of CO_2 [42]–[44]. Consequently, NO_2^- leads to a reduction in photosynthesis which promotes the generation of ROS such as O_2^- by accelerating the one-electron reduction of O_2 [40]. Therefore, accumulation of NO_2^- after NO_2 exposure leads to oxidative stress, which in turn causes the observed damage to the plant [33], [41]

The beneficial influence of NO_2 on plants

It was mentioned earlier that the plants' response to NO_2 is highly dependent on the applied concentration. This becomes more evident when other observations are considered, which

demonstrated that exposure of plants to low concentrations of NO_2 can benefit the plants general constitution. For instance, tomato plants fumigated with 0.5 ppm for 10 days displayed an increase in shoot length [45]. Similar observations were made for sunflowers that were exposed to up to 3 ppm for 3 weeks [46]. Furthermore, the fumigation of tomato during their entire growth period with 0.05 ppm resulted in augmented numbers of flowers which led to an increase in yield [47]. Likewise, when Arabidopsis plants were fumigated with the same concentration of NO_2 for 4 weeks they displayed a significant enhancement in leaf size [48].

Since atmospheric NO_2 is likely assimilated into the plants primary nitrogen metabolism after stomatal uptake [49] (Figure 2), it is assumed that NO_2 functions as an air-born fertilizer leading to increased protein levels and growth promotion [4], [6]–[8], [46]. On the contrary, Takahashi *et al.* (2005) reported that the total nitrogen content comprised of less than 5 % of NO_2-derived N in fumigated plants that were sufficiently supplied with soil-nitrogen [50]. Nevertheless, their nutrient uptake and metabolism as well as their photosynthetic rate accelerated, which led to an increase in biomass due to enhanced cell proliferation and enlargement [48], [50]–[52]. The authors further described that approximately one third of the incorporated NO_2-derived N was not assimilated into the N metabolism but rather into a previously unknown nitrogen species, which was further identified in various other plant species [53], [54]. Therefore, the authors postulated that exogenously supplied NO_2 functions as a multifaceted signal that stimulates plant growth. This further encouraged them to hypothesize that NO_2 may be of physiological importance as an endogenous signal in plants [30], [50], [51].

Plants generate a multitude of endogenous signaling molecules to execute important physiological functions. However, convincing evidence has yet to be found for a plant-specific biosynthetic pathway which yields NO_2. Several reports indicated that NO_2 may be generated enzymatically *in planta*. It was demonstrated *in vitro* that horseradish peroxidase as well as mammalian myeloperoxidase (MPO) and lactoperoxidase (LPO) can utilize NO_2^- as a one-electron donor during the detoxification of H_2O_2 resulting in its oxidation to NO_2 [55], [56]. In addition, non-symbiotic hemoglobins such as the Arabidopsis GLB1 or *Medicago sativa* MHB1 were reported to produce NO_2 mechanistically similar to the heme-containing peroxidases [57], [58].

1.1.2 The signal transmission potential of NO_2

The aforementioned studies revealed that an enzymatic production of NO_2 is conceivable. Nonetheless, its generation *in planta* has yet to be demonstrated, though its emission from herbicide-treated plants was already reported [13], [59]. Assuming that NO_2 functions as an endogenous signaling molecule, the question remains of how it may be involved in signal transduction, since

action sites or receptors of NO_2 have yet to be identified [30]. One indication of its mode of action was delivered by observations made during the NO_2-producing enzymatic reactions *in vitro*. Here, several studies demonstrated that NO_2 post-translationally nitrates tyrosine residues of proteins, which is a known protein modification that occurs for instance during plant defense responses [55]–[58], [60], [61]. Moreover, the highly reactive radical state of NO_2 predestines it to be converted to other RNS, which in turn may activate signaling cascades. The following chapter will focus on the direct and indirect signal transmission potential of NO_2.

Reactive nitrogen species and their involvement in plant signaling

NO_2 is one of many reactive molecules that are classified as RNS, which are nitrogen-containing oxo-derivatives such as NO, $ONOO^-$, or dinitrogen trioxide (N_2O_3). NO is known to be an important mediator of a variety of physiological responses. For instance, abscisic acid (ABA)-induced NO production mediates stomatal closure via the second messenger cyclic guanosine monophosphate (cGMP) [62]–[64]. Moreover, while auxin-induced NO formation is a prerequisite for adventitious root formation in cucumber [65], NO is best known for its involvement in pathogen defense and HR-PCD induction (see section 1.2).

As mentioned previously, NO_2 disproportionates to NO_3^- and NO_2^- (Figure 2). The latter is known to be a valuable source for NO production either due to spontaneous reduction [66], non-enzymatic electron transfer from the mitochondrial respiratory chain [67], [68], or even due to enzymatic reactions [69], [70], [71]. Since a considerable increase in NO_2^- has been measured at several occasions after NO_2 treatment of a variety of plant species, an accumulation of the signaling molecule NO may likely be involved in NO_2-induced plant responses [4], [39], [40]. Besides NO, $ONOO^-$ is another highly reactive RNS that is capable of altering electrophilic molecules such as lipids or nucleic acids via one or two-electron oxidation, nitration, or radical formation [72]–[75]. In plants, $ONOO^-$ is commonly generated during the spontaneous reaction of NO with O_2^- and was demonstrated to accumulate during HR-mediated cell death [60], [76]. Accordingly, Alamillo and Garcia-Olmedo (2001) showed that urate-mediated $ONOO^-$ scavenging in Arabidopsis leaves upon *P. syringae* pv. *phaseolicola* infection reduced the plants HR-PCD and defense gene expression [77].

How NO and RNS implement their bioactivity is still under heavy investigation in order to obtain further mechanistic details. Nonetheless, two major signal transduction mechanisms have been confirmed to occur in plants upon accumulation of NO and RNS: indirect signal transmission via second messengers such as cGMP and signal transduction via the direct interaction with proteins [64], [65], [78]. NO and RNS can confer their bioactivity through post-translational protein

modifications which cause conformational alterations, protein-protein interactions, or influence the subcellular location of the target protein that ultimately leads to changes in protein activity [79]. The best described post-translational protein modifications mediated by RNS are the S-nitrosylation of cysteines and the nitration of tyrosine residues, which shall be characterized in more detail in the upcoming chapter.

Protein modifications mediated by reactive nitrogen species

The RNS-mediated S-nitrosylation of proteins is a potent post-translational modification that has been shown to play central roles in the regulation of disease resistance and HR within plants [80]–[83]. Here, an NO-moiety is covalently bound to the thiol group of cysteines leading to the formation of S-nitrosothiols (SNO, Table 1 left). However, NO itself is an inadequate oxidant of amino acid side chains under physiological conditions [84]. Therefore, S-nitrosylation is usually mediated by oxo-derivatives of NO (e.g. NO_2, N_2O_3, and $ONOO^-$) or metal-NO complexes (Table 1 (1) and (2) [85]). However, the common assumption is that trans-nitrosylation is the dominant reaction within cellular signal transmission [86]. Here, S-nitrosylated proteins directly transfer their NO-moiety to a thiol group of another cysteine (Table 1 (3)). The major physiological mediator of this reaction is S-nitrosoglutathione (GSNO), which functions as an NO reservoir and is predestined as an important signaling-mediator [87].

Table 1 Overview of S-nitrosylation and tyrosine nitration pathways.
Left) Pathways leading to S-nitrosylation of cysteine (Cys) residues. **Right)** Pathways resulting in the nitration of tyrosine (Tyr) residues. RNS = reactive nitrogen species, S = thiol group, • = indication for radical, $CO_3•^-$ = carbonate radical, Me = metal complex, PRX = peroxidase.

(1) ***Oxidative S-nitrosylation***	**(4)** ***Radical-mediated tyrosine nitration***
RNS ($NO_2•$, N_2O_3, $ONOO^-$) + Protein-Cys-S^- ⟶ Protein-Cys-S-NO	$ONOO^-$ + CO_2 ⟶ $CO_3•^-$ + $NO_2•$
(2) ***Metal-catalyzed S-nitrosylation***	$CO_3•^-$ + Protein-Tyr ⟶ Protein-Tyr •
NO• + Me ⟶ Me-NO	Protein- Tyr • + $NO_2•$ ⟶ Protein-Tyr-NO_2
Me-NO + Protein-Cys-S^- ⟶ Me + Protein-Cys-S-NO	**(5)** ***Oxo-metal-catalyzed tyrosine nitration***
(3) ***Trans-nitrosylation***	Peroxidase + H_2O_2 ⟶ PRX Intermediate + H_2O
Protein-Cys-S-NO + Protein-Cys-S^- ⟶ Protein-Cys-S^- + Protein-Cys-S-NO	PRX Intermediate + NO_2^- ⟶ PRX Intermediate + $NO_2•$
	PRX Intermediate + Protein-Tyr ⟶ Peroxidase + Protein-Tyr •
	Protein- Tyr • + $NO_2•$ ⟶ Protein-Tyr-NO_2

To date, several studies have provided proof of the physiological importance of SNO, especially during disease resistance and HR-PCD. For instance, in 2006 Lindermayr *et al.* demonstrated that the recombinant Arabidopsis methionine adenosyltransferase 1 (MAT1) is S-nitrosylated upon GSNO

incubation which led to a reversible inhibition of this enzyme necessary for ET biosynthesis [88]. Moreover, GSNO was reported to S-nitrosylate NPR1, the key regulator of SA-mediated defense signaling, as well as its nuclear interaction partner TGA1 [80], [82]. Here, GSNO-treatment facilitated the translocation of NPR1 to the nucleus and increased the TGA1 DNA binding affinity leading to an enhanced defense gene expression [82], [89]. Contradictory however, the S-nitrosylation of NPR1 was also reported to promote the oligomerization of the protein and thereby detaining it to the cytoplasm [80]. Another indication of the importance of S-nitrosylation during plant-pathogen interaction was presented by Yun *et al.* in 2011, who demonstrated that the Arabidopsis NADPH oxidase RESPIRATORY BURST OXIDASE HOMOLOGUE PROTEIN D (RBOHD) was S-nitrosylated during HR upon the infection with *P. syringae* DC3000. This modification dampened the NADPH oxidase activity resulting in reduced ROS accumulation which in turn curbed excessive cell death during HR [83].

Another major RNS-mediated post-translational protein modification is the nitration of tyrosine residues, where a NO_2-moiety is added to an *ortho*-carbon of the aromatic ring of a tyrosine forming the negatively charged 3-nitrotyrosine (nTyr) [61]. Presumably, there are multiple pathways that generate nTyr, however *in vitro* and *in vivo* studies indicated that the participation of free radicals is a commonality amongst them. One major route of nTyr generation involves the formation of the NO_2 and carbonate radicals during the rapid reaction of $ONOO^-$ with carbon dioxide (CO_2). In turn, the two radicals radicalize tyrosine residues which leads to the addition of the NO_2-moiety to the tyrosyl-radical intermediate (Table 1 (4), [90], [91]). Another potentially biologically relevant mechanism involves *oxo*-metal complexes as is found in peroxidases that oxidize tyrosine to the tyrosyl radical, which is then followed by the addition of the NO_2-moiety (Table 1 (5), [91], [92]). This mechanism was described in several *in vitro* studies where the nitration of tyrosine residues was observed during the enzymatic formation of NO_2 from NO_2^- and can be used as an indirect marker for NO_2 formation ([55]–[58]).

The nitration of tyrosines increases the hydrophobicity and dimension of the affected protein and therefore causes structural changes and steric restrictions of the protein [93]. These impediments often lead to a loss of function or the degradation of the protein as described by Castillo *et al.* (2015) for the nitrated ABA receptor PYR/PYL/RCAR [94]. Increases in tyrosine nitration has been demonstrated for a variety of plant species under various stress conditions, e.g. in wounded pumpkin, Arabidopsis undergoing pathogen-induced HR, or salt-stressed sunflower seedlings [95]–[97]. However, so far only a small number of nitrated proteins have been characterized in detail to identify the physiological relevance of the occurring tyrosine nitration [93].

As emphasized in the previous chapters, NO_2 has promising potential in the induction and transmission of signaling in plants and therefore it may be capable of modulating defense responses

such as HR-PCD and pathogen defense as has been reported extensively for other RNS [1]–[3]. Hence, this work was focused on the investigation of potential signaling interfaces and pathways which may be modulated by NO_2 during these defense responses. The plants' immune response is regulated via a well-orchestrated and highly elaborate signaling network, which will be outlined in the upcoming introductory chapters.

1.2 Plant innate immunity

During their life cycle plants have to face many challenges from foragers, since their sessile lifestyle condemns them to be an effortless and rich food source for a variety of organisms. Besides the imminent threat of herbivores, plants are often plagued with diseases caused by bacteria, fungi, or oomycetes. These organisms evolved various feeding strategies; from nourishing on nutrients from living cells (termed biotrophic pathogens) to killing the host in order to feed on the dead cell contents (necrotrophic pathogens). Other pathogens, termed hemibiotrophs, can pursue both feeding strategies [98]. No matter the pathogenic lifestyle, infestation entails reduced biomass, decrease in fertility and can ultimately lead to the death of the plant [99]. In turn, this threatens humanities food security, since crop diseases such as the potato blight (inflicted by *Phytophthora infestans*) or wheat stem rust (*Puccinia graminis*) annihilate annual yields [100]. However, plants are not defenseless against these pathogenic microbes. By virtue of constant exposure to these threats, plants have evolved a highly sophisticated defense and immune system to fend off microbial intruders.

The first challenges which microbes must overcome in order to successfully penetrate the plant are the physical barriers of the plant. Microbes first encounter the hydrophobic cutin and wax-containing cuticle that protects the plants external surface of the epidermis [101]. Secondly, microbes must penetrate the rigid cell wall, which is actively modified and reinforced at the infection sites to prevent microbe penetration [102]. However, most fungi are able to overcome these physical barriers by excreting enzymes that degrade their components such as cutinases, cellulases, or pectinases. On the contrary, bacteria often access the plant through natural openings such as the stomata or wounds [99], [103]. Once inside the plant, microbes are confronted with the plants second line of defense: its innate immune system. Here, the plant perceives the invading pathogen by recognizing conserved pathogen-associated molecular patterns (PAMPs) and initiates an elaborate arsenal of customized defenses, termed PAMP-triggered immunity (PTI) [104].

1.2.1 The onset of PAMP-triggered immunity – a potential site of action for NO_2

The initiating stimulus of the PAMP-triggered immunity is the perception of pathogen- or damage-associated molecular patterns (PAMPs or DAMPs). PAMPs are conserved, microbe-derived molecules of various types such as proteins (bacterial flagellin and elongation factor Tu) or carbohydrates such as the fungal chitin (reviewed by [105]). DAMPs on the other hand, are plant-derived molecules that are generated by the lytic activity of the pathogen, like oligogalacturonides (OGs) that are released during cell wall fragmentation [106] (Figure 3).

PAMP recognition occurs via plasma membrane-bound pattern-recognition receptors (PRRs), whose extracellular domains specifically bind individual PAMPs [107]. Few PRR/PAMP couples have been identified to date, such as the Arabidopsis FLAGELLIN-SENSITIVE 2 (FLS2) receptor which is specific for flagellin, or the chitin-specific LysM-CONTAINING RECEPTOR-LIKE KINASE 5 (LYK5) receptor [108], [109]. Following ligand binding, PRRs complex with specific regulatory receptor kinases to initiate immune signaling by associating with receptor-like cytoplasmic kinases (RLCKs) such as the Arabidopsis BOTRYTIS-INDUCED KINASE1 (BIK1) [105], [110]–[112] (Figure 3). These cytoplasmic kinases dissociate from the receptor complex upon PAMP binding and initiate downstream signaling cascades, as illustrated in Figure 3 [99].

One immediate cellular response upon PAMP-recognition is the production of ROS such as O_2^- or H_2O_2 which are detectable 2-3 min after PAMP recognition [99]. In Arabidopsis, O_2^- is largely generated by the NADPH oxidase RBOHD. Reportedly, the ROS burst can be initiated by the activating phosphorylation of RBOHD by BIK1 and other PAMP-initiated signaling [113]–[115]. ROS themselves are a key component of the plants defense system since they mediate stomatal closure, directly inhibit pathogen growth, and impede their penetration by crosslinking the cell wall [116]–[118]. Moreover, ROS take part in PTI progression by stimulating downstream signaling [119].

A further immediate physiological response upon pathogen infection is the rapid influx of calcium ions (Ca^{2+}) into the cytosol, which is initiated 30 sec to 2 min after PAMP perception [99], [120] (Figure 3). Studies have shown that BIK1 and other cytoplasmic kinases are required for Ca^{2+} signaling [113], [121]. Besides Ca^{2+} and ROS, RNS were also described to be involved in PAMP signaling. NO, whose production was reported to be inducible by the Ca^{2+} influx, was demonstrated to be crucial for various steps during PTI [122], [123]. The concerted action of ROS, Ca^{2+}, RNS, and cytosolic kinases further transmit the PAMP-induced signal to mitogen-activated protein kinase (MAPK) cascades and Ca^{2+}-dependent protein kinases (CDPKs), which finally convey the signal to the nucleus [99] (Figure 3).

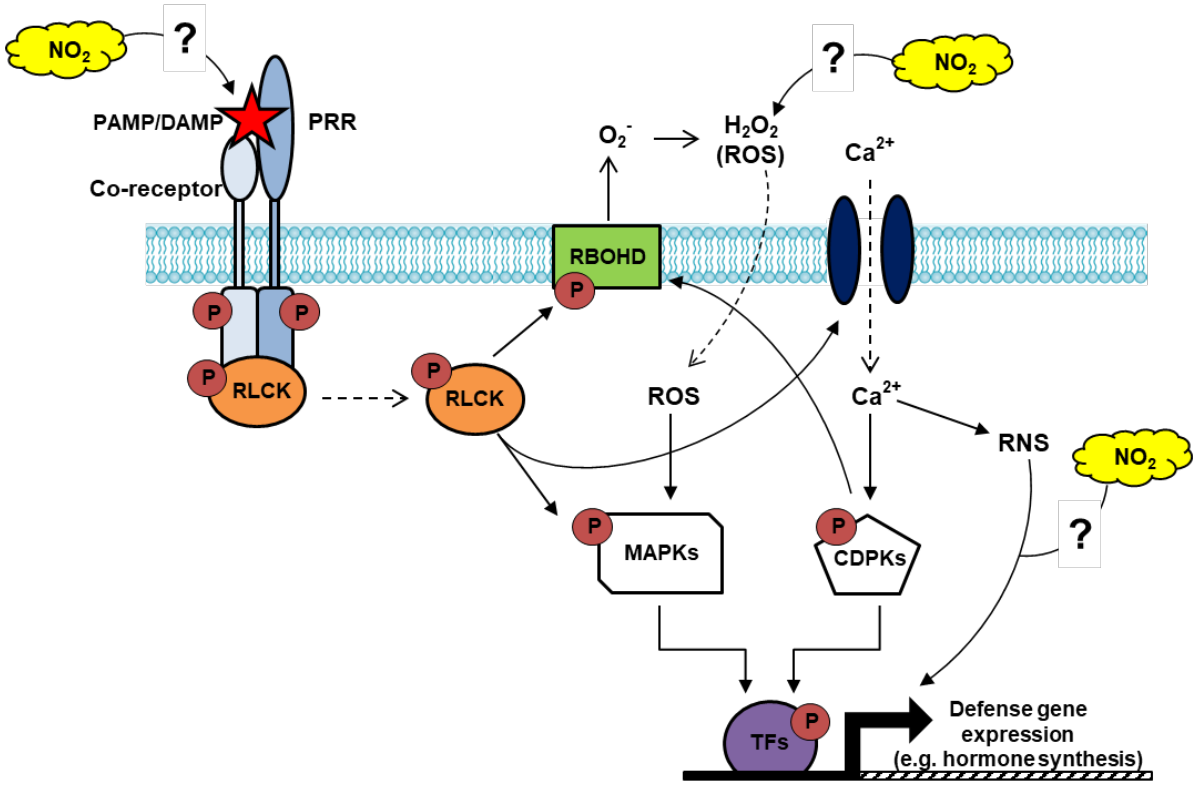

Figure 3: Potential sites of action for NO_2 to induce initial PAMP-induced signaling
PAMP/DAMP-binding causes complex-formation of PRRs with co-receptors and RLCKs. This induces cooperative phosphorylation that leads to the dissociation of the RLCKs. These can promote ROS burst by activating RBOHD. Both are able to activate MAPK cascades that activate defense gene expression. Moreover, RLCKs can initiate Ca^{2+}-influx to the cytoplasm that in turn can activate CDPKs and promote RNS formation resulting in TF-activation that induces defense gene expression. PAMP/DAMP = pathogen/damage-associated-molecular pattern, PRR = pattern-recognition receptor, RLCK = receptor-like cytoplasmic kinase, P = Phosphorylation, RBOHD = NADPH oxidase, ROS = reactive oxygen species, MAPKs = MAP Kinase cascade, CDPKs = Ca^{2+}-dependent protein kinases, RNS = reactive nitrogen species, TFs = transcription factors. Solid arrows with filled head = activation/induction, Solid arrows with open head = production, dashed arrows = translocation, arrows with question mark = potential site of action for NO_2.

MAPK cascades, which are activated within minutes of PAMP recognition, are multi-layered phosphorylation chains consisting of multiple kinases which ultimately lead to the activation of specific MAP kinases [124] (abbreviated as MAPKs in Figure 3). In Arabidopsis, MPK3 and 6, as well as MPK4, are well described MAP kinases that establish distinct PTI responses by inducing transcriptional reprogramming [99]. For instance, MPK4 and MPK6 activate various transcription factors like WRKY33 which is essential for the synthesis of the antimicrobial compounds [125]–[127]. Moreover, MPK3 and MPK6 are involved in regulating the production of the defense hormone ethylene [128].

Another signal transmission path to the nucleus is mediated by CDPKs, which are transiently activated between 5 and 30 min after PAMP recognition [129]. Amongst others, they were shown to

convey the flagellin-mediated ROS burst by activating RBOHD and induce transcriptional reprogramming in Arabidopsis as well as phytohormone accumulation in *Nicotiana benthamiana* [130].

As indicated in Figure 3, several sites of action for NO_2 can be hypothesized to initiate PTI signaling. NO_2 may indirectly trigger this defense signaling by initiating the release of DAMPs due to its reported potential to cause acute injuries [4], [5]. Moreover, the formation of ROS and RNS after exposure to NO_2 [34], [35], [40], [66] may be effective in activating PTI, since both reactive species are well described in the modulation of crucial steps during PTI initiation [99], [122], [123]. Additionally, a direct role of NO_2 during PTI induction can be theorized, based on its ability to promote signal transmitting protein modifications.

PTI signaling downstream of MAPKs and CDPKs activates a number of transcription factors that execute the immune response by activating antimicrobial compound production, cell wall reinforcement, and the synthesis of phytohormones which further induce secondary transcriptional changes for maintaining the defense state [99].

1.2.2 Phytohormones fine-tune pathogen-triggered immunity

Phytohormones are small endogenously produced signaling molecules that occur in low concentrations within the plant and can freely diffuse or are actively transported to their location of action. They regulate a broad spectrum of physiological processes such as growth, development, reproduction, and play a crucial role in the plants pathogen response [131]. The compounds salicylic acid (SA) as well as jasmonic acid (JA) and its derivatives are considered to be major mediators of plant defense [132], [133]. Additionally, other hormones such as abscisic acid (ABA), gibberellins (GA), ethylene (ET), brassinosteroids, and auxins were reported to modulate the plants immune signaling network [134]–[137]. Changes in hormone concentration as well as the composition and timing of the hormone blend determine a wide range of plant responses [131], [138]. As mentioned above, these changes can be initiated by PAMP-triggered signaling leading to a customized response against individual pathogens [99]. For instance, the invasion of biotrophic or hemibiotrophic pathogens commonly activates SA synthesis and signaling hours after PAMP perception, whereas necrotrophic invaders regularly trigger the induction of JA and ET synthesis and signaling [98], [139]. An overview of the hormone-mediated signaling during pathogen defense that may be stimulated by NO_2 is shown in Figure 4.

Salicylic acid-mediated defense against Pseudomonas syringae

Since the 1980s, the gram-negative bacterial pathogen *Pseudomonas syringae* has been utilized to unravel the plants interaction with hemibiotrophic pathogens [140]. Arabidopsis perceives *P. syringae* via the FLS2 receptor that recognizes flagellin, which then initiates various responses, such as Ca^{2+}-influx that activates CDPKs and Ca^{2+}-sensor proteins [99]. Several reports have demonstrated that Ca^{2+}-sensors such as calmodulin-binding proteins activate the transcription of the SA-biosynthetic gene *ICS1* upon *P. syringae* infection [141], [142]. SA accumulation initiates transcriptional reprogramming via its key regulator NONEXPRESSOR of PATHOGENESIS–RELATED GENES 1 (NPR1) [143]. Under normal conditions, NPR1 resides in the cytoplasm as an oligomer due to redox-sensitive intermolecular disulfide bonds. Upon pathogen-perception, ROS and RNS, as well as SA are generated and shift the cellular redox-state, leading to the reduction of these intermolecular bonds and the release of NPR1 monomers which can translocate to the nucleus [80] (Figure 4, green panel). Here, NPR1-mediated transcription is regulated by its close homologs NPR3 and NPR4, which function as SA receptors [144]. In the absence of SA, NPR4 binds to NPR1 and rapidly induces its degradation. Increasing SA levels disrupt the NPR1-NPR4 interaction and facilitate NPR1-induced transcription. Exceeding SA levels however, favor NPR1-NPR3 binding, which flags NPR1 again for degradation [143]–[145]. Thus, NPR1-mediated signaling is highly controlled and defined by prevailing SA concentrations. Active NPR1 interacts with various transcription factors such as TGACG SEQUENCE-SPECIFIC BINDING PROTEINs (TGAs) or WRKYs which subsequently promote the transcription of SA-responsive genes such as PATHOGENESIS-RELATED1 and 5 (PR1, PR5), or the beta-glucanase PR2 [146], [147], [148]. Despite various efforts, the exact mode of the action of SA is still not fully understood [143]. Nonetheless, SA-mediated defense signaling is crucial for the defense against biotrophic or hemibiotrophic pathogens such as *P. syringae,* as evident by extended bacterial growth and increased susceptibility of Arabidopsis mutants which are impaired in SA accumulation and signaling [149].

Jasmonic acid/Ethylene-mediated defense upon B. cinerea infection

The widespread necrotrophic fungus *Botrytis cinerea* is the second most threatening plant pathogen and causes 15-40 % loss of crops on the field and in storage [150]. *B. cinerea* is the causal agent of gray mold disease that leads to soft rot symptoms in berries, tomato, or ornamental flowers, to name just a few of its over 200 dicot crop hosts [150]. *B. cinerea* secretes over 40 different toxins, including botrydial and botcinic acid, in order to kill the hosts cells to obtain nutrients [151].

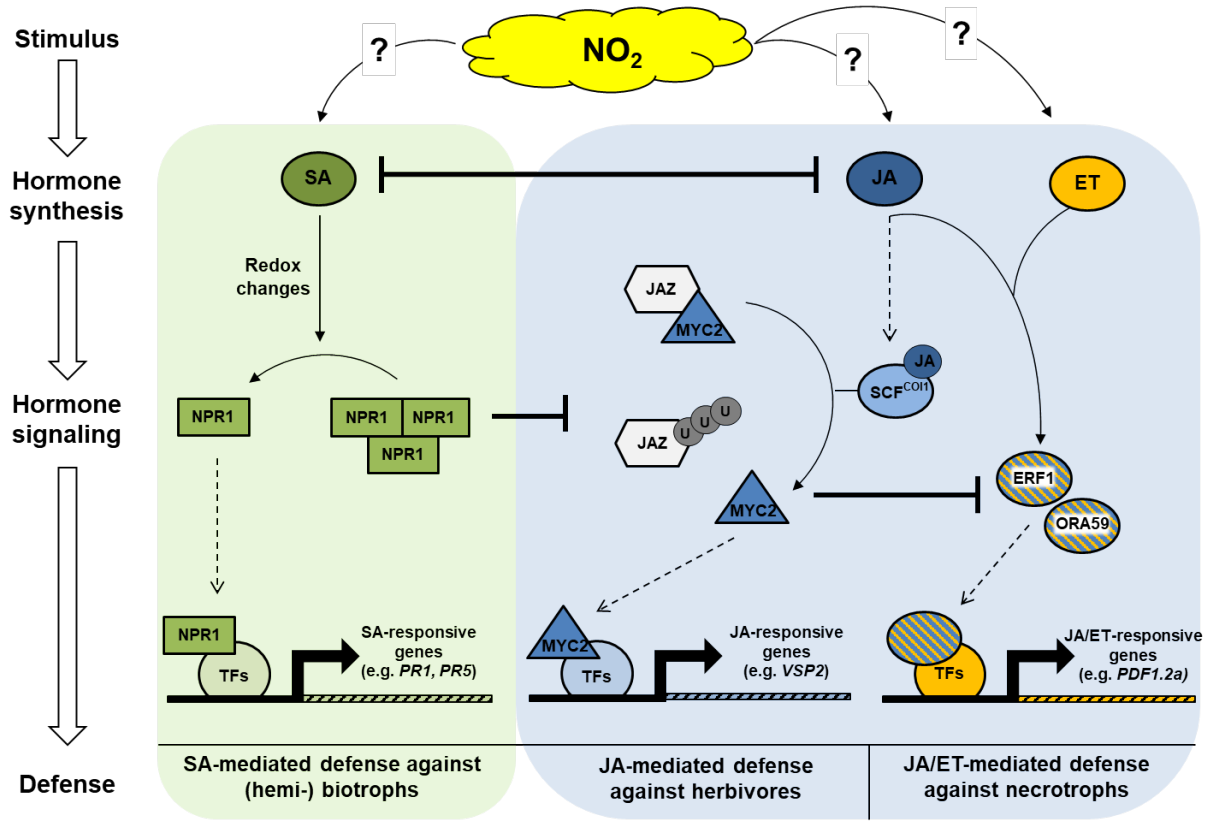

Figure 4: Abridgement of hormone signaling and networking during the immune response
Green panel) Defense signaling against (hemi-) biotrophs mediated by SA. SA shifts the cellular redox state and thereby releases NPR1 monomers. At balanced levels of SA, NPR1 can translate to the nucleus and activates TFs that induce the transcription of SA-responsive genes. For simplification, NPR3 and NPR4 were not depicted. **Blue panel)** Defense signaling against necrotrophs and herbivores mediated by JA and ET. JA binds to the SCF^{COI1}-complex that ubiquitinylates JAZ proteins leading to their degradation. This releases MYC2 that activates TFs that induce the expression of JA-responsive genes effective against herbivores (e.g. *Vsp2*). In concert with ET (orange), JA activates the TFs ERF1 and ORA59 that promote the transcription of JA/ET-responsive genes effective against necrotrophs (orange). SA = salicylic acid, JA = jasmonic acid, ET = ethylene, U = ubiquitin, TFs = transcription factor. Solid arrows = activation/release, dashed arrows = translocation/binding, bars = inhibition.

The perception of fungal-specific PAMPs like chitin, as well as fungus-generated DAMPs triggers the biosynthesis of JA and its derivatives [150]. During JA perception and signaling (Figure 4, blue panel), the CORONATINE INSENSITIVE 1 (COI1) F-box protein occupies a key role as it is required for most JA-dependent responses [152], [153]. COI1 is integrated in the SKIP-CULLIN-F-box-type E3 ubiquitin ligase complex (SCF^{COI1}-complex) which perceives elevated JA levels. Upon JA detection, the SCF^{COI1}-complex promotes the ubiquitin-mediated degradation of JASMONATE-ZIM-DOMAIN (JAZ) proteins which releases transcription factors that induce the transcription of JA responsive genes [154]–[156]. One of these transcription factors is MYC2 that is encoded by *JASMONATE INSENSITIVE 1* (*JIN1*) and promotes the expression of genes involved in wound and herbivore response, such as *VEGATIVE STORAGE PROTEIN 2* (*VSP2*) [157]–[159] (Figure 4, blue panel). However, the MYC2-mediated signaling pathway is less important during the defense against *B.*

cinerea, since Arabidopsis *myc2* mutants still display a wild-type (WT) like resistance to this fungus [158]. *B. cinerea* infection also triggers the biosynthesis of ET via MPK3/ MPK6 [99], [128]. In concert with JA, ET induces the expression of *OCTADECANOID-RESPONSIVE ARABIDOPSIS AP2/ERF 59* (*ORA59*) and *ETHYLENE-RESPONSIVE FACTOR 1* (*ERF1*) [160], [161]. These transcription factors promote the expression of defense genes such as the *PLANT DEFENSIN 1.2a* (*PDF1.2a*) or the PATHOGENESIS-RELATED *BASIC CHITINASE* (*CHI-B/PR3*) and *HEVEIN-LIKE* (*HEL/PR4*) [158], [159], [162]. The fact that JA-treatment of ET insensitive mutants does not trigger *ERF1*, *ORA59*, or *PDF1.2a* expression demonstrates the importance of the concomitant action of both JA and ET during the defense response against necrotrophs [163]. Moreover, mutants impaired in JA- as well as ET- production and signaling (e.g. *aos, opr,3* and *coi1* for JA and *etr1, ein3,* and *eil1* for ET) are highly susceptible to *B. cinerea,* which further implicates both hormones in the implementation of the plants response to this pathogen [164]–[167].

Antagonistic effects of salicylic acid- and jasmonic acid-mediated signaling

Even though the SA and JA/ET signaling pathways appear to be distinct, they do not function independently from each other. Rather, they interconnect via complex regulatory networks in order to customize suitable defense responses and commonly antagonize each other actively as a trade-off between biotrophic and necrotrophic resistance. This was first established by various pharmacological and genetic studies which demonstrated that SA is a potent suppressor of JA-responsive gene expression [168], [169]. This was further attested by Spoel *et al.* in 2003, who recorded a 25-fold increase in JA levels of SA-deficient Arabidopsis plants infected with *P. syringae* DC3000 [170]. The SA-mediated suppression of the JA-pathway was demonstrated to be of physiological relevance on many occasions. For instance, the activated SA signaling in *P. syringae*-infected Arabidopsis plants rendered them highly susceptible to subsequent infection with the necrotrophic fungus *Alternaria brassicicola* [171].

Within the hormonal signaling cascades, there are many key nodes which regulate the switch between SA- and JA-mediated defenses. One of those switches is the MAP kinase MPK4, which is a positive regulator of JA signaling due to its repressive effect on SA biosynthesis [172]. Moreover, a crucial role of NPR1 in the regulation of SA- and JA-mediated signaling was established. Mutants impaired in this SA key regulator failed to block the SA-mediated suppression of JA-responsive genes [170]. It was further demonstrated that retained cytosolic NPR1 is sufficient to repress JA-mediated signaling without activating SA-responsive genes [170]. Nevertheless, several representatives of TGA or WRKY transcription factors that are regulated by nuclear NPR1 have been implicated to be involved in JA-signal suppression [138].

1.2.3 Prominent defense mechanisms activated during PTI

Despite the pathogens best efforts, the plant is typically capable of employing a variety of defense mechanisms which efficiently inhibit the progression of the pathogen. Besides the previously mentioned transcription of pathogen-specific defense genes which encode antimicrobial peptides that savage the pathogen itself, plants are further able to initiate the production of antimicrobial secondary metabolites. Moreover, pathogens can be confined to the site of infection by cell wall modifications or induced cell death to prevent the progression of the infection.

The hypersensitive response

Plants often prevent the spreading of (hemi-) biotrophic pathogens by the induction of programmed cell death (PCD) during the hypersensitive response (HR) which leads to the confinement of the pathogen to the site of infection, ultimately leading to the intruders' starvation [173]. Early studies demonstrated that a sustained increase in cytosolic Ca^{2+} is essential for the onset of HR-PCD, since a general inhibition of Ca^{2+} channels suppressed cell death in pathogen-infected soybean cultures and cowpea [174], [175]. However, the central role in HR-PCD is occupied by ROS, which can induce cell death by lipid peroxidation that disrupts membrane integrity or by modifying the cellular redox-status [173]. This was confirmed by pharmacological inhibition or knock-out of the major ROS source (NADPH oxidases) in various plant species. These plants exhibit decreased levels of ROS and subsequent reduction in cell death [176]. Furthermore, NO was reported to be an additional player in HR induction. Delledonne *et al.* (1998) demonstrated that the exogenous application of NO in combination with H_2O_2 or O_2^- activated HR-PCD synergistically since neither ROS nor NO alone were able to trigger an advanced HR [177]. This was further confirmed by the observation that the inhibition of NO accumulation in Arabidopsis compromised the plants HR development upon infection with an avirulent *Pseudomonas* strain leading to enhanced bacterial growth [177].

These multifaceted HR-induction signals indicate that HR-PCD is regulated on a genetic level, which is further supported by several Arabidopsis, maize, or tomato mutants which impulsively develop HR-induced lesions [178]. Moreover, HR-PCD remains under tight hormonal control (reviewed in [176]). SA occupies the most prominent role, since this hormone and ROS amplify each other in a feed-forward mechanism which promotes cell death propagation. The involvement of SA in the onset of HR-PD was verified due to the lack of pathogen-induced cell death in SA-deficient Arabidopsis *NahG* mutants [179]. Furthermore, co-treatment of wild-type (WT) Arabidopsis with SA and O_2^- significantly enhanced cell death induction [180]. Additionally, the induction of ET biosynthesis is in part required for the continuation of the cell death-driving ROS accumulation [181], [182]. Finally, JA accumulation

is involved in the containment of cell death propagation as shown by intensified HR-PCD of JA-insensitive Arabidopsis mutants after ozone treatment [183], [184].

Callose deposition

Another effective defense mechanism of plants against various pathogens and wounding is the deposition of the (1,3)-β-glucan polymer callose [185] which can occur in papillae between the plasma membrane and the cell wall at infection sites [186], [187]. In previous studies it was demonstrated that callose deposition is induced after *B. cinerea* infection of Arabidopsis [188]. Furthermore, elevated callose depositions at early time points after infection provide penetration resistance against the biotrophic powdery mildew fungus and *A. brassicicola* [186], [189]. In Arabidopsis, callose is synthesized by a group of 12 mostly membrane-localized callose synthases encoding *GLUCAN SYNTHASE-LIKE* (*GSL*) genes. GSL5, herein referred to as PMR4 (POWDERY MILDEW RESISTANT 4), was identified as the predominant callose synthase during wounding and pathogen infection, since *pmr4*-deficient plants failed to deposit callose at affected sites [189]–[191]. The induction of callose biosynthesis upon pathogen infection is a complex process where the involvement of ROS, SA, and indole glucosinolates (IGs) has been reported [192]–[194]. It was demonstrated that *PMR4* expression is significantly up-regulated upon SA-treatment in an NPR1-dependent manner, though a transcription factor regulating its gene expression has not yet been identified [195]–[197]. However, the effectiveness of callose deposition against biotrophic pathogens is still debated, since *pmr4* mutants exhibited a hyperinduction of SA biosynthesis as well as a constitutive expression of defense genes. This consequently renders the *pmr4* mutant resistant to these type of pathogens [191], [197]. On the contrary, Scalschi et al. (2015) revealed that a functional JA-biosynthetic pathway is crucial for proper callose deposition and basal resistance of *B. cinerea*-infected tomato [198].

Camalexin production

Other components of the plants' arsenal against pathogens are the low molecular weight secondary metabolites termed phytoalexins which affect the invader's functionality. The most investigated representative of this heterogeneous group of compounds is camalexin (3-thiazol-2'yl-indole) which is found in Arabidopsis. Its antimicrobial activity has been tested successfully *in vitro* for instance against the hemi-biotrophic bacterium *P. syringae* pv *maculicola*, or the necrotrophic fungi *A. brassicicola* and *B. cinerea* [199]–[202]. Camalexin disrupts bacterial and fungal cell membranes, reduces fungal cell wall permeability, and induces fungal apoptotic-like programmed cell death [199],

[201], [203], [204]. *In planta*, camalexin is synthesized locally around the infection site upon detection of a large variety of PAMPs and DAMPs such as fungal chitosan, bacterial flagellin, and endogenous OGs [200], [205]. Conclusively, as mutant analysis reveals, camalexin plays a crucial role in the resistance against a variety of pathogens such as the necrotrophic fungi *A. brassicicola* or *B. cinerea*, as well as the hemibiotrophic oomycete *Phytophthora brassicae* and the biotrophic powdery mildew [206]–[209]. Interestingly, camalexin-deficient mutants are not susceptible to *P. syringae*, even though its effectiveness was reported in *in vitro* assays [199], [210].

Upon PAMP/DAMP recognition, camalexin is produced *de novo* in close proximity to the infection site as a result of an elaborate defense signaling network. Various studies indicated that JA, ET, as well as SA and ROS are important players in camalexin synthesis induction [211]. Their involvement however, appears to be dependent on the infecting pathogen. Reports are available that claim that JAs' contribution to camalexin synthesis induction is negligible upon *A. brassicicola* infection, but crucial when plants are invaded by *B. cinerea* [202], [212], [213]. Similar observations were made for the involvement of SA. For instance, transgenic Arabidopsis which is impeded in SA accumulation due to the expression of the bacterial SA-hydroxylase (NahG) did not accumulate any detectable camalexin upon *P. syringae* DC3000 infection. However, these transgenic plants generated a WT-like increase in camalexin when infected with *Phytophthora porri* [214], [215] Furthermore, ET was reported to play a role in camalexin induction, since mutants impaired in ET signaling accumulated less camalexin after *P. syringae* or *A. brassicicola* treatment [202], [216]. Since camalexin accumulation can also be stimulated with various oxidative-stress-inducing chemicals such as paraquat, it is assumed that ROS may also be essential for camalexin biosynthesis [217]. In general, various reports have demonstrated that camalexin synthesis is regulated via a MAPK cascade that ultimately leads to the activation of MPK3 and MPK6. These kinases activate the transcription factor WRKY33, which in turn regulates genes involved in the biosynthesis of tryptophan, the precursor of camalexin, as well as the expression of camalexin biosynthetic genes such as the key cytochrome P450 *PHYTOALEXIN DEFICIENT 3* (*PAD3)* [205]. Furthermore, WRKY33-induced camalexin accumulation is positively regulated by MPK4 that is activated upon *P. syringae* or flagellin treatment [125].

1.2.4 Defense priming as a measure to enhance resistance

The activation of appropriate defense mechanisms is highly effective to protect the plant against pathogens. However, the induction of ample defenses negatively affects the plants fitness due to the inevitable consumption of resources. Moreover, the time required to implement a successful defense may leave the plant vulnerable to considerable damage during the early stages of infection [218].

Consequently, plants evolved mechanisms which sense environmental cues in order to promote a state of alertness and prepare itself for potential pathogen invasions enables a faster and stronger defense response [219]. This approach of defense readiness is termed priming, which is postulated to be an adaptive, low-cost defensive state that is characterized by either no or only a slight and transient induction of defense responses after detection of a priming stimulus. Upon detection of a challenging signal (e.g. pathogen infection) however, a primed plant is able to deploy a more rapid and enhanced defense than naïve, non-stimulated plants [220]. So far, a variety of stimuli are reported to trigger the primed state, like naturally occurring compounds such as beta-aminobutyric acid (BABA), SA, or volatile organic compounds (VOCs). Also mild abiotic or biotic stresses such as temperature changes, or PAMPs and DAMPs, as well as stimuli derived from beneficial symbiotic microbes (e.g. *Trichoderma*) are known to induce a primed state [221]. The multitude of environmental cues which were reported to function as priming agents further encourages the hypothesis that exposure to NO_2 may be sufficient to prime the plant into a state of alertness, therefore rendering it more resistant against future pathogen attacks.

On the molecular level, priming is assumed to involve the accumulation of signaling molecules and proteins, as well as DNA modifications which convey the timely advanced and/or enhanced defense response in a concerted effort [222], [223]. For instance, in 2009, Beckers *et al.* demonstrated that the mRNA and dormant proteins of the MAPK cascade, MPK3 and MPK6 in particular, are accumulating after treatment with the SA analogue benzothiadiazole (BTH). Upon challenge with *P. syringae* pv *maculicola,* the BTH-primed plants showed a greater abundance of active (phosphorylated) MPK3/6, leading to an enhanced defense gene expression that consequently resulted in an enhanced resistance to the pathogen [224].

Another effect associated with priming is the increase in pattern-recognition receptors such as FLS2, as well as their affiliated co-receptors as reported after prolonged BTH-treatment of Arabidopsis by Tateda *et al.* (2014) [225]. This is speculated to result in an enhanced sensitivity to PAMPs and an intensified activation of downstream signaling e.g. via MAPK cascades [223]. Yet another hypothesis for the molecular conveyance of priming is associated with epigenetics. Here, it is proposed that priming agents induce modifications of chromatin that encourage a faster and more robust activation of defense-related genes [223].

1.3 Project objective

The steady increase in anthropogenic environmental pollution with NO_2 is a newsworthy topic due to the broad spectrum of detrimental effects which NO_2 inflicts on human health and the environment, especially plants. However, deeper understanding of the underlying mechanisms that cause these detrimental effects is still unknown. In plants, a common assumption is that the accumulation of toxic levels of NO_2^- upon NO_2 uptake causes severe oxidative damage which leads to cell collapse and ultimately culminates in the death of the plant. However, the identification of NO_2-resistant or susceptible plant species [40], as well as reported beneficial effects of low NO_2 doses indicate that NO_2 may induce specific signaling cascades leading to a self-programmed death of the plant cell rather than randomly inflicting damage as a phytotoxin.

Therefore, the first aim of this work was to expand the knowledge of the NO_2-induced cell death by establishing a NO_2-fumigation system that generates consistently-reproducible damage to *Arabidopsis thaliana*, to be used for further analysis. The established fumigation system was utilized to evaluate if NO_2-induced cell death is solely based on NO_2^- toxicity or if NO_2 is capable of initiating signaling leading to HR-like cell death. Therefore, the NO_2 disproportionation products within NO_2-damaged plants were analyzed to assess the accumulation of NO_2^-. Moreover, levels of molecules and protein modifications that are associated with HR-PCD signaling (ROS, NO, SNO, and nTyr) were determined by applying histochemical and biochemical methods. In order to investigate the importance of these signaling molecules, their abundance was pharmacologically manipulated during the onset of NO_2-induced cell death. Finally, Arabidopsis plants were treated with NO_2^- to assess if it induces similar responses within the plant as they were observed after NO_2 exposure.

Independently, Arabidopsis plants were evaluated for their response to short-term exposure to non-damaging concentrations of NO_2, since a variety of beneficial effects were described for low NO_2 doses. In the literature, two main hypotheses arose for this phenomenon. First, NO_2 may operate as an air-born fertilizer which encourages plant growth by promoting the plants nitrogen metabolism and secondly, NO_2 may induce growth-promoting signaling.

Examination of the immediate plant response to short-term exposure of non-damaging NO_2 concentrations via microarray analysis revealed a rapid transcriptional reprogramming, pointing to a previously undescribed capability of NO_2 to induce a pathogen defense response. Accordingly, a NO_2-induced resistance against the necrotroph *B. cinerea* and the hemibiotroph *P. syringae* pv *tomato* DC3000 was observed. Based on this, an attempt to unravel the underlying mechanisms of this induced resistance against *B. cinerea* was made by screening various mutants impaired in defense mechanisms and hormone signaling for their NO_2-induced resistance phenotype.

Additionally, commonly known defense responses such as hormone and camalexin synthesis, callose deposition, and PR gene expression were examined in *B. cinerea*-infected plants after NO_2 fumigation. This approach was intended to provide insights into the underlying hormone and defense signaling pathways and to identify the executing mechanisms which cause the NO_2-induced resistance.

2 Results

2.1 Characterization of the NO_2-induced cell death

In recent years, multiple reports have indicated that the exposure to high dosages of NO_2 caused detrimental effects such as growth retardation, necrosis, and cell death in various plant species such as *Arabidopsis thaliana*, pinto bean, or *Nicotiana glutinosa* [4], [5], [30]. However, the underlying mechanisms of the NO_2-induced cell death have not yet been investigated in detail. To address the question of how NO_2 triggers the plant to undergo cell death, *Arabidopsis thaliana* was exposed to various concentrations of NO_2 for 1 h which caused varying degrees of damage. Changes in signaling molecules, protein modifications, and nitrogen-containing compounds were determined to highlight important players during NO_2-induced cell death.

2.1.1 Visualization and quantification of the NO_2-induced cell death

To characterize NO_2-induced cell death, the severity of leaf damage in Arabidopsis plants caused by raising concentrations of NO_2 needed to be assessed. Therefore, four-week-old Col-0 plants were fumigated for 1 h with 10, 20, or 30 ppm NO_2. As a negative control plants were placed into the fumigation chamber and fumigated with air. After 24 h the damage was documented (Figure 5 A) and the dead leaf areas were visualized by Trypan Blue (Figure 5 B), which is only able to permeate and stain cells if the membranes are disrupted [226]. Fumigation with air and 10 ppm NO_2 did not cause any apparent leaf damage, whereas 20 ppm NO_2 visibly induced severe necrotic lesions which were also detected by the Trypan Blue staining. Fumigation for 1 h with 30 ppm NO_2 however, resulted in complete leaf collapse and rapid wilting which was already apparent during the exposure period to NO_2 (Figure 5 A, B).

The observed development of cell death was quantified over time via electrolyte leakage. Here, whole rosettes were harvested directly after fumigation and submerged in water for 24 h. During that time, electrolytes leaked through disrupted membranes of dead cells, thereby increasing the water conductivity, which was measured at various time points (Figure 5 C). Plants fumigated with 10 ppm NO_2 leaked 13 % of their electrolytes after 24 h. This was similar to the 15 % leakage in air fumigated plants, which supported the lack of visible symptoms or cell death staining after these treatments. Fumigating plants with 20 ppm NO_2 resulted in a relative electrolyte leakage of 27 % that was excelled to 63 % for plants treated with 30 ppm NO_2 (Figure 5 C). Therefore, cell death quantification via electrolyte leakage confirmed that NO_2-induced leaf damage is dependent on its concentration.

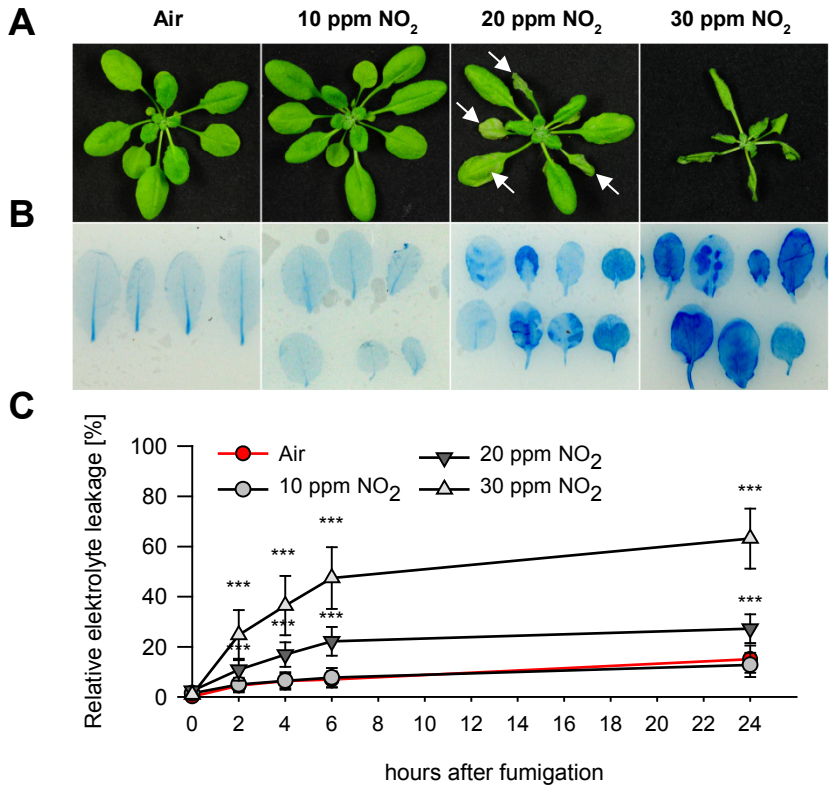

Figure 5: Concentration-dependent cell death induced by NO_2

Col-0 plants were exposed to air (control), or 10, 20, and 30 ppm NO_2 for 1 h. **A)** Visible cell damage. Arrows indicate damaged leaf areas. **B)** Trypan Blue staining of dead leaf areas 24 h after fumigation. **A, B)** Representative pictures of 2 independent experiments are shown. **C)** Cell death quantification by electrolyte leakage at various time points after fumigation. Data points represent means ± SD (n = 10-19). The figure was modified after Kasten *et al*., 2017 by permission of Oxford University Press. ***Statistics:*** Asterisks indicate significant differences from control samples via Kruskal Wallis test and Wilcoxon test with FDR correction (***p < 0.001).

2.1.2 Quantification of nitrogen compounds and protein modifications after NO_2 fumigation

As mentioned in section 1.1.1, NO_2 rapidly disproportionates into equimolar amounts of NO_2^- and NO_3^- in aqueous solutions. This hydrolyzation was demonstrated to occur in plants upon NO_2 uptake by Zeevaart in 1976. Here, it was also determined that NO_2-induced leaf damage correlated with NO_2^- accumulation in various plant species such as *Phaseolus vulgaris* (pinto bean), *Datura stramonium* (devil's snare), *Pisum sativum* (pea), or *Spinacea oleracea* (spinach) [4].

To investigate if the NO_2-induced cell death in *Arabidopsis thaliana* is accompanied by NO_2^- and NO_3^- accumulation, their contents were quantified immediately after fumigation with various NO_2 concentrations using a Sievers Nitric Oxide Analyzer NOA 280i (NOA; Figure 6 A, B). In air fumigated control leaves, average basal NO_2^- concentrations of 1.6 nmol/mg protein were detected. Upon NO_2 fumigation the NO_2^- content gradually increased in a concentration-dependent manner, reaching significant peak values of up to 3478 nmol/mg protein after fumigation with 30 ppm NO_2. Even in plants treated with 10 ppm NO_2 which did not cause detectable leaf damage, NO_2^- levels

increased on average 110-fold to 177 nmol/mg protein (Figure 6 A). Contrariwise, the insignificant variations in the NO_3^- content, ranging from 27 µmol/mg protein in control samples to 47 µmol/mg protein after 30 ppm NO_2 (Figure 6 B), were negligible when considering the massive increase in NO_2^-.

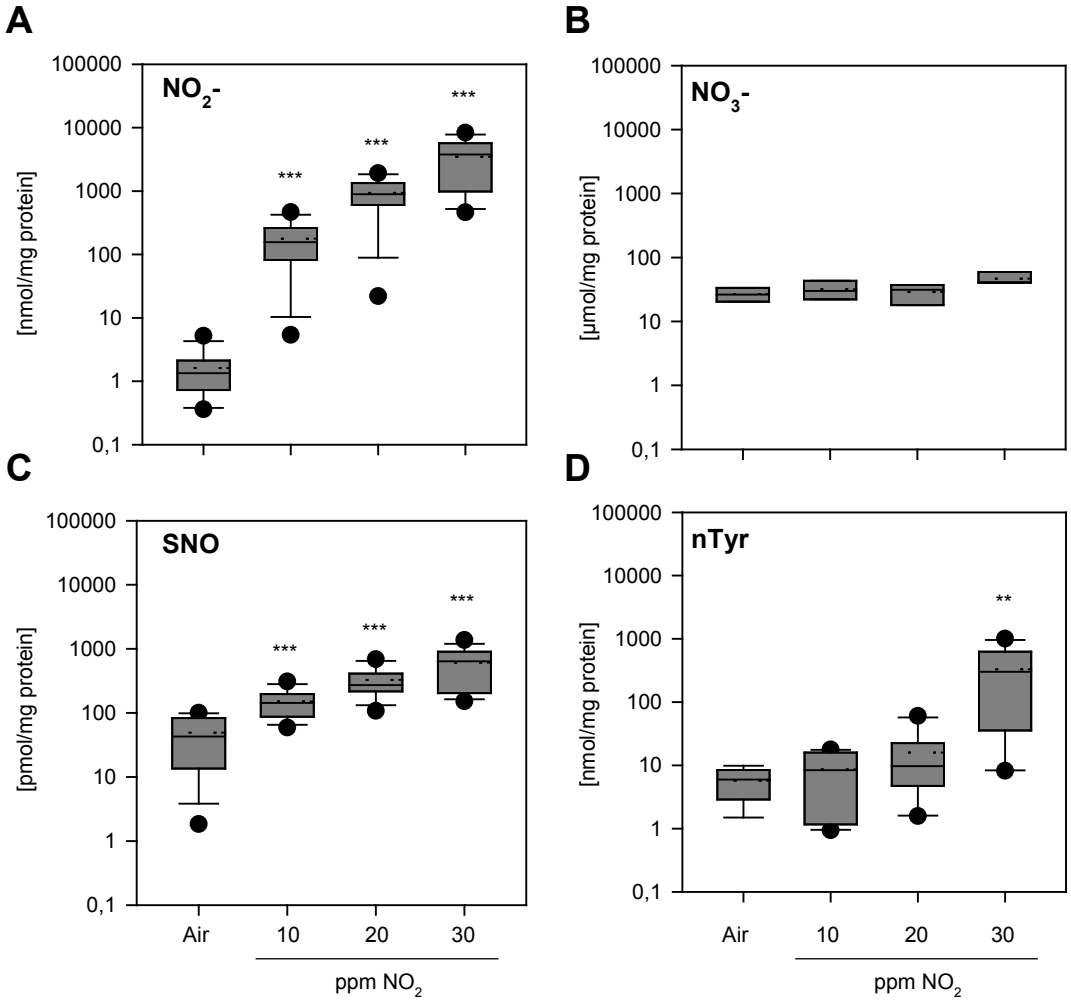

Figure 6: Nitrite, nitrate, S-nitrosothiols, and nitrated proteins content upon NO_2 fumigation
Arabidopsis Col-0 plants were exposed to air (control) or different concentrations of NO_2 for 1 h. **A)** Nitrite (NO_2^-), **B)** nitrate (NO_3^-), and **C)** S-nitrosothiols (SNO) were measured with the Nitric Oxide Analyzer, whereas in **D)** a commercial enzyme-linked immunoassay was used to quantify tyrosine-nitrated proteins (nTyr). Box plots represent median (solid line), mean (dashed line), and $25^{th}/75^{th}$ percentiles (grey box) from 3 independent experiments (except 1 for B). n = 12-14 (A), 3 (B), 8-14 (C), 8-11(D). Whiskers represent 5^{th} and 95^{th} percentiles (only when n > 3), black dots are outliers. The labeling of the x-axes is identical in all graphs. The figure was modified after Kasten *et al*., 2017 by permission of Oxford University Press. ***Statistics:*** Asterisks indicate significant differences from the control samples via Kruskal Wallis Test and Wilcoxon Test with FDR correction (*p < 0.05, **p < 0.01, ***p < 0.001).

Due to its reactive nature, it is likely that NO_2 or its oxo-derivatives such as NO_2^- or $ONOO^-$ post-translationally modify protein residues and thereby alter their activity. One example for these modifications is the S-nitrosylation (SNO) of proteins, where a NO moiety is covalently added to a

reactive thiol group of cysteines [80]–[83]. Furthermore, it was reported that NO_2 and $ONOO^-$ are capable of mediating the nitration of tyrosine (nTyr) residues [60], [87], [95], [227], [228]. To investigate whether the frequency of these protein modifications is altered during the NO_2-induced cell death, SNO and nTyr levels were quantified immediately after fumigation with air, 10, 20, or 30 ppm NO_2. SNO content was determined using the NOA (Figure 6 C), whereas nTyr levels were quantified with a commercial Nitrotyrosine Assay Kit (Figure 6 D).

The NOA analysis revealed that SNO increased significantly with raising NO_2 concentrations. SNO levels in air fumigated control plants averaged to 49 pmol/mg protein. This amount tripled after exposure to 10 ppm NO_2 to 151 pmol/mg protein and culminated in 610 pmol/mg protein after 30 ppm NO_2 (Figure 6 C). Such a continuous increase was not detected for the nitration of tyrosine residues. Here, basal nTyr levels of 6 nmol/mg protein in air-fumigated plants only increased insignificantly after exposure to 10 or 20 ppm NO_2 but significantly rose 55-fold to 330 nmol/mg protein when fumigated with 30 ppm NO_2 (Figure 6 D).

Taken together, NO_2 fumigation loaded the leaf with NO_2^- and SNO even when non-damaging NO_2 concentrations (10 ppm) were applied, whereas pronounced tyrosine nitration only occurred in collapsing leaves after exposure to 30 ppm NO_2. Though NO_2 equimolarly disproportionates to NO_2^- and NO_3^- the latter was not affected by any treatment.

2.1.3 NO and H_2O_2 production is crucial for the NO_2-induced cell death

NO and H_2O_2 are well-known signaling molecules in plants which synergistically trigger the induction of the HR during incompatible plant-pathogen interactions [177], [229]. To investigate their roles in the NO_2-induced cell death, the formation of intracellular NO was evaluated with the fluorescent probe di-amino-fluorescein diacetate (DAF-FM DA), whereas H_2O_2 production was determined via diaminobenzidine tetrahydrochloride (DAB) staining (Figure 7 A, B). The signaling molecules were quantified immediately after fumigation of Arabidopsis Col-0 with various concentrations of NO_2.

The DAF-FM DA fluorescence signal representing intracellular NO was significantly increased 2.2-fold after fumigation with 30 ppm NO_2 when compared to the air-fumigated control (Figure 7A). This fluorescence signal in turn was significantly reduced by 31 %, when 30 ppm NO_2-treated plants were simultaneously infiltrated with DAF-FM DA and the NO scavenger 2-(4-carboxyphenyl)-4,4,5,5-tetramethylimidazoline-1-oxyl-3-oxide (cPTIO, 500 µM). This demonstrated the specificity of the DAF-FM DA probe towards NO. Plants fumigated with 10 or 20 ppm NO_2 did not show a significant

increase in fluorescence intensity when compared to the air-fumigated control, indicating that only an insignificant amount of NO may have accumulated as a result of these treatments (Figure 7 A).

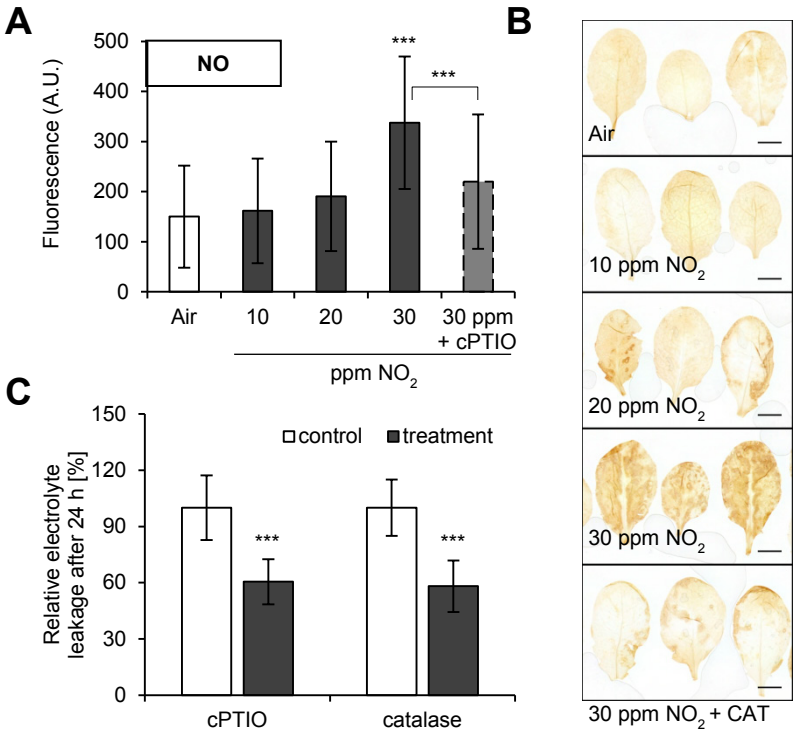

Figure 7: NO_2 fumigation triggers NO and H_2O_2 production important for NO_2-induced cell death
Col-0 plants were exposed to air (control) or NO_2 for 1 h with the indicated concentrations. **A)** Intracellular NO was quantified immediately after fumigation with a photometric assay using 5 µM DAF-FM DA that was infiltrated into leaves 1 h before fumigation. Injection of the NO scavenger cPTIO (500 µM) alongside DAF-FM DA before fumigation with 30 ppm NO_2 served as a DAF-FM DA specificity control (dashed-lined column). Columns represent means ± SD of 3 independent experiments; n = 23-24. **B)** H_2O_2 was detected directly after fumigation via DAB staining. Injection of the H_2O_2-degrading enzyme catalase (CAT, 100 U/ml) before fumigation with 30 ppm NO_2 served as a specificity control for the DAB staining. Representative pictures of 2 independent experiments (except 1 for NO_2 + CAT) are shown; n = 14-16, 8 for NO_2 + CAT; Scale = 5 mm. **C)** Scavengers of NO (500 µM cPTIO) and H_2O_2 (100 U/ml catalase) were infiltrated into leaves 30 min before exposure to 30 ppm NO_2. Immediately after fumigation plant cell death was quantified via electrolyte leakage (cPTIO control = H_2O; catalase control = 0.38 M potassium phosphate buffer pH 7). Columns represent means ± SD; n = 11. A.U. = arbitrary unit. The figure was modified after Kasten *et al*., 2017 by permission of Oxford University Press. ***Statistics:*** Asterisks indicate significant differences from control samples via One Way ANOVA with Holm-Sidak post-hoc Test for multiple comparisons versus control group (**p < 0.01, ***p < 0.001).

In line with the observations made for NO, DAB staining revealed an increase of H_2O_2 immediately after fumigation with 30 ppm NO_2, as was evident by the conspicuous brown areas (Figure 7 B). Infiltration of plants with 100 U/ml of the H_2O_2-detoxifying enzyme catalase (CAT) before fumigation with 30 ppm NO_2 largely prevented DAB staining and verified the dyes' specificity towards H_2O_2. Less pronounced DAB staining was observed after fumigation with 20 ppm NO_2. However, exposure to air or 10 ppm NO_2 (Figure 7 B) did not produce staining results, which correlated with the described concentration-dependent NO_2-induced cell death (see 2.1.1).

According to the literature, the development of HR requires the synergistic action of NO and ROS such as H_2O_2, since neither ROS nor NO are capable of triggering an advanced HR by themselves [177], [229]. This was substantiated by infiltrating leaves with cPTIO or catalase prior to fumigation with 30 ppm NO_2 followed by ion leakage measurements after 24 h to assess cell death propagation (Figure 7 C). Scavenging NO with 500 µM cPTIO significantly reduced total electrolyte leakage by 39.5 % when compared to the H_2O-infiltrated control. Similarly, detoxification of H_2O_2 by catalase led to a 41.9 % decrease in total electrolyte leakage in comparison with the infiltration-control (0.38 M potassium phosphate buffer, pH 7) (Figure 7 C).

In summary, these findings demonstrated that high concentrations of NO_2 stimulate the accumulation of NO and H_2O_2 and corroborated the importance of these two signaling molecules in promoting the NO_2-induced cell death.

2.1.4 Nitrite infiltration resembles the effects of NO_2 fumigation

As shown in 2.1.2, exposure to non-damaging NO_2 concentrations loaded the leaves with an excessive quantity of NO_2^-. Since NO_2^- accumulation is well-known to cause plant injury [230], [231] it was investigated whether NO_2^- infiltration was able to mimic the effects of NO_2 fumigation that lead to cell death induction. Therefore, leaves were infiltrated with 10 and 100 mM $NaNO_2$ or H_2O as control. Electrolyte leakage was performed 1 h after infiltration (Figure 8 A) and leaves were stained with Trypan Blue 24 h treatment (Figure 8 B).

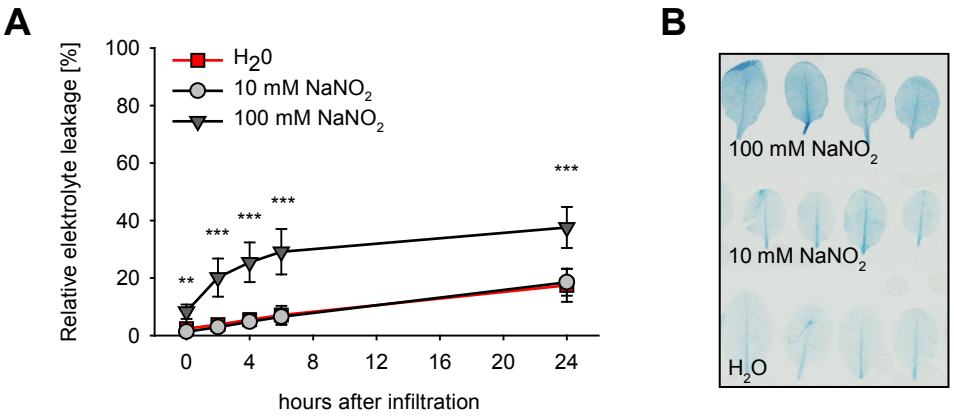

Figure 8: Nitrite infiltration mimics NO_2 -induced cell death
A) Four leaves per plant were injected with H_2O (control), 10 mM, or 100 mM $NaNO_2$. Cell death was quantified over time by electrolyte leakage of whole rosettes starting 1 h after injection. Data points are means ± SD from 2 independent experiments (except 1 for 10 mM $NaNO_2$); n = 15-22. **B)** Trypan Blue cell death staining was performed 24 h after infiltration. Representative pictures are shown; n = 6-8. The figure was modified after Kasten *et al.*, 2017 by permission of Oxford University Press. ***Statistics:*** Asterisks indicate significant differences from control samples via Kruskal Wallis Test and Wilcoxon Test with FDR correction (**p<0.01, ***p<0.001).

Infiltration of 100 mM $NaNO_2$ into Arabidopsis Col-0 leaves led to rapid cell death as evidenced by a total electrolyte leakage of 37.6 % (Figure 8 A) and positive Trypan Blue staining (Figure 8 B) 24 h after infiltration. However, the cell death extent was not as severe as observed after fumigation with 30 ppm NO_2, where 63 % of the total electrolytes leaked through the damaged membranes (Figure 5 C). Compared to the H_2O-infiltrated control, infiltration of 10 mM $NaNO_2$ did not enhance electrolyte leakage or Trypan Blue staining (Figure 8 A, B).

Additionally, leaf material was harvested 3 h after $NaNO_2$ infiltration for analysis of NO_2^-, SNO, H_2O_2, NO_3^-, and nTyr contents. The 3 h time point was chosen since the visible damage of 100 mM $NaNO_2$-treated leaves closely resembled that, which was observed directly after fumigation with 30 ppm NO_2. As anticipated, a drastic increase of NO_2^- in the $NaNO_2$-infiltrated leaves was detected by using the NOA. Treatment with 10 mM $NaNO_2$ raised the mean NO_2^- levels by 4.6-fold from 11 nmol/mg protein in H_2O-infiltrated leaves to 51 nmol/mg protein. Infiltration of 100 mM $NaNO_2$ resulted in an average NO_2^- content of 14070 nmol/mg protein, which corresponded to a significant 1279-fold increase (Figure 9 A).

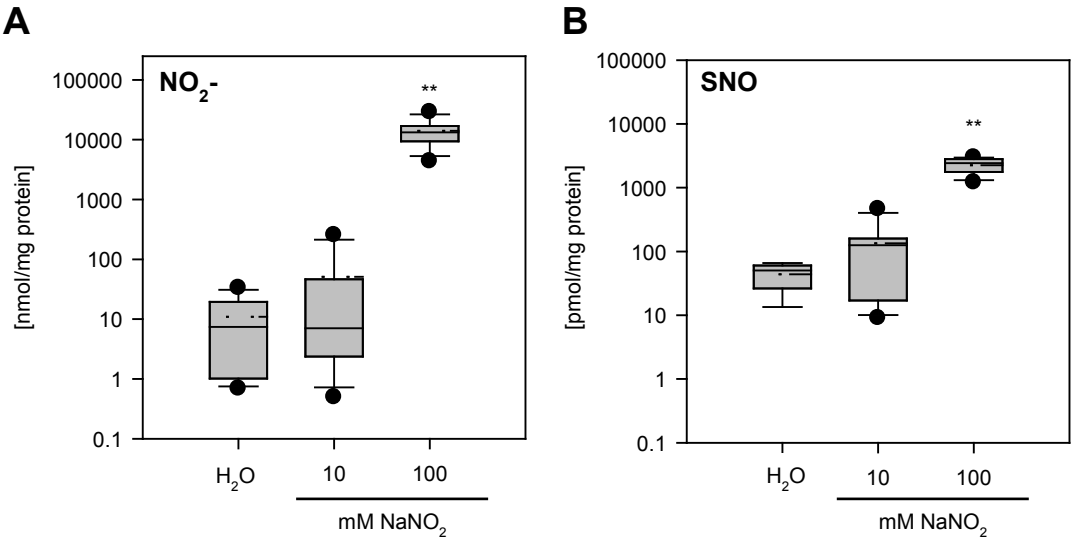

Figure 9: $NaNO_2$ injection elevates nitrite and S-nitrosothiol levels

Leaves were infiltrated with H_2O (control), 10 mM, or 100 mM $NaNO_2$. All measurements were performed 3 h after infiltration. A Nitric Oxide Analyzer was used to quantify **A)** nitrite (NO_2^-) and **B)** S-nitrosothiols (SNO). Box plots represent median (solid line), mean (dashed line), and 25^{th}/75^{th} percentiles (grey box) from 2 independent experiments; n = 7 (A), 4-7 (B). Whiskers represent 5^{th} and 95^{th} percentiles, black dots are outliers. The figure was modified after Kasten *et al*., 2017 by permission of Oxford University Press. ***Statistics:*** Asterisks indicate significant differences from control samples via Kruskal Wallis Test and Wilcoxon Test with FDR correction (**p < 0.01).

Similar observations were made for SNO, whose content tripled from 44 pmol/mg protein in H_2O-infiltrated leaves to 134 pmol/mg protein after infiltration of 10 mM $NaNO_2$ and was further increased by 52-fold to 2249 pmol/mg protein after treatment with 100 mM (Figure 9 B). The absolute levels of

NO_2^- and SNO measured after treatment with 10 mM $NaNO_2$ were comparable to those determined after fumigation with 10 ppm NO_2. On the other hand, leaves treated with 100 mM $NaNO_2$ accumulated approximately four times the quantity of both compounds when compared to those which were treated with 30 ppm NO_2. Changes in NO_3^- and nTyr level were also measured after $NaNO_2$ infiltration, which did not show any significant differences when compared to the content in H_2O-treated leaves (Supplemental Figure 1).

Furthermore, the accumulation of H_2O_2 and NO after $NaNO_2$ treatment was investigated since the production of both signaling molecules was induced after fumigation with NO_2 and was crucial for the induction of cell death, as described in 2.1.3. Intracellular NO strongly accumulated upon treatment with $NaNO_2$ as determined via the increased fluorescence intensity of DAF-FM DA 1 h after infiltration (Figure 10 A). The fluorescence signal was intensified by 4.7-fold upon infiltration with 10 mM $NaNO_2$ and further augmented to 7.1-fold when using 100 mM. This exceeded the amount of NO detected after fumigation with 30 ppm NO_2 by a factor of 2.5 (see Figure 7 A). To ensure that the strong fluorescence signal specifically represented NO accumulation, 100 mM $NaNO_2$ were co-infiltrated with the NO scavenger cPTIO, which led to a signal reduction of 70 % (Figure 10 A, grey, dashed-lined column).

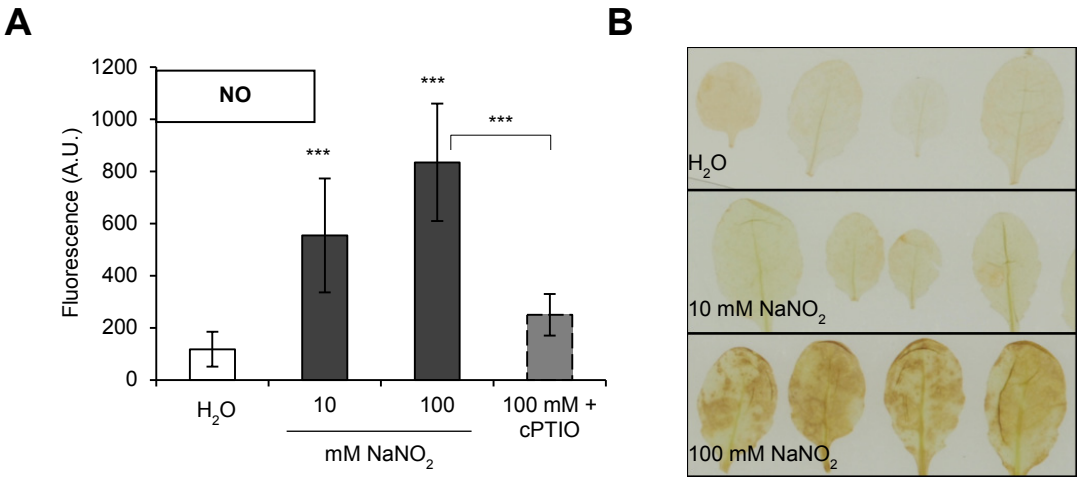

Figure 10: $NaNO_2$ infiltration triggers NO and H_2O_2 accumulation
A) Intracellular NO was measured using the fluorescent probe DAF-FM DA. H_2O (control), 10 mM, or 100 mM $NaNO_2$ were co-infiltrated with 5 µM DAF-FM DA. The resulting fluorescence signal was measured 1 h after infiltration. Injection of the NO scavenger cPTIO (500 µM) alongside DAF-FM DA and 100 mM $NaNO_2$ served as a DAF-FM DA specificity control (dashed-lined column). Columns represent means ± SD; n = 10.). **B)** H_2O_2 was detected by diaminobenzidine (DAB) staining 3 h after nitrite infiltration (representative pictures are shown); n = 8-10. A.U. = arbitrary unit. The figure was modified after Kasten *et al*., 2017 by permission of Oxford University Press. ***Statistics:*** Asterisks indicate significant differences from control samples via Kruskal Wallis Test and Wilcoxon Test with FDR correction (**p < 0.01, ***p < 0.001).

H_2O_2 accumulation after $NaNO_2$ infiltration resembled the results obtained after NO_2 fumigation. DAB staining and therefore H_2O_2 production was most prominent after applying the highest concentration of $NaNO_2$ (Figure 10 B). No distinct staining was detected in leaves infiltrated with H_2O or 10 mM $NaNO_2$, which led to the conclusion that, at most, an insignificant amount of H_2O_2 was produced upon those treatments.

Taken together, the infiltration of a high concentration of NO_2^- (100 mM) induced less pronounced cell death than 30 ppm NO_2 but was accompanied by a greater increase in SNO and NO. Similar to the observations made during the NO_2-induced cell death, 100 mM $NaNO_2$ led to an accumulation of H_2O_2 but did not alter NO_3^- levels. Nitrated proteins that were enriched after fumigation with 30 ppm NO_2 were however not affected by $NaNO_2$.

2.2 NO_2 induces changes in the gene expression profile

Previous research revealed that exposure to low dosages of NO_2 had a beneficial impact on plants by enhancing growth, biomass, flowering, and yield in various plant species such as tomato, sun flower, or Arabidopsis (see 1.1.1, [45]–[47]). Hence, the second part of this work aimed to investigate the molecular processes in plants exposed to NO_2 concentrations which did not cause any visible damage. In accordance with the previous results, fumigation of Arabidopsis Col-0 with 10 ppm NO_2 for 1 h suited this criterion and therefore was used to examine the plants response to this moderate, non-damaging dose of NO_2. To obtain a comprehensive overview of processes that were affected by NO_2, a genome-wide gene expression analysis was performed using an Agilent At8x60K one-color microarray.

2.2.1 Microarray data evaluation

Arabidopsis Col-0 plants were fumigated with air or 10 ppm NO_2 for 1 h and leaf material was obtained directly or 6 h after fumigation for microarray analysis. Preprocessing of the data was kindly performed by Dr. Elisabeth Georgii and included background correction, quantile normalization, and $\log_2$ transformation. Since four biological replicates per treatment were evaluated, the obtained values of the same gene (as classified by the TAIR 10 genome annotation [232]) were averaged across these replicates. Differential gene expression analysis of NO_2- against air-fumigated samples was also conducted by Dr. Elisabeth Georgii and revealed large sets of genes that were differentially expressed after NO_2-fumigation at both time points. The microarray data has been deposited in the

ArrayExpress database at EMBL-EBI (www.ebi.ac.uk/arrayexpress) under the accession number E-MTAB-6522. The access however, is restricted until the work is published (preliminary access via username: Reviewer_E-MTAB-6522, password: Nyonpqvw).

The large set of approximately 21600 genes was filtered according to their adjusted p-value and fold change (FC) to the air treatment to identify relevant NO_2-specific responses. Figure 11 depicts this data confinement. Volcano plots were generated by plotting the log_2(FC) of each gene against the negative decadic logarithm of its respective adjusted p-value. These plots aimed to illustrate the comprehensive effect of NO_2 upon gene regulation for each investigated time point after fumigation (Figure 11 A). The Venn diagrams in Figure 11 B illustrate the number of significantly regulated genes which were highlighted in the volcano plots using an identical color code.

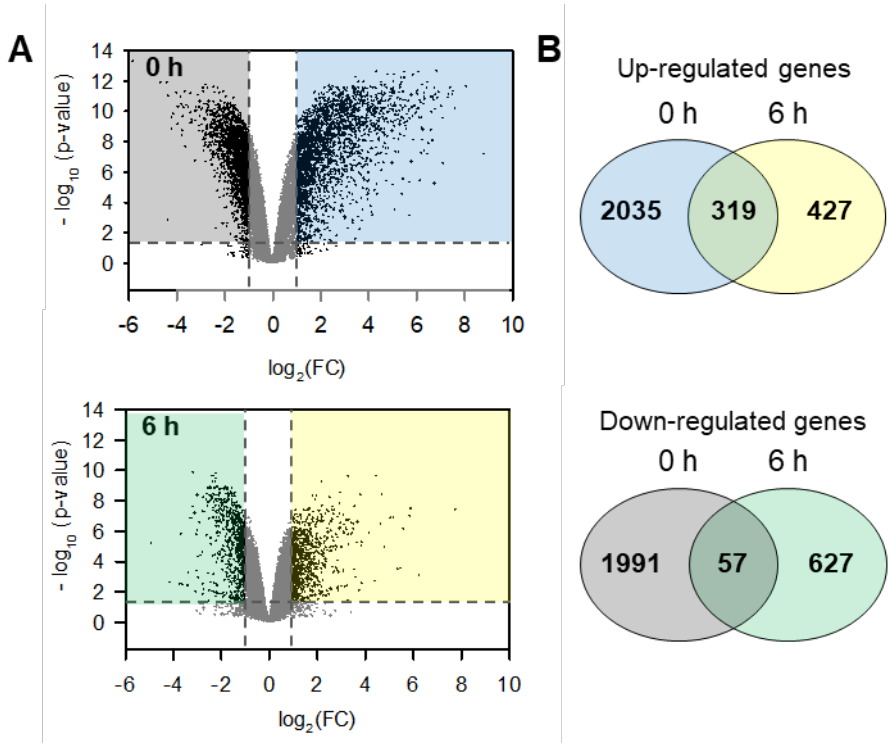

Figure 11: Illustration of changes in gene expression induced by 10 ppm NO_2
Col-0 plants were fumigated with 10 ppm NO_2 or air for 1 h and leaf material was harvested for microarray analysis immediately (0 h) or 6 h after fumigation; n = 4. Changes in gene expression were determined by the fold change (FC) of their fluorescent signal after NO_2 treatment compared to the air control. **A)** Volcano plots visualizing the changes in gene expression 0 h (top) and 6 h (bottom) after fumigation by plotting the adjusted p-value over the fold change. Horizontal dashed lines mark p = 0.05; vertical dashed lines indicate log_2(FC) ± 1. Data points represent expression of individual genes. The expression of genes appearing in the colored left panels is significantly down-regulated ($p < 0.05$, $log_2(FC) < 1$), whereas expression of genes within the colored right panel shows significant up-regulation ($p < 0.05$, $log_2(FC) > 1$). **B)** Venn diagrams illustrating the number of significant genes that are up- (top) or down-regulated (bottom) with $p < 0.05$ and log_2(FC) ± 1. Right: genes were exclusively regulated 0 h after fumigation, left: genes were exclusively regulated 6 h after fumigation, middle: genes were mutually regulated at both time points. Color code is consistent in A and B indicating genes down-regulated at 0 h (purple) and 6 h (green), or up-regulated at 0 h (blue) and 6 h (yellow).

When comparing the volcano plots of each investigated time point it became evident that NO_2 caused rapid, highly significant transcriptional reprogramming. The data points at the 0 h time point (Figure 11 A, top) covered a larger area within the plot plane than those at the 6 h time point (Figure 11 A, bottom). This indicated that the changes in gene expression immediately after fumigation were highly significant (plot height) and more pronounced (plot width) than after 6 h. Moreover, approximately 2400 genes were significantly up-regulated, while approximately 2000 genes were down-regulated significantly immediately after fumigation, whereas only about one third as much (750 up- and 680 down-regulated genes) were affected after 6 h (Figure 11 B). Interestingly, the regulated genes scarcely overlapped across the two time points (Figure 11 B, middle). Only 11.5 % of all up- and 2.1 % of all down-regulated genes were affected at both time points, which hinted towards transient or discrete time-dependent responses of the plant to NO_2.

2.2.2 Ontology enrichment of genes regulated by NO_2

In the attempt to unravel the underlying biological processes induced by NO_2, functional profiles of the up- ($p < 0.05$, $\log_2(FC) > 1$) or down- regulated ($p < 0.05$, $\log_2(FC) < -1$) gene sets were retrieved via Gene Ontology (GO) term enrichment analysis using the PANTHER 11.0 overrepresentation test. Here, each gene within the analyzed data set was classified into GO-terms. These annotation categories were then tested for their overrepresentation when compared to an Arabidopsis reference list (Figure 12).

Immediately after fumigation 122 GO-terms were significantly enriched in the up-regulated gene set (Supplemental Table 1). Many of them were related to plant defense processes, which is graphically represented by the clustering of numerous GO-terms according to their distance within the gene ontology hierarchy (Figure 12, left). Here, major GO-terms included defense against wounding, fungi, and bacteria. Furthermore, the enrichment revealed that NO_2 activated genes involved in JA metabolism and signaling, as well as genes responsible for mediating the response to SA and ET. Moreover, NO_2 induced the expression of genes involved in camalexin biosynthesis and flavonoid glucuronidation, as well as programmed cell death, which are effective defense mechanisms against a variety of pathogens [199], [233]–[235].

Even though, only 13.5 % (319 out of 2354) of the genes up-regulated directly after fumigation were still highly expressed after 6 h, similar GO-terms where enriched at both time points. In total 69 GO-terms were enriched within the set of genes up-regulated 6 h after fumigation (Figure 12, right). 40 of those annotations, were already enriched directly after fumigation, including responses to chitin, fungus, wounding, as well as JA metabolic processes (Supplemental Figure 2 and Supplemental Table 2). GO-terms exclusively enriched in the gene set up-regulated 6 h after fumigation

represented cellular water homeostasis, cell wall metabolic processes involving xyloglucan and polysaccharides, as well as responses to light and nutrient stimuli (Figure 12, right).

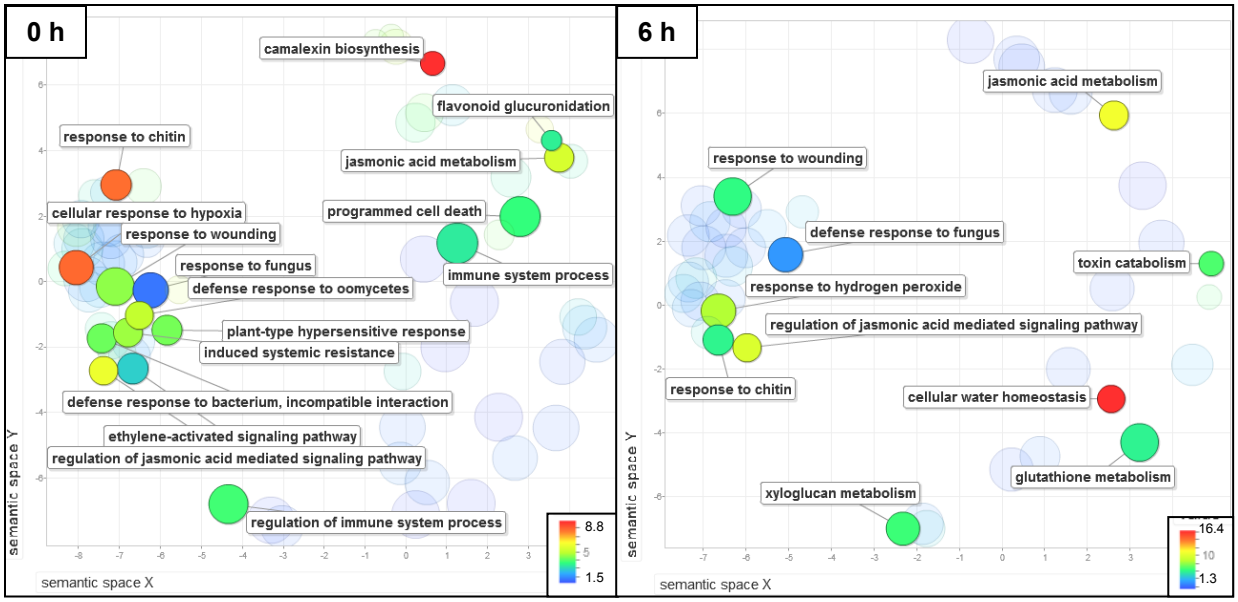

Figure 12: Gene ontology (GO) enrichment analysis of genes up-regulated by 10 ppm NO_2
Enriched GO terms (Fold enrichment > 1, $p < 0.05$) of genes up-regulated directly (0 h, left) or 6 h (right) after fumigation were identified using the PANTHER 11.0 overrepresentation test and visualized in scatter plots using the REVIGO tool. Each circle represents a GO term, whereat the number of genes it encompasses is represented by the circle size. The color code depicts the fold enrichment of the respective GO term within the data set compared to the PANTHER *Arabidopsis thaliana* reference list. Circles are clustered according to the distance of the respective GO terms within the GO hierarchical tree. Axes have no intrinsic meaning. Highly enriched or interesting GO terms are labeled.

Genes down-regulated immediately after fumigation encompassed 57 significantly enriched GO-terms (Supplemental Table 3). These included general processes such as the primary metabolism, rhythmic and developmental processes as well as growth regulation. Furthermore, responses to the phytohormones auxin and gibberellin were actively repressed upon NO_2 fumigation (Supplemental Figure 3, left and Supplemental Table 3). Six hours after exposure to 10 ppm NO_2, genes involved in DNA maintenance such as replication and repair as well as cell cycle processes were significantly down-regulated (Supplemental Figure 3 right and Supplemental Table 4).

In summary, the comparison of the gene expression profile of NO_2-fumigated against air-fumigated plants revealed that defense responses where initiated upon exposure to moderate, non-damaging concentrations of NO_2. More specifically, NO_2 activated genes involved in the biosynthesis and signaling of the plant hormones JA, SA, and ET and induced the expression of genes related to defense mechanisms such as camalexin and flavonoid biosynthesis, programmed cell death, and metabolic processes within the cell wall.

2.3 Quantification of hormone levels after fumigation with 10 ppm NO_2

The transcriptional profiling of plants fumigated with 10 ppm NO_2 suggests that NO_2 promotes JA and SA signaling. Since both hormones are well-known to be important regulators of plant immunity and pathogen defense [131], the influence of NO_2 upon SA and JA accumulation was investigated further. Therefore, SA and various jasmonates were quantified via LC-MS/MS at different time points after NO_2 treatment to assess whether the enriched abundance of the biosynthetic gene transcripts was translated to an accumulation of these hormones. The phytohormone measurements were performed in collaboration with Dr. Axel Mithöfer (Max-Planck Institute for Chemical Ecology in Jena, Germany).

2.3.1 NO_2 stimulates a rapid turnover of active jasmonates

The term jasmonates encompasses all biologically active intermediates during the JA biosynthesis, such as *cis*-(+)-12-oxophytodienoic acid (*cis*-OPDA), as well as JA derivatives that are able to modulate biological processes, such as jasmonoyl-isoleucine (JA-Ile), methyl-jasmonate (MeJA), and JA itself [236], [237]. Jasmonates derive from the fatty acid linolenic acid which undergoes oxidation via lipoxigenases (LOX), dehydration via the allene oxide synthase (AOS), followed by subsequent cyclization to *cis*-OPDA via the allene oxide cyclases (AOC). After *cis*-OPDA is reduced by the OPDA-reductase (OPR3), three rounds of β-oxidation (e.g. via Acyl-CoA oxidase ACX1 and OPC-8:0 CoA ligase OPCL1) are necessary to form JA. JA in turn, can be modified to JA-Ile or MeJA via the jasmonates-amid synthetase JAR1 and JA-carboxyl methyltransferase JMT, respectively [237]. The JA biosynthetic pathway is outlined in Figure 13 A, which also illustrates the gene expression levels of the major biosynthetic genes directly and 6 h after fumigation as they were obtained from the microarray data sets. The majority of the depicted genes were significantly up-regulated immediately after fumigation (Figure 13 A, right underlying panel), ranging in $\log_2$(FC) relative to the air control from 1.1 for *AOS* to 5.9 for *AOC3*. Only *LOX2* and *JAR1* were negligibly expressed ($0 < \log_2 FC < 1$). At 6 h after fumigation the expression levels had declined to a maximum of $\log_2$(FC) = 2.1 for *AOC1* (Figure 13 A, left underlying panel).

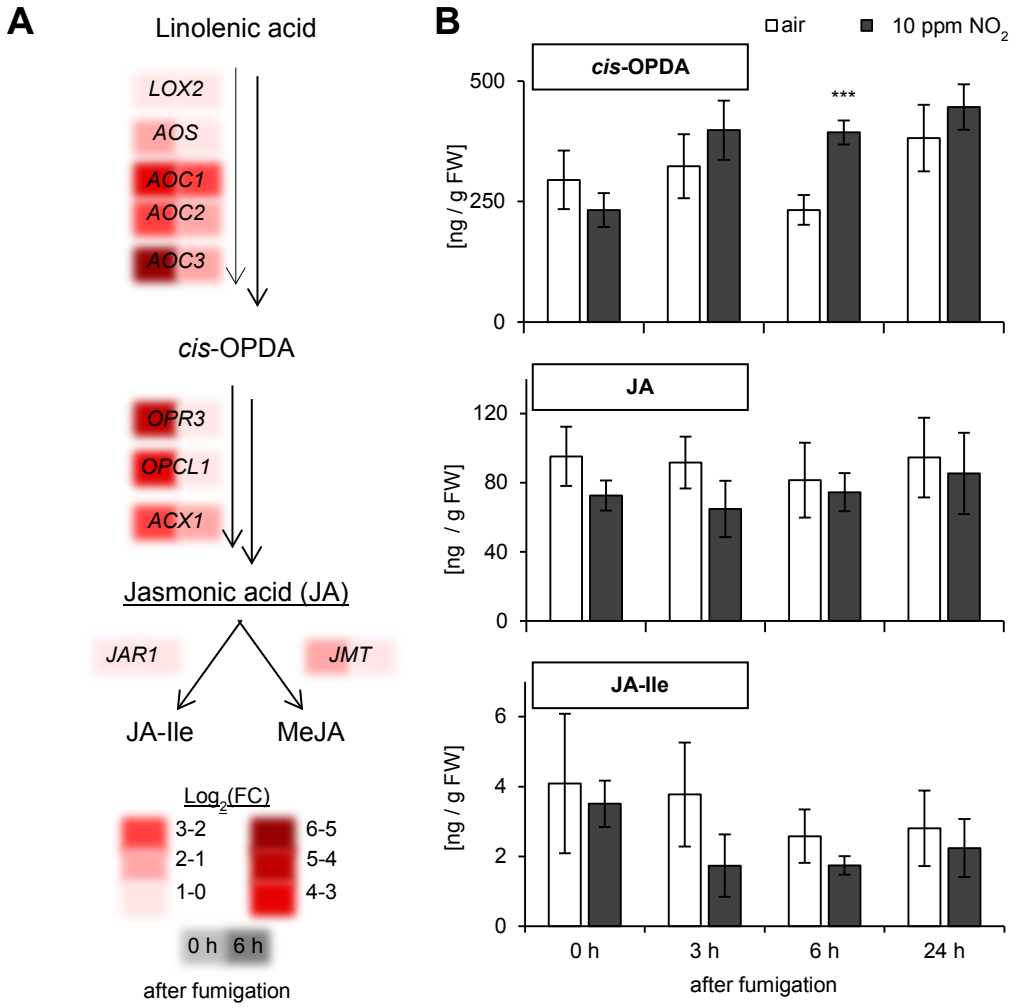

Figure 13: NO_2 stimulates the expression of JA synthesis genes but not jasmonate accumulation
A) Schematic JA biosynthesis pathway illustrating the expression levels (log_2(FC)) of the respective genes obtained from the microarray directly (0 h) or 6 h after fumigation with 10 ppm NO_2. Colored panels depict log_2(FC) of the genes compared to the air fumigated control, left = 0 h, right = 6 h after fumigation. **B)** Quantification of various jasmonates (top: *cis*-OPDA, middle: JA, bottom: JA-Ile) at different time points after fumigation with air or 10 ppm NO_2 was done via LC-MS/MS and normalized to the sample's fresh weight (FW). Columns represent means ± SD; n = 5. *Cis*-OPDA = *cis*-(+)-12-oxophytodienoic acid, JA = jasmonic acid, JA-Ile = jasmonoyl-L-isoleucine, MeJA = methyl jasmonate. The figure legends and labeling of the x-axes are identical in all graphs. ***Statistics:*** Asterisks indicate significant differences within the time points via Two Way ANOVA + Holm-Sidak post-hoc Test (***p < 0.001). Two Way ANOVA showed that fumigation-induced changes in hormone levels significantly depended on the time in case of *cis*-OPDA (p = 0.002) but not for JA or JA-Ile.

The enrichment of biosynthetic gene transcripts directly after NO_2 fumigation, suggested that NO_2 may lead to a rapid accumulation of jasmonates. However, increased levels were only measured for *cis*-OPDA starting at 3 h after fumigation (Figure 13 B, top). No significant changes were detected for JA or JA-Ile (Figure 13 B, middle and bottom). These findings contradict previous research which demonstrated that an increase in transcription levels of JA biosynthetic genes generally coincides

with the accumulation of jasmonates [238]. Therefore, it was investigated whether NO_2 was promoting a rapid decomposition of jasmonates.

A major step during the catabolic turnover of active jasmonates is the oxidation of JA-Ile by members of the cytochrome P45 family (CYP94) resulting in biologically inactive 12-OH-JA-Ile and 12-COOH-JA-Ile [239]–[241]. Additionally, JA-Ile and its hydroxylated form can be catabolized to tuberonic acid (12-OH-JA) by the amidohydrolases IAR3 and ILL6 [242]. Moreover, jasmonate-induced oxygenases (JOXs) were recently identified, which hydroxylate JA to its inactive 12-OH-JA derivative [243] and represents yet another catabolic pathway of active jasmonates. All the described pathways, including the corresponding gene expression levels were summarized in Figure 14 A.

The microarray analysis revealed that NO_2 strongly promoted the inactivation of jasmonates. Immediately after fumigation, the majority of genes involved in these catabolic reactions were highly up-regulated with fold changes (log_2(FC)) to the respective air controls ranging from 1.3 up to 7.4. Here, especially the genes encoding the CYP94 proteins and members of JOXs were highly induced. Particularly in case of the latter, the transcript levels remained significantly elevated up to a log_2(FC) of 7.8 at 6 h after NO_2 treatment. Besides the JOXs, the gene transcripts of most of the aforementioned catabolic enzymes remained highly abundant at this time point after fumigation. All accurate expression levels of the genes depicted in Figure 13 A and Figure 14 A can be found in Supplemental Table 6.

The rapid and extensive NO_2-induced transcription of genes whose products are necessary for jasmonate catabolism strengthens the hypothesis that NO_2 stimulates rapid jasmonate turnover. To further reinforce this theory, intermediates of the catabolic reactions were quantified by LC-MS/MS in cooperation with Dr. Axel Mithöfer (Max-Planck Institute for Chemical Ecology in Jena, Germany). In Figure 14 B the levels of 12-OH-JA, 12-OH-JA-Ile, and 12-COOH-JA-Ile at various time points after air and NO_2 fumigation are shown. All catabolic intermediates rapidly increased and peaked in their concentrations at 3 h after NO_2 fumigation. Specifically, 12-OH-JA increased significantly by a factor of 3.2 from 21.9 ng/g FW in air-fumigated plants to 71 ng/g FW after NO_2 treatment. A similar 3.1-fold increase was observed for 12-COOH-JA-Ile from 6 ng/g FW (air) to 18.9 ng/g FW (NO_2). OH-JA-Ile levels elevated significantly by 2.3-fold at 3 h after fumigation when compared to the air-fumigated control. After 3 h, the levels of the catabolic products gradually declined to base line levels at 24 h after NO_2 treatment (Figure 14 B).

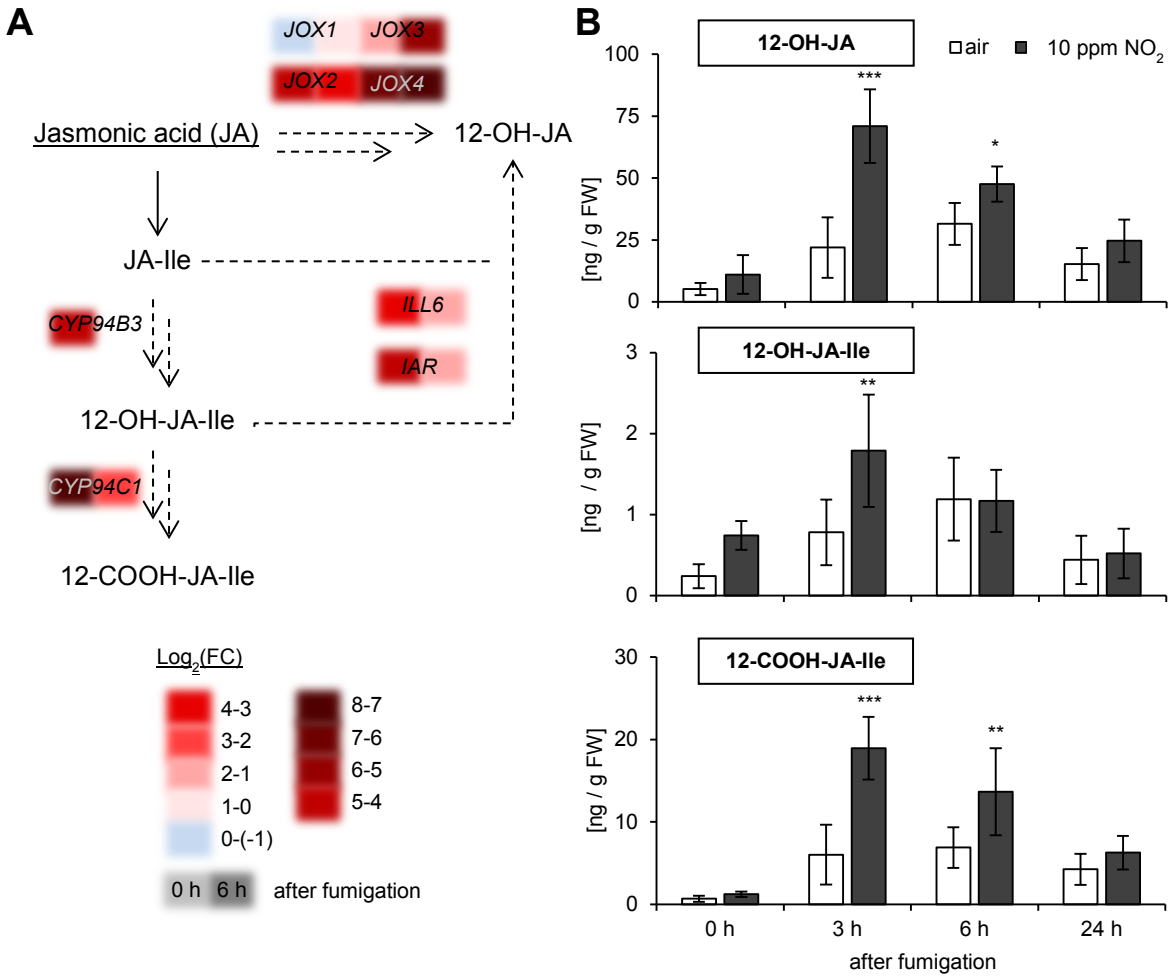

Figure 14: NO_2 stimulates the catabolism of active jasmonates
A) Schematic pathway of the catabolism of active jasmonates (JA, JA-Ile) illustrating the expression levels (log_2(FC)) of the respective genes obtained from the microarray directly (0 h) or 6 h after fumigation with 10 ppm NO_2. Colored panels depict log_2(FC) of the genes compared to air fumigated control, left = 0 h, right = 6 h after fumigation. **B)** Levels of various jasmonate degradation products (top: 12-OH-JA, middle: 12-OH-JA-Ile, bottom: 12-COOH-JA-Ile) at different time points after fumigation with air or 10 ppm NO_2 were measured via LC-MS/MS and normalized to the sample's fresh weight (FW). Columns represent means ± SD; n = 5. 12-OH-JA = 12-hydroxyl jasmonic acid, JA-Ile = jasmonoyl-L-isoleucine, 12-OH-JA-Ile = 12-hydroxyl-JA-Ile, 12-COOH-JA-Ile = 12-dicarboxy-JA-Ile. The figure legends and labeling of the x-axes are identical in all graphs. ***Statistics:*** Asterisks indicate significant differences within the time points via Two Way ANOVA + Holm-Sidak post-hoc Test (*p < 0.05, **p < 0.01, ***p < 0.001). Two Way ANOVA showed that fumigation-induced changes significantly depended on the time for OH-JA (p < 0.001) and COOH-JA-Ile (p < 0.001) but not for 12-OH-JA-Ile.

Taken in conjunction, the results suggested that exposure to NO_2 has the potential to induce jasmonate production due to its ability of activating the transcription of genes necessary for their biosynthesis. However, an accumulation of jasmonates was not detectable at any time after NO_2 fumigation. According to the gene expression data, NO_2 fumigation simultaneously promoted the induction of catabolic pathways and therefore may likely have stimulated a rapid turnover of

biologically active jasmonates. This hypothesis was strengthened by the observed accumulation of inactive jasmonate metabolites after NO_2 exposure.

2.3.2 NO_2 promotes a transient accumulation of salicylic acid

In addition to jasmonates, the accumulation of SA after fumigation with 10 ppm NO_2 was investigated, since this hormone is known to be an important signal in the plants defense against pathogens [133], [244]. In Arabidopsis, the *de novo* synthesis of SA upon pathogen infection can occur via two distinct pathways. In the first, chorismate can be transformed to isochorismate by the isochorismate synthase ICS1 (or SA INDUCTION-DEFICIENT 2, SID2) [245]. Isochorismate is then further metabolized to SA potentially by the action of PBS3, a member of the acyl-adenylate/thioester-forming enzyme family, and the acetyltransferase-family member EPS1 [246]. The second source of SA is the phenylpropanoid pathway, where phenylalanine is non-oxidatively deaminized by Phenylalanine ammonia-lyases (PAL) to cinnamate. Subsequent intermediate reactions lead to the formation of benzoic acid, which is finally converted to salicylic acid [247], [248]. Several regulatory proteins are involved in SA synthesis, including ENHANCED DISEASE SUSCEPTIBILTY 1 (EDS1), and PHYTOALEXIN DEFICIENT 4 (PAD4) [249]–[251]. Finally, SA is transported out of the chloroplast by the Multi-Antimicrobial Extrusion (MATE) transporter ENHANCED DISEASE SUSCEPTIBILTY 5 (EDS5) [252], [253]. The SA biosynthetic pathways are outlined in Figure 15 A, which also illustrates the gene expression levels of the major biosynthetic genes directly and 6 h after fumigation as they were obtained from the microarray data sets.

The gene transcripts of the aforementioned proteins involved in SA biosynthesis were at least 2.2-fold up-regulated (except *EPS1, PAL3/4*) immediately after fumigation with NO_2 (Figure 15 A). Nonetheless, the transcript levels of the biosynthetic genes declined to levels comparable to those in air-fumigated plants at 6 h after NO_2 fumigation ($\log_2$(FC) between -0.9 and 1.3). The accurate expression levels of the genes depicted in Figure 15 A can be found in Supplemental Table 5.

Since an enhanced expression of biosynthetic genes such as *SID2* was reported to coincide with SA accumulation [245], levels of this hormone were quantified after fumigation with 10 ppm NO_2. LC-MS/MS analysis revealed that the NO_2-induced expression of SA biosynthetic genes was indeed causing a significant increase in SA levels immediately after fumigation (Figure 15 B). Basal SA level averaged out to approximately 90 ng/g FW in air fumigated leaves, which was exceeded by 34.5 % and 36.3 % directly or 3 h after fumigation, respectively. Over time the SA content rapidly declined from 132.6 ng/g FW at 3 h, to 73.4 ng/g FW at 6 h after fumigation. At this time point, the SA levels significantly decreased by 31 % when compared to the concentration in the respective air fumigated

control. This is in line with the previous observation that the transcript levels of the biosynthetic genes declined at this time point as well.

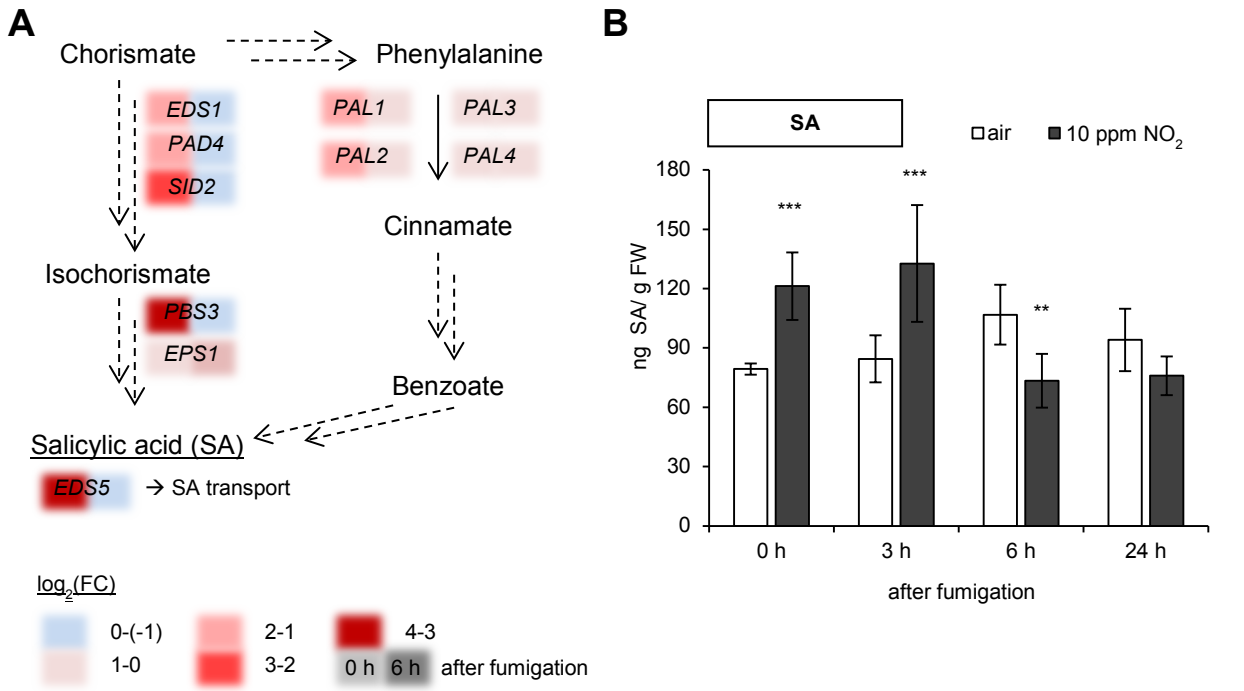

Figure 15: NO_2 promotes a rapid but transient accumulation of SA
A) Schematic salicylic acid (SA) biosynthesis pathway illustrating the expression levels (log_2(FC)) of the respective genes obtained from the microarray directly (0 h) or 6 h after fumigation with 10 ppm NO_2. Colored panels depict log_2(FC) of the genes compared to air fumigated control, left = 0 h, right = 6 h after fumigation. **B)** SA levels at different time points after fumigation with air or 10 ppm NO_2 were measured via LC-MS/MS and normalized to the sample's fresh weight (FW). Columns represent means ± SD; n = 5. ***Statistics:*** Asterisks indicate significant differences within the time points via Two Way ANOVA + Holm-Sidak post-hoc Test (**p < 0.01, ***p < 0.001). Two Way ANOVA showed that fumigation-induced changes in SA levels significantly depended on the time (p < 0.001).

In summary, exposure to 10 ppm NO_2 activated the expression of genes involved in SA biosynthesis, particularly those associated with the isochorismate pathway like *SID2*. Even though, the enhancement in gene expression only occurred immediately after fumigation and was almost abolished 6 h after NO_2 fumigation, it provoked a rapid, but transient accumulation of SA.

2.4 Deciphering the role of phytohormones in NO_2-induced pathogen resistance

The gene expression profile obtained by the microarray analysis revealed that NO_2 exposure activates genes associated with pathogen defense and immune system processes (see section 2.2.2). These findings led to the conclusion that NO_2 exposure may be sufficient to provide pathogen resistance. Here, induced resistance against necrotrophic fungi appeared to be a reasonable assumption, since enriched GO-terms encompassed responses against fungi and the fungal elicitor chitin, as well as JA- and ethylene-mediated responses, all of which are known to be involved in necrotrophic defense [98]. Moreover, GO-terms regarding the synthesis of metabolites with antifungal properties, such as camalexin [167] were highly enriched directly after fumigation.

2.4.1 NO_2-induced resistance against *Botrytis cinerea*

To investigate whether NO_2 induces resistance against necrotrophic fungi, NO_2 fumigated plants were infected with *Botrytis cinerea*. The areas of the developing necrotic lesions were analyzed to assess the potential of NO_2 to provide resistance against this pathogen. In detail, Arabidopsis Col-0 plants were fumigated with 10 ppm NO_2 for 1 h, followed by droplet-infection of detached leaves after 6 h with approximately 1000 spores of *B. cinerea* which were maintained in half-strength grape juice during the infection period. To obtain an infection reference, unfumigated leaves were exposed to *B. cinerea*. Three days after infection the necrotic areas which had formed on fumigated leaves were measured and normalized to the mean necrotic area of unfumigated leaves (= 100 %).

Since unfumigated plants were used as a control, it had to be ensured that the fumigation process of plants treated with NO_2 did not influence the infection assay (e.g. temperature or light variation and wind speed in the fumigation chamber). Therefore, *B. cinerea*-induced lesion formation on air-fumigated and unfumigated leaves was compared in prior experiments. Here, no significant differences in lesion size were detected (Supplemental Figure 5).

Figure 16 A (top) illustrates a representative example of the necrotic lesions formed on NO_2 fumigated and non-treated plants. Evidently, lesions on NO_2 fumigated plants were considerably smaller than those which developed on unfumigated leaves. This observation was made in numerous independent experiments. It was also noted that the application of half-strength grape juice alone did not induce lesions (Figure 16 A, bottom). Quantification of the necrotic areas revealed that the

necrotic lesions formed on NO_2 fumigated plants were significantly reduced by approximately 30 % when compared to the average necrotic area which formed on unfumigated leaves (Figure 16 B).

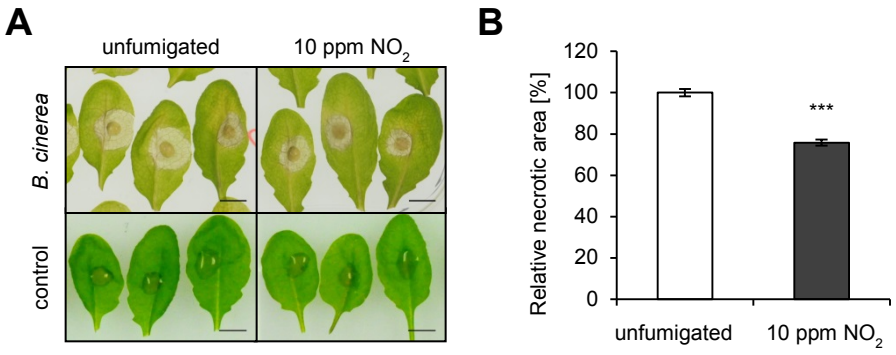

Figure 16: NO_2 induces resistance against *Botrytis cinerea*
Col-0 plants were fumigated with 10 ppm NO_2 for 1 h (unfumigated as control) followed by droplet-infection of detached leaves with approx. 1000 spores of *B. cinerea* 6 h after fumigation (half-strength grape juice as control). **A)** Representative pictures of necrotic lesions 3 days after droplet-infection with *B. cinerea* (top) or half-strength grape juice as control (bottom). Scale = 5 mm. **B)** Evaluation of necrotic lesion development occurred 3 days after infection by measuring the necrotic area via ImageJ. The necrotic areas formed on fumigated leaves were normalized to the mean necrotic area of unfumigated leaves (= 100 %). Columns represent means of 18 independent experiments ± SEM; n_{leaves} = 624-640. ***Statistics:*** Asterisks indicate significant differences from control via Mann Whitney Rank Sum Test (***$p < 0.001$).

Taken together, The *B. cinerea* infection assay confirmed the hypothesis that NO_2 induces resistance against necrotrophic fungi.

2.4.2 The role of jasmonic acid in the NO_2-induced resistance against *B. cinerea*

As previously mentioned, it is commonly assumed that the defense against necrotrophic fungi is primarily mediated by jasmonates [139], [238]. According to the obtained microarray data, genes involved in the synthesis and signaling of this phytohormone are highly up-regulated after NO_2 exposure (see section 2.2.2). However, only a minor increase in *cis*-OPDA was detected after fumigation, while no changes of the remaining active jasmonates were determined. Nonetheless, the detected increase in inactive jasmonate-catabolic products without a concurrent depletion of the active jasmonate pool strongly suggested a NO_2-induced production of jasmonates (see section 2.3.1). To investigate whether this regulation of jasmonates is of biological significance, Arabidopsis knock-out mutants impaired in JA-biosynthesis and –signaling were subjected to the *B. cinerea* infection assay after NO_2-fumigation.

Initially, mutants impaired in JA-synthesis were tested for their NO_2-induced resistance phenotype. Here, the *aos* and *opr3* mutant were utilized, as both knock-out mutants are known to be impeded or deficient of JA accumulation upon wounding or *B. cinerea* infection [165], [254], [255]. The corresponding genetic background controls (WT) of the mutants were concurrently fumigated and infected to ensure that the respective WT plants can develop the NO_2-induced resistance. Representative pictures of the necrotic lesions are shown in Supplemental Figure 6.

As shown in Figure 17, both WT controls developed a resistance to *B. cinerea* when they were exposed to NO_2 before infection. The necrotic lesions on NO_2-treated *Col-gl* (*aos* background control, Figure 17 A) were significantly reduced by 33.2 %, whereas WS (WT of *opr3*, Figure 17 B) displayed a 31.1 % reduction in lesion size upon NO_2 fumigation. In case of both JA-deficient mutants the size of the *B. cinerea*-induced lesions was not affected by NO_2 treatment, demonstrating that *opr3* and *aos* lack the NO_2-induced resistance phenotype (Figure 17). Statistical analysis using Two Way ANOVA further revealed that the observed fumigation-induced effects on the lesion size significantly depended on the genotype (*aos* vs. *Col-gl*: p = 0.004, *opr3* vs. WS: p = 0,007). Conclusively, the NO_2-induced resistance against *B. cinerea* is dependent on a functional JA-biosynthesis.

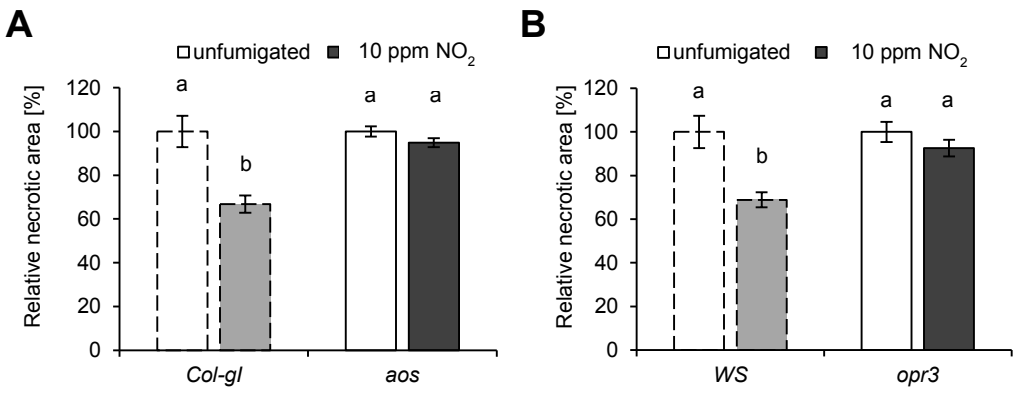

Figure 17: Mutants impaired in JA synthesis lack the NO_2-induced resistance against *B. cinerea*
JA-deficient mutants were subjected to *B. cinerea* droplet-infection 6 h after fumigation with 10 ppm NO_2 for 1 h (unfumigated as control). Necrotic areas formed on fumigated leaves after 3 days were normalized to the mean necrotic area of the respective unfumigated leaves (= 100 %). Relative necrotic area of **A)** *aos* and its WT-like genetic background *Col-gl* or **B)** *opr3* and its WT ecotype WS. Columns represent means of 3 independent experiments ± SEM; n_{leaves} = 66-74 (*Col-gl*), 125-129 (*aos*), 70-90 (WS), 105-117 (*opr3*). Dashed-lined columns represent respective WT. ***Statistics:*** Letters indicate significant differences of all pairwise comparisons via Kruskal Wallis Test + Dunn's post-hoc Test ($p < 0.01$). Multifactorial Two Way ANOVA analysis demonstrated that fumigation-induced effects depended on the genotype (*aos vs. Col-gl*: p = 0.004; *opr3 vs. WS*: p = 0.007).

Additional experiments were conducted to investigate the involvement of JA signaling in the NO_2-induced resistance against *B. cinerea* in more detail, since several genes involved in the propagation of the JA response were up-regulated upon NO_2 fumigation. An overview of the JA signaling pathway

is depicted in Figure 18 A, while a detailed description of the signaling pathway can be found in section 1.2.2. The expression profile of the genes relevant during JA/ET-signaling revealed that *COI1* expression was not strongly influenced by NO_2, whereas the transcription factors *JIN1*, *ORA59*, and *ERF1* were highly up-regulated immediately after NO_2 treatment (log_2(FC) of 3.0, 2.1, and 3.3, respectively, Figure 18 A).

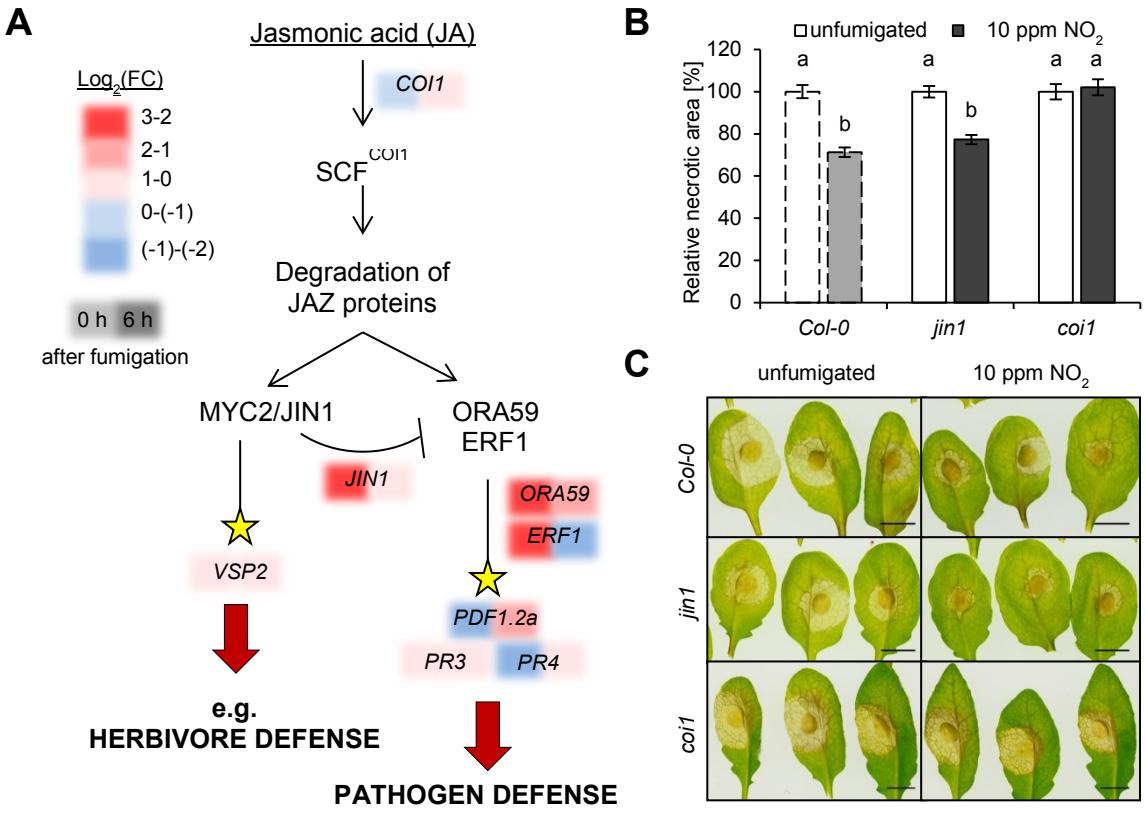

Figure 18: NO_2-induced resistance is dependent on COI1- but not JIN1-mediated JA signaling
A) Schematic pathway of jasmonic acid (JA) signaling illustrating the expression levels (log_2(FC)) of the respective genes obtained from the microarray directly (0 h) or 6 h after fumigation with 10 ppm NO_2. Colored panels depict log_2(FC) of the genes compared to air fumigated control, left = 0 h, right = 6 h after fumigation. Stars indicate gene activation. **B)** Mutants impaired in JA signaling (*coi1*, *jin1*) were subjected to *B. cinerea* droplet-infection 6 h after fumigation with 10 ppm NO_2 for 1 h (unfumigated as control). Necrotic areas formed after 3 days on fumigated leaves were normalized to the mean necrotic area of the respective unfumigated leaves (= 100 %). Columns represent means of 3 independent experiments ± SEM; n_{leaves} = 126-128 (Col-0), 93-99 (*jin1*, *coi1*). Dashed-lined columns represent respective WT. **C)** Representative pictures of necrotic lesions formed on NO_2-treated and unfumigated leaves of Col-0, *jin1*, and *coi1* 3 days after infection. Scale = 5 mm. ***Statistics:*** Letters indicate significant differences of all pairwise comparisons via Kruskal Wallis Test + Dunn's post-hoc Test ($p < 0.01$). Multifactorial analysis using Two Way ANOVA demonstrated that the observed fumigation-induced effects significantly differed between the examined genotypes ($p = 0.034$).

However, their transcript levels declined to basal levels at 6 h after fumigation. Interestingly, the expression of the defense genes *PDF1.2a* and *PR4* was only induced at the later time point and repressed directly after NO_2 treatment. The transcript levels of *VSP2* and *PR3* remained relatively

unaffected by NO_2 when compared to the air-fumigated control treatment (Figure 18 A). The accurate expression levels of the genes depicted in Figure 18 A can be found in Supplemental Table 6.

Knock-out mutants which were impaired in JA-responsive signaling were examined for their NO_2-induced resistance phenotype using the same experimental set-up as described previously (Figure 18 B). The JA-insensitive *coi1* mutant did not show any significant differences in the size of the necrotic lesions that developed on NO_2 - or non-fumigated leaves upon *B. cinerea* infection. NO_2 fumigation of *jin1* however, resulted in a significant decrease of the lesion size by 22.7 %, which was comparable to the observation made for the Col-0 WT control (Figure 18 B, C). Taken together, the NO_2-induced resistance against *B. cinerea* was evident in Col-0 and *jin1*, but not in *coi1*.

These results indicated that the NO_2-induced resistance against *B. cinerea* is dependent on JA accumulation and COI1- but not JIN1-mediated signaling. Therefore, the up-regulation of genes involved in jasmonate biosynthesis and signaling was suggested to be of biological relevance during the plants response to NO_2.

2.4.3 NO_2–induced resistance in plants impaired in SA biosynthesis and signaling

Since SA biosynthetic genes were up-regulated and SA level transiently increased upon NO_2 fumigation (see section 2.3.2), the role of SA in the NO_2-induced resistance against *B. cinerea* was examined. In order to assess the necessity of SA accumulation during this type of resistance, mutants which were defective in *SID2* and plants expressing the *Pseudomonas putida NahG* gene were utilized. The *sid2* mutant is impaired in the main SA biosynthesis pathway and therefore does not accumulate SA upon pathogen infection [214], [245], whereas *NahG* plants express a bacterial SA hydroxylase which degrades SA to catechol [256], [257].

The NO_2-induced resistance in WT (Col-0) manifested itself in a 22 % reduction of the relative necrotic area. In the case of *sid2* and *NahG* NO_2-pretreatment facilitated a 18.4 % and 14 % reduction in lesion size, respectively (Figure 19, representative pictures of necrotic lesions see Supplemental Figure 6). Therefore, functional *SID2* is not essential for the development of the NO_2-induced resistance, whereas the degradation of SA by *NahG* slightly impeded the establishment of the NO_2-induced resistance phenotype. In addition, the SA-insensitive *npr1* mutant was included in the *B. cinerea* infection assay after NO_2 fumigation. Plants defective in *NPR1* are largely impeded in the SA-induced defense response since they do not express certain *PR* genes which are characteristic and essential SA responses [258]. The expression of *NPR1* and its responsive gene *PR2* was induced directly after NO_2 fumigation (log_2(FC) = 1.13 and 1.4, respectively), followed by a

decline of both transcripts to a log_2(FC) of -0.6 at 6 h after NO_2 treatment. However, the expression of the SA-inducible *PR1* and *PR5* genes was only negligibly altered upon NO_2 fumigation. (see Supplemental Table 5). Interestingly, NO_2-pretreatment of *npr1* did not accomplish the establishment of the NO_2-induced resistance against *B. cinerea* (Figure 19, representative pictures of necrotic lesions see Supplemental Figure 6).

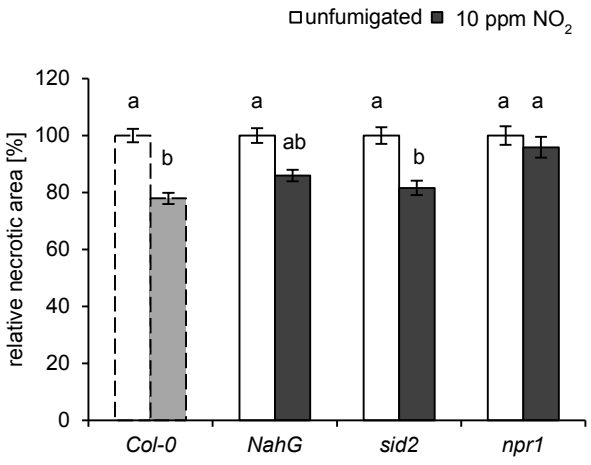

Figure 19: NO_2-induced resistance against *B. cinerea* is dependent on NPR1 but not SA
SA-deficient (NahG, *sid2*) or SA-signaling (*npr1*) mutants were subjected to *B. cinerea* droplet-infection 6 h after fumigation with 10 ppm NO_2 for 1 h (unfumigated as control). Necrotic areas formed on fumigated leaves after 3 days were normalized to the mean necrotic area of the respective unfumigated leaves (= 100 %). Columns represent means of 3 (8 for Col-0, 5 for NahG) independent experiments ± SEM; n_{leaves} = 303-331 (Col-0), 223-244 (NahG), 148-153 (*sid2*), 95-104 (*npr1*). Dashed-lined columns represent respective WT. ***Statistics:*** Letters indicate significant differences of all pairwise comparisons via Kruskal Wallis Test + Dunn's post-hoc Test ($p < 0.01$). Two Way ANOVA showed that the fumigation-induced effects significantly depended on the genotypes ($p = 0.015$).

Taken together, these results suggest that the NO_2-induced resistance against *B. cinerea* is mediated by *NPR1*. However, it did not require SA synthesis via *SID2*, whereas the degradation of SA by bacterial *NahG* partially abolished the NO_2-induced resistance phenotype.

2.5 NO_2-induced plant defense mechanisms leading to the resistance against *B. cinerea*

Plants evolved complex, ornately-orchestrated signaling networks to tailor appropriate responses against pathogens of different lifestyles. The first line of defense commonly includes the reinforcement of the cell wall e.g. via callose and lignin deposition. This fortification aims to impede the penetration of pathogens or their spreading within the plant [189], [233]. Another mechanism affective against a variety of pathogens is the production of antimicrobial secondary metabolites. In Arabidopsis glucosinolates and the phytoalexin camalexin are both well-studied examples of these inducible metabolites that exhibit growth-inhibiting antifungal and antimicrobial properties [199], [202], [259]. Upon pathogen attack, plants also induce the expression of PR genes and defensins which

encode peptides that savage the pathogen itself, such as chitinases (PR3) or glucanases (PR2) [148].

Considering the enormous arsenal of defense mechanisms that an attacked plant has at its disposal, a question arose: which ones may precipitate the NO_2-induced resistance against *B. cinerea.* In order to investigate this issue, various defense mechanisms were analyzed for potential differences in their development when *B. cinerea*-infected plants were pretreated with NO_2. It was hypothesized that NO_2 fumigation may enhance or temporally advance the development of selective defense mechanisms and thereby promoting the plants resistance to the fungus.

2.5.1 Defense gene expression in NO_2-preteated, *B. cinerea* infected plants

As mentioned above, the expression of *PR*- and defensin genes is a major response of pathogen-infected plants. For instance, the increase in transcript levels of the *PR1* gene is considered to be a marker for pathogen-induced SA-signaling, since its expression is induced via NPR1 upon SA accumulation [258], [260], [261]. A marker for JA-inducible defense responses is the enhanced expression of the plant defensin *PDF1.2a*, whose transcripts increase upon fungal infection and external JA application [262], [263]. Hence, the effect of NO_2-pretreatment upon the expression of *PR1* and *PDF1.2a* after *B. cinerea* infection was examined via qPCR. Since the *B. cinerea* mutant screen revealed that jasmonate- and SA-signaling were both necessary for the full development of NO_2-induced resistance (see section 2.4.2 and 2.4.3), pretreatment with NO_2 may affect the *B. cinerea*-induced defense gene expression. Gene transcript levels of both genes were analyzed via qPCR 48 h after *B. cinerea* spray-infection of NO_2-fumigated and non-fumigated Col-0 plants. The obtained transcript levels were normalized to the reference genes *UBC*, *PDF2*, and *ACTIN2* whose transcription did not differ among the treatments.

Collectively, the infection with *B. cinerea* significantly enhanced the expression of *PDF1.2a* in unfumigated and NO_2-treated plants when compared to the grape juice-sprayed control. Here, NO_2 fumigation stimulated a significant 2.9-fold increase of *PDF1.2a* transcripts from 49.8 in unfumigated plants compared to 144.9 after NO_2 fumigation (Figure 20 A). Conclusively, NO_2-pretreatment promoted an enhanced accumulation of *PDF1.2a* upon *B. cinerea* infection which likely contributed to the NO_2-induced resistance phenotype. The expression of *PR1* was also significantly enhanced upon *B. cinerea* infection in both NO_2 - and non-fumigated plants (Figure 20 B). However, NO_2-pretreatment did not influence the accumulation of *PR1* transcripts upon *B. cinerea* infection (Figure

20 B) and therefore is likely not involved in the development of the NO_2-induced resistance phenotype.

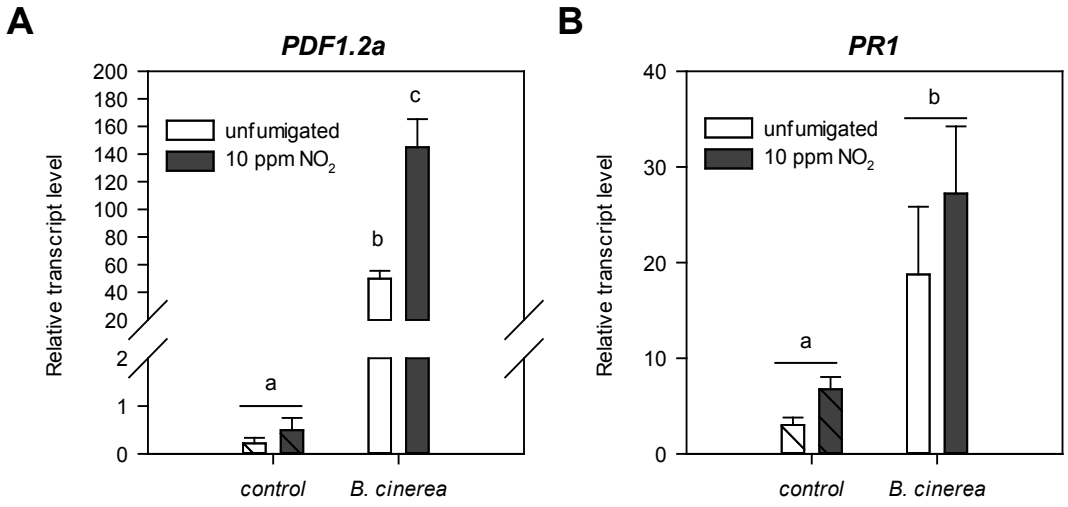

Figure 20: NO_2-treatment enhances *PDF1.2a* but not *PR1* expression upon *B. cinerea* infection
Col-0 plants were fumigated with 10 ppm NO_2 for 1 h (unfumigated as control) followed by spray-infection with 2 x 10^5 *B. cinerea* spores (half-strength grape juice as infection control) 6 h after fumigation. Leaf material was harvested 48 h after infection to determine mRNA transcript levels via qPCR. Transcript levels were normalized to the geometric mean of the reference genes *UBC, PDF2*, and *ACTIN2*. **A)** Relative transcript level of *PDF1.2a*. Columns represent means ± SD; n = 4. **B)** Relative transcript level of *PR1*. Columns represent means ± SD; n = 3-4. **A, B)** Hachured columns distinguish infection controls. ***Statistics:*** Letters indicate significant differences of all pairwise comparisons via Two Way ANOVA + Holm-Sidak post-hoc Test ($p < 0.05$). Two Way ANOVA revealed that control and *B. cinerea* infection differentially affect gene expression in case off both genes ($p < 0.001$) but a significant difference between air and NO_2-induced effects was only detected for *PDF1.2a* ($p = 0.017$).

To investigate whether the NO_2-induced enhancement of *PDF1.2a* expression after *B. cinerea* infection correlated with the observed NO_2-induced resistance, mutants which lacked this phenotype were analyzed for their *PDF1.2*a transcript levels via qPCR (Figure 21).

The WT-like genetic background (*Col-gl*) of the jasmonate-deficient *aos* displayed a significant Col-0-like NO_2-induced enhancement of *PDF1.2a* after *B. cinerea* infection. As expected, *aos* did not exhibit any transcriptional activation of *PDF1.2a,* after either NO_2 fumigation or *B. cinerea* infection (Figure 21 B). The SA-insensitive *npr1* mutant exhibited a significant transcriptional activation of *PDF1.2a* after *B. cinerea* infection but did not display an enhanced transcript accumulation upon NO_2 pretreatment (Figure 21 A). Moreover, the *PDF1.2a* copy numbers did not increase upon NO_2 fumigation in uninfected plants, as was observed in the Col-0 WT. These results demonstrated that NO_2-induced enhancement of *PDF1.2a* transcription upon *B. cinerea* infection may be sufficient to facilitate the NO_2-induced resistance, since mutants lacking this phenotype did not display this enhanced (*npr1*) or any *B. cinerea*-induced *PDF1.2a* expression (*aos*).

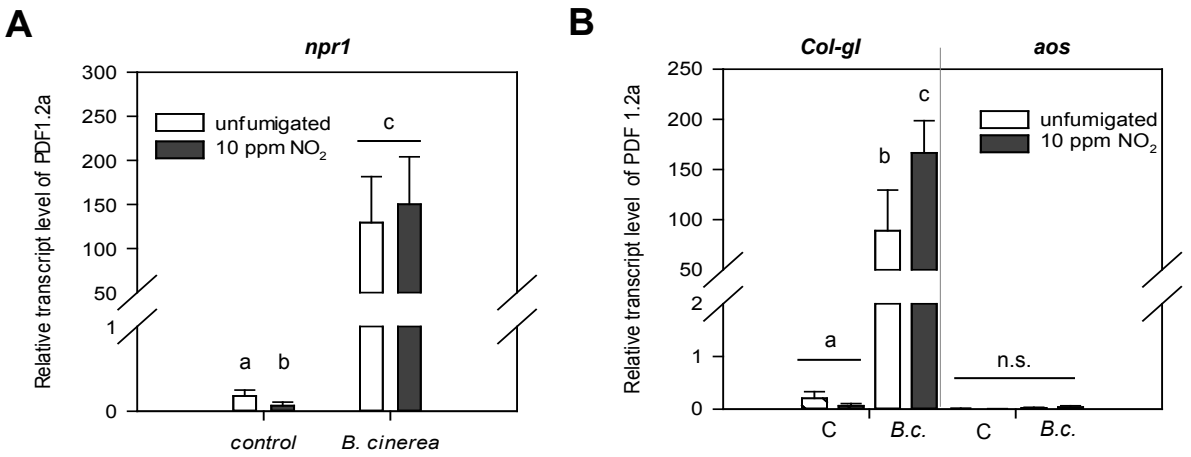

Figure 21: Mutants impeded in the NO_2-induced resistance against *B. cinerea* do not display an enhanced or any *PDF1.2a* expression upon infection
Mutants were fumigated with 10 ppm NO_2 for 1 h (unfumigated as control) followed by spray-infection with 2 x 10^5 *B. cinerea* spores 6 h after fumigation. Leaf material was harvested 48 h after infection to determine *PDF1.2a* transcript levels via qPCR that were normalized to the geometric mean of the reference genes *UBC, PDF2*, and *ACTIN2*. **A)** Relative *PDF1.2a* transcript level in *npr1*. Columns represent means ± SD; n = 4. **B)** Relative *PDF1.2a* transcript level in *aos* and its WT-like *Col-gl* genetic background. Columns represent means ± SD; n = 3-4. **A, B)** Hachured columns distinguish infection controls. C = half-strength grape juice as infection control, *B.c.* = *Botrytis cinerea*. ***Statistics:*** **A, B)** Letters indicate significant differences of all pairwise comparisons within the genotypes via Two Way ANOVA + Holm-Sidak post-hoc Test ($p < 0.01$). **A)** Two Way ANOVA showed that the changes in gene expression depended on the type of infection ($p < 0.001$) but not fumigation. **B)** Two Way ANOVA demonstrated that significant differences in gene expression were dependent on the type of infection ($p < 0.001$) and fumigation ($p = 0.025$) for *Col-gl* but not *aos*. Three Way ANOVA showed that the infection-induced expression changes depended on the genotype ($p < 0.001$). n.s. = not significant.

2.5.2 The influence of NO_2 on camalexin production

As mentioned above, the phytoalexin camalexin is a characteristic secondary metabolite with antimicrobial and antifungal properties whose production is induced in Arabidopsis upon infection with various pathogens including *B. cinerea* [167], [199], [264], [265].

Camalexin is produced from tryptophan, which is converted to indole-3-acetaldoxime (IAOx) via the cytochrome P450 CYP79B2 or its homolog CYP79B3 [266]–[268]. This reaction is tightly controlled by the transcription factors MYB34, MYB51, and MYB122 [269]. IAOx is further dehydrated to indole-3-acetonitrile (IAN) by CYP71A12 and CYP71A13 [270]. During camalexin biosynthesis glutathione S-transferases, including GSTF6, conjugate glutathione (GSH) to IAN [206], [271]–[273] that is further formed to a cysteine conjugate (Cys-IAN) with the aid of gamma-glutamyl-peptidases 1 and 3 (GGP1/3) [274]. This compound is the substrate for the Cytochrome P450 CYP71B15/PAD3 which ultimately catalyzes its reaction to camalexin [210], [272], [275]. An important regulator of camalexin synthesis is the transcription factor WRKY33 that binds to the promoters of PAD3 and CYP71A13 and thereby promotes their transcription at an early stage of infection [276].

The camalexin synthesis pathway is outlined in Figure 22 A. Here, the expression profiles of the biosynthetic genes obtained during the microarray directly (0 h) and 6 h after NO_2 fumigation were indicated by the colored panels underlying the respective genes. The gene expression profile indicated that NO_2 treatment may activate camalexin synthesis by rapidly enhancing the expression of the required genes. The expression of the transcriptional regulators *MYB122*, *MYB51*, and *WRKY33* were highly induced immediately after NO_2 fumigation, which likely contributed to the significant increase in the biosynthetic gene transcripts such as *CYP79B2*, *CYP71A13*, and *PAD3* (for exact log_2(FC) values see Supplemental Table 7). According to Frerigmann *et al*. (2015) the up-regulation of these genes is essential for camalexin synthesis [269]. The hypothesis of a NO_2-induced camalexin synthesis was further substantiated by the GO-Term enrichment analysis that was described earlier (see 2.2.2). Here, camalexin synthesis was ranked as the most enriched GO-Term with a fold enrichment value of 8.88 (Supplemental Table 1).

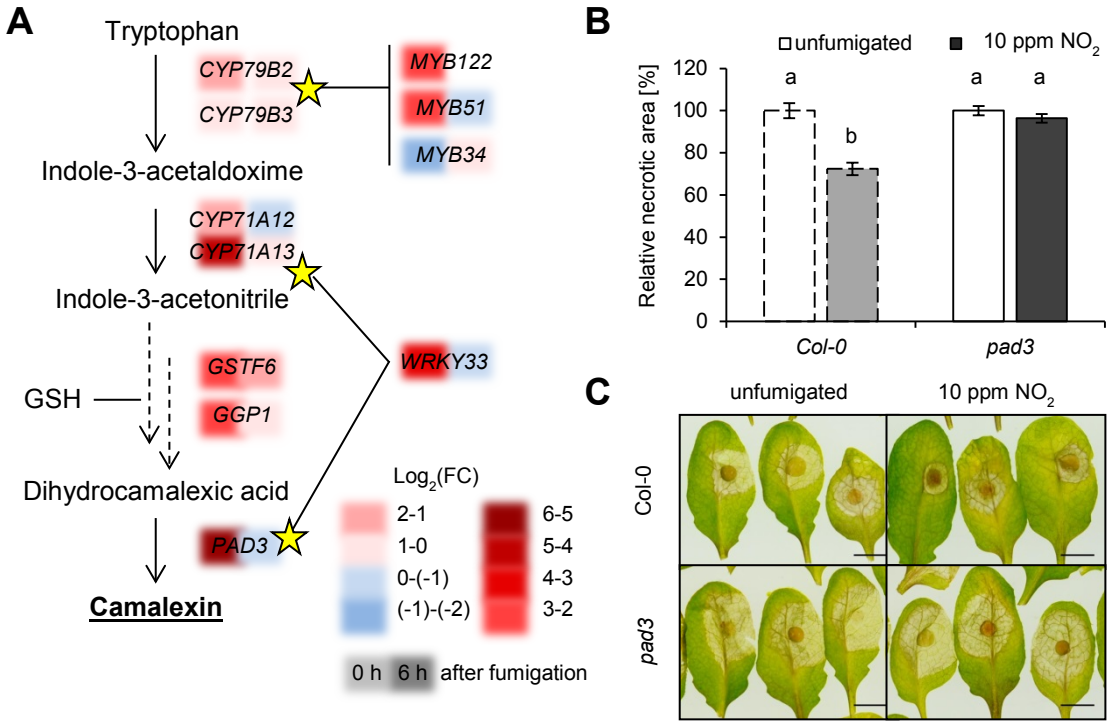

Figure 22: Camalexin-deficient *pad3* does not display NO_2-induced resistance against *B. cinerea*
A) Schematic pathway of camalexin synthesis illustrating the expression levels (log_2(FC)) of the respective genes obtained from the microarray directly (0 h) or 6 h after fumigation with 10 ppm NO_2. Colored panels depict log_2(FC) of the genes compared to air fumigated control, left = 0 h, right = 6 h after fumigation. Stars indicate gene activation. **B)** Camalexin-deficient *pad3* mutants were subjected to *B. cinerea* droplet-infection 6 h after fumigation with 10 ppm NO_2 for 1 h (unfumigated as control). Necrotic areas formed on fumigated leaves after 3 days were normalized to the mean necrotic area of the respective unfumigated leaves (= 100 %). Columns represent means of 3 independent experiments ± SEM; n_{leaves} = 83-93. Dashed-lined columns represent respective WT. **C)** Representative pictures of necrotic lesions formed on NO_2-treated and unfumigated leaves of Col-0 and *pad3 3* days after infection. Scale = 5 mm. GSH = glutathione. ***Statistics:*** Letters indicate significant differences of all pairwise comparisons via Kruskal Wallis Test + Dunn's post-hoc Test ($p < 0.01$). Two Way ANOVA showed that the effect of fumigation is dependent on the genotypes ($p < 0.001$).

It was reported that plants which were deficient in camalexin, such as the *pad3* mutant, displayed enhanced susceptibility towards pathogens like *B. cinerea* [167]. This was confirmed during this work by comparing the necrotic lesion size which developed on unfumigated Col-0 and *pad3* plants (Supplemental Figure 10). To investigate whether camalexin may be involved in the NO_2-induced resistance, the *pad3* mutant was subjected to the *B. cinerea* infection assay after NO_2 fumigation (Figure 22 B, C). Three days after infection the necrotic lesions on NO_2-pretreated *pad3* did not significantly differ in size when compared to the unfumigated control. However, the NO_2-induced resistance was fully developed in Col-0 WT, where the necrotic lesion size was significantly reduced by 27.6 % upon NO_2 pretreatment (Figure 22 B, C). The abolishment of the NO_2-induced resistance phenotype in *pad3* led to the conclusion that the induction of *PAD3* transcription contributed to the NO_2-induced resistance against *B. cinerea*.

Surprisingly, NO_2 fumigation did not alter *PAD3* expression upon *B. cinerea* infection (Figure 23 A). qPCR analysis 16 and 24 h after infection demonstrated that *PAD3* transcript levels significantly increased to the same extend upon *B. cinerea* infection in unfumigated and NO_2-treated Col-0 plants (Figure 23 A). Multi-factorial statistical analysis via Three Way ANOVA further confirmed that the significant differences in expression levels depended on the time ($p < 0.001$) and the type of infection ($p < 0.001$) but not on the type fumigation.

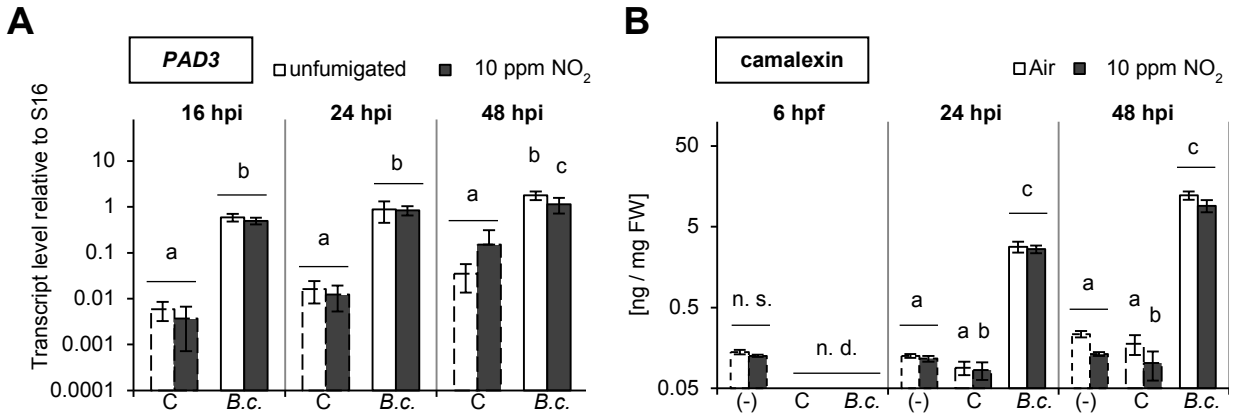

Figure 23: NO_2-treatment does not alter *PAD3* and camalexin level upon *B. cinerea* infection
Col-0 plants were fumigated with 10 ppm NO_2 for 1 h (unfumigated or air as control) followed by spray-infection with 2 x 10^5 *B. cinerea* spores 6 h after fumigation. Leaf material was harvested immediately before (6 hpf) or 16, 24, and 48 h after infection (hpi). **A)** Quantification of *PAD3* transcript levels relative to S16 expression via qPCR. Columns represent means of 2 independent experiments ± SD; n = 5. **B)** Camalexin levels were measured via reverse-phase HPLC 6, 24, and 48 h after fumigation or 24 and 48 h after infection of fumigated plants. Columns represent means of 2 independent experiments (one for uninfected samples) ± SEM; n = 6-12. **A, B)** Dashed-lined columns distinguish infection controls. C = half-strength grape juice as infection control, *B.c.* = *Botrytis cinerea*, (-) = uninfected NO_2- or air-fumigated plants, n. d. = not determined, hpf = hours post fumigation, hpi = hours post infection. ***Statistics:*** **A)** Letters indicate significant differences of all pairwise comparisons within the time points via Two Way ANOVA + Holm-Sidak post-hoc Test (16, 24 hpi: $p < 0.001$, 48 hpi: $p < 0.01$). **B)** Letters indicate significant differences of all pairwise comparisons within the time points via Two Way ANOVA + Holm-Sidak post-hoc Test ($p < 0.05$).**A, B)** Multifactorial analysis via Three Way ANOVA showed that significant differences in *PAD3* expression or camalexin levels depended on the time ($p < 0.001$) and type of infection ($p < 0.001$) but not the type of fumigation. n. s. = not significant.

The quantification of camalexin via HPLC at various time points after NO_2 fumigation did not reveal a NO_2-induced accumulation of this secondary metabolite (Figure 23 B, labelled with (-)). This demonstrated that the enhanced expression of biosynthetic genes in NO_2-fumigated plants was not sufficient to induce camalexin production. The analysis of the camalexin content revealed that *B. cinerea* infection led to a significant gradual increase from basal 0.1 ng/mg FW, over 2.8 and 2.6 ng/mg FW at 24 h, to 12.2 and 9.1 ng/mg FW after 48 h in air-fumigated and NO_2-treated plants, respectively. However, no statistical differences in the camalexin content after *B. cinerea* infection of air- and NO_2-treated Col-0 plants were detected (Figure 23 B). In line with this, multifactorial analysis via Three Way ANOVA revealed that significant differences in camalexin levels only depended on the time ($p < 0.001$) and the type of infection ($p< 0.001$) but not on the type of fumigation.

Taken together, these results indicated that although NO_2 fumigation rapidly induced the expression of biosynthetic genes, NO_2 treatment was not sufficient to activate camalexin production after fumigation and did not enhance camalexin levels upon *B. cinerea* infection. However, plants impaired in camalexin accumulation due to a non-functional key biosynthetic enzyme (PAD3), did not exhibit the NO_2-induced resistance against this pathogen. Conclusively, functional PAD3 but not camalexin was crucial for the NO_2-induced resistance phenotype.

2.5.3 The effect of NO_2 on callose deposition after *B. cinerea* infection

Another effective defense mechanism utilized by plants against various pathogens and wounding is the deposition of the (1,3)-β-glucan polymer callose [185] which can occur in papillae between the plasma membrane and the cell wall at infection sites [186], [187]. The induction of callose biosynthesis is a complex process where the involvement of ROS, SA, or indole glucosinolates (IGs) have all been reported [192], [194]. Since the activation of these pathways was evident in the microarray data after fumigation, the influence of a potential early or enhanced callose deposition during the NO_2-induced resistance was examined.

The *pmr4* mutant is defective in the callose synthase gene *GSL5* and therefore does not deposit callose upon pathogen infection [190], [277]. This mutant was subjected to the *B. cinerea* infection assay after NO_2 fumigation (Figure 24 A). The necrotic lesions that developed on NO_2-treated *pmr4* did not significantly differ in size from its unfumigated control, whereas the Col-0 WT exhibited a significant 23.7 % reduction of the necrotic area when pretreated with NO_2 under the same conditions. Hence, the callose-deficient *pmr4* mutant did not display the NO_2-induced resistance phenotype.

In an independent experimental set-up, 2-deoxy-D-glucose (2-DDG) was applied to Col-0 in order to inhibit callose deposition. 2-DDG is commonly utilized as a potent callose inhibitor, although its mode of action has yet to be clarified in detail [278]–[281]. It presumably affects the biosynthesis of lipid-linked oligosaccharides and subsequently inhibits protein glycosylation [281], [282]. Here, leaves were infiltrated with the inhibitor or H_2O 24 h before NO_2-treatment, followed by *B. cinerea* droplet-infection 6 h after fumigation. As a reference, non-infiltrated Col-0 plants were identically treated. In all treatments, the *B. cinerea*-induced necrotic lesions were normalized to the average necrotic area which developed on unfumigated, non-infiltrated leaves. Regardless of the executed treatment, all unfumigated leaves developed lesions of similar size without any significant variations. This demonstrated that neither the infiltration process nor 2-DDG or H_2O affected the plants basal defense response or fungal growth (Figure 24 B). H_2O-infiltrated and non-infiltrated plants both developed a pronounced NO_2-induced resistance against *B. cinerea* which was successfully suppressed by 2-DDG treatment (Figure 24 B).

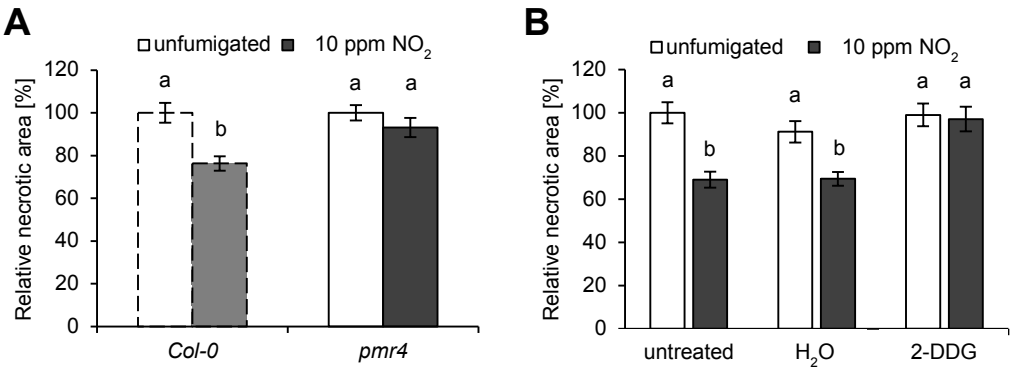

Figure 24: Impaired callose formation impedes the NO_2-induced resistance against *B. cinerea*
A) Relative necrotic area of NO_2-treated, callose-deficient *pmr4* mutants (Col-0 as WT control). Col-0 and *pmr4* plants were subjected to *B. cinerea* droplet-infection 6 h after fumigation with 10 ppm NO_2 for 1 h (unfumigated as control). Necrotic areas formed after 3 days on fumigated leaves were normalized to the mean necrotic area of the respective unfumigated leaves (= 100 %). Columns represent means of 4 independent experiments ± SEM; n_{leaves} = 134-145. Dashed-lined columns represent WT. **B)** Relative necrotic area determined on Col-0 plants that were infiltrated with 1.2 mM of the callose-synthesis inhibitor 2-DDG (H_2O as control) 24 h before fumigation, followed by *B. cinerea* droplet-infection. Columns represent means of 2 independent experiments ± SEM; n = 70-76 (untreated), 105-120 (H_2O), 123-130 (2-DDG). 2-DDG = 2-deoxy-D-glucose. ***Statistics:*** **A)** Letters indicate significant differences of all pairwise comparisons via Kruskal Wallis Test + Dunn's post-hoc Test ($p < 0.05$). Two Way ANOVA showed that the effect of fumigation is dependent on the genotype ($p < 0.001$). **B)** Letters indicate significant differences of all pairwise comparisons via Kruskal Wallis Test + Dunn's post-hoc Test ($p < 0.05$). Two Way ANOVA showed that the fumigation-induced effects were significantly dependent on the treatments ($p = 0.014$).

The inhibition of the NO_2-induced resistance in Col-0 after treatment with the callose inhibitor 2-DDG correlated with the observations made for the callose-deficient *pmr4* mutant described above. Therefore, these results implied that NO_2 induced callose deposition ultimately led to NO_2-induced resistance.

2.5.4 Callose quantification in chitosan-elicited plants after NO_2-fumigation

Since the previous results indicated that callose deposition plays a role in the NO_2-induced resistance, changes in the abundance of callose after NO_2 fumigation were quantified. However, preliminary experiments showed that the autofluorescence of *B. cinerea* interfered with the detection method of callose via Aniline Blue. As a mitigation, plants were treated with chitosan, a deacetylated form of chitin and a known component of the fungal cell wall [283]. Chitosan is a potent elicitor of responses similar to those observed during fungal infection, such as camalexin production, lignification, the induction of a JA response, and callose deposition [192], [284]–[286]. Therefore, chitosan infiltration was ideal to induce a response similar to a fungal infection without impeding callose detection. Aniline Blue fluorescence in leaf discs was determined 4, 16, and 24 h after NO_2-treated Col-0 and *pmr4* plants were infiltrated with 500 µg/ml chitosan (Figure 25).

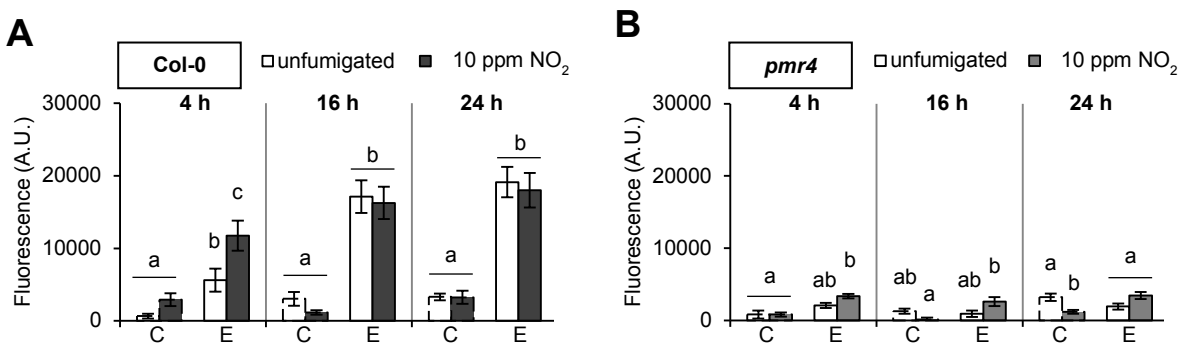

Figure 25: NO_2-treatment enhances callose deposition upon treatment with the elicitor chitosan
Plants were fumigated with 10 ppm NO_2 for 1 h (unfumigated as control) and infiltrated with 500 µg/ml chitosan (0.04 % acetic acid as control) 4 h after fumigation. Leaf discs were obtained for callose quantification with Aniline Blue 4, 16, and 24 h after chitosan treatment. **A)** Callose quantification in Col-0. **B)** Callose quantification in *pmr4*. **A, B)** Columns represent means ± SEM; n_{leaves} = 34-44 (Col-0), 27-35 (*pmr4*) from 10 plants per time point and treatment. Dashed-lined columns represent 0.04 % acetic acid as infiltration control. C = infiltration control, E = Elicitor chitosan treatment, A.U. = arbitrary unit. ***Statistics:*** **A, B)** Letters indicate significant differences of all pairwise comparisons within the genotypes and time points via Kruskal Wallis Test + Dunn's post-hoc Test ($p < 0.05$). Three Way ANOVA (genotype *vs*. fumigation *vs*. treatment) showed that at 4 h after elicitation, callose deposition significantly differed among Col-0 and *pmr4* ($p < 0.001$), the treatments ($p < 0.001$), and the fumigations ($p = 0.013$). At 16 and 24 h the differences in callose were only significant among the genotypes and treatments ($p < 0.001$). **A)** Two Way ANOVA showed that chitosan-induced callose deposition significantly differed from the control treatment ($p < 0.001$) at all time points. Fumigation-induced differences in callose were only detected 4h after treatment ($p < 0.004$). **B)** Two Way ANOVA within the time points showed no significant effect of fumigation on callose deposition. Chitosan significantly influenced callose deposition 4 h ($p < 0.001$) and 16 h ($p = 0.007$) after treatment

As anticipated, chitosan elicitation (E) of Col-0 triggered a significant ($p < 0.001$) gradual increase in Aniline Blue fluorescence in both NO_2- and unfumigated leaves as revealed by Two Way ANOVA when compared to the unelicited control (Figure 25 A). The slight increase in fluorescence intensity in the callose-deficient *pmr4* mutant was negligible when compared to WT and therefore confirmed the

specificity of Aniline Blue for callose (Figure 25 B). Although Two Way ANOVA analysis of these results revealed that chitosan significantly influenced the fluorescence intensity in *pmr4* after 4 h ($p < 0.001$) and 16 h ($p = 0.007$), no meaningful differences were detected between NO_2-treated and unfumigated *pmr4* plants (Figure 25 B). Notably, 4 h after elicitation, the fluorescence intensity in NO_2-treated Col-0 plants was significantly higher than in its unfumigated counterpart (Figure 25 A). Multifactorial analysis via Two Way ANOVA confirmed that fumigation-induced differences in the fluorescence intensity were detected 4h after treatment ($p < 0.004$). The enhanced fluorescence intensity in NO_2-fumigated Col-0 was compensated at later time points after elicitation (16 and 24 h).

Confocal microscopy of Aniline Blue-stained leaf discs revealed that the callose deposition occurred in the extracellular space or in the cell wall, which became apparent when the UV and bright field channels were merged (Figure 26 bottom). Confocal microscopy further visualized the aforementioned measurements and attested that the fluorescence was more intense in NO_2-treated Col-0 plants at 4 h after chitosan elicitation (Figure 26 A). The previously-mentioned compensation of the fluorescence intensities in NO_2-treated and unfumigated Col-0 leaf discs starting 16 h after elicitation was also detectable via confocal microscopy (Supplemental Figure 8 A). In addition, microscopy revealed that fumigation with NO_2 alone caused a slight increase in callose fluorescence (Figure 26 A).

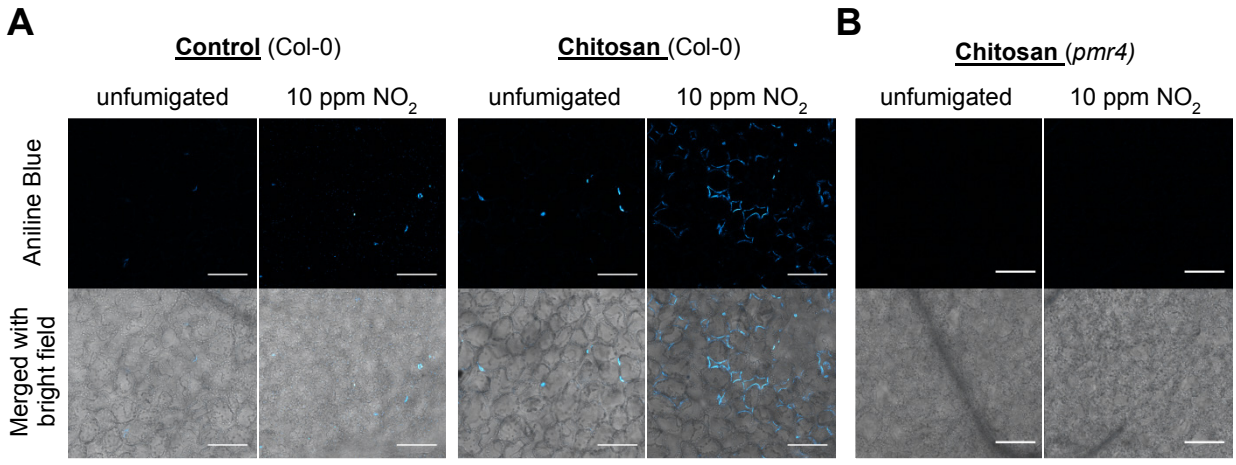

Figure 26: NO_2-induced enhancement of callose upon chitosan elicitation
Plants were fumigated with 10 ppm NO_2 for 1 h (unfumigated as control) and infiltrated with 500 µg/ml chitosan (0.04 % acetic acid as control) 4 h after fumigation. Leaf discs were obtained 4 h after chitosan treatment and stained with Aniline Blue. Fluorescence was detected with the TCS SP8 X confocal laser scanning microscope (Leica). Excitation was done with a Diode Laser UV 405 nm (0.1 % intensity), Emission was set from 480 – 500 nm. Bright field pictures were taken using the Transmission PMT. Channels were merged using the ImageJ software. Representative pictures of the Aniline Blue fluorescence (blue) were taken of NO_2-fumigated or unfumigated **A)** Col-0 leaf discs 4 h after treatment with chitosan or control and **B)** of *pmr4* leaf discs 4 h after treatment with chitosan. **A, B)** 3 different areas of 3 independent leaf discs were examined with similar results. Scale = 100 µm.

The visual detection of Aniline Blue-stained callose was done by exciting the samples with a 405 nm (UV) Diode Laser at 0.1 % laser intensity. When using the same laser intensity for leaf discs obtained from the callose-deficient *pmr4* mutant, Aniline Blue fluorescence was detectable neither 4 h or 16 h after elicitation (Figure 26 B, Supplemental Figure 8 B) which confirmed the dyes' specificity to callose.

Taken together, the Aniline Blue-mediated detection of callose demonstrated that NO_2-pretreated plants deposited more callose at an early stage after treatment with a fungal elicitor than unfumigated plants. This further supported the previously-stated hypothesis that callose deposition is of importance during the NO_2-induced resistance against *B. cinerea*.

To investigate whether this early enhancement of callose deposition is a key defense mechanism that drives the NO_2-induced resistance, mutant analyses were conducted. NO_2-pretreated mutants which were previously identified to not develop the NO_2-induced resistance were evaluated for their callose content 4 h after chitosan elicitation. The selected mutants were impaired in SA-synthesis (*sid2*) and –signaling (*npr1*), jasmonate-signaling (*coi1*), camalexin synthesis (*pad3*), and callose deposition (*pmr4*). Except for *sid2,* all selected mutants were impaired in NO_2-induced resistance development.

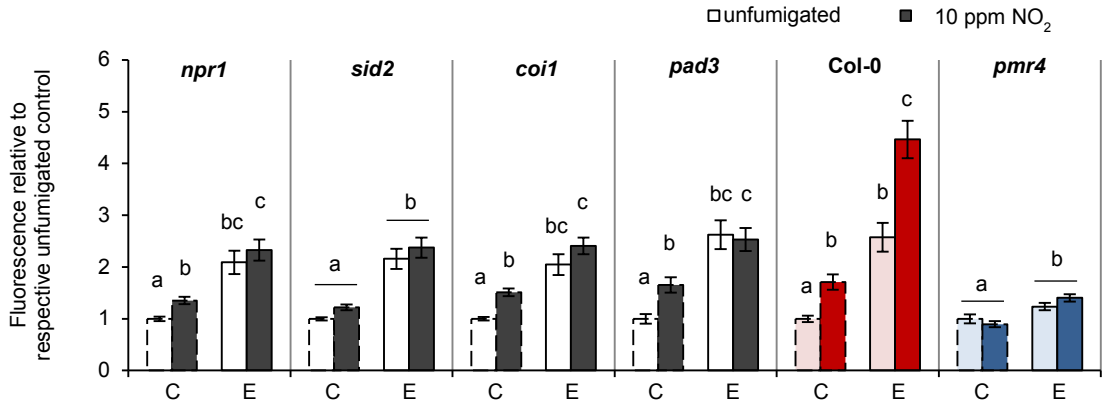

Figure 27: Callose quantification of NO_2-pretreated mutants after chitosan elicitation
Mutants impaired in SA-synthesis (*sid2*) and -signaling (*npr1*), JA-signaling (*coi1*), camalexin synthesis (*pad3*), and callose deposition (*pmr4*) were fumigated with 10 ppm NO_2 for 1 h (unfumigated as control) and infiltrated with 500 µg/ml chitosan (0.04 % acetic acid as control) 4 h after fumigation. Leaf discs were obtained for callose quantification with Aniline Blue 4 h after chitosan treatment. Measured Aniline Blue fluorescence was normalized to the respective unfumigated controls. Columns represent means ± SEM from 3 (4 for Col-0 and *pmr4*) independent experiments; n_{leaves} = 138-159 (Col-0), 103-119 (*pmr4*) from 40 plants per treatment, n_{leaves} = 57-65 for the remaining mutants from 16-23 plants per treatment. red = Col-0 positive control (lightly colored = unfumigated, intensely colored = NO_2-treated), blue = *pmr4* negative control (lightly colored = unfumigated, intensely colored = NO_2-treated). Dashed-lined columns represent 0.04 % acetic acid as infiltration control. C = infiltration control, E = Elicitor chitosan treatment, A.U. = arbitrary unit. ***Statistics:*** Letters indicate significant differences of all pairwise comparisons within the genotypes via Kruskal Wallis Test + Dunn's post-hoc Test ($p < 0.05$).

As expected, a significant increase in callose-specific fluorescence intensity after chitosan elicitation was detected in NO_2-fumigated Col-0 plants while *pmr4* showed only a negligible enhancement in fluorescence upon elicitation without any differences between NO_2-treated and unfumigated plants (Figure 27, red and blue, respectively). The callose-specific fluorescence of all other mutants tested was intensified upon chitosan elicitation to a similar extent as was observed in unfumigated Col-0. However, none of the elicited mutants tested exhibited the NO_2-induced enhancement in fluorescence intensity (Figure 27). Here, the fluorescence signals were indistinguishable from those detected in the unfumigated controls. Hence the NO_2-induced early enhancement of callose upon chitosan elicitation only occurred in Col-0 WT plants. Since most of the mutants tested did not develop a NO_2-induced resistance, it was assumed that the NO_2-induced early enhancement of callose may be a crucial factor for the development of this phenotype. However, *sid2* was able to develop a similar NO_2-induced resistance phenotype as observed in Col-0 (see 2.4.3), but no early enhancement of callose was detected after fumigation. Hence, additional defense mechanisms are likely to be involved in the propagation of the NO_2-induced resistance.

Another observation made during this experiment was that, with the exception of *sid2* and *pmr4,* NO_2 pretreatment caused significant increases in the fluorescence intensity of non-elicited mutants. This correlated with observations made during confocal microscopy of Col-0 and *pmr4* (Figure 26). However, these observations were not consistent throughout all experiments (see Figure 25 A), likely due to limitations in the sensitivity of the photometric assay. Nonetheless, it can be assumed that NO_2 treatment alone was capable of inducing callose deposition.

2.6 NO_2-induced resistance against *Pseudomonas syringae* DC3000

Up to this point, the obtained results indicate that the NO_2-induced response included the activation of jasmonate- and SA-mediated signaling which led to defense-related expression of genes such as *PDF1.2a*, as well as genes involved in camalexin biosynthesis. Furthermore, NO_2 temporally advanced the deposition of callose upon pathogen infection, ultimately leading to resistance against *B. cinerea*. However, these responses are not limited to the defense against necrotrophic fungi. Particularly defenses induced via the SA-mediated signaling pathway are commonly considered to be the most effective against biotrophic pathogens [98], [139], [287]. For instance, the bacterial elicitor flagellin 22 (flg22) which triggers SA accumulation is a potent inducer of callose deposition [287]–[289]. Therefore, it was investigated whether NO_2 pretreatment may also provide resistance

against the hemi-biotrophic bacterium *Pseudomonas syringae* pv. *tomato* DC3000 (*Pst.* DC3000). 5-week-old Col-0 plants were fumigated with NO_2, followed by syringe infiltration with $1x10^5$ cfu/ml *Pst.* DC3000 4 h after fumigation. The bacterial titer in the infected leaves were determined 2 h after infection in order to ensure that NO_2- and unfumigated leaves were exposed to the same initial bacterial concentration. The bacterial titer was further evaluated 1 and 2 days after infection in order to determine if NO_2 pretreatment influenced bacterial growth.

As shown in Figure 28, infected leaves which were pretreated with 10 ppm NO_2 harbored fewer bacteria than their unfumigated counterpart. The mean colony forming unit per ml (cfu/ml) in unfumigated leaves was 1.5- and 2.8-fold higher than in NO_2-treated plants, one and two days after infection (dpi), respectively. This was indicative of a $\log_{10}$ (cfu/ml) at 2 dpi of 5.3 in the control and 4.8 in NO_2-treated samples. Multifactorial statistical analysis via Two Way ANOVA revealed that the changes in the bacterial titer over time was significantly influenced by the pretreatment with NO_2 ($p = 0.008$). This observation was similar to that reported by Cao *et al*. (2014), who reported that treatment of Arabidopsis with chitin oligomers triggered a resistance against *Pst.* DC3000 which was dependent on the PAMP-recognition receptors CERK1 and LYK5 [109]. Therefore, it can be concluded that NO_2-induced signaling provided a PTI-like resistance against the hemi-biotrophic bacterium *Pst*. DC3000.

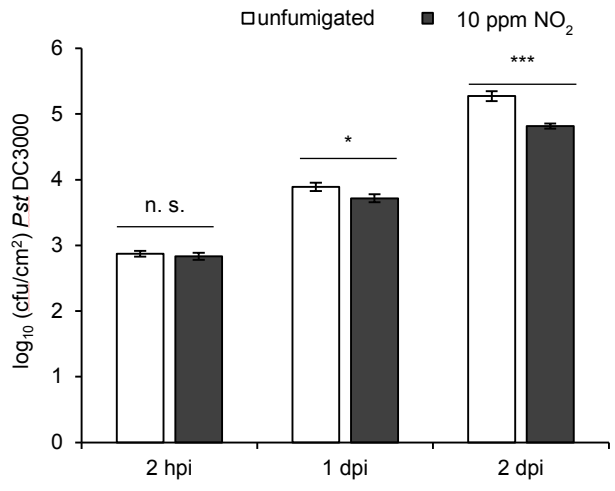

Figure 28: NO_2 provides resistance against *Pst.* DC3000
Col-0 plants were fumigated with 10 ppm NO_2 for 1 h (unfumigated as control) and infiltrated with $1x10^5$ cfu/ml *Pst.* DC3000 4 h after fumigation. Leaf discs of infected leaves were obtained 2 hours, and 1 and 2 days after infection to determine the bacterial titer (cfu/cm^2 leaf material). Columns represent means ± SEM from 7 independent experiments; n = 26-27 (2 hpi), 72 (1 dpi), 66 (2 dpi). One biological replicate consisted of 3 leaves from 3 different plants. hpi = hours post infection, dpi = days post infection, cfu = colony forming units. ***Statistics:*** Asterisks indicate significant differences of all pairwise comparisons via Two Way ANOVA + Holm-Sidak post-hoc Test (*$p < 0.05$, ***$p < 0.001$). The bacterial titer significantly changed over time ($p < 0.001$), which was influenced by the type of fumigation ($p = 0.008$), n. s. = not significant.

2.6.1 Callose quantification in *Pst.* DC3000-infected Col-0 plants after NO_2-fumigation

As mentioned earlier, bacterial elicitors such as the flg22 epitope are capable of inducing callose deposition [288]. Since the NO_2-induced resistance against *B. cinerea* was at least partially ascribed to an early enhanced induction of callose deposition in response to the fungal elicitation (see 2.5.3), it was investigated whether the same can be assumed for the NO_2-induced resistance against *Pst.* DC3000. Hence, NO_2-fumigated Col-0 and callose-deficient *pmr4* leaves were subjected to the callose-quantifying Aniline Blue staining 4 h after *Pst.* DC3000 infection.

As anticipated, neither *Pst.* DC3000 infection nor NO_2-fumigation of the callose-deficient *pmr4* led to changes in Aniline Blue fluorescence intensity, which confirmed the specificity of the callose detection method (Figure 29, right). In unfumigated Col-0, *Pst.* DC3000 infection did not lead to a significant increase of the fluorescence signal at the examined time point. However, NO_2 pretreatment caused a significant increase in the fluorescence intensity of infected leaves, which was indicative of an NO_2-stimulated induction of callose deposition (Figure 29, left). A significant NO_2-induced increase in fluorescence intensity was also observed in MOCK treated samples when compared to the unfumigated control treatment. Moreover, Two Way ANOVA within the genotypes confirmed that callose deposition in Col-0 significantly changed after *Pst.* DC3000 infection ($p = 0.004$) and fumigation ($p < 0.001$).

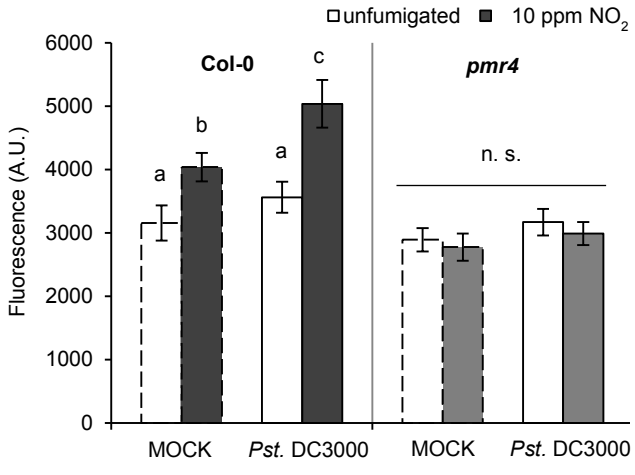

Figure 29: NO_2-treatment enhances callose deposition upon *Pst.* DC3000 infection
Col-0 and callose-impaired *pmr4* plants were fumigated with 10 ppm NO_2 for 1 h (unfumigated as control) and infiltrated with $1x10^5$ cfu/ml *Pst.* DC3000 (MOCK as control) 4 h after fumigation. Leaf discs were obtained for callose quantification with Aniline Blue 4 h after infection. Columns represent means ± SEM from 2 independent experiments; n_{leaves} = 46-52 from 15 plants per treatment. Dashed-lined columns distinguish infection controls. MOCK = 10 mM $MgCl_2$. ***Statistics:*** Letters indicate significant differences of all pairwise comparisons within the genotypes via Two Way ANOVA + Holm Sidak post-hoc Test ($p < 0.05$). Three Way ANOVA (genotype *vs.* fumigation *vs.* treatment) showed that callose depositions significantly varied between the genotypes ($p < 0.001$), n. s. = not significant

Taken in conjunction, these results demonstrated that NO_2 induced an early induction of callose deposition upon infection with *Pst.* DC3000, similar to the observations made after treatment with a fungal elicitor. Hence, the early enhanced induction of callose may play a crucial role in conveying the NO_2-induced resistance against the hemi-biotrophic bacterium *Pst.* DC3000.

3 Discussion

3.1 The characterization of the NO_2-induced cell death

For more than half a century, devastating effects of NO_2 on plants were described and attempted to characterize. Here, the majority of studies postulated that increasing NO_2^- in the leaves causes the NO_2-induced cell death, as it was hypothesized that the metabolization of NO_2^- consumes important cofactors such as NADP/NADPH. Consequently, the availability of these cofactors is limited during photosynthetic processes, which leads to a documented reduction in photosynthesis and subsequent promotion of ROS generation, ultimately culminating in oxidative stress [42]–[44]. This hypothesis agrees with the fact that ROS are crucial for the onset of HR-PCD during pathogen infection [173], [176], [290]. Hence it was assumed that NO_2-induced cell death may resemble an HR-like PCD. However, ROS are not the only players involved in the onset of HR-PCD instead acting synergistically with NO, since neither ROS nor NO alone are able to initiate an advanced HR-PCD [177]. This interplay demonstrates that the onset of programmed cell death is a multifaceted, tightly regulated process. By investigating HR-PCD characteristic features, the presented work aimed to strengthen the hypothesis that the observed NO_2-induced cell death bears resemblance to an HR-like PCD to further broaden the knowledge of the onset of the NO_2-induced cell death.

3.1.1 Nitrite accumulation initiates the NO_2-induced cell death

An experimental set-up was established where four-week-old Arabidopsis Col-0 plants were fumigated with increasing concentrations of NO_2 for 1 h. Under these controlled conditions, highly reproducible effects of NO_2 were produced. After entering the leaf through the stomata [39], NO_2 caused cell death which positively correlated with the applied concentration, as demonstrated by electrolyte leakage and trypan blue staining (Figure 5). Exposure to 10 ppm NO_2 did not cause any detectable damage to the plant, whereas 20 ppm evoked severe lesion formation and fumigation with 30 ppm NO_2 resulted in complete leaf collapse that already occurred within the hour of fumigation.

Evaluation of the disproportionation products of NO_2 within leaf tissue directly after fumigation confirmed previous reports that NO_2 exposure causes an increase in NO_2^- (Figure 6 A). Even though NO_2 equally disproportionates in the leaf to NO_2^- and NO_3^-, no significant changes in NO_3^- accumulation were detected after NO_2 exposure (Figure 6 B). Previously, similar observations had

been made by Zeevaart (1976) in pea plants fumigated with up to 20 ppm NO_2 for 15 min [4] or when loading Arabidopsis leaves with NO_2^- by infiltrating $NaNO_2$ (Supplemental Figure 1 A). Zeevaart demonstrated in an earlier study that NO_2 fumigation led to a considerable induction of nitrate reductase (NR) activity [291], which suggests that the NO_2-induced NR activity quickly converts NO_3^- to NO_2^-, and further contributes to the dramatic increase of NO_2^- [4], [291]. Studies with pathogen infected tomato plants have also reported elevated NO_2^- levels. Here, the increase in NO_2^- was attributed to elevated NR activity that provided an excess amount of NO_2^- which was subsequently reduced to NO in order to facilitate the imminent defense response [292]. Moreover, massive accumulation of NO_2^- further indicates that the nitrite reductase (NiR), which converts NO_2^- to ammonia, is the rate-limiting enzyme during the metabolization of NO_2.

In the present work, the increase in NO_2^- positively correlated with the NO_2 concentrations the plants were exposed to, peaking at a 2100-fold increase after fumigation with 30 ppm NO_2. Interestingly, NO_2^- levels also rose up to 110-fold in plants fumigated with 10 ppm NO_2, which did not cause any visible damage (Figure 6 A, Figure 5 A). Therefore, it can be concluded that NO_2^- accumulation does not necessarily entail cell death. Similar observations were made when infiltrating leaves with 10 mM $NaNO_2$, which elevated the NO_2^- content within the tissue by a factor of 4.6 but did not result in leaf damage (Figure 9 A and Figure 8). In this experimental set-up, leaf damage was only visible after infiltrating 100 mM $NaNO_2$ which was equivalent to a 1300-fold increase in NO_2^-. These experiments demonstrated that plants can countervail rapid changes in their cellular chemistry up to a certain threshold that is likely defined by subsequent accumulation of the cell death signals ROS and/or NO.

3.1.2 Accumulation of ROS is essential for the execution of the NO_2-induced cell death

In the case of unintended ROS production, plants employ a well-tuned antioxidant defense system. This includes enzymes such as catalase (CAT), superoxide dismutase (SOD), and peroxidases (POD) which detoxify ROS with the aid of the antioxidant redox-couples ascorbate (AsA) - dehydroascorbate (DHA) and glutathione (GSH) - glutathione disulfide (GSSG). Under non- or low stress conditions the enzymatic oxidation and reduction of these antioxidants prevents ROS accumulation and avoids oxidative damage [293], [294]. This is likely the case during the fumigation of Arabidopsis with 10 ppm NO_2 or infiltration with 10 mM $NaNO_2$, since no accumulation of the ROS H_2O_2 was detected via DAB staining despite the observed increase in NO_2^- (Figure 7 B and Figure 10 B). This hypothesis is supported by observations made by Chen *et al.* (2010) who exposed camphor seedlings to 0.1 – 4 ppm NO_2 for 10 h a day over a 60-day period which did not induce NO_2-induced cell death [33]. In this study, the SOD and AsA-GSH cycle activity increased in correlation with the

applied NO_2 concentration. The authors concluded that the activation of ROS scavenging mechanisms protected the plant from excessive damage caused by NO_2 [33]. Though they reported negative effects such as chlorophyll degradation and reduction in photosynthesis at higher NO_2 concentrations. In another study, an enhanced antioxidant activity of SOD and CAT were associated with a tolerance to the air pollutant ozone by successfully scavenging ROS [295].

When ROS accumulate excessively, as observed after fumigation with 20 or 30 ppm NO_2 or after infiltration of 100 mM $NaNO_2$ (Figure 7 B and Figure 10 B), they likely are not eliminated sufficiently due to a congestion of the antioxidant defense system. Insufficient ROS scavenging then inflicts damage by lipid peroxidation, oxidation of proteins, or interference with nucleic acids and enzyme activities. This ROS-induced damage can ultimately culminate in the death of the cell or the entire organism [33], [39]–[41], [296]. The importance of ROS for the onset of the NO_2-induced cell death is further emphasized when the H_2O_2-detoxyfying enzyme CAT was infiltrated into the leaves prior to fumigation with 30 ppm NO_2. Here, DAB staining confirmed that CAT successfully reduced the NO_2-induced accumulation of H_2O_2 and subsequent electrolyte leakage demonstrated that this ROS decrease attenuated the NO_2-induced cell death by 42 % (Figure 7 B and C).

The remaining question is: how do ROS accumulate during NO_2 fumigation? During pathogen-induced HR-PCD, the ROS burst responsible for the onset of cell death is primarily generated by the NADPH oxidases RBOHD and RBOHF [297]–[299]. However, during the NO_2-induced cell death, these enzymes do not appear to be the major source of ROS, as their corresponding mutants were not compromised in cell death development when fumigated with 30 ppm NO_2 for 1 h [39]. Alternatively, H_2O_2 may be produced by peroxidases as previously observed during *P. syringae* infection of Arabidopsis [300], [301]. Several peroxidase genes such as *PER4, PER36,* and *PRX71* were highly expressed within the microarray data set immediately after fumigation with 10 ppm NO_2 ($log_2(FC) > 6$, see raw microarray data set E-MTAB-6522 at the Array Express database at EMBL-EBI). However, this hypothesis was not examined further through the course of this work. Moreover, ROS may be generated according to the above-stated assumption that the NO_2-induced reduction in photosynthesis promotes ROS accumulation by accelerating the one-electron reduction of O_2 [40].

3.1.3 Nitric oxide is an additional cell death signal upon NO_2 fumigation

During the onset of pathogen-growth-restricting HR, NO is a crucial mediator of the programmed cell death. Initial studies on this topic were performed with soy bean cell suspensions by Delledonne *et al*. (1998) [177]. They demonstrated that the exogenous application of NO in combination with H_2O_2

or O_2^- activated the HR-induced cell death synergistically, as neither ROS nor NO alone were able to trigger an advanced HR. This was further supported by the use of RBOH activity inhibitors or CAT-mediated H_2O_2 detoxification as well as the scavenging of NO by cPTIO, where each treatment reduced the onset of HR [177]. This is in line with observations made during NO_2-induced cell death. Here, NO accumulated 2.2- and 7.1-fold after fumigation with 30 ppm NO_2 or infiltration with $NaNO_2$, respectively (Figure 7A and Figure 10 A). However, cell death induction was only observed when the NO increase coincided with ROS accumulation, as was the case for the treatments with 30 ppm NO_2 and 100 mM $NaNO_2$. NO also accumulated after infiltration with 10 mM $NaNO_2$. However, no ROS increase was detected via DAB staining after this treatment, which provided a reasonable explanation as to why no cell death was observed. The importance of NO during NO_2-induced cell death was further substantiated by the 40 % reduction in NO_2-induced electrolyte leakage upon infiltration of leaves with the NO scavenger cPTIO prior to fumigation with 30 ppm NO_2 (Figure 7 A). Unexpectedly, no increase in NO was detected with DAF-FM DA after treatment with 20 ppm NO_2 that induced localized cell death that was accompanied by H_2O_2 accumulation. However, due to method constraints, a spatially limited accumulation of NO at the site of cell death induction cannot be excluded.

Major sources of NO during pathogen defense are the enzymatic reduction of NO_2^- by NR as well as the oxidation of arginine by yet-unknown enzymes with nitric oxide synthase (NOS)-like activity [228], [302]. Even though NR is commonly known for its reduction of NO_3^-, it was reported that, upon elevated cytoplasmic NO_2^- levels, NR reduces this nitrogen compound to NO instead [70], [71]. Since NO_2 fumigation overloads the leaf with NO_2^-, the enzymatic reduction by NR may be a likely source of NO during the NO_2-induced cell death. However, analysis of the *nia1nia2noa2* triple mutant which is devoid of both, the NR (NIA1, NIA2) and NOS-like (NOA1) activity disputes this hypothesis. During a mutant screen, *nia1nia2noa2* did not display a reduced NO_2-induced cell death after exposure to 30 ppm for 1 h. Therefore NR and NOS-like activities may not be crucial for the onset of NO_2-induced cell death [39]. Nonetheless, NO_2^- is considered a valuable source of NO production. For instance, exogenously applied NO_2^- is spontaneously reduced to NO in the acetic conditions of the apoplast [66]. Furthermore, NO can be generated non-enzymatically from NO_2^- when it accepts electrons from the mitochondrial respiratory chain, as is observed during the infection of Arabidopsis with the avirulent pathogen *P. syringae* pv. *maculicola* or in tobacco plants during anoxic conditions [67], [68]. Hence, a major role of NO_2^- during the NO_2-induced NO accumulation and subsequent cell death induction can be assumed.

In summary, the concerted accumulation and action of ROS and NO are crucial for the onset of the NO_2-induced cell death. This was further supported by the aforementioned mutant screen which revealed that mutants accumulating NO (*nox1)* or ROS (*cad2, vtc1*) were more sensitive to NO_2 [39].

Recent models suggest that NO is an amplifier of ROS signaling by impeding its turn-over through the antioxidant system. As reviewed in detail by Begara-Morales *et al.* (2016), NO affects various enzymes crucial for ROS detoxification by inhibiting their enzymatic activity via post-translational modifications [87]. This corresponds with reports of antioxidant depletion in H_2O_2 - and NO-treated tobacco BY-2 cells that undergo cell death [229]. A significant decline in the antioxidants glutathione and ascorbate was also described after fumigation of Arabidopsis with 30 ppm NO_2 for 1 h [39]. However, it was not examined whether NO promotes the accumulation of ROS by regulating its turn-over. Here, testing whether NO scavenging may cause a reduction in ROS after NO_2 fumigation, will be a revealing experiment to reasonably confirm for the hypothesis.

The presented results and reports from the literature imply that NO-mediated post-translational modifications are essential regulatory mechanisms during the onset of programmed cell death and shall be discussed further in the next chapter.

3.1.4 RNS-mediated protein modifications correlate with the NO_2-induced cell death

Post-translational modifications of proteins that are mediated by NO and its oxo-derivatives are well-documented in plants. For example, during HR-PCD, S-nitrosylation (SNO) of cysteine and nitration of tyrosine residues (nTyr) were demonstrated to be of physiological relevance [83], [96], [227]. Therefore, the abundance of these regulatory protein modifications was analyzed immediately after treating Arabidopsis plants with NO_2 or NO_2^-. Here, the SNO content gradually increased with the applied NO_2 concentrations, up to 610 pmol/mg protein (12-fold increase) after 30 ppm NO_2 (Figure 6 C). Similar observations were made after loading leaves with NO_2^-, where SNO concentrations increased up to 52-fold after treatment with 100 mM $NaNO_2$ (Figure 9 B). However, protein nitration was only induced after fumigation with 30 ppm NO_2 and was not detected after $NaNO_2$ infiltration (Figure 6 D, Supplemental Figure 1 B). Tyrosine nitration is mostly generated via $ONOO^-$ which is formed during the reaction of NO with O_2^- (Table 1(5), [90], [91]). However, if NO levels exceed the amount of O_2^-, the reaction to N_2O_3 is favored over the formation of $ONOO^-$ [303]. After $NaNO_2$ infiltration, O_2^- is likely converted to H_2O_2 e.g. via an enhanced activation of SOD, as reported upon NO_2 treatment [33], which leads to the depletion of O_2^-. Since the presented results demonstrate that NO and H_2O_2 are both highly abundant after treatment with 100 mM $NaNO_2$, NO may exceed O_2^-. Therefore, it was concluded that $NaNO_2$ infiltration promotes the formation of N_2O_3 instead of $ONOO^-$. In turn, N_2O_3 favors the S-nitrosylation of cysteines instead of nTyr formation, which was demonstrated to occur heavily after loading leaves with NO_2^- [84] (Table 1(1)).

An alternative mechanism which leads to nTyr formation involves the enzymatic reduction of NO_2^- by *oxo*-metal complexes such as peroxidases in the presence of H_2O_2 (Table 1(5), [91], [92]). Although both educts of this enzymatic reduction (NO_2^- and H_2O_2) were highly abundant after infiltration of 100 mM $NaNO_2$, they did not encourage nTyr formation. Considering the lack of protein nitration in $NaNO_2$-infiltrated leaves, the question becomes: how nTyr formation could occur in leaves which were exposed to NO_2. One reasonable explanation is that the introduction of ample levels of free radical NO_2 into the leaf can directly react with tyrosine residues resulting in the formation of nTyr [90], [304]. Furthermore, the *oxo*-metal complexes may participate in nTyr formation by reducing NO_2^- in the presence of H_2O_2.

Taken together, the previous results strongly suggest that SNO modifications play an important role during the NO_2-induced cell death, as its increase correlates with the applied concentrations of NO_2 and $NaNO_2$ as well as the induced cell death. However, the role of nTyr is less distinct, as only the cell death induced by NO_2 was accompanied by an increase in nTyr, while $NaNO_2$ did not show any increase in this protein modification. Nonetheless, increases in tyrosine nitration are reported in Arabidopsis undergoing pathogen-induced HR [96], where nTyr likely regulate protein inhibition or degradation [93], [94], [305].

But how do protein modifications influence the onset of cell death? For instance, NO-mediated protein modifications amplify ROS accumulation by disturbing the regulation of the antioxidant system [87], [306]. In this regard, nTyr has been shown to inhibit various isozymes of the Arabidopsis SOD *in vitro*, as well as cytosolic pea ascorbate peroxidase (APX) and its monohydroascorbate reductase (MDAR) which is involved in the regeneration of ascorbate [307]–[309]. Since ascorbate and APX are important for the detoxification of H_2O_2, the inhibition of their regeneration or enzymatic activity may lead to oxidative damage [308].

The S-nitrosylation of proteins also has been accredited to play a pivotal role in the regulation of the antioxidant system. It was demonstrated that S-nitrosylated Arabidopsis peroxiredoxin (Prx) II E and pea PrxIIF were inhibited in their ability to detoxify H_2O_2 as well as $ONOO^-$ (in case of PrxIIE) [227], [310]. Furthermore, studies with pea revealed that SNO inhibits peroxisomal catalase as well as MDAR activity [309], [311]. Additionally, an inhibitory effect of SNO was reported for APX in tobacco BY-2 cells during the onset of HR-PCD [312]. However, protein regulations induced by SNO are highly complex and cannot be generalized as strictly inhibitory. For instance, it was reported that SNO stimulates APX activity in pea and Arabidopsis *in vivo* [304], [309]. This is in line with the finding that SNO-modifications of RBOHD led to a reduction of ROS during the HR-PCD of *P. syringae* DC3000 infected Arabidopsis [83].

Taken in conjunction, the involvement of cysteine S-nitrosylation and tyrosine nitration of proteins are well described during the onset of HR-PCD by regulating the accumulation of ROS. These protein modifications often result in the impediment of ROS detoxification which subsequently causes oxidative damage. The accumulation of SNO during the NO_2 and $NaNO_2$-induced cell death suggests that this protein modification plays a critical role during this response. However, further research is necessary to indisputably identify SNO as a crucial mediator during this type of cell death. Here, knowledge about SNO levels after suppressing the NO_2-induced cell death by scavenging NO or ROS may give vital clues about the role of SNO during cell death. Furthermore, the identification of distinct S-nitrosylated proteins whose regulation may convey the NO_2-induced cell death has the potential to deepen the understanding of processes which initiate this type of cell death. Similar statements can be made for the tyrosine nitration of proteins during the NO_2-induced cell death.

3.1.5 Suggested work model of NO_2-mediated cell death induction

Upon entering the leaf through the stomata (Supplemental Figure 9), NO_2^- levels within the leaf increase due to the disproportionation of NO_2 and possible NR activity which converts the accumulating NO_3^- to NO_2^- [34], [35], [39], [291]. The enzymatic metabolization of the disproportionation products likely consumes cofactors which would otherwise be used during photosynthesis. This cofactor depletion is assumed to impede the photosynthetic fixation of CO_2, leading to the acceleration of the one-electron reduction of O_2 to O_2^- [42]–[44]. NO_2 exposure was also reported to reduce the chlorophyll content which further impairs proper photosynthetic processes and promotes ROS accumulation. Simultaneously, NO_2 and NO_2^- give rise to RNS such as NO or $ONOO^-$, which then orchestrate the modification of proteins by S-nitrosylation or tyrosine nitration (Figure 30).

When plants are exposed to high doses of NO_2, dramatic increases of NO_2^-, ROS, and NO were detected. NO_2, NO, and other accumulating RNS mediate extensive S-nitrosylation and nitration of proteins, as demonstrated by increases in SNO and nTyr levels. These protein modifications were reported to target and inhibit several enzymes of the antioxidant system and therefore impair ROS detoxification [87]. An imbalance of the AsA/GSH-antioxidant cycle during the NO_2-induced cell death was demonstrated in previous work which was not presented in this thesis. Here, fumigation with 30 ppm NO_2 for 1 h caused a depletion of reduced GSH and AsA by 90 and 80 %, respectively, while the oxidized GSSG increased by approximately 5-fold [39]. Therefore, NO_2 exposure promotes the amplification of ROS which ultimately leads to oxidative damage and cell death. This hypothetic mode of NO_2-induced cell death was outlined in Figure 30 (Top).

Contrariwise, in the case of exposure to moderate, non-damaging doses of NO_2, the activities of the enzymes integrated into the antioxidant system were reported to be stimulated [33], [295]. This may be facilitated by the detected increase of SNO, as stimulatory effects of SNO upon APX activity were reported in Arabidopsis [313]. Under these conditions, the antioxidant system may successfully scavenge accumulating ROS, thereby protecting the cell from oxidative damage and facilitating survival (Figure 30, Bottom).

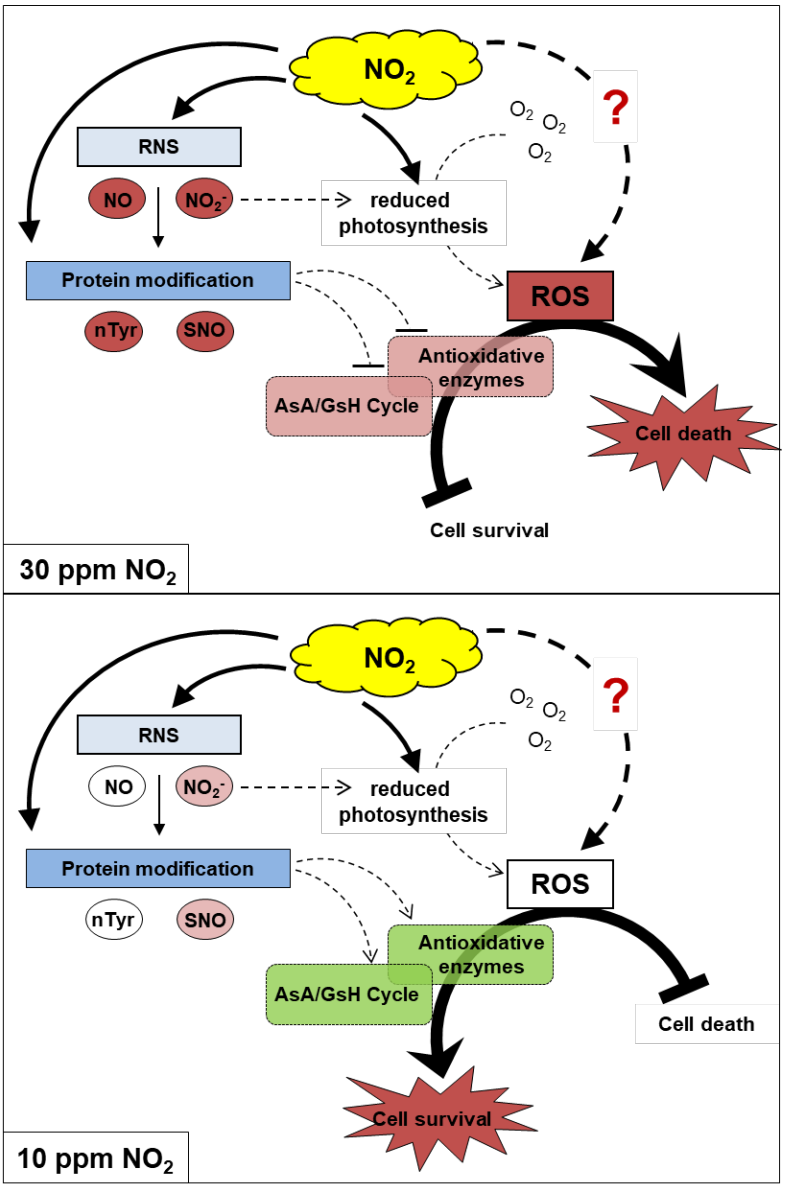

Figure 30: Hypothetical model of NO_2-mediated cell death and survival
Top) High NO_2 doses (30 ppm) induce dramatic increases in RNS such as NO and NO_2^- that mediate protein modifications such as SNO and nTyr which can negatively affect the activity of the AsA/GSH cycle and detoxifying antioxidative enzymes. NO_2 and its disproportionation product NO_2^- can impede photosynthesis that causes the one-electron reduction of O_2 to the ROS O_2^-, which are converted to H_2O_2. The NO_2-induced inhibition of the antioxidant system impedes the detoxification of accumulating ROS which facilitates oxidative damage at high concentrations which culminates in cell death. Shapes highlighted in red indicate an NO_2-induced accumulation (compounds and modifications) or inhibition (enzymes). **Bottom)** Moderate doses of NO_2 (10 ppm) cause comparatively minor increases in NO_2^- and SNO (highlighted in a pastel red) and no augmentations in NO and nTyr. Hence, NO_2 likely does not inhibit but stimulate the antioxidant system by activating enzyme modifications (Shapes highlighted in green). This prevents a build-up of ROS that are generated by the NO_2-induced reduction in photosynthesis. The avoidance of oxidative stress protects the plant from cell death. NO_2 = nitrogen dioxide, NO = nitric oxide, RNS = reactive nitrogen species, NO_2^- = nitrite, SNO = S-nitrosylation, nTyr = tyrosine nitration, GSH = glutathione, AsA = ascorbate, O_2^- = superoxide anion, ? = hypothetical modes of action.

Taken together, the NO_2-induced cell death shows a high degree of similarity to HR-PCD. Central roles are occupied by NO and ROS (H_2O_2), which concertedly stimulate the onset of HR-PCD upon pathogen infection [177]. Additionally, nTyr and SNO modifications of proteins are reported to

increase during HR-PCD [83], [96], [227] and facilitate the accumulation of ROS by impeding the antioxidant system [227], [310], [307]–[309]. These HR-PCD characteristics were also observed during the NO_2-induced cell death which was driven by the accumulation of NO_2^-. Moreover, the regulation of HR-PCD is significantly mediated by hormones such as SA, ET, and JA, and was also reported to occur on a genetic level [178], [179], [181], [182], [183], [184]. The gene expression profiling performed in this work suggests that similar regulatory processes also occur during the NO_2-induced cell death. The obtained microarray data revealed the potential of NO_2 to stimulate hormone synthesis and signaling along with the expression of genes related to HR and PCD (see GO-term enrichment Figure 12). Though, the NO_2 concentration used in the microarray experiment did not induce cell death, it demonstrates that NO_2 exposure can enable the stimulation of pathways leading to HR-PCD. In summary, the results strongly suggest that NO_2 induced an HR-PCD-like cell death.

3.2 NO_2 induces PTI-like basal disease resistance

Previous research demonstrated that the cellular effect of NO_2 is highly dependent on the dose which the plant is exposed to. As illustrated above, high doses of this gas can lead to rapid cell death. On the contrary, low to moderate doses were described to beneficially impact various plants species such as tomato, sun flower, or Arabidopsis by supporting growth, biomass formation, flowering or yield [45]–[47]. Several reports claimed that a fertilizing effect of NO_2 is the underlying cause of these observations [6]–[8], [46]. Conversely, other work hypothesized that exogenously applied NO_2 induces endogenous signaling rather than boosting the metabolism [30], [50]–[52]. This hypothesis is strengthened by the results described above, which demonstrated that NO_2 promotes the formation of signal-transmitting protein modifications (SNO, nTyr), as well as the accumulation of relevant signaling molecules (NO, H_2O_2). However, to date little is known about as to how non-damaging exposure to NO_2 impacts physiological and molecular processes of the plant. In order to address this issue, Arabidopsis plants were fumigated with non-damaging concentrations of NO_2 (10 ppm for 1 h) and subjected to transcriptome analysis. This approach aimed to obtain a comprehensive overview of NO_2-induced signaling cascades or metabolic processes based on the regulation of associated genes.

3.2.1 The NO_2-induced resistance is commissioned by transcriptional reprogramming

The evaluation of the gene expression analysis revealed that NO_2 fumigation induces extensive transcriptional reprogramming. Immediately after fumigation, more than 2300 genes were significantly up-regulated, whereas the transcription of approximately 2000 genes was suppressed simultaneously. Six hours after fumigation, the number of regulated genes was reduced to approximately 750 and 680 genes which were significantly up- or down-regulated, respectively (Figure 11). This demonstrated that NO_2 is rapidly perceived by the plant leading to a fast but transient transcriptional reprogramming. This temporary response was further supported by the observation that only a small number of 319 up- and 57 down-regulated genes were regulated continuously at both time points (Figure 11).

To obtain insights into the biological processes which were initiated upon exposure to NO_2, functional profiles of the up- and down-regulated gene sets were generated via Gene Ontology (GO) term enrichment analysis. This approach revealed that NO_2 induced a rapid and transient transcriptional activation of signaling cascades and metabolic pathways associated with basal pathogen defense (Figure 12, Supplemental Table 1, Supplemental Table 2). Specifically, NO_2 activated genes involved in biosynthesis and signaling of the plant hormones JA, ET, and SA, all of which are well-known as primary signals in defense response regulation [132], [133], [314]. Responses involving JA metabolism and signaling and those inducible by chitin and fungi were persistent regulatory effects induced by NO_2 as they were still facilitated 6 h after fumigation. Furthermore, NO_2 treatment promoted the activation of genes involved in defense mechanisms which are directly effective against pathogen invasion, such as camalexin and flavonoid glucuronidation, programmed cell death, and metabolic processes concerning the plant cell wall [199], [233]–[235]

However, the functional profile of genes which were down-regulated after NO_2 fumigation was less defined. Immediately after fumigation, the transcription of genes involved in the primary metabolism as well as plant growth and development were highly suppressed. This was likely induced by the active repression of auxin- and gibberellin-mediated signaling cascades, since these phytohormones implement various developmental processes [315], [316] (Supplemental Table 3, Supplemental Figure 3). At the later time point, a significant number of genes involved in defense response or SA were repressed, which was indicative of the attenuation of the NO_2-induced defense response. Furthermore, processes involving DNA maintenance and replication were repressed (Supplemental Table 4, Supplemental Figure 3). Presumably, this active suppression of primary physiological processes upon NO_2 treatment reflects the plants deviation of resources in order to favor defense over growth and development [317], [318].

PCA meta-analysis performed by Dr. Elisabeth Georgii revealed that the NO_2-induced gene expression profile was highly similar to previously-published microarray data sets obtained after *B. cinerea* [164] and *P. syringae* infection [319] or after chitin [320] and flg22 treatment [129], [321]. On the contrary, gene expression profiles after drought or heat treatment [322] were less comparable to the NO_2-induced response (Supplemental Figure 4). In accordance with this, NO_2 fumigation caused a 30 % reduction in necrotic lesion formation after infection with the necrotrophic fungus *B. cinerea* and inhibited the growth of *P. syringae* DC3000 (Figure 16, Figure 28). A similar observation was made by Ferrari *et al*. (2007), who compared gene expression profiles of Arabidopsis treated with the endogenous DAMP OG or *B. cinerea*. Here, they reported that the OG-induced gene expression profile overlapped by approximately 50 % with the profile obtained after *B. cinerea* infection. Accordingly, they reported that OG-pretreatment was sufficient to render Arabidopsis resistant to this necrotrophic fungus [164].

The NO_2-induced resistance demonstrated that the observed transcriptional reprogramming was transmitted to a physiologically relevant response leading to PTI. Conclusively, the question needs to be answered by which mechanisms NO_2 is able to induce PTI.

3.2.2 Exposure to NO_2 alters hormone homeostasis

GO-term enrichment analysis revealed that NO_2 fumigation stimulated a persistent transcriptional activation of JA metabolic processes and signaling. Surprisingly, NO_2 fumigation did not promote the accumulation of JA or JA-Ile at any time point after fumigation. Even though NO_2 fumigation led to an increased abundance of biosynthetic gene transcripts, only the JA precursor *cis*-OPDA showed a significant increase at 6 h after fumigation (Figure 13). At several occasions in the past, *cis*-OPDA was reported to possess signaling capabilities which were distinct from other jasmonates [198], [236], [323]. As an example, during development, it has been shown that *cis*-OPDA is involved in the inhibition of seed germination in Arabidopsis and plays a role in tomato embryo development [324], [325]. More importantly, it was found that *cis*-OPDA can activate the expression of genes in concert or independently of other jasmonates during plant defense [323], [326]. Hence, a role of *cis*-OPDA during pathogen resistance should not be underestimated. For instance, the belated accumulation of *cis*-OPDA as a precursor of jasmonates may indicate a deferred production of JA and its derivatives which in turn ultimately stimulate the NO_2-induced PTI. The involvement of *cis*-OPDA during pathogen defense is also evident when considering the findings of Scalschi *et al.* (2015) in *cis*-OPDA- and JA-Ile-deficient *OPR3*-silenced tomato plants. These plants were highly susceptible to *B. cinerea* due to an impediment in the deposition of callose. Interestingly, the application of *cis*-OPDA but not JA restored the plants' capability to deposit callose and subsequently reinstated basal

resistance to *B. cinerea*. Moreover, *cis*-OPDA treatment of WT tomato plants facilitated an enhanced resistance [198]. These findings may encourage the hypothesis that the NO_2-induced accumulation of *cis*-OPDA is partially responsible for the NO_2-induced resistance which is mainly implemented by the deposition of callose. However, this hypothesis was not pursued during this work as a direct link between *cis*-OPDA and callose formation as observed in tomato has yet to be identified in Arabidopsis. Moreover, the lack of the NO_2-induced resistance in the *opr3* mutant (Figure 17), which is devoid of jasmonates but is still able to produce *cis*-OPDA, demonstrates that the accumulation of *cis*-OPDA is of minor importance during the NO_2-induced resistance.

Interestingly, upon examination of the microarray data, it became apparent that gene transcripts associated with the catabolism of jasmonates accumulated alongside those involved in JA biosynthesis. During the catabolic processes, JA and JA-Ile are converted to 12-OH-JA-Ile, 12-COOH-JA-Ile, and 12-OH-JA. The simultaneous transcriptional induction of metabolic and catabolic processes was previously described by Koo *et al.* (2011). They demonstrated that the transcription of the metabolic enzymes responsible for the conversion of the active jasmonates to 12-OH-JA-Ile and 12-COOH-JA-Ile (CYP94C1, CYP94B3) overlapped with the expression of the JA biosynthetic genes after wounding [240]. Consequently, they determined that the accumulation of 12-OH-JA-Ile and 12-COOH-JA-Ile after wounding coincided with a decline in JA and JA-Ile levels, which was dependent on COI1 [240], [327]. Other studies demonstrated that the application of MeJA, as well as wounding or *B. cinerea* infection, triggered an enhanced transcription of Jasmonate-Induced Oxygenases (JOXs) genes [243], [328]. JOXs were identified to metabolize JA to its inactive form 12-OH-JA. Accordingly, a JOX-deficient quadruple mutant (*jox1jox2jox3jox4*) hyperaccumulated JA and JA-Ile and was highly resistant to *B. cinerea* due to a constitutive expression of defense-related genes such as *PDF1.2a* [243]. Hence, the transcriptional activation of JOX and other jasmonate-catabolic enzymes terminate JA-induced defense signaling by diminishing the pool of available active jasmonates. Additionally, it was reported that the catabolic products 12-OH-JA-Ile, 12-COOH-JA-Ile, and 12-OH-JA all fail to facilitate the complex formation of COI1 with JAZ proteins and consequently prevent JA-mediated signaling and the activation of defense related genes [240], [243], [327]. The fact that the application of MeJA can initiate the transcriptional activation of JOXs demonstrates that jasmonates are capable of inhibiting their own signaling by arresting their production in a regulatory feed-back mechanism [243], [328]. Consequently, the simultaneous transcriptional activation of JA biosynthetic and catabolic genes provided a reasonable explanation for the lack of active jasmonates after NO_2-fumigation. Intriguingly, the significant accumulation of the aforementioned JA catabolites starting at 3 h after fumigation confirmed this hypothesis (Figure 14). It is likely that NO_2 induced the production of active jasmonates (as indicated by the increase in *cis*-OPDA), which in turn stimulates the activation of their own catabolic turn-over as a rapid feed-back mechanism. This may enable the preservation of resources which otherwise would have been consumed by an excessive

accumulation of jasmonates that escalate the induction of defense responses. Hence, no changes in active jasmonate levels were detected.

Additionally, it is known that SA antagonizes JA signaling [329]. Though it predominately represses JA-responsive gene expression, rather than downregulating JA biosynthesis [330], SA may be involved in the degradation of JA. Since the gene expression analysis indicated an NO_2-induced activation of SA biosynthetic genes and the induction of processes mediated by SA, the phytohormone was quantified at various time points after fumigation. In contrast to the jasmonates, NO_2 induces a transient but significant accumulation of SA up to 3 h after fumigation (Figure 15). Since this transient SA peak precedes the accumulation of the jasmonate degradation products, it suggests that SA plays a part in the initiation of the JA-catabolic gene transcription. However, up-to-date information on the regulation of these catabolic genes is scarce [331].

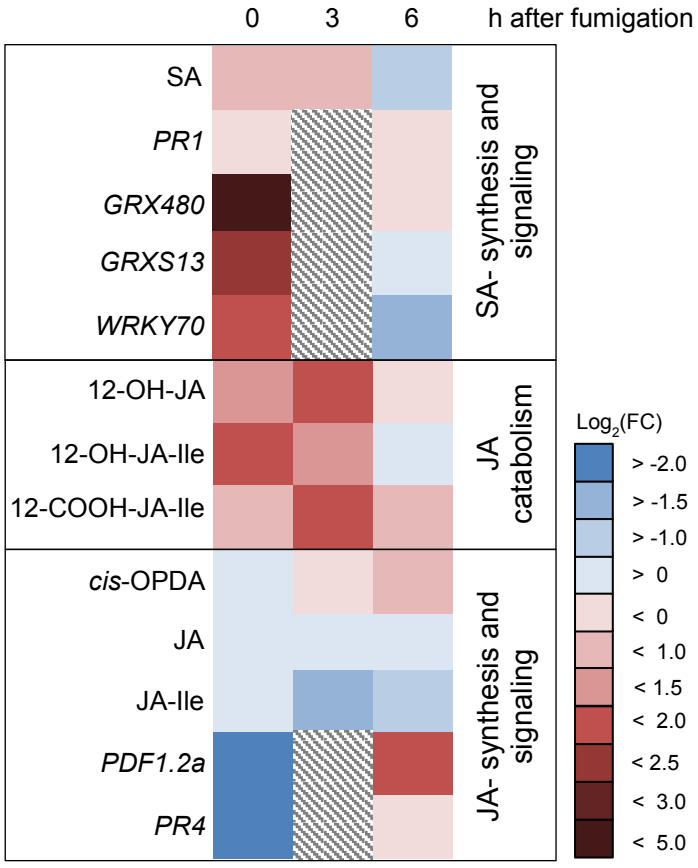

Figure 31: Chronological illustration of the SA/JA antagonism after NO_2 fumigation
Directly (0-3 h) after fumigation SA levels and SA-responsive genes as well as JA degradation products are up-regulated, which decrease after 6 h. At this time point the levels of *cis*-OPDA augmented and the expression of JA-responsive genes increase to their maximum, whereas SA synthesis and signaling components as well as JA catabolite levels decline. Colored panels represent fold change (log_2) of concentration or expression from the air fumigated controls. SA = salicylic acid, PR = PATHOGENESIS-RELATED, GRX = glutaredoxin, 12-OH-JA = 12-hydroxyl jasmonic acid, 12-OH-JA-Ile = 12-hydroxyl-JA-Ile, 12-COOH-JA-Ile = 12-dicarboxy-JA-Ile, *cis*-OPDA = *cis*-(+)-12-oxophytodienoic acid, JA = jasmonic acid, JA-Ile = jasmonoyl-L-isoleucine, PDF1.2a = DEFENSINE-LIKE protein1.2a. Hatched boxes = no data available for this time point.

Nonetheless, the SA-induced repression of JA-responsive genes was evident when considering the suppression of *PDF1.2a* and *PR4* transcription. The transcriptional repression of these JA-inducible genes chronologically coincided with the detected SA peak as well as the increased transcription of

essential SA-inducible regulators of JA repression, such as the glutaredoxins GRX480 and GRXS13, as well as several WRKY (e.g. WRKY70) [332], [333] (Figure 31, Supplemental Table 5). As soon as the SA peak subsides, the transcripts of JA-inducible *PDF1.2a* and *PR4* begin to accumulate 6 h after fumigation. However, whether the NO_2-induced transient increase of SA is sufficient to induce SA-mediated defense signaling must still be resolved , as the expression of *PR1* – the major marker of SA-induced defense [138] was not altered upon NO_2 fumigation. Nonetheless, the results evidently demonstrated an extensive SA/JA crosstalk which is induced by NO_2 (Figure 31, Supplemental Table 5).

Taken together, these results indicate that exposure to NO_2 rapidly alters hormone homeostasis by inducing a fast but transient accumulation of SA. Since SA accumulation overlapped with the suppression of JA-responsive genes followed by a subsequent increase in JA-degradation products, SA likely plays a crucial role in containing JA-augmentation and –signaling.

3.2.3 Jasmonate signaling via COI1 is essential for the NO_2-induced *B. cinerea* resistance

Though jasmonate accumulation was not detectable after NO_2 fumigation, it was presumed that the enrichment of GO-terms involved in JA-mediated defense signaling is of physiological relevance during the NO_2-induced resistance against *B. cinerea*. The defense against this necrotrophic fungus is highly dependent on JA biosynthesis and signaling, as was demonstrated on several occasions by utilizing mutant analyses. For instance, the JA-deficient Arabidopsis *aos* mutant developed necrotic lesions which were approximately 400 % larger than those observed on the respective WT control. The susceptibility of *aos* was preventable by exogenous application of JA [165]. Another mutant impaired in JA synthesis is *opr3,* which was unaffected in the production of the JA precursor *cis*-OPDA but displays a reduction in JA levels by about 70 % when infected with *B. cinerea*. Correspondingly, *opr3* mutants are susceptible to *B. cinerea*, although to a lesser extent than *aos* [165]. Similar susceptibilities of these mutants to *B. cinerea* were also observed throughout the course of this work (Supplemental Figure 10*).*

NO_2 pretreatment of the aforementioned JA-deficient mutants revealed that jasmonate biosynthesis was crucial for the development of the NO_2-induced resistance, since neither *aos* nor *opr3* showed a reduction in necrotic lesion formation upon fumigation (Figure 17). Complementary LC-MS/MS measurements to quantify *cis*-OPDA, JA, and JA-Ile in NO_2- and air-fumigated Col-0 plants at various time points after spray-infection with *B. cinerea* demonstrated that JA and JA-Ile increased upon pathogen infection. However, NO_2 pretreatment did not induce an enhanced or early accumulation of

cis-OPDA or the jasmonates (see Supplemental Figure 7 A, B, C). Therefore, a NO_2-induced enhancement of jasmonate biosynthesis can be excluded as a major cause for resistance development. Nonetheless, it was previously demonstrated that JA-inducible genes can be activated without a detectable increase in endogenous jasmonate levels during pathogen infection of rice [334]. Thus, the NO_2-induced resistance may still be conveyed by enhanced JA-dependent plant responses without requiring a coincided enhancement of jasmonates. This was underlined when examining the *B. cinerea*-susceptible Arabidopsis *coi1* mutant which lacks a key regulator of JA-mediated defense signaling (Supplemental Figure 10*)* [139], [164]. Here, the NO_2-induced resistance was completely abolished, which demonstrates the importance of a functional JA-signaling pathway (Figure 18). Another key regulator of JA-induced defenses is MYC2 (JIN1) which positively regulates the herbivore and wound defense by activating the expression of *VSP2*, but inhibits pathogen defense by suppressing ERF1 and ORA59-mediated expression of *PDF1.2a* and other defense-related genes [158], [159], [335]. Therefore, it is comprehensible that NO_2-pretreated *jin1* mutants displayed a fully-developed NO_2-mediated resistance against *B. cinerea* (Figure 18).

Taken together, the results demonstrated that the NO_2-induced resistance against *B. cinerea* requires a functional but does not demand an enhanced synthesis of jasmonates that activate COI1-dependent signaling. This was supported by the observation that NO_2-pretreated plants exhibited an enhanced transcription of *PDF1.2a* upon *B. cinerea* infection (Figure 20 A). This is indicative of an NO_2-mediated acceleration of JA-signaling. The expression of the plant defensin PDF1.2a has often been associated with the resistance to necrotrophic pathogens such as *B. cinerea* or *A. brassicicola*, and was reported to inhibit the growth of the latter *in vitro* [139], [262], [263]. Therefore, the NO_2-induced resistance may be conveyed by the enhanced induction of *PDF1.2a* transcription which likely increases the amount of this antifungal peptide. However, further investigation is necessary in order to strengthen this hypothesis e.g. by quantifying PDF1.2a peptide levels after the treatments or by analyzing mutants that are solely deficient in PDF1.2a.

3.2.4 Distinct and ambiguous roles of NPR1 and SA during NO_2-induced *B. cinerea* resistance

Ferrari *et al.* (2003) reported that exogenous application of SA increases the resistance of Arabidopsis against *B. cinerea* which is indicative of the involvement of SA during the defense against this pathogen [167]. This was in accordance with the observation made in complementary LC-MS/MS measurements that *B. cinerea* spray-infection stimulates a continuous increase in SA (Supplemental Figure 7D). Furthermore, Ferrari *et al.* observed that transgenic *NahG* plants which contain a bacterial salicylate 1-hydrolase to induce SA degradation showed enhanced disease

symptoms. In contrast, the *sid2* mutant which is impaired in SA biosynthesis pathway via ICS1 exhibited WT-like resistance (similar observations were made in this work, Supplemental Figure 10). Therefore, the authors concluded that SA which is produced independently of ICS1 may be important during the defense against *B. cinerea*. They suggested a role of the SA biosynthetic pathway via PAL, since PAL-inhibition led to an enhanced susceptibility in WT and *sid2,* but only had a small impact on *NahG* plants [245], [167]. Similar to the findings of Ferrari *et al*., the NO_2-induced resistance against *B. cinerea was* fully established in *sid2*, but partially impeded in *NahG* (Figure 19). This observation indicates that SA may be involved in the development of the NO_2-induced resistance, when generated in an ICS1-independent manner. However, the quantification of SA via LC-MS/MS demonstrated that NO_2 does not facilitate an early or enhanced production of SA upon *B. cinerea* spray-infection. This indicates that NO_2 does not induce alterations in SA levels upon *B. cinerea* infection which convey the NO_2-induced resistance (Supplemental Figure 7 D). Nevertheless, plants treated exclusively with NO_2 showed a transient increase in SA which may be sufficient to initiate responses that ultimately lead to resistance upon *B. cinerea* infection Figure 15 B).

Alternatively, it is known that mutants which are deficient in SA (such as *sid2*) accumulate higher levels of JA due to the aforementioned SA/JA antagonism, and therefore display enhanced JA-responsive gene expression upon pathogen attack [170]. Thus, the NO_2-induced resistance observed in *sid2* as well as the partial resistance in *NahG,* could be caused by an enhanced activation of JA-signaling. This would indicate that a functional JA- rather than SA-signaling is important for the NO_2-induced resistance against *B. cinerea*. A negligible role of SA-mediated signaling during the NO_2-induced resistance is further supported when the expression pattern of the SA-defense signaling marker *PR1* is considered. Although *PR1* is up-regulated upon *B. cinerea* infection, its expression is neither enhanced nor advanced when pretreated with NO_2 (Figure 20 B). This is consistent with reports that *sid2*, which developed the NO_2-induced resistance to its full extent, is known to be impaired in *PR1* induction [214]. Contradictory to the hypothesis that SA-signaling is inconsequential for NO_2-induced resistance is the observation that a knock-out of the key regulator of SA-mediated defense signaling NPR1 led to a complete abolishment of the resistance phenotype (Figure 19). In case JA- rather than SA-signaling is involved in this type of resistance, it would have been expected that NO_2-pretreated *npr1* establishes a WT-like *B. cinerea* resistance. This is due to the fact that the *NPR1* knock-out causes an alleviation of the SA-mediated suppression of the JA response, leading to increased JA- and *PDF1.2a* expression levels [170]. However, *npr1* did not develop an NO_2-mediated enhancement of *PDF1.2a* expression as observed in WT, which may explain the lack of the NO_2-induced resistance in this mutant (Figure 21 A).

Interestingly, NPR1 was associated with a SA-independent mode of induced resistance which requires JA and ethylene (ET). In 1998 Pieterse *et al.* demonstrated that the non-pathogenic

rhizobacterium *Pseudomonas fluorescens* triggers an induced systemic resistance (ISR) response against *P. syringae*. This induced resistance remained in SA-non-accumulating *NahG* transgenic lines, but neither the JA-signaling-impeded *jar1* nor the ethylene response mutant *etr1* displayed the protective *P. fluorescens*-induced resistance. Moreover, they reported that the *npr1* mutant also failed to develop this resistance. Therefore, they proposed that this ISR is triggered by an SA-independent pathway in which components from the JA and ET response activate a systemic resistance which is dependent on NPR1 [336]. Similar observations were made by Nie *et al.* 2017, who determined that the beneficial rhizobacterium *Bacillus cereus* AR156 triggered ISR against *B. cinerea* and *P. syringae* DC3000 which was dependent on NPR1- as well as JA/ET-signaling but did not require SA [337], [338]. Analogous to these observations, the NO_2-induced resistance is blocked in mutants impaired in JA- (*coi1*), as well as NPR1-signaling (*npr1*), whereas SA-deficient mutants (*sid2, NahG*) remain partially resistant. Preliminary experiments also suggested that the ethylene insensitive *etr1* mutant which is defective of the ethylene receptor, is impaired in the NO_2-induced resistance (Supplemental Figure 11). These findings suggest that root symbionts and NO_2 may stimulate similar hormonal signaling pathways leading to induced resistance against the necrotrophic fungus *B. cinerea*. Moreover, the induced signaling also protected against the hemibiotrophic *P. syringae* DC3000, in case of the root symbionts [338] and NO_2, as demonstrated by a reduced bacterial titer in NO_2-pretreated Col-0 when compared to its untreated counterpart (Figure 28).

Taken together, NO_2 induces resistance against *B. cinerea* by simultaneously activating NPR1- and JA-dependent signaling. The concomitant induction of these pathways is effective in providing a basal resistance against various pathogens of different lifestyles, as was already demonstrated for root symbiont-induced resistance. However, this remains to be validated for NO_2. Although NO_2-treated WT plants developed a resistance against *P. syringae* DC3000, mutant screens to determine the involved signaling pathways are still pending. Nonetheless, these findings reflect the ornately-orchestrated defense signaling networks in Arabidopsis and demonstrate that the interplay between JA- and SA-mediated signaling is far more complex than simply antagonistic.

3.2.5 The propagation of NO_2-induced signaling leading to PTI

Pattern-triggered immunity (PTI) characterizes the development of basal disease resistance against a variety of pathogens, since a multitude of pathogen- or endogenously derived elicitors (PAMPs/DAMPs) can induce this type of defense [105], [339]. After the perception of PAMPs by PRR receptors, the plant rapidly deploys signal transmitters such as ROS, Ca^{2+}, RNS, and activated cytosolic kinases in order to initiate appropriate defense gene induction through MAPK and CDPK cascades [99]. The activation of these highly variable signaling cascades were reported numerous

times when plants were invaded by *P. syringae* DC3000 or *B. cinerea* where they customize pathogen-specific defense responses e.g. by inducing a fine-tuned production of an effective hormone blend [99], [150].

NO_2 provides resistance against both *B. cinerea* and *P. syringae* DC3000 which is indicative of a NO_2-induced basal immunity which resembles PTI. This is supported by the finding that a multitude of early PTI-signaling components are highly induced immediately after fumigation with NO_2 (Supplemental Table 8). Amongst others, various receptor kinases such as *BRI1-ASSOCIATED RECEPTOR KINASE 1 (*BAK1) that interacts with FLS2 and other PRRs [340], PEPR1,2 that are associated with DAMP-perception [107], or the Lectin receptor Kinase (LecRK) –VI.2, which was demonstrated to be required for priming and *P. syringae*-induced PTI [341], are all highly up-regulated. Moreover, receptor-like cytoplasmic kinases such as BIK1 or PCRK1, which are involved in PTI against *P. syringae* [342]*,* are up-regulated in the gene expression data set immediately after fumigation (Supplemental Table 8). These kinases lead to the activation of MAP kinase cascades which generally consist of multi-layered phosphorylation chains involving MAP kinase kinase kinases (MEKK) which activate MAP kinase kinases (MEK) that subsequently phosphorylate MAP kinases (MPK). Finally, the latter induces transcriptional reprogramming e.g. by activating transcription factors such as WRKYs [343]. The Arabidopsis genome encodes 60 MEKKs, 10 MEKs, and 20 MPKs which demonstrates that MAPK cascades offer a highly versatile network to induce a multitude of responses [344]. After NO_2 fumigation, numerous MAPK cascade components are highly induced (Supplemental Table 8). Moreover, several CDPKs such as CPK1, 4, and 6 that are associated with PTI and defense are expressed upon NO_2 fumigation (Supplemental Table 8) [345].

Taken together, the NO_2-induced enhanced expression of the aforementioned signal transmitters provide further evidence that NO_2 promotes resistance by initiating PTI. However, transcriptional regulation only allows for the assumption of such mechanistic induction, since it does not provide evidence about the genuine availability of the active proteins that ultimately transmit the signal. Hence, further experiments are necessary to strengthen this hypothesis. However, studies by Nie *et al.*, have previously demonstrated that an induced resistance against *B. cinerea* by *B. cereus* can be conveyed by an increase in crucial MAPK protein levels that initiate an augmented expression of PTI marker genes [337].

Making the assumption that NO_2 stimulates basal resistance which is mechanistically similar to PTI, the question remains as to how NO_2 is perceived by the plant to initiate defense signaling. On one hand, NO_2 may induce signaling via DAMP-perceiving PRRs such as WALL-ASSOCIATED KINASE 1 (WAK1) [346]. NO_2 is a highly reactive molecule and therefore likely to inflict damage to the cell wall or membrane e.g. by oxidizing or nitrating lipids [347]. Thereby, endogenous DAMPs may be generated upon NO_2 exposure which initiate further signaling cascades that lead to pathogen

resistance. The elicitation of DAMP signaling e.g. by exogenous application or endogenous generation of oligogalacturonides (OG) was demonstrated to induce the accumulation of phytoalexins, the expression of defense-related genes, and the production of ROS. Accordingly, OG-treatment rendered Arabidopsis plants resistant to *B. cinerea* [106], [164], [348].

However, the endogenous production of DAMPs is difficult to determine *in vivo* unless a large amount is present, which would be typically associated with massive tissue degradation [348], [349]. Therefore, an NO_2-induced DAMP generation is challenging to convincingly confirm. Alternately, the results presented here demonstrate that NO_2 induces the accumulation of signaling molecules such as ROS and RNS as well as inducing the S-nitrosylation and nitration of proteins which are reported to facilitate signal transmission during plant-pathogen interactions (see 1.1.2). For instance, fumigation with 10 ppm NO_2 causes an increase in SNO (Figure 6), the involvement of which is well described in the regulation of NPR1 or the ROS-producing NADPH oxidase RBOHD [82], [83], [89]. Moreover, on several occasions, ROS- and RNS-mediated signaling was reported to be involved in PTI and pathogen defense [116]–[119], [122], [123]. Although H_2O_2 or NO accumulation was not detected after fumigation with 10 ppm NO_2 for 1 h (Figure 7), the utilized methods may not have been sensitive enough to detect the low but physiologically-significant concentrations of these molecules, since the techniques were based on the qualitative determination of a histochemical staining (ROS) or a fluorescence signal (NO). Another possibility of NO_2-induced signal induction may be that NO_2 itself functions as a signaling molecule as proposed by Takahashi and Morikawa in 2014 [30].

3.2.6 The NO_2 induced resistance is conveyed by early enhanced callose deposition but not camalexin

The purpose of PTI is to deploy an arsenal of defense mechanisms which impede the propagation of pathogens [104]. Common outcomes of PTI induction include the *de novo* production of the antimicrobial secondary metabolite camalexin or the pathogen-confining deposition of callose at the site of infection [185], [200], [205]. As it is evident that NO_2 fumigation triggers PTI, the induction of these defense mechanisms during the NO_2-induced resistance against *B. cinerea* was examined. It was assumed that NO_2 stimulates an enhanced induction of these defense mechanisms, thereby promoting the induced resistance. The gene expression analysis revealed that a majority of genes involved in the regulation and biosynthesis of camalexin were highly up-regulated immediately after NO_2 fumigation (Supplemental Table 7). This was further confirmed by GO-term analysis which demonstrated that “camalexin biosynthesis” was the most enriched GO-term in the up-regulated data set (Supplemental Table 1). Therefore, an enhanced synthesis of camalexin was a likely candidate to

convey the NO_2-induced resistance against *B. cinerea*. This hypothesis was supported by reports that claim that the camalexin-deficient *pad3* mutant displays an enhanced susceptibility to this fungus [167] (Supplemental Figure 10). When subjecting this mutant to the NO_2 resistance assay, it became evident that functional PAD3 is crucial for the NO_2-mediated resistance (Figure 22). Surprisingly, HPLC quantification revealed that camalexin did not accumulate after NO_2 fumigation. Moreover, NO_2-pretreatment did not impact the expression of *PAD3* or enhance the accumulation of camalexin upon *B. cinerea* infection of WT (Figure 23). These findings led to the conclusion that the NO_2-induced resistance against *B. cinerea* is dependent on functional PAD3, but not camalexin. A similar observation was previously reported by Ferrari *et al*., who demonstrated an increased expression in *PAD3* upon treatment of Arabidopsis with OGs. However, they could not detect an OG-induced accumulation of camalexin [164]. The authors argued that elicitor treatments may not induce camalexin accumulation, instead they may prime plants in order to enhance camalexin production upon pathogen infection. However, this hypothesis was invalid for the NO_2-elicited resistance, since NO_2-pretreatment did not influence camalexin levels after infection. Previously, Zhou *et al*. showed that SA treatment activates *PAD3* expression but is not sufficient to induce camalexin synthesis [210], [249]. Therefore, the observed transient peak in SA immediately after fumigation may have induced the expression of camalexin biosynthetic genes but was insufficient to initiate camalexin production.

Alternatively, PAD3 may be involved in the biosynthesis of currently-unknown antimicrobial compounds which either originate from the degradation of camalexin or are derived from other indolic compounds [164]. In 2009, Bottcher *et al*. reported that PAD3 not only mediates the formation of camalexin from dihydrocamalexic acid (DHCA), but is also involved in the formation of DHCA itself [272]. Therefore, it is conceivable that yet unknown compounds which originate from DHCA are associated with the NO_2-induced resistance. Moreover, Bottcher *et al*. identified several compounds as putative metabolites downstream of PAD3 in Arabidopsis undergoing biotic or abiotic stress which may exhibit a unknown potential to induce resistance [272].

Besides camalexin, the fortification of the cell wall by callose was investigated for its potential role in the NO_2-induced resistance, as it is a common readout for PTI induction [339]. The *pmr4* mutant which is deficient in the deposition of callose upon pathogen infection displayed no NO_2-induced resistance against *B. cinerea* (Figure 24 A) [190], [191], [193], [197]. Additionally, the resistance was compromised in WT plants which were treated with the callose synthesis inhibitor 2-DDG prior to fumigation with NO_2 (Figure 24 B). These findings strongly implied the involvement of callose in the induced resistance against *B. cinerea*. This was examined in more detail by the photometric detection of callose via Aniline Blue in WT and *pmr4* plants which were treated with the fungal elicitor chitosan after NO_2 fumigation. The quantification of the Aniline Blue fluorescence revealed that, at an

early stage after chitosan treatment, NO_2-pretreatment significantly promoted the deposition of callose (Figure 25, Figure 26). The experiments demonstrated that the timely response of NO_2-induced enhanced callose formation provides a reasonable explanation to the mechanism by which NO_2-pretreatment facilitates resistance against *B. cinerea*. The effectiveness of early callose deposition against fungal infection was previously demonstrated during powdery mildew infection of Arabidopsis, which impeded the penetration capabilities of the fungus [189].

Consequently, mutants associated with the NO_2-induced resistance (*npr1, sid2, coi1, pmr4,* and *pad3)* were tested for the NO_2-mediated enhancement of callose deposition after chitosan elicitation. Besides the callose-deficient *pmr4*, all mutants were generally capable of depositing callose upon elicitation and/or NO_2 exposure (Figure 27). Except for *sid2,* all mutants were deficient in cultivating the NO_2-induced resistance, an observation which led to the conclusion that the NO_2-stimulated enhancement of callose upon elicitation was indispensable for resistance, rather than the callose induction upon NO_2 exposure *per se*. More importantly, the stimulatory effect of NO_2 on chitosan-elicited callose deposition was not detected in the *npr1*, *sid2*, or *coi1* mutants, which suggested that both SA and JA-signaling are important prerequisites for the early enhancement of callose, but not for the basal onset of its deposition.

The induction of callose synthesis is a complex process where the regulating pathways differ according to the perceived PAMP and the prevalent growth conditions. Thus, multiple signals are involved in the onset of callose deposition, rather than one conserved signaling pathway [192]. Therefore, defense hormones may have varying functions during the formation of callose in Arabidopsis. For instance, it was reported that exogenous application of SA or MeJA in the absence of the elicitor flagellin did not induce callose formation [193]. However, SA was reported to potentiate the flagellin-elicited callose formation in an NPR1-dependent manner [350]. The role of JA during callose deposition is similarly ambiguous. In the case of Arabidopsis, Garcia-Andrade *et al*. (2011) reported that basal callose deposition upon *B. cinerea* infection of WT was independent of COI1. However, they further claimed that the potentiated callose formation in the *B. cinerea*-resistant knock-out mutant of the transcription factor OCP3 necessitated functional COI1 [188]. These studies demonstrated that both SA- and JA- signaling are dispensable for basal callose deposition but are essential for an elicitor-triggered potentiation of callose upon pathogen infection. Analogous conclusions can be drawn for the NO_2-induced resistance against *B. cinerea* based on the aforementioned results.

Basal callose formation can by initiated via ROS and indole glucosinolates (IGs) in a hormone-independent manner. It was reported on several occasions that callose deposition is positively regulated by ROS accumulation, which is one of the first responses during the onset of PTI [192], [350]. Moreover, it is well established that IGs, such as breakdown products of methoxy-indol-3-

ylmethyl glucosinolate, induce flagellin-induced callose deposition independent of phytohormones [193], [194]. IGs are closely related to camalexin, as they largely share the same biosynthetic pathway and are known to be potent antimicrobial compounds, whose formation is induced during PTI [211], [268], [351], [352]. Since a multitude of IG-biosynthetic genes were up-regulated immediately after NO_2 fumigation (Supplemental Table 7), they may be involved in the basal callose deposition upon NO_2 exposure. Though camalexin and IGs share similar features, the unaffected deposition of callose upon flagellin-, chitosan-, or NO_2-treatment in the *pad3* mutant demonstrated that basal callose formation was not dependent on camalexin [193] (Figure 27). However, the lack of NO_2-stimulated callose potentiation upon elicitation in *pad3* may hint towards a PAD3-generated metabolite being involved in this process.

Taken together, these obtained results suggest that NO_2 triggers an early enhanced deposition of callose which facilitates the induced resistance against *B. cinerea*. Similar observations were made by Nie *et al*. (2017), who specified that the *B. cereus*-induced resistance against *B. cinerea* was conveyed by the early and enhanced production of ROS and callose [337]. In combination with published studies, the obtained data further suggests that the enhanced deposition of callose was dependent on PAD3, as well as functional SA- and JA-signaling pathways mediated by NPR1 and COI1, respectively [188], [350]. However, the data obtained while investigating the *sid2* mutant demonstrated that the NO_2-mediated potentiation of callose is likely not the sole catalyst of the NO_2-induced resistance. Despite lacking the enhanced callose formation, *sid2* was still capable of developing the NO_2-induced resistance against *B. cinerea*.

Moreover, NO_2 was demonstrated to cause a significantly enhanced deposition of callose 4 h after Col-0 plants were infected with *Pst.* DC3000 suggesting that similar mechanisms convey the NO_2-induced resistance against this pathogen as well. Therefore, it can be concluded that NO_2 stimulates a PTI-resembling basal defense response that ultimately leads to an accelerated augmentation of callose which protects the plant against *B. cinerea* and *P. syringae* in concert with other non-pathogen specific defense mechanisms.

3.2.7 Suggested model of the NO_2-induced signaling leading to induced resistance

The fact the NO_2 provides a general resistance against pathogens of different lifestyles – the necrotrophic fungus *B. cinerea* and the hemibiotrophic bacterium *P. syringae* strongly implies that NO_2 stimulates PTI. Upon exposure to NO_2, several events are likely to initiate signaling which ultimately leads to PTI and NO_2-induced pathogen resistance. First, the damaging effects of the

highly reactive radical NO_2 on the cell wall or membrane [347] may generate endogenous DAMPs, which are perceived by PRRs that subsequently launch PTI-triggering signals (Figure 32).

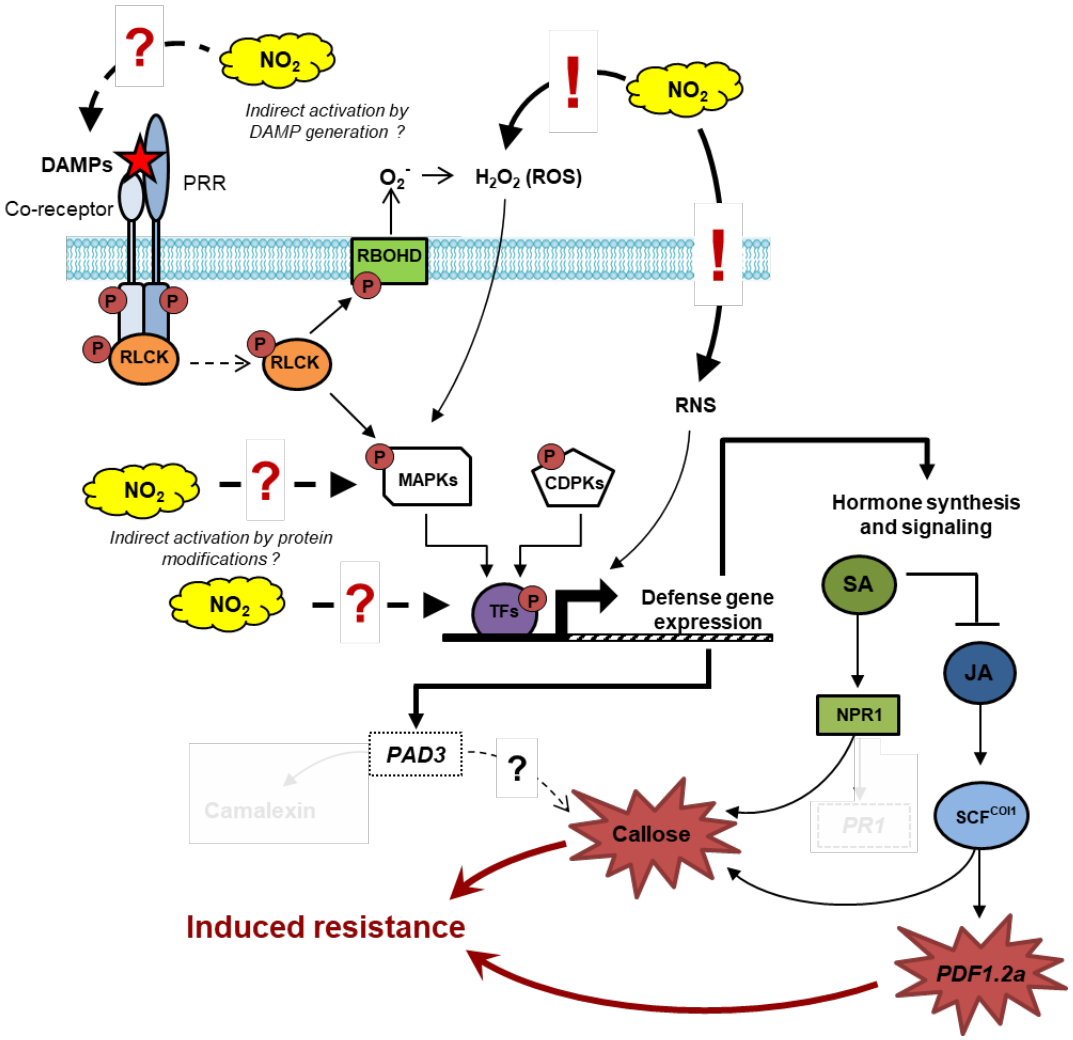

Figure 32: Working model of the establishment of the NO_2-induced resistance
The uptake of NO_2 leads to the formation of ROS, RNS, and protein modifications and potentially induces the generation of endogenous DAMPs. These signaling components and possibly NO_2 itself can initiate the activation of MAP kinase cascades and CDPKs either directly or indirectly via PRRs. These in turn, transmit the signaling to the nucleus via the activation of transcription factors (TFs). The activity of TFs can be modulated by protein modifications and via ROS or RNS accumulation. TFs then can initiate the expression and synthesis of defense-related compounds such as SA and JA or the camalexin biosynthetic enzyme PAD3. Camalexin itself, was determined to not be essential for the NO_2-induced resistance. In concert with *PAD3* gene expression, NPR1- and COI1-mediated SA- and JA signaling stimulate the early enhanced deposition of callose that contributes to the induced resistance. NO_2-induced JA signaling further promotes the enhanced expression of *PDF1.2a* upon *B. cinerea* infection. The expression of the SA-responsive *PR1* was not altered during the NO_2-induced resistance. DAMP = Damage associated molecular pattern, PRR = pattern recognition receptor, ROS = reactive oxygen species, RNS = reactive nitrogen species, MAPK = Mitogen-activated protein kinase, CDPK = Ca^{2+}dependent protein kinase, SA = salicylic acid, JA = jasmonic acid. Solid arrows = activation/accumulation, dashed arrows = hypothetical/ mechanism unclear. Masked (bleached) items were determined not to be involved in the NO_2-induced resistance against *B. cinerea*.

Secondly, NO_2 fumigation triggers the accumulation of signaling molecules such as ROS and NO and promotes signal-transmitting protein modifications like S-nitrosylation, all of which are well known to facilitate the propagation of the PTI response [116]–[119], [122], [123] [82], [83], [89]. Finally, NO_2 itself may function as a signaling molecule which stimulates PTI by activating downstream signaling [30].

PTI signaling after perception of a triggering stimulus include the activation of MAPK and CDPK cascades [124], [129] that transmit the signal to the nucleus by activating transcription factors or potentiate the initial signal e.g. by promoting ROS accumulation [125]–[127], [130]. It was demonstrated that NO_2 fumigation stimulates transcription of multiple players within the PTI signaling cascade (Supplemental Table 8), which emphasizes that this signaling network is utilized to induce the NO_2-induced resistance. By these means, NO_2 exposure initiates a rapid transcriptional reprogramming which stimulates a transient increase in SA. The brief peak in this phytohormone may facilitate further transcriptional changes such as the up-regulation of genes involved in jasmonate catabolism and signaling repression which lead to a net-zero turn-over rate of these phytohormones and ultimately results in the initial repression of jasmonate signaling (e.g. *PDF1.2a*). Moreover, the transient SA peak may stimulate the enhanced expression of camalexin biosynthetic genes (especially *PAD3*) [114]. Although suggested by the NO_2-induced up-regulation of the respective biosynthetic genes, the NO_2-induced resistance against *B. cinerea* was not facilitated by an enhanced or accelerated production of defense hormones or camalexin. Nonetheless, SA- and JA-signaling mediated by NPR1 and COI1, respectively, as well as PAD3 are essential for the NO_2-induced resistance, since their functionality is indispensable for the early enhanced deposition of callose which is assumed to convey the resistance against *B. cinerea*. Moreover, NO_2 promotes the enhanced expression of the antimicrobial JA-responsive plant defensin *PDF1.2a* which presumably contributes to the enhanced-resistance of NO_2-fumigated plants (for summary see Figure 32).

3.2.8 Is the NO_2-induced basal disease resistance a result of priming for PTI?

The effects of NO_2 on disease resistance fuel the hypothesis that NO_2 may function as a priming stimulus which triggers the plant into a state of alert that ultimately facilitates the acceleration and potentiation of defenses upon pathogen infection [223]. Commonly, a priming stimulus induces either no or only a slight and transient induction of defense responses [220]. The same phenomenon was observed after NO_2 fumigation. NO_2 exposure induced massive transcriptional reprogramming which should have promoted hormone synthesis and signaling - instead SA only increased transiently whereas JA did not accumulate at all. Moreover, the expression of defense-related and PR genes

was, at most, only slightly activated after NO_2 fumigation. Furthermore, the gene expression analysis demonstrated that NO_2-treatment had the capability to induce camalexin synthesis, which however was not implemented. Finally, exclusive NO_2 exposure only induced a negligible, basal deposition of callose which was only slightly above the methodical detection limit.

Another characteristic of defense priming is that primed plants can deploy more rapid and/or enhanced defenses upon perception of a challenging stimulus (e.g. pathogens) than naïve, unstimulated plants and are therefore more resistant to the stressor [220]. This was applicable for NO_2-treated plants. NO_2 treatment potentiated the transcription of the JA-responsive *PDF1.2a* upon *B. cinerea* infection and further facilitated the early enhanced deposition of callose which provided resistance against *B. cinerea* and *P. syringae*.

On the molecular level, it is assumed that a priming stimulus triggers the accumulation or transcription of defense signaling components, thereby promoting a more rapid activation of defense mechanisms that subsequently conveys the development of resistance [222], [223]. An enhanced transcription of defense-mediating genes was previously described for the priming agent BTH, as well as during *B. cereus*-induced *B. cinerea* resistance [224], [337]. Both treatments led to augmented levels of MAP kinase mRNA and proteins, and ultimately led to a greater abundance of active proteins upon pathogen challenge and enhanced disease resistance [224]. Since numerous players involved in PTI signaling, such as MAP kinases, Ca^{2+} dependent protein kinases, and transcription factors were up-regulated after NO_2 treatment, it is conceivable that the elevated abundance of their transcripts may contribute to a more rapid response against subsequent pathogen infection. Similarly, priming is associated with an increase in PRRs and their respective co-receptors which render the primed plant more sensitive to a following perception of PAMPs and DAMPs and therefore enhances the subsequent activation of defense signaling [223], [225]. An increase in mRNA levels of various PRRs was also detected after NO_2 treatment (Supplemental Table 8).

Taken in conjunction, the molecular processes initiated by NO_2 that facilitate a potentiation of callose deposition, PDF1.2a expression, and subsequent pathogen resistance resemble those observed during priming. However, stating that NO_2 is a priming agent is not recommended at this point, since the obtained results are suggestive. It must still be clarified if the NO_2-induced transcriptional alterations are actually translated to enhanced levels of physiologically active protein, which ultimately facilitate the NO_2-induced resistance.

4 Outlook

The ability of NO_2 to induce a broad range of effects on plants offers a multitude of possibilities to unravel and characterize their ornate signaling networks in more detail. By utilizing comparative transcriptional and proteome analysis alongside mutant screens, the molecular mechanisms of cell death and induced resistance triggered by NO_2 could further be clarified. Though this work expanded the understanding of the NO_2-induced signaling, many questions remain unsolved. First, it is still ambiguous how the plant perceives NO_2. During the NO_2-induced cell death, evidence accumulated that NO_2^- rather than NO_2 occupies a catalyzing role. However, this must still be reviewed for the induced resistance. Furthermore, the hypothesis that NO_2 generates endogenous DAMPs as well as NO_2 itself functioning as an endogenous signaling molecule in plants remains unsolved, due to the lack of accurate quantification methods for DAMPs [348], [349] or NO_2 *in vivo*.

NO_2 is one of the major man-made air pollutants which threatens human health and the environment, and has raised overt concern in public, media, and the government. The development of physical injuries in plants highly correlates with the concentration of NO_2 which they are exposed to. This provides the opportunity to use NO_2-sensitive species as bioindicators to monitor, assess, and potentially alert for harmful concentrations of NO_2 in highly polluted areas, as is already implemented for O_3 via the Bel-W3 tobacco variety [353], [354]. Moreover, it also may be worthwhile to investigate whether plants can be utilized to diminish the quantity of NO_2 in the air. It has been recently shown that plants are able to fix NO from ambient air [355]; therefore, they may also be capable of absorbing and purging the air of excess NO_2.

Finally, the ability of NO_2 to induce disease resistance against pathogens of different lifestyles which was outlined during this work, as well as observations made as a result of prior work indicate that exposure to low doses of NO_2 promote biomass formation and yield [45], [47], [48] may institute new research approaches for green house agriculture. Here, the potential identification of an NO_2-induced resistance in crop plants would be crucial. Moreover, it would be worthwhile to investigate whether the NO_2-induced resistance is effective against other pests and abiotic stresses. However, in order to utilize the beneficial effects of NO_2 in agriculture, its dose must be well adjusted, to ensure that the potential build-up of toxic metabolites and other negative effects are minimized.

In conclusion, this work demonstrates that NO_2 induces versatile signaling and effects in plants that suggest a regulatory role of NO_2 and its reaction products in plant defense. This provides new opportunities to unravel signaling pathways in plants as well as it enables new prospects in utilizing plants to counter environmental pollution or in establishing NO_2 in pest control management.

5 Material

5.1 Plant material

All experiments were performed with *Arabidopsis thaliana*. The utilized genotypes and their description and origin are summarized in Table 2.

Table 2: Plant material information

Line	Eco type	Gene Identifier	Sources	Reference	Description
Col-0			Lehle Seeds, (Round Rock, USA)		WT eco-type Columbia-0 (Col-0)
npr1	Col-0	AT1G64280	Xinnian Dong	[258]	Knock-out of *NONEXPRESSOR OF PR GENES 1*
sid2-1	Col-0	AT1G74710	Mikael Brosché	[245]	Knock-out of *SALICYLIC ACID INDUCTION DEFICIENT 2*
NahG	Col-0		Novartis AG (Basel, CHE)	[256], [257]	Transgenic Arabidopsis expressing the bacterial *nahG* gene encoding the salicylate 1-hydrolase for SA degradation
pad3	Col-0	AT3G26830	Own lab stock	[265]	Knock-out of *PHYTOALEXIN DEFICIENT 3*
pmr4-1	Col-0	AT4G03550	Nottingham Arabidopsis Stock Centre (NASC)	[356]	Knock-out of *POWDERY MILDEW RESISTANT 4* (NASC Number: N3858)
coi1-16	Col-0	AT2G39940	Mikael Brosché	[357]	Knock-out of *CORONATINE INSENSITIVE 1,* back-crossed with Col-0 to remove *glabra1* and *penetration2* background mutations

Line	Eco type	Gene Identifier	Sources	Reference	Description
jin1	Col-0	AT1G32640	Own lab stock	[157]	Knock-out of *JASMONATE INSENSITIVE 1*
Col-gl1	Col-0	AT3G27920	Mikael Brosché	[358]	Knock-out of *GLABRA 1* used as genetic background of *aos*
aos	Col-gl1	AT5G42650	Mikael Brosché	[254]	Knock-out of *ALLENE OXIDE SYNTHASE*
WS			Lehle Seeds, (Round Rock, USA)		WT eco-type Wassilewskija (WS)
opr3	WS	AT2G06050	John Browse	[255]	Knock-out of *OXOPHYTODIENOATE-REDUCTASE 3*

5.2 Pathogens

Pathogen stocks were maintained and provided by the group of Dr. Corina Vlot-Schuster (Institute of Biochemical Plant Pathology, Helmholtz-Zentrum Munich, Germany).

Table 3: Utilized Pathogens

Species	Strain	source
Botrytis cinerea	SAS 56	Vlot-Schuster group
Pseudomonas syringae	*pv tomato DC3000*	Vlot-Schuster group

5.3 Kits

Table 4: Purchased Kits

Kit	Company	Application
Nitrotyrosine Assay Kit, Chemiluminescence Detection, No. 17-10006	Merck Millipore, Darmstadt, DEU	Tyrosine nitration quantification
QuantiTect® Reverse	Qiagen GmbH, Hilden, DEU	cDNA synthesis

Kit	Company	Application
Transcription Kit, No. 205311		
RNase-free DNase Set, No. 79254	Qiagen GmbH, Hilden, DEU	gDNA digest
RNeasy® Mini Kit, No. 74104	Qiagen GmbH, Hilden, DEU	RNA purification
RNeasy® Plant Mini Kit, No. 74904	Qiagen GmbH, Hilden, DEU	RNA extraction
SensiMix™ SYBR® Low-ROX Kit, No. QT6250	Bioline, London, GBR	qPCR

5.4 Chemicals and enzymes

Commonly used chemicals not listed in Table 5 were purchased from Sigma-Aldrich (St. Luis, USA), Merck (Darmstadt, DEU), or Carl-Roth GmbH (Karlsruhe, DEU).

Table 5: Utilized chemicals and Enzymes

Chemical/ Enzyme	Company
15 % NO in N_2	Linde Group, Munich, DEU
cPTIO, No. C221 (2-(4-carboxyphenyl)-4,4,5,5-tetramethylimidazoline-1-oxyl-3-oxide)	Sigma-Aldrich, St. Luis, USA
2-DDG, No. D8375 (2-Deoxy-D-glucose)	Sigma-Aldrich, St. Luis, USA
DAB, No. D5637 (3,3'-diaminobenzidine tetrahydrochloride)	Sigma-Aldrich, St. Luis, USA
6x DNA Gel Loading Dye, No R0611	Thermo Fisher Scientific, Freiburg, DEU
BSA, No. 9048-46-8 (Bovine Serum Albumin – Albumin Bovine Fraction V)	Serva Electrophoresis GmbH, Heidelberg, DEU
Catalase from bovine liver, No. C9322	Sigma-Aldrich, St. Luis, USA
Chloral hydrate, No. 23100	Sigma-Aldrich, St. Luis, USA
DAF-FM DA, No. D9194 (Di-amino-fluorescein diacetate)	Sigma-Aldrich, St. Luis, USA
Medium molecular weight chitosan, No. 448877	Sigma-Aldrich, St. Luis, USA
Aniline Blue WS (Methyl Blue), No. M6900	Sigma-Aldrich,

Chemical/ Enzyme	Company
	St. Luis, USA
Protein Assay Dye Reagent Concentrate, No. 5000006	Bio-Rad, Munich, DEU
Silwet L-77, No. VIS-01	Lehle Seeds, Round Rock, USA
Sulfanilamide, No. S9251	Sigma-Aldrich, St. Luis, USA
Trypan Blue, No. 93590	Sigma-Aldrich, St. Luis, USA

5.5 Buffers and solutions

The components used to prepare buffers and solutions were purchased from Carl-Roth GmbH (Karlsruhe, DEU), Sigma-Aldrich (St. Luis, USA), and Merck (Darmstadt, DEU) if they were not explicitly listed in 5.4.

Table 6: Preparation of buffers and solutions

Buffer/ solution	Composition	Application
1x Phosphate buffered saline (PBS)	137 mM NaCl, 10 mM Na_2HPO_4, 2.7 mM KCl, 1.8 mM KH_2PO_4	Sample extraction from leaf material
Sulfanilamide solution	5 % sulfanilamide (w/v) in 1 M HCl	Nitrite scavenging (NO Analyzer)
Triiodide solution	325 mg I_2, 500 mg KI, 10 ml ddH_2O, 35 ml glacial acetic acid	NO Analyzer
VCl_3 solution	50 mM VCl_3 in 0.8 M HCl	NO Analyzer
K_2HPO_4 buffer	150 mM K_2HPO_4 in ddH_2O, pH 9.5	Callose quantification
Aniline Blue staining solution	0.01 % (w/v) Aniline Blue in K_2HPO_4 buffer, pH 9.5	Callose quantification
Alcoholic lactophenol-Trypan Blue solution	30 ml 96 % ethanol, 10 ml 90 % lactic acid, 10 ml glycerol, 9.43 ml phenol, 20 mg Trypan Blue, 10 ml ddH_2O	Trypan Blue cell death staining
MOCK	10 mM $MgCl_2$ in ddH_2O	*Pst* DC3000 infection
1x Tris-acetate-EDTA (TAE) buffer	40 mM Tris, 1mM EDTA, 0.1 % (v/v) glacial acetic acid	Gel electrophoresis

Buffer/ solution	Composition	Application
50 mM Potassium phosphate buffer	19.1 mM K_2HPO_4, 30.9 mM KH_2PO_4, pH 7	Buffer for catalase infiltration
DAB buffer	1 mg/ml DAB, 0.05 % (v/v) Tween 20 in ddH_2O, pH 3.8 (KOH)	H_2O_2 visualzation
DAF-FM DA buffer	5 µM DAF-FM DA, 0.05 % (v/v) Tween 20 in 0.1 % (v/v) DMSO	NO detection

5.6 Media

The media were consistently prepared with ddH_2O and autoclaved before use. The components used for media preparation were purchased from Sigma-Aldrich (St. Luis, USA), Merck (Darmstadt, DEU), and Becton Dickinson GmbH (Le Pont de Claix, FRA).

Table 7: Medium preparation

Medium	Composition	Application
Agar	0.8 % (w/v) agar in ddH_2O	Infection of detached leaves
NYGA	0.5 % (w/v) bactoprotease pepton 0.3 % (w/v) yeast extract 2 % (v/v) glycerol 1.8 % (w/v) agar	Cultivation of *Pst* DC3000
Oatmeal	2 % (w/v) oatmeal 1.5 % (w/v) agar	Cultivation of *B. cinerea*
Malt	3 % (w/v) malt extract 1.5 % (w/v) agar	Cultivation of *B. cinerea*

5.7 Antibiotics

Antibiotics were purchased from Duchefa Biochemie (Haarlem, NLD).

Table 8: Commonly used antibiotics

Antibiotic	Stock solution	Final concentration
Kanamycin (Kan), No. K0126-0025	50 mg/ml in ddH_2O	50 µg/ml
Rifampicin (Rif), No. R0146-0005	10 mg/ml in methanol	50 µg/ml

5.8 Oligonucleotides

The following primers for quantitative PCR were kindly provided by the group of Dr. Christian Lindermayr (1) and Dr. Anton Schäffner (2) from the Institute of Biochemical Plant Pathology, Helmholtz-Zentrum Munich, Germany. The oligonucleotides were purchased from Eurofins Genomics, Ebersberg, DEU.

Table 9: Primers used for quantitative PCR

name	Gene Identifier	orientation	Sequence 5' → 3'	source
UBC21	AT5G25760	Forward	CTGCGACTCAGGGAATCTTCTAA	1
		Reverse	TTGTGCCATTGAATTGAACCC	1
PDF2	AT1G13320	Forward	TAACGTGGCCAAAATGATGC	1
		Reverse	GTTCTCCACAACCGCTTGGT	1
ACTIN2	At3g18780	Forward	ACTTTCATCAGCCGTTTTGA	1
		Reverse	ACGATTGGTTGAATATCATCAG	1
TUB9	At4g20890	Forward	GTACCTTGAAGCTTGCTAATCCTA	2
		Reverse	GTCAAAGGTGCAAAACCAAC	2
S16	At5g18380	Forward	TTTACGCCATCCGTCAGAGTAT	2
		Reverse	TCTGGTAACGAGAACGAGCAC	2
PAD3	AT3G26830	Forward	TACTTGTTGAGATGGCATTGTTGAA	2
		Reverse	CTTCCTCCTGCTTCGCCAAT	2
PR1	AT2G14610	Forward	GTGCCAAAGTGAGGTGTAACAA	2
		Reverse	CGTGTGTATGCATGATCACATC	2
PDF1.2a	AT5G44420	Forward	CCAAGTGGGACATGGTCAG	2
		Reverse	ACTTGTGTGCTGGGAAGACA	2

5.9 Appliances

Table 10: Commonly used Appliances

Appliance	Type	Company
Camera	Nikon DC300	Minato, Tokyo, JPN
Microscope	TCS SP8 X confocal laser scanning microscope	Leica Microsystems GmbH, Wetzlar, DEU

Appliance	Type	Company
	Phase-contrast microscope	Carl Zeiss GmbH, Jena, DEU
Centrifuge	Centrifuge 4530 R/ Rotor FA-45-48-11	Eppendorf, Hamburg, DEU
	Mikro 220R / Rotor No. 1189-A	Hettich GmbH, Tuttlingen, DEU
	Qiagen Sigma 4K15C / 091000F-Rotor, 09366F-Swing Bucket	Sigma Laborzentrifugen GmH, Osterode, DEU
Spectrophotometer	Infinite M1000 Pro	Tecan Trading AG, Maennedorf, CHE
	NanoDrop ND-1000	NanoDrop Technologies, Freiburg, DEU
	Tecan GENios microplate reader	Tecan Trading AG, Maennedorf, CHE
	DU 640 Spectrophotometer	Beckman, Hamburg, DEU
Thermal cycler	T100 Thermal Cycler	Bio-Rad, Munich, DEU
Real time thermal cycler	Applied Biosystems 7500 Fast Real-Time PCR system (ABI 750 Fast)	Applied Biosystems, Freiburg, DEU
Homogenizer	Silamat S6	Ivoclar Vivadent, Ellwangen, DEU
NO Analyzer	Sievers Nitric Oxide Analyzer NOA 280i	Analytix Ltd, Boldon, GBR
	AC32M	Environnement S.A., Poissy, FRA
Conductivity meter	GLM 020A	Greisinger Electronic GmbH, Regenstauf, DEU
Stomatal conductance measurement	SC-1 Leaf Porometer	Decagon Devices Inc., Pullman, USA
Microarray analysis	8×60K custom Arabidopsis microarrays Design ID 29132, A-GEOD-16892 Low Input Quick Amp Labeling	Agilent Technologies, Santa Clara, USA

5.10 Web applications and software

Table 11: Used web applications and software

Software	Reference and Source	Application
Real-time PCR-Miner 4.0	[359] http://ewindup.info/miner/	qPCR data analysis
QuantPrime	[360] http://www.quantprime.de/	Primer design for qPCR
geNorm	[361]	Identification of reference genes for qPCR
Sequence Detection software 1.3.1	Applied Biosystems, Freiburg, DEU	qPCR amplification plot visualization and data collection
Sievers NO Analysis Software	Analytix Ltd, Boldon, GBR	Peak area integration during nitrite, nitrate, and SNO quantification
SigmaPlot 12.0	Systat Software, San Jose, USA	Statistical analysis and graph design
ImageJ 1.49m	Rasband, W.S., U.S. National Institutes of Health, Bethesda MD, USA, http://imagej.nih.gov/ij/	Picture analysis (necrotic area determination) and management (microscopy)
Arabidopsis Information Resource (TAIR)	[362] https://www.arabidopsis.org/	Database for genetic and molecular biology data of *Arabidopsis thaliana*
PANTHER 11.0	[363] http://pantherdb.org/	Gene Ontology (GO) Term Enrichment
REVIGO	[364] http://revigo.irb.hr/	Summary and visualization of GO Term enrichments
jvenn	[365] http://jvenn.toulouse.inra.fr/app/index.html	Venn diagram generation
ArrayExpress	[366] http://www.ebi.ac.uk/arrayexpress/	Publication of microarray data
PubMed	National Center of Biotechnology Information, U.S. National Library of Medicine, Bethesda MD, USA, https://www.ncbi.nlm.nih.gov/pubmed	Literature database

6 Methods

6.1 Plant treatments

6.1.1 Plant cultivation

Arabidopsis thaliana seeds were sown on a mixture of soil and sand in a 4:1 ratio and vernalized for two days at 4 °C in the dark before being transferred to long-day growth conditions (14 h light/10 h dark; 65-85 µmol m^{-2} sec^{-1} light intensity; 20°C day /18°C night; 65-68 % relative humidity). To ensure proper germination and growth, the plants were covered with a plastic foil for the first week after sowing, which was replaced with a plastic lid for the following two weeks. Plants were watered from the bottom up three times a week until they were utilized four to five weeks after sowing.

6.1.2 Fumigation of plants with NO_2

The fumigation of four to five-week-old plants with various concentrations of NO_2 (10, 20, 30 ppm) was performed as described in Kasten *et al*., 2016 [39]. In brief, all fumigations were carried out for one hour in an air-tight flow-through fumigation chamber where illumination and temperature were monitored. A schematic layout of the flow-through fumigation system is depicted in Figure 33.

To ensure a uniform fumigation the air-flow rate within the chamber was manipulated by adjustable inlet and outlet air flows (influx and efflux regulation). Here, Slight negative pressure was maintained in order to avoid inadvertent NOx reactions as air withdrawal from the chamber exceeded the air intake. For NO_2 fumigation, 15 % NO in N_2 was diverted to a mixing chamber containing Raschig glass rings where it reacted with 100 % O_2 to NO_2 before entering the fumigation chamber. The final NO_2 concentration within the chamber was monitored by branching off the outlet flow to an AC32M NO Analyzer (Environnement S.A.) when it exited the chamber. Adjustments to the gas concentrations within the chamber were done by regulating the volume of NO introduced to the system per time unit (ml NO/min) with a mass flow controller and by manipulating the overall flow rate within the system. The O_2 volumes were not altered.

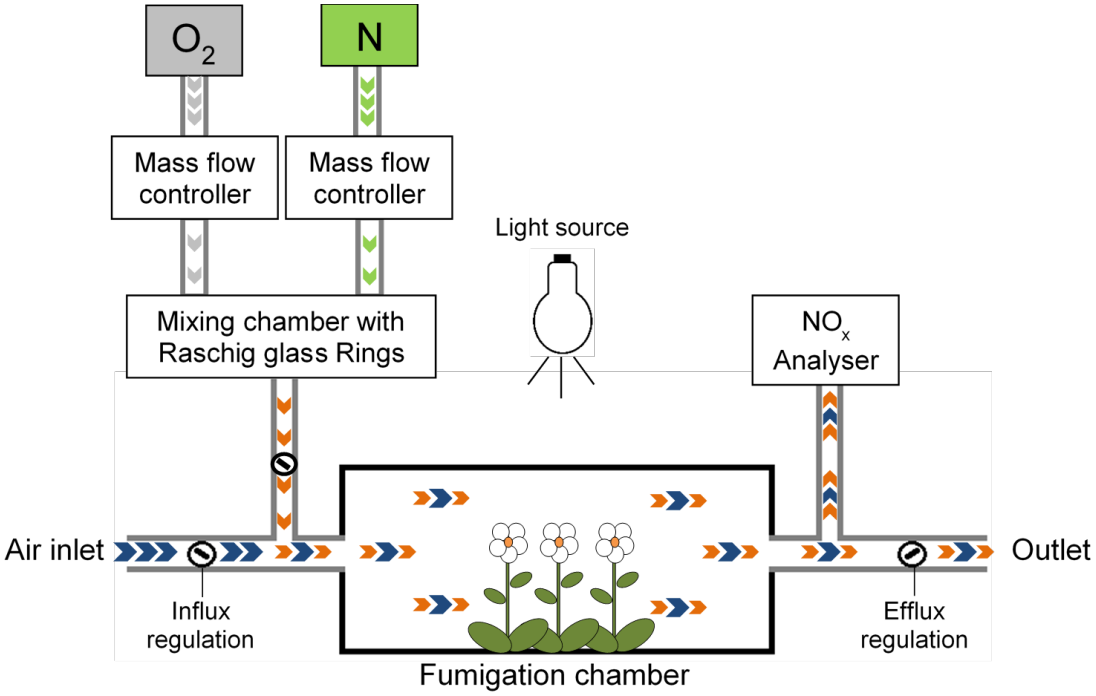

Figure 33: Schematic layout of the flow-through fumigation system
For NO_2 fumigation, NO and O_2, whose flow rates were defined by mass flow controllers, were introduced to a mixing chamber with Raschig glass rings to react to NO_2. The gas was then introduced to the air inlet flow that enters the fumigation chamber. To monitor the NO_x (NO and NO_2) within the fumigation chamber, part of the outlet flow was diverted to a NO_x analyzer. Arrows symbolize gas flow, NO: green; O_2: grey; NO_2: orange; Air: blue. Modified after Kasten *et al*., 2017 [380].

6.1.3 Nitrite infiltration

Four leaves of four-week-old Col-0 plants were infiltrated with 10 or 100 mM sodium nitrite ($NaNO_2$) or ddH_2O (negative control) from their abaxial side using a 1 ml needle-less syringe. After infiltration, the plants were kept in the climate chamber under long-day conditions until required for further experiments [39].

6.2 Cell death evaluation

6.2.1 Electrolyte leakage

Tissue damage was assessed via electrolyte leakage as described in Kasten *et al*., 2016 [39]. Whole plant rosettes were harvested, rinsed with ddH_2O, and incubated individually in 30 ml ddH_2O under gentle agitation at room temperature (RT). The water conductivity (µS/cm) was determined with a GLM 020A conductivity meter (Greisinger Electronic) after 0, 2, 4, 6, and 24 h. After capture of the

final measurement, the samples were frozen overnight at -20°C, followed by reheating to RT. The subsequent conductivity measurement of each sample was defined as 100 % electrolyte leakage and was used for normalization of the time course conductivities of the respective sample.

Plants fumigated with various concentrations of NO_2 or air as a control were used for electrolyte leakage immediately after fumigation, whereas plants infiltrated with $NaNO_2$ or ddH_2O were subjected to this method after air-drying for 1 h in the climate chamber.

6.2.2 Trypan Blue staining

Cell death was visualized histochemically 24 h after the various treatments by Trypan Blue staining as described by Joo *et al.,* 2005 [367] with slight modifications. Whole leaves were boiled for 1 min in an alcoholic lactophenol-Trypan Blue solution followed by an incubation for 1 h at RT and gentle agitation. The leaves were distained by boiling for 20 min in a chloral hydrate solution (2.5 g/ml in ddH_2O) using a water bath. The chloral hydrate solution was changed before the distaining continued at RT and gentle agitation until the leaves of the respective negative control treatments were fully distained. The leaves were mounted in 50 % glycerol and photographed with a Nikon DC300.

6.3 Pathogen infection

NO_2 fumigated plants were infected with pathogens exhibiting different lifestyles: the virulent hemi-biotrophic bacterium *Pseudomonas syringae pv. tomato* (*Pst*) DC3000 and the necrotrophic fungus *Botrytis cinerea*.

6.3.1 *Pseudomonas syringae pv. tomato* DC3000

Cultivation

Pst DC3000 was cultivated for two days at 28 °C on selective NYGA agar supplemented with the antibiotics rifampicin and kanamycin (50 µg/ml). For each experiment a new bacteria culture was prepared.

Infection method

Five-week-old plants that were fumigated with 10 ppm NO_2 (unfumigated plants as control) were inoculated 4 h after fumigation with 1 x 10^5 colony forming units per ml *Pst* DC3000 suspension (cfu/ml). To accomplish this, bacterial cells were scraped from the cultivation plate and resuspended in sterile 10 mM $MgCl_2$. The absorbance of the undiluted suspension was measured at a wavelength of 600 nm (OD_{600nm}) using a DU 640 spectrophotometer (Beckman). The suspension was diluted according to the assumption that a *Pst* DC3000 solution with an OD_{600nm} of 0.2 contains 1 x 10^8 cfu/ml [149]. Three to four leaves per plant were infiltrated with the bacterial suspension or 10 mM $MgCl_2$ (MOCK control) from their abaxial side using a 1 ml needle-less syringe. The inoculated plants were covered with a clear lid to ensure high humidity for proper infection while they were kept in the climate chamber under long-day conditions until required for further experiments.

Bacterial growth assay

The *Pst* DC3000 bacterial titer within the leaves was determined 2 h and 1 and 2 days after infection. 6 mm leaf discs were obtained at the required time points with a cork borer from each infected leaf. In case of the 2 h time point, the sample was surface sterilized for 30 s in 80 % ethanol. Three leaf discs from different plants were merged to one biological replicate and homogenized for 20 s in 200 µl 10 mM $MgCl_2$ using a Silamat S6 Tissue Homogenizer (Ivoclar Vivadent) and 1.7-2.0 mm glass beads. The resulting bacterial suspension was diluted in 10 mM $MgCl_2$ in a serial logarithmic dilution (10-fold) with a dilution factor range from 10^0 to 10^5. Subsequently, 20 µl of each dilution was spotted onto selective NYGA agar before incubating them for two days at 28 °C. Bacterial colonies were counted in spots containing between 10 and 100 colonies and the bacterial titer (cfu/cm^2) per biological replicate was calculated as follows:

$$cfu/cm^2 = colony\ count \times dilution\ factor \times \frac{V_{total}}{V_{spotted}} \times leaf\ disc\ factor$$

$$(with: V_{total} = 200\ \mu l;\ V_{spotted} = 20\ \mu l;\ leaf\ disc\ factor = 1.18\ cm^{-1})$$

6.3.2 *Botrytis cinerea*

Cultivation

B. cinerea (strain SAS 56) hyphae stored at –80 °C were cultivated on oatmeal-containing agar in the dark and at RT. After two weeks, an approximately 1 cm^2 piece of hyphae-containing agar was transferred onto malt agar and the incubation was continued until grey fungal spores emerged. These spores were transferred onto halves of canned apricots which were soaked for several hours

in ddH_2O to reduce their sugar content. After cultivating *B. cinerea* on the apricots for approximately one week, the spores were used for infection experiments. *B. cinerea* was continuously subcultured on apricots until their virulence began to reduce, then a new culture was started on oatmeal-containing agar and the process restarted.

Droplet-infection and necrotic lesion evaluation of detached leaves

Four-week-old plants of various genotypes were fumigated with 10 ppm NO_2 (unfumigated plants as control). *B. cinerea* spores were resuspended in ddH_2O and the number of spores in 1 µl was determined using a phase-contrast microscope (Zeiss) at 20x magnification (minimum spore number required: 200/µl). The spore suspension was then diluted 1:2 in sterile-filtered grape juice and the volume of the droplet necessary to infect a leaf with 1000 spores was calculated accordingly (maximum droplet volume = 10 µl). Leaves were harvested 6 h after fumigation and placed with their abaxial side down onto 0.8 % agar. The calculated volume of the *B. cinerea* spores in the half-strength grape juice was spotted onto the leaves, while avoiding the middle vein. The agar plates were sealed and incubated in the climate chamber under long-day conditions. After Three days the necrotic lesions were documented with a Nikon DC300 and their areas were determined via ImageJ (version 1.49m). Since the volume of the droplet containing the *B. cinerea* spores used for infection varied between individual experiments, the areas of the necrotic lesions developed on fumigated leaves were normalized to those formed on unfumigated leaves (= 100 %) for each individual experiment. Moreover, NO_2-treated and untreated WT plants were always included during the evaluation of mutants to assess the mutants' general susceptibility to *B. cinerea* and to verify the virulence of the fungus and the functionality of the assay during each individual experiment.

Spray infection of entire plants

Entire plants were infected with *B. cinerea* 6 h after fumigation with 10 ppm NO_2 (unfumigated or air fumigated plants as control) by spraying a half-strength grape juice suspension containing 2 x 10^5 fungal spores/ml and 0.01 % Silwet L-77 onto the plants until run-off. The *B. cinerea* spore suspension was prepared as described above. As a negative control, plants were sprayed with the half-strength grape juice suspension containing 0.01 % Silwet L-77 without fungal spores. The infected plants were covered with a clear lid to ensure high humidity for proper infection and kept in the climate chamber under long-day conditions until used for further experiments.

6.3.3 Chitosan elicitation

To mimic a fungal infection, plants were inoculated with the fungal elicitor chitosan 4 h after they had been fumigated with 10 ppm NO_2 (unfumigated plants as control). Here, three to four leaves per plant

were infiltrated from their abaxial side with 500 µg/ml medium molecular weight chitosan in 0.04 % acetic acid using a 1 ml needle-less syringe. As a negative control plants were treated with 0.04 % acetic acid. The treated plants were covered with a clear lid and were kept in the climate chamber under long-day conditions until required for further experiments.

6.4 Analytical techniques

6.4.1 Preparation of plant extracts

Approximately 100 mg of leaf material was harvested and frozen in liquid nitrogen either immediately after NO_2- or air-fumigation with various concentrations or 3 h after $NaNO_2$ (H_2O) infiltration. The samples were homogenized twice for 10 s using a Silamat S6 Tissue Homogenizer and 1.7-2.0 mm glass beads. The leaf material was incubated on ice for 10 min in 500 µl 1x phosphate-buffered saline (PBS). After centrifugation for 10 min at 14000 rpm, the supernatant was divided into aliquots for quantification of NO_2^-, NO_3^-, SNO, nTyr, and protein content.

6.4.2 Measurement of nitrite, nitrate, and S-nitrosothiol contents

The content of NO_2^-, NO_3^-, and SNO in leaves was determined using the Sievers Nitric Oxide Analyzer NOA 280i (Analytix Ltd.) as described in Kasten *et al*., 2016 [39]. Here, the leaf extract is injected into strongly-reducing reagents which convert the aforementioned compounds within the sample to NO. In turn, NO is oxidized by internally generated ozone resulting in NO_2 (excited state) and O_2. The emission of a photon when NO_2 relaxes to its ground state is detected by a photomultiplier resulting in quantifiable chemiluminescence peaks.

Endogenous NO_2^- was reduced to gaseous NO by injecting leaf extracts (see 6.4.1) into a reaction vessel containing a triiodide solution heated to 30 °C. In order to quantify SNO, endogenous NO_2^- was scavenged by adding 5 % sulfanilamide (w/v, in 1 M HCl) to the sample at a 1:9 dilution before injection into the triiodide solution. To determine the NO_3^- content in the leaf extract, its total nitrogen content was quantified using a 50 mM vanadium chloride (VCl_3) solution heated to 90 °C as the reducing agent. The nitrate content in the sample was then determined by subtracting the obtained NO_2^- and SNO content from the total amount of nitrogen. Chemiluminescence peak area integration was performed using the Sievers NO Analysis Software. SNO, NO_2^-, and NO_3^- concentrations were quantified using $NaNO_2$ and $NaNO_3$ calibration curves, respectively. The measured concentrations were normalized to the protein content in the examined leaf extracts.

6.4.3 Tyrosine nitration determination

Tyrosine nitration in plant extracts (see 6.4.1) was determined using a competitive enzyme-linked immunosorbent assay (ELISA) from Merck Millipore (Nitrotyrosine Assay Kit, Chemiluminescence Detection) and an Infinite M1000 Pro plate reader (Tecan Trading AG) according to the manufacturers' instructions. The nitrotyrosine content in the plant extracts was calculated from a generated calibration curve using nitrotyrosine peptide standards (0.1024 µM – 1600 µM) and correlated to the protein content in the leaf extracts.

6.4.4 Determination of protein concentration

The protein content of plant extracts (see 6.4.1) was determined using the Protein Assay Dye Reagent Concentrate (Bio-Rad) which is based on the Bradford method [368]. Briefly, 5 µl of plant extract were incubated with a 1:5 dilution of the Bradford reagent in a total volume of 1 ml. After incubation for 10 min at RT the absorbance at 595 nm was determined using the DU 640 spectrophotometer. The protein concentration of each sample was calculated from a standard curve that was recorded using various amounts of BSA (1 – 10 µg).

6.4.5 Phytohormone measurements via LC-MS/MS

To quantify phytohormones, approximately 250 mg leaf material (exact weight was recorded) of four-week-old Col-0 plants that were fumigated with NO_2 or air was harvested 0, 3, 6, and 24 h after fumigation. Similarly, leaf material from plants that were spray-infected with *B. cinerea* (see 6.3.2) 6 h after fumigation was collected 16, 24, and 48 h after infection. The samples were frozen in liquid nitrogen and kept at -80˚C until further use. The extraction of JA, OH-JA, *cis*-OPDA, JA-Ile, OH-JA-Ile, COOH-JA-Ile, and SA as well as the liquid chromatography-tandem mass spectrometry (LC-MS/MS) analyses were performed by Dr. Axel Mithöfer at the Max-Planck Institute for Chemical Ecology in Jena, Germany as described in Vadassery *et al.*, 2012 [369]. In brief, the LC-MS/MS analyses were performed with an Agilent 1200 HPLC system (Agilent, Waldbronn, DEU) and subsequent API 5000 tandem mass spectrometer (Applied Biosystems, Darmstadt, DEU) equipped with a Turbo spray ion source in negative ionization mode [369]. The elution profile from Vadassery *et al.*, 2012 [369] was changed to 0 - 0.5 min, 10% B; 0.5 - 4.0 min, 10 - 90% B; 4.0 - 4.02 min, 90 - 100% B; 4.02 - 4.5 min, 100% B and 4.41 - 7.0 min, 10% B at a flow rate of 1.1 ml/min. The amounts of the phytohormones were calculated relative to the signal of their respective internal standards [369] and correlated to the sample fresh weight.

6.4.6 Camalexin measurements via reverse-phase HPLC

Four-week-old Col-0 plants were fumigated with 10 ppm NO_2 or air and approximately 100 mg (exact weight was recorded) of leaf material was collected and frozen in liquid nitrogen 6 h after fumigation. Simultaneously, the remaining plants were spray-infected with *B. cinerea* (see 6.3.2) and harvested 24 and 48 h after infection as described above. Camalexin extraction and quantification was performed by Prof. Dr. Erich Glawischnig from the Technical University of Munich at the School of Life Sciences Weihenstephan in Freising, Germany. The procedures were done as previously described, but with slight modifications [269], [270], [275]. In brief, the obtained leaf material was extracted twice for 30 min in 200 µl of a 4:1 (v/v) dilution of MeOH in H_2O at 65°C. Afterwards, the extracts were combined and centrifuged for 15 min at 17,000 g. The samples were then analyzed via reverse-phase high performance liquid chromatography, (HPLC, LiChroCART 250-4, RP-18, 5 µm, Merck) using a flow rate of 1 $mL \cdot min^{-1}$ and the following elution profile: MeOH/H_2O (1:1; v/v) for 2 min, followed by a 10 min linear gradient to 100% MeOH and subsequent 3 min 100% MeOH. The quantification of camalexin was done using a Shimadzu F-10AXL fluorescence detector (318 nm excitation/370 nm emission) and via UV absorption at 318 nm using a calibration curve generated from an authentic standard.

6.5 Staining

6.5.1 Detection of intracellular NO

Intracellular NO was detected using DAF-FM DA as described in Kasten *et al.*, 2016 [39]. This cell-permeable fluorescent probe is diacetylated to DAF-FM within the cell where it reacts with NO to form a fluorescent benzotriazole [370]–[372].

Leaves of four-week-old Col-0 plants were infiltrated with 5 µM DAF-FM DA in 0.1 % DMSO and 0.05% Tween 20 using a 1 ml syringe without a needle. After air-drying for 1 h in the climate chamber, the infiltrated plants were fumigated with NO_2 (10, 20, or 30 ppm) or air as described in 6.1.2. Immediately after fumigation, 6 mm leaf discs were obtained using a cork borer. The leaf discs were placed with the abaxial side up into wells of a black flat-bottom 96-well plate containing 50 µl ddH_2O. The fluorescence was measured at 485 nm excitation and 535 nm emission using a Tecan GENios microplate reader (Tecan Trading AG). The average fluorescence value of leaf discs infiltrated with 0.1% DMSO containing 0.05 % Tween 20 (negative control) was subtracted from the sample readings. To ensure the specificity of the fluorescent probe to NO, leaves were infiltrated with 500 µM of the NO scavenger cPTIO alongside DAF-FM DA.

In other experiments 5 µM DAF-FM DA in 0.1 % DMSO and 0.05 % Tween 20 with or without 500 µM cPTIO was co-infiltrated with 10 or 100 mM $NaNO_2$ (see 6.1.3). Here, leaf discs were obtained 1 h after infiltration and the NO content was measured as described above.

6.5.2 Visualization of H_2O_2 production

Hydrogen peroxide (H_2O_2) generation in leaves was visualized using DAB, which is oxidized to a brown precipitate by H_2O_2 in the presence of peroxidases [373]. The procedure was modified from Ramel *et al.*, 2009 [374] and described in Kasten *et al.*, 2016 [39]. Briefly, leaves of four-week-old plants were detached immediately after fumigation with various concentrations of NO_2, or air, or 3 h after $NaNO_2$ infiltration (see 6.1.2 and 6.1.3). The leaves were subsequently vacuum-infiltrated with 1 mg/ml DAB in ddH_2O (pH 3.8, KOH) containing 0.05 % Tween 20 and incubated for 45 min in the climate chamber. After rinsing with ddH_2O the leaves were incubated in 96 % ethanol in a water bath at 80 °C until all chlorophyll was removed. Finally, the leaves were mounted in 50 % glycerol and documented with a Nikon DC300. To confirm the H_2O_2 specificity of the DAB staining, plants were infiltrated with 100 U/ml catalase in 0.38 M potassium phosphate buffer (pH 7). After air-drying the plants for 1 h in the climate chamber, they were fumigated with 30 ppm NO_2 and stained as described above.

6.5.3 Callose quantification

Callose staining and quantification was done with five-week-old NO_2-fumigated Col-0 and *pmr4* plants 4 h after they have been syringe-infiltrated with *Pst* DC3000 (see 6.3.1). Moreover, four to-five-week-old plants of various genotypes were elicited with chitosan (6.3.3) 4 h after NO_2 treatment before subjecting them to the callose staining 4 h after the elicitation (additional 16 and 24 h time point for Col-0 and *pmr4*).

Leaf discs (6 mm) were obtained from treated leaves with a cork borer at the indicated time points and incubated overnight in 96 % ethanol to remove chlorophyll. The distained leaf discs were gently dried off with paper towels and then incubated for 1 h in 150 mM K_2HPO_4 buffer (pH 9.5) at RT and mild agitation. Meanwhile, a 0.01 % Aniline Blue staining solution was prepared and stirred until decolorized, while protecting it from light. The samples were stained overnight in the dark at RT and gentle agitation. After rinsing the leaf discs in the K_2HPO_4 buffer, they were transferred into wells of a black flat-bottom 96-well plate containing 50 µl of the same buffer. Callose was quantified by measuring the Aniline Blue fluorescence (mean of nine reads per leaf disc) with the Infinite M1000 Pro plate reader after adjusting the Z-positioning of the fluorescence top optics. Aniline Blue

fluorescence was excited with 405 nm (5 nm bandwidth of the excitation monochromator) and the emission wavelength was set to 490 nm (bandwidth of the emission monochromator: 20 nm). To minimize noise of potential autofluorescence, the fluorescence of leaf discs which were incubated overnight in 150 mM K_2HPO_4 buffer (pH 9.5) without Aniline Blue, was subtracted from the values of stained samples for each treatment.

6.5.4 Confocal microscopy of callose depositions

Leaf discs of treated plant were stained with Aniline Blue as described above (6.5.3), mounted in 50 % glycerol on a microscope slide with a coverslip, and analyzed for callose depositions with the TCS SP8 X confocal laser scanning microscope (Leica) using the HC PL APO CS2 20x/0.75 IMM objective. The samples were excited with a Diode 405 Laser (Laser line UV 405 nm) at 0.1 % laser intensity. The emitted fluorescence was detected with a photomultiplier (PMT) at 480 – 500 nm (gain 800), whereas bright field pictures were taken at gain 400 using the Transmission PMT.

6.6 Molecular biological methods

6.6.1 RNA extraction and cDNA synthesis

RNA was isolated from approximately 100 mg leaf material which was frozen in liquid nitrogen immediately after obtaining the samples and homogenized twice for 10 s using a Silamat S6 Tissue Homogenizer and 1.7-2.0 mm glass beads. RNA extraction was performed using the RNeasy® Plant Mini Kit (Qiagen) according to the manufacturers' instructions. The concentration and purity of the obtained RNA was estimated spectrophotometrically using the NanoDrop ND-1000 (NanoDrop Technologies). Samples which did not fulfill the aspired spectrophotometric ratios (A260/230 = 1.8 – 2.2; A260/280 = 2.0 - 2.2) were subjected to the RNA Clean Up Protocol of the RNeasy® Mini Kit (Qiagen). RNA integrity and purity were additionally confirmed via agarose gel electrophoresis (6.6.2). Reverse transcription of 1 µg total RNA to cDNA was performed using the QuantiTect® Reverse Transcription Kit (Qiagen) according to the manufacturers' instructions.

6.6.2 Agarose gel electrophoresis

To separate RNA, 1.5 % agarose gels were prepared (1.5 g agarose in 100 ml 1x TAE buffer) and supplemented with ethidium bromide. 1 µg RNA in 10 µl RNase-free H_2O and 2 µl 6x loading dye

was loaded and the gel was run in a gel electrophoresis unit at 120 V for approximately 30 min. The separated RNA was visualized with the Gel DOC 200 (Bio-Rad).

6.6.3 Quantitative Polymerase Chain Reaction (qPCR)

qPCR performance

Generated cDNA (6.6.1) was diluted 1:16 in ddH_2O prior to qPCR, which was performed according to the manufacturers' instructions of the SensiMix™ SYBR® Low-ROX Kit (Bioline). The qPCR reactions were prepared in a system-suitable 96-well plate that was then sealed and centrifuged for 1 min at 3500 rpm. Subsequently, the qPCR was started in an Applied Biosystems 7500 Fast Real-Time PCR system (Applied Biosystems) using the following conditions: 1 cycle at 95°C for 15 min; 40 cycles of 95°C for 15 sec, 60°C for 30 sec, 72°C for 45 sec. If primer pairs were used for the first time, a dissociation curve was recorded after the qPCR was finished to exclude primer dimerization (1 cycle of 95°C for 15 sec, 60°C for 1 min, 95°C for 15 sec).

qPCR data analysis

Data analysis was performed using the Real-Time PCR-Miner 4.0 application [359] to obtain the weighted average efficiency and the number of PCR cycles required for crossing the threshold (CT) for each reaction. The weighted average efficiencies of each reaction for a single primer pair were averaged to give the average efficiency (E) for each primer pair. The efficiency corrected CT values $(1 + E^{-CT})$ of the genes of interest were then normalized to the geometric mean of those obtained for the reference genes giving the relative transcription levels of the genes of interest.

Selection of suitable reference genes

To identify suitable reference genes whose transcriptions were unaffected by the various applied plant treatments, cDNA from NO_2-fumigated, *B. cinerea* spray-infected Col-0 plants (see 6.3.2) and their respective control samples were subjected to qPCR using primer pairs for various reference genes. Their non-normalized expression levels were processed via the geNorm extension for Microsoft Excel [361]. This application calculates the internal reference gene-stability measure (M) which identifies the most stably expressed reference genes among treatments [361]. For qPCR analysis of NO_2-fumigated, *B. cinerea*-infected plants *UBC21* (M = 0.182), *PDF2* (M = 0.182), and *ACTIN2* (M = 0.038) were chosen as reference genes. In other experiments, *TUB9* or *S16* were used as reference genes after it was ensured that their amplification plots were not varying among the treatments.

6.6.4 Expression profile generation via microarray analysis

Sample preparation and microarray performance

Four-week-old Arabidopsis Col-0 plants were fumigated with 10 ppm NO_2 or air. Approximately 50 mg of leaf material was harvested immediately (0 h) and 6 h after fumigation and frozen in liquid nitrogen. The samples were homogenized twice for 10 s using a Silamat S6 Tissue Homogenizer and 1.7-2.0 mm glass beads. RNA was extracted with the RNeasy® Plant Mini Kit (Qiagen) as described in 6.6.1, with the exception that a digest of any potentially remaining DNA was included, using the RNase-free DNase Set for on-column DNA digestion (Qiagen) according to the RNeasy® Plant Mini Kit protocol. The RNA integrity was confirmed via agarose gel electrophoresis (6.6.2).

The gene expression analysis was kindly performed by Claudia Knappe (Institute of Biochemical Plant Pathology, Helmholtz-Zentrum Munich, Germany) using Agilent At860K one-color microarrays (Design ID: 29132, A-GEOD-16892) according to the manufacturers' One-Color Microarray-Based Gene Expression Analysis protocol for low input quick Amp labeling. After 17 h hybridization at 65 °C and washing, slides were scanned using the Agilent Microarray Scanner and data was extracted using the Agilent Feature Extraction Software with the template GE1_1010_Sep11.

Data evaluation and analysis

Preprocessing of the data was kindly performed by Dr. Elisabeth Georgii (Institute of Biochemical Plant Pathology, Helmholtz-Zentrum Munich, Germany). The data preprocessing was done with the Bioconductor 2.13 software package limma, version 3.18.13 [375] and included background correction, quantile normalization, $\log_2$ transformation, and averaging across probes of the same gene according to the TAIR10 genome annotation [232]. The differential expression analysis was also conducted with the limma package considering two factors (time and treatment) and a nested interaction formula [376], [377]. Genes with adjusted p-values < 0.05 (based on the false discovery rate method for adjustment) and absolute $\log_2$ fold changes > 1 or < -1 were selected for further analysis. The differential expressions of processed data sets were visualized via volcano plots generated by SigmaPlot 12.0 (Systat Software) and Venn diagrams created with jvenn [365].

Annotated gene sets which were differentially expressed in air and NO_2-treated samples were selected according to their adjusted p-value ($p < 0.05$) and their $\log_2$ fold changes ($\log_2(FC) < -1$ or > 1) and were subjected to GO-Term enrichment analysis. This was done with PANTHER 11.0 using the PANTHER overrepresentation Test (release date: 2016-07-15) [363]. The gene sets were annotated and categorized to GO terms using the GO Ontology database (release date: 2016-12-28) and compared to a reference list of the PANTHER database for *Arabidopsis thaliana*. The overrepresentation test included Bonferroni correction for multiple testing and compared

classifications of multiple clusters of the given gene list to the reference list in order to statistically determine over- or under-representation of the classification categories using the binomial test for each gene ontology [378]. The obtained enriched GO terms ($p < 0.05$) were visualized in semantic similarity-based scatterplots generated with the REVIGO tool [364].

6.7 Pharmacological manipulation

6.7.1 Pharmacological cell death manipulation

Four leaves of four-week-old Col-0 plants were infiltrated from the abaxial side with either 500 µM cPTIO, ddH_2O (control), 100 U/ml catalase in 0.38 M potassium phosphate buffer pH 7, or phosphate buffer alone (control) using a 1 ml needle-less syringe. After air-drying for 30 min in the climate chamber under long-day conditions, the plants were fumigated with 30 ppm NO_2 for 1 h, followed by immediate electrolyte leakage measurements (see 6.2.1).

6.7.2 Callose synthesis inhibition via 2-Deoxy-D-glucose

Leaves of four-week-old Col-0 plants were syringe-infiltrated with 1.2 mM of the callose synthesis inhibitor 2-deoxy-D-glucose (2-DDG) or ddH_2O 24 h before fumigation with 10 ppm NO_2 (unfumigated as control) [279]. Six hours after fumigation the infiltrated leaves were detached, placed on 0.8 % agar, droplet-infected with *B. cinerea* and the necrotic lesions were analyzed after three days as described in section 6.3.2. The necrotic areas were compared to those formed on unfumigated and non-infiltrated leaves (= 100 %).

6.8 Statistical analysis

Data that was obtained from experiments with only one variable parameter (e.g. fumigation) was analyzed using unifactorial statistical analysis. When comparing only two independent groups, the Student's t-test was used, in cases where the Shapiro-Wilk normality test ($p > 0.05$) was passed. If the normality test failed, the analysis was done with the non-parametric Mann-Whitney rank Sum Test. The comparison of more than two independent groups that were passing the Shapiro-Wilk normality test ($p > 0.05$) was done by One-Way ANOVA and subsequent Holm-Sidak post-hoc test for all pairwise comparisons (indicated with letters) or comparisons against a control group. When the normality assumption of ANOVA failed on original or log-transformed data (Shapiro-Wilk test), the

non-parametric Kruskal-Wallis test with subsequent Dunn's Method post-hoc test was performed to test for differences between the groups.

Data that was obtained from experiments with two or three independent variables (fumigation, infection, and genotype) were analyzed using multifactorial statistical analysis. Here, Two- and Three-Way ANOVA was used to investigate relationships among these independent variables and their influence upon the investigated dependent variable. Unfortunately, the data analyzed with these parametric methods often failed the normality assumption. While the advantages of non-parametric statistical methods are acknowledged and understood, the requisite multifactorial analysis techniques are complex and not widely available for non-parametric data [379]. Therefore, the aforementioned non-parametric unifactorial Kruskal-Wallis test and Dunn's Method for all pairwise comparisons was performed in addition to the multifactorial ANOVA, even though it forgoes the examination of interaction effects [379]. All statistical analyses were conducted using SigmaPlot 12.0 (Systat Software).

In case of the cell death data presented here that was already published in Kasten *et al.*, 2016 [39] the statistical analysis of data that failed the normality assumption was performed by Dr. Elisabeth Georgii (Institute of Biochemical Plant Pathology, Helmholtz-Zentrum München,Germany) Here, the non-parametric Kruskal-Wallis test using Wilcoxon tests with FDR correction for post-hoc analysis was performed via R version 3.0.3. Statistical significances were indicated with asterisks (***$p < 0.001$, **$p < 0.01$, *$p < 0.05$).

7 References

[1] Y. Wang, G. J. Loake, and C. Chu, “Cross-talk of nitric oxide and reactive oxygen species in plant programed cell death.,” *Front. Plant Sci.*, vol. 4, no. August, p. 314, 2013.

[2] C. Scheler, J. Durner, and J. Astier, “Nitric oxide and reactive oxygen species in plant biotic interactions,” *Curr. Opin. Plant Biol.*, vol. 16, no. 4, pp. 534–539, 2013.

[3] A. Molassiotis and V. Fotopoulos, “Oxidative and nitrosative signaling in plants: two branches in the same tree?,” *Plant Signal. Behav.*, vol. 6, no. 2, pp. 210–214, 2011.

[4] A. J. Zeevaart, “Some effects of fumigating plants for short periods with NO2,” *Environ. Pollut.*, vol. 11, no. 2, pp. 97–108, 1976.

[5] O. C. Taylor and F. M. Eaton, “Suppression of plant growth by nitrogen dioxide.,” *Plant Physiol.*, vol. 41, no. 1, pp. 132–135, 1966.

[6] K. Okano and T. Totsuka, “Absorption of Nitrogen-Dioxide by Sunflower Plants Grown at Various Levels of Nitrate,” *New Phytol.*, vol. 102, no. 4, pp. 551–562, 1986.

[7] M. Takahashi, D. Konaka, A. Sakamoto, and H. Morikawa, “Nocturnal uptake and assimilation of nitrogen dioxide by C3 and CAM plants,” *Zeitschrift fur Naturforsch. - Sect. C J. Biosci.*, vol. 60, no. 3–4, pp. 279–284, 2005.

[8] Y. Hu, V. Fernández, and L. Ma, “Nitrate transporters in leaves and their potential roles in foliar uptake of nitrogen dioxide.,” *Front. Plant Sci.*, vol. 5, no. July, p. 360, 2014.

[9] A. Altshuller, “Thermodynamic considerations in the interactions of nitrogen oxides and oxy-acids in the atmosphere,” *J. Air Pollut. Control Assoc.*, vol. 6, pp. 97–100, 1956.

[10] World Health Organization and UNAIDS, *Air quality guidelines: global update 2005, Particulate matter, ozone, nitrogen dioxide and sulfur dioxide*. Copenhagen: World Health Organization, 2006.

[11] D. Jarvis, G. Adamkiewicz, M.-E. Heroux, R. Rapp, and F. Kelly, *WHO Guidelines for Indoor Air Quality: Selected Pollutants.* Geneva: World Health Organization, 2010.

[12] A. Schindlbacher and Zechmeister-Boltenstern, “Effects of soil moisture and temperature on NO, NO2 , and N2O emissions from European forest soils,” *J. Geophys. Res.*, vol. 109, no. D17, p. doi:10.1029/2004JD004590, 2004.

[13] L. Klepper, “Nitric oxide (NO) and nitrogen dioxide (NO2) emissions from herbicide-treated soybean plants,” *Atmos. Environ.*, vol. 13, pp. 537–542, 1979.

[14] M. Berglund, “Health risk evaluation of nitrogen oxides.,” *Scand. J. Work. Environ. Heal.*, vol. 19, 1993.

[15] “Urban air quality in the United Kingdom.,” Quality of urban air review group, Department of the Environment, London, 1993.

[16] A. Hickman, M. Bevan, and D. Colwill, *Atmospheric pollution from vehicle emissions at four sites in Coventry (Report No. CR 695)*. Crowthorne: Department of the Environment, Transport and Road Research Laboratory, 1976.

[17] U. Gehring *et al.*, “Traffic-related air pollution and respiratory health during the first 2 yrs of life,” *Eur. Respir. J.*, vol. 19, no. 4, pp. 690–698, 2002.

[18] J. James Gauderman, W., Avol, E., Gilliland, MF., Vora, H., Thomas, D., Berhane, K., McConnell, R., Kuenzli, N., Lurmann, F., Rappaport, E., Margolis, H., Bates, D & Peters, “The Effect of Air Pollution on Lung Development from 10 to 18 Years of Age,” *N Engl J Med*, no. 351, pp. 1057–1067, 2004.

[19] S. Esposito *et al.*, “Impact of air pollution on respiratory diseases in children with recurrent wheezing or asthma,” *BMC Pulm. Med.*, vol. 14, no. 1, p. 130, 2014.

[20] W. James Gauderman *et al.*, “Association between air pollution and lung function growth in Southern California children: Results from a second cohort,” *Am. J. Respir. Crit. Care Med.*, vol. 166, no. 1, pp. 76–84, 2002.

[21] S. Madronisch, *The Role of the Stratosphere in Global Change. Vol. 18. NATO-ASI Series*, vol. 18. Amsterdam: Springer-Verlag, 1993.

[22] World Health Organization (WHO), “WHO Air quality guidelines for particulate matter, ozone, nitrogen dioxide and sulfur dioxide: global update 2005: summary of risk assessment.,” WHO Press, Geneva, 2006.

[23] G. E. Southon, C. Field, S. J. M. Caporn, A. J. Britton, and S. A. Power, “Nitrogen Deposition Reduces Plant Diversity and Alters Ecosystem Functioning: Field-Scale Evidence from a Nationwide Survey of UK Heathlands,” *PLoS One*, vol. 8, no. 4, pp. 1–12, 2013.

[24] A. G. Jones and S. A. Power, “Field-scale evaluation of effects of nitrogen deposition on the functioning of heathland ecosystems,” *J. Ecol.*, vol. 100, no. 2, pp. 331–342, 2012.

[25] P. Angold, “The impact of a road upon adjacent heathland vegetation: effects on plant species composition,” *J. Appl. Ecol.*, vol. 34, pp. 409–417, 1997.

[26] M. Bernhardt-Römermann, M. Kirchner, T. Kudernatsch, G. Jakobi, and A. Fischer, “Changed vegetation composition in coniferous forests near to motorways in Southern Germany: The effects of traffic-born pollution,” *Environ. Pollut.*, vol. 143, no. 3, pp. 572–581, 2006.

[27] K. L. Bignal, M. R. Ashmore, A. D. Headley, K. Stewart, and K. Weigert, “Ecological impacts of air pollution from road transport on local vegetation,” *Appl. Geochemistry*, vol. 22, no. 6, pp. 1265–1271, 2007.

[28] Umweltbundesamt, “Air quality 2016: Nitrogen dioxide still the top pollutant.” p. Press release No.4/2017, 31.01.2017.

[29] W. Heck and D. Tingey, “Nitrogen dioxide: Time-concentration Model to predict acute foliar injury. report No: EPA-600/3-79-057,” U.S. Environmental Protection Agency, Washington, D.C., EPA/600/3-79/057 (NTIS PB299218), Springfield, 1979.

[30] M. Takahashi and H. Morikawa, “Nitrogen dioxide is a positive regulator of plant growth,” *Plant Signal. Behav.*, vol. 9, no. e28033, pp. 8–11, 2014.

[31] X. Liu, F. Hou, G. Li, and N. Sang, “Effects of nitrogen dioxide and its acid mist on reactive oxygen species production and antioxidant enzyme activity in Arabidopsis plants,” *J. Environ. Sci.*, vol. 34, pp. 93–99, 2015.

[32] C. Thompson, E. Hensel, G. Kats, and O. Taylor, “Effects of continuous exposure of navel oranges to nitrogen dioxide,” *Atmos*, vol. 4, pp. 349–355, 1970.

[33] Z. Chen, Y. Chen, G. Du, X. Wu, and F. Li, “Effects of 60-day NO2 fumigation on growth, oxidative stress and antioxidative response in Cinnamomum camphora seedlings,” *J. Zhejiang Univ. B (Biomed Biotechnol)*, vol. 11, no. 3, pp. 190–199, 2010.

[34] S. Schwartz and W. White, “Kinetics of reactive dissolution of nitrogen oxide in aqueous solution.,” *Adv. Environ. Sci. Teh.*, vol. 12, pp. 1–16, 1983.
[35] O. Augusto, M. G. Bonini, A. M. Amanso, E. Linares, C. C. X. Santos, and S. L. De Menezes, “Nitrogen dioxide and carbonate radical anion: two emerging radicals in biology,” *Free Radic. Biol. Med.*, vol. 32, no. 9, pp. 841–859, 2002.
[36] L. Beevers and R. H. Hageman, “Nitrate reduction in higher plants,” *Annu. Rev. Plant Physiol.*, vol. 20, no. 1, pp. 495–522, 1969.
[37] N. M. Crawford, “Nitrate: nutrient and signal for plant growth.,” *Plant Cell*, vol. 7, pp. 859–868, 1995.
[38] Z. Qiao and F. Murray, “The effects of NO2 on the uptake and assimilation of nitrate by soybean plants,” *Environ. Exp. Bot.*, vol. 39, no. 1, pp. 33–40, 1998.
[39] D. Kasten, A. Mithöfer, E. Georgii, H. Lang, J. Durner, and F. Gaupels, “Nitrite is the driver, phytohormones are modulators while NO and H2O2 act as promoters of NO2 -induced cell death,” *J. Exp. Bot.*, vol. 67, no. 22, pp. 6337–6349, 2016.
[40] K. Shimazaki, S. Yu, T. Sakaki, and K. Tanaka, “Differences between Spinach and Kidney Bean Plants in Terms of Sensitivity to Fumigation with NO2,” *Plant Cell Physiol.*, vol. 33, no. 3, pp. 267–273, 1992.
[41] X. Liu, F. Hou, G. Li, and N. Sang, “Effects of nitrogen dioxide and its acid mist on reactive oxygen species production and antioxidant enzyme activity in Arabidopsis plants,” *J. Environ. Sci.*, vol. 34, pp. 93–99, 2015.
[42] A. Hill and J. Bennett, “Inhibition of Apparent Photosynthesis by Nitrogen Oxides,” *Atmos. Environ.*, vol. 4, pp. 341–348, 1970.
[43] P. Purczeld, C. Chon, A. Portis Jr., H. Heldt, and U. Heber, “The mechanism of the control of Carbon fixation by the pH in the Chloroplast stroma - Studies with Nitrte-mediated proton transfer across the envelope,” *Biochim. Biophys. Acta*, vol. 501, pp. 488–498, 1978.
[44] S. Sabaratnam, G. Gupta, and C. Mulchi, “Effects of nitrogen dioxide on leaf chlorophyll and nitrogen content of soybean,” *Environ. Pollut.*, vol. 51, no. 2, pp. 113–120, 1988.
[45] F. H. F. G. Spierings, “Influence of fumigations with NO2 on growth and yield of tomato plants,” *Netherlands J. Plant Pathol.*, vol. 77, no. 6, pp. 194–200, 1971.
[46] N. Faller, “Schwefeldioxid, Schwefelwasserstoff, nitrose Gase und Ammoniak als ausschliessliche S- bzw. N-Qellen der hoheren Pflanze,” *Zeitschrift für Pflanzenernährung und Bodenkd.*, vol. 131, no. 2, pp. 120–130, 1972.
[47] M. Takahashi, A. Sakamoto, H. Ezura, and H. Morikawa, “Prolonged exposure to atmospheric nitrogen dioxide increases fruit yield of tomato plants,” *Plant Biotechnol.*, vol. 28, no. 5, pp. 485–487, 2011.
[48] M. Takahashi *et al.*, “Nitrogen dioxide regulates organ growth by controlling cell proliferation and enlargement in Arabidopsis,” *New Phytol.*, vol. 201, no. 4, pp. 1304–1315, 2014.
[49] M. Takahashi, Y. Sasaki, S. Ida, and H. Morikawa, “Nitrite reductase gene enrichment improves assimilation of NO(2) in Arabidopsis.,” *Plant Physiol.*, vol. 126, no. 2, pp. 731–741, 2001.
[50] M. Takahashi, M. Nakagawa, A. Sakamoto, C. Ohsumi, T. Matsubara, and H. Morikawa, “Atmospheric nitrogen dioxide gas is a plant vitalization signal to increase plant size and the contents of cell constituents,” *New Phytol.*, vol. 168, no. 1, pp. 149–154, 2005.
[51] S. E. H. Adam, J. Shigeto, A. Sakamoto, M. M. Takahashi, and H. Morikawa, “Atmospheric nitrogen dioxide at ambient levels stimulates growth and development of horticultural plants,” *Botany*, vol. 86, no. 2, pp. 213–217, 2008.
[52] Q. Xu *et al.*, “Salicylic acid-altering Arabidopsis mutants response to NO2 Exposure,” *Bull. Environ. Contam. Toxicol.*, vol. 84, no. 1, pp. 106–111, 2010.
[53] H. Morikawa *et al.*, “Formation of unidentified nitrogen in plants: An implication for a novel nitrogen metabolism,” *Planta*, vol. 219, no. 1, pp. 14–22, 2004.
[54] H. Morikawa *et al.*, “Novel metabolism of nitrogen in plants,” *Zeitschrift fur Naturforsch. - Sect. C J. Biosci.*, vol. 60, no. 3–4, pp. 265–271, 2005.
[55] H. Shibata, Y. Kono, S. Yamshita, Y. Sawa, H. Ochiai, and K. Tanaka, “Degradation of chlorophyll by nitrogen dioxide generated from the peroxidase reaction,” *Biochim. Biophys. Acta*, vol. 1230, pp. 45–50, 1995.
[56] A. Van Der Vliet, J. P. Eiserich, B. Halliwell, and C. E. Cross, “Formation of reactive nitrogen species during peroxidase-catalyzed oxidation of nitrite: A potential additional mechanism of nitric oxide- dependent toxicity,” *J. Biol. Chem.*, vol. 272, no. 12, pp. 7617–7625, 1997.
[57] A. Sakamoto *et al.*, “Three distinct Arabidopsis hemoglobins exhibit peroxidase-like activity and differentially mediate nitrite-dependent protein nitration,” *FEBS Lett.*, vol. 572, no. 1, pp. 27–32, 2004.
[58] A. Maassen and J. Hennig, “Effect of Medicago sativa Mhb1 gene expression on defense response of Arabidopsis thaliana plants,” *Acta Biochim. Pol.*, vol. 58, no. 3, pp. 427–432, 2011.
[59] L. Klepper, “Comparison between NO(x) Evolution Mechanisms of Wild-Type and nr(1) Mutant Soybean Leaves.,” *Plant Physiol.*, vol. 93, no. 1, pp. 26–32, 1990.
[60] S. Saito, A. Yamamoto-Katou, H. Yoshioka, N. Doke, and K. Kawakita, “Peroxynitrite generation and tyrosine nitration in defense responses in tobacco BY-2 cells,” *Plant Cell Physiol.*, vol. 47, no. 6, pp. 689–697, 2006.
[61] F. J. Corpas, M. Chaki, M. Leterrier, and J. B. Barroso, “Protein tyrosine nitration A new challenge in plants,” *Plant Signal. Behav.*, vol. 4, no. 10, pp. 920–923, 2009.
[62] S. J. Neill, R. Desikan, A. Clarke, and J. T. Hancock, “Nitric oxide is a novel component of abscisic acid signaling in stomatal guard cells,” *Plant Physiol.*, vol. 128, no. 1, pp. 13–16, 2002.
[63] C. García-Mata and L. Lamattina, “Nitric oxide induces stomatal closure and enhances the adaptive plant responses against drought stress.,” *Plant Physiol.*, vol. 126, no. 3, pp. 1196–1204, 2001.
[64] C. Garcia-Mata, R. Gay, S. Sokolovski, A. Hills, L. Lamattina, and M. R. Blatt, “Nitric oxide regulates K+ and Cl- channels in guard cells through a subset of abscisic acid-evoked signaling pathways.,” *Proc. Natl. Acad. Sci. U. S. A.*, vol. 100, no. 19, pp. 11116–11121, 2003.
[65] G. C. Pagnussat, L. Lanteri, and L. Lamattina, “Nitric Oxide and Cyclic GMP Are Messengers in the Indole Acetic Acid-Induced Adventitious Rooting Process,” *Plant Physiol.*, vol. 132, pp. 1241–1248, 2003.
[66] P. C. Bethke, “Apoplastic Synthesis of Nitric Oxide by Plant Tissues,” *Plant Cell*, vol. 16, no. 2, pp. 332–341, 2004.
[67] L. V. Modolo, O. Augusto, I. M. G. Almeida, J. R. Magalhaes, and I. Salgado, “Nitrite as the major source of nitric oxide production by Arabidopsis thaliana in response to Pseudomonas syringae,” *FEBS Lett.*, vol. 579, no. 17, pp. 3814–3820, 2005.
[68] E. Planchet, K. Jagadis Gupta, M. Sonoda, and W. M. Kaiser, “Nitric oxide emission from tobacco leaves and cell

suspensions: rate limiting factors and evidence for the involvement of mitochondrial electron transport.," *Plant J.*, vol. 41, no. 5, pp. 732–743, 2005.
[69] C. Stöhr, F. Strube, G. Marx, W. R. Ullrich, and P. Rockel, "A plasma membrane-bound enzyme of tobacco roots catalyses the formation of nitric oxide from nitrite," *Planta*, vol. 212, pp. 835–841, 2001.
[70] H. Yamasaki, Y. Sakihama, and S. Takahashi, "An alternative pathway for nitric oxide production in plants: new features of an old enzyme.," *Trends Plant Sci.*, vol. 4, no. 4, pp. 128–129, 1999.
[71] P. Rockel, F. Strube, A. Rockel, J. Wildt, and W. M. Kaiser, "Regulation of nitric oxide (NO) production by plant nitrate reductase in vivo and in vitro.," *J. Exp. Bot.*, vol. 53, no. 366, pp. 103–10, 2002.
[72] M. Arasimowicz-Jelonek and J. Floryszak-Wieczorek, "Understanding the fate of peroxynitrite in plant cells - From physiology to pathophysiology," *Phytochemistry*, vol. 72, no. 8, pp. 681–688, 2011.
[73] L. Virag, E. Szabo, P. Gergely, and C. Syabo, "Peroxynitrite-induced cytotoxicity: mechanism and opportunities for intervention.," *Toxicol. Lett.*, vol. 140–141, pp. 113–124, 2003.
[74] H. Rubbo *et al.*, "Nitric oxide regulation of superoxide and peroxynitrite-dependent lipid peroxidation.," *J. Biol. Chem.*, vol. 269, pp. 26066–26075, 1994.
[75] M. G. Salgo, E. Bermúdez, G. L. Squadrito, and W. A. Pryor, "DNA damage and oxidation of thiols peroxynitrite causes in rat thymocytes," *Arch. Biochem. Biophys*, vol. 322, no. 2, pp. 500–505, 1995.
[76] F. Gaupels, E. Spiazzi-Vandelle, D. Yang, and M. Delledonne, "Detection of peroxynitrite accumulation in Arabidopsis thaliana during the hypersensitive defense response," *Nitric Oxide - Biol. Chem.*, vol. 25, no. 2, pp. 222–228, 2011.
[77] J. M. Alamillo and F. Garcia-Olmedo, "Effects of urate, a natural inhibitor of peroxynitrite-mediated toxicity, in the response of Arabidopsis thaliana to the bacterial pathogen Pseudomonas syringae," *Plant J.*, vol. 25, no. 5, pp. 529–540, 2001.
[78] J. Durner, D. Wendehenne, and D. F. Klessig, "Defense gene induction in tobacco by nitric oxide, cyclic GMP, and cyclic ADP-ribose.," *Proc. Natl. Acad. Sci. U. S. A.*, vol. 95, no. 17, pp. 10328–10333, 1998.
[79] D. T. Hess and J. S. Stamler, "Regulation by S-nitrosylation of protein post-translational modification," *J. Biol. Chem.*, vol. 287, no. 7, pp. 4411–4418, 2012.
[80] Y. Tada *et al.*, "Plant immunity requires conformational charges of NPR1 via S-nitrosylation and thioredoxins," *Science.*, vol. 321, no. 5891, pp. 952–956, 2008.
[81] M. C. Romero-Puertas *et al.*, "Proteomic analysis of S-nitrosylated proteins in Arabidopsis thaliana undergoing hypersensitive response," *Proteomics*, vol. 8, no. 7, pp. 1459–1469, 2008.
[82] C. Lindermayr, S. Sell, B. Müller, D. Leister, and J. Durner, "Redox regulation of the NPR1-TGA1 system of Arabidopsis thaliana by nitric oxide.," *Plant Cell*, vol. 22, no. 8, pp. 2894–2907, 2010.
[83] B.-W. Yun *et al.*, "S-nitrosylation of NADPH oxidase regulates cell death in plant immunity," *Nature*, vol. 478, pp. 264–268, 2011.
[84] K. A. Broniowska and N. Hogg, "The Chemical Biology of S-Nitrosothiols," *Antioxid. Redox Signal.*, vol. 17, no. 7, pp. 969–980, 2012.
[85] I. Kovacs and C. Lindermayr, "Nitric oxide-based protein modification: formation and site-specificity of protein S-nitrosylation," *Front. Plant Sci.*, vol. 4, p. 137, 2013.
[86] T. Nakamura and S. a. Lipton, "Emerging Role of Protein-Protein Transnitrosylation in Cell Signaling Pathways," *Antioxid. Redox Signal.*, vol. 18, no. 3, pp. 239–249, 2013.
[87] J. C. Begara-Morales *et al.*, "Antioxidant systems are regulated by nitric oxide-mediated post-translational modifications (NO-PTMs)," *Front. Plant Sci.*, vol. 7, no. 152, p. doi: 10.3389/fpls.2016.00152, 2016.
[88] C. Lindermayr, G. Saalbach, G. Bahnweg, and J. Durner, "Differential inhibition of arabidopsis methionine adenosyltransferases by protein S-nitrosylation," *J. Biol. Chem.*, vol. 281, no. 7, pp. 4285–4291, 2006.
[89] I. Kovacs, J. Durner, and C. Lindermayr, "Crosstalk between nitric oxide and glutathione is required for NONEXPRESSOR OF PATHOGENESIS-RELATED GENES 1 (NPR1)-dependent defense signaling in Arabidopsis thaliana," *New Phytol.*, vol. 208, no. 3, pp. 860–872, 2015.
[90] H. Gunaydin and K. Houk, "Mechanisms of Peroxynitrite Mediated Nitration of Tyrosine," *Chemi Res Toxicol*, vol. 22, no. 5, pp. 894–898, 2009.
[91] R. Radi, "Nitric oxide, oxidants, and protein tyrosine nitration.," *Proc. Natl. Acad. Sci. U. S. A.*, vol. 101, no. 12, pp. 4003–8, 2004.
[92] K. Bian, Z. Gao, N. Weisbrodt, and F. Murad, "The nature of heme/iron-induced protein tyrosine nitration.," *Proc. Natl. Acad. Sci. U. S. A.*, vol. 100, no. 10, pp. 5712–5717, 2003.
[93] Z. Kolbert, G. Feigl, Á. Bordé, Á. Molnár, and L. Erdei, "Protein tyrosine nitration in plants: Present knowledge, computational prediction and future perspectives," *Plant Physiol. Biochem.*, vol. 113, pp. 56–63, 2017.
[94] M.-C. Castillo, J. Lozano-Juste, M. González-Guzmán, L. Rodriguez, P. Rodriguez, and J. León, "Inactivation of PYR/PYL/RCAR ABA receptors by tyrosine nitration may enable rapid inhibition of ABA signaling by nitric oxide in plants.," *Sci. Signal*, vol. 8, no. 392, p. DOI: 10.1126/scisignal.aaa7981, 2015.
[95] F. Gaupels *et al.*, "Systemic induction of NO-, redox-, and cGMP signaling in the pumpkin extrafascicular phloem upon local leaf wounding," *Front. Plant Sci.*, vol. 7, no. 154, p. doi: 10.3389/fpls.2016.00154, 2016.
[96] D. Cecconi, S. Orzetti, E. Vandelle, S. Rinalducci, L. Zolla, and M. Delledonne, "Protein nitration during defense response in Arabidopsis thaliana," *Electrophoresis*, vol. 30, no. 14, pp. 2460–2468, 2009.
[97] A. David, S. Yadav, F. Baluška, and S. Bhatla, "Nitric oxide accumulation and protein tyrosine nitration as a rapid and long distance signalling response to salt stress in sunflower seedlings," *Nitric Oxide*, vol. 50, pp. 28–37, 2016.
[98] J. Glazebrook, "Contrasting Mechanisms of Defense Against Biotrophic and Necrotrophic Pathogens," *Annu. Rev. Phytopathol.*, vol. 43, no. 1, pp. 205–227, 2005.
[99] J. Bigeard, J. Colcombet, and H. Hirt, "Signaling mechanisms in pattern-triggered immunity (PTI)," *Mol. Plant*, vol. 8, no. 4, pp. 521–539, 2015.
[100] E. Pennisi, "Armed and Dangerous," *Science.*, vol. 327, no. 5967, pp. 804–805, 2010.
[101] T. H. Yeats and J. K. C. Rose, "The Formation and Function of Plant Cuticles," *Plant Physiol.*, vol. 163, no. 1, pp. 5–20, 2013.
[102] W. Underwood, "The Plant Cell Wall: A Dynamic Barrier Against Pathogen Invasion," *Front. Plant Sci.*, vol. 3, no. 85, p. doi: 10.3389/fpls.2012.00085, 2012.
[103] S. Zeilinger *et al.*, "Friends or foes? Emerging insights from fungal interactions with plants," *FEMS Microbiol Rev.*, vol. 40,

no. 2, pp. 182–207, 2016.
[104] J. D. G. G. Jones and J. L. Dangl, “The plant immune system,” *Nature*, vol. 444, no. 7117, pp. 323–329, 2006.
[105] D. Couto and C. Zipfel, “Regulation of pattern recognition receptor signalling in plants,” *Nat. Rev. Immunol.*, vol. 16, no. 9, pp. 537–552, 2016.
[106] M. Benedetti *et al.*, “Plant immunity triggered by engineered in vivo release of oligogalacturonides, damage-associated molecular patterns,” *Proc. Natl. Acad. Sci.*, vol. 112, no. 17, pp. 5533–5538, 2015.
[107] C. Zipfel, “Plant pattern-recognition receptors,” *Trends Immunol.*, vol. 35, no. 7, pp. 345–351, 2014.
[108] D. Chinchilla, Z. Bauer, M. Regenass, T. Boller, and G. Felix, “The Arabidopsis Receptor Kinase FLS2 Binds flg22 and determines the specificity of Flagellin perception,” *Plant Cell*, vol. 18, no. 2, pp. 465–476, 2006.
[109] Y. Cao *et al.*, “The kinase LYK5 is a major chitin receptor in Arabidopsis and forms a chitin-induced complex with related kinase CERK1,” *Elife*, vol. 3, pp. 1–19, 2014.
[110] D. Lu, S. Wu, X. Gao, Y. Zhang, L. Shan, and P. He, “A receptor-like cytoplasmic kinase, BIK1, associates with a flagellin receptor complex to initiate plant innate immunity,” *Proc. Natl. Acad. Sci.*, vol. 107, no. 1, pp. 496–501, 2010.
[111] M. Roux *et al.*, “The Arabidopsis Leucine-Rich Repeat Receptor–Like Kinases BAK1/SERK3 and BKK1/SERK4 are required for innate immunity to hemibiotrophic and biotrophic pathogens,” *Plant Cell*, vol. 23, no. 6, pp. 2440–2455, 2011.
[112] Y. Sun *et al.*, “Structural basis for flg22-induced activation of the Arabidopsis FLS2-BAK1 immune complex,” *Science.*, vol. 342, pp. 624–629, 2013.
[113] L. Li *et al.*, “The FLS2-associated kinase BIK1 directly phosphorylates the NADPH oxidase RbohD to control plant immunity,” *Cell Host Microbe*, vol. 15, no. 3, pp. 329–338, 2014.
[114] U. Dubiella *et al.*, “Calcium-dependent protein kinase/NADPH oxidase activation circuit is required for rapid defense signal propagation,” *Proc. Natl. Acad. Sci.*, vol. 110, no. 21, pp. 8744–8749, 2013.
[115] Y. Kadota, K. Shirasu, and C. Zipfel, “Regulation of the NADPH Oxidase RBOHD During Plant Immunity.,” *Plant Cell Physiol.*, vol. 56, no. 8, pp. 1472–80, 2015.
[116] R. Singh, P. Parihar, S. Singh, R. K. Mishra, V. P. Singh, and S. M. Prasad, “Reactive oxygen species signaling and stomatal movement: Current updates and future perspectives,” *Redox Biol.*, vol. 11, pp. 213–218, 2017.
[117] C. Lamb and R. A. Dixon, “The oxidative burst in plant disease resistance,” *Annu. Mol.Biol.*, vol. 48, pp. 251–275, 1997.
[118] D. J. Bradley, P. Kjellbom, and C. J. Lamb, “Elicitor- and wound-induced oxidative cross-linking of a proline-rich plant cell wall protein: A novel, rapid defense response,” *Cell*, vol. 70, no. 1, pp. 21–30, 1992.
[119] Y. Liu and C. He, “A review of redox signaling and the control of MAP kinase pathway in plants,” *Redox Biol.*, vol. 11, pp. 192–204, 2017.
[120] S. Ranf, L. Eschen-Lippold, P. Pecher, J. Lee, and D. Scheel, “Interplay between calcium signalling and early signalling elements during defence responses to microbe- or damage-associated molecular patterns,” *Plant J.*, vol. 68, no. 1, pp. 100–113, 2011.
[121] S. Ranf, L. Eschen-Lippold, K. Fröhlich, L. Westphal, D. Scheel, and J. Lee, “Microbe-associated molecular pattern-induced calcium signaling requires the receptor-like cytoplasmic kinases, PBL1 and BIK1,” *BMC Plant Biol.*, vol. 14, no. 1, p. 374, 2014.
[122] F. Groß, J. Durner, and F. Gaupels, “Nitric oxide, antioxidants and prooxidants in plant defence responses.,” *Front. Plant Sci.*, vol. 4, no. 419, p. doi: 10.3389/fpls.2013.00419 Nitric, 2013.
[123] W. Ma, A. Smigel, Y.-C. Tsai, J. Braam, and G. A. Berkowitz, “Innate immunity signaling: cytosolic Ca2+ elevation is linked to downstream nitric oxide generation through the action of calmodulin or a calmodulin-like protein.,” *Plant Physiol.*, vol. 148, no. 2, pp. 818–828, 2008.
[124] X. Meng and S. Zhang, “MAPK Cascades in Plant Disease Resistance Signaling,” *Annu. Rev. Phytopathol.*, vol. 51, no. 1, pp. 245–266, 2013.
[125] J.-L. Qiu *et al.*, “Arabidopsis MAP kinase 4 regulates gene expression through transcription factor release in the nucleus,” *EMBO J.*, vol. 27, no. 16, pp. 2214–2221, 2008.
[126] G. Mao, X. Meng, Y. Liu, Z. Zheng, Z. Chen, and S. Zhang, “Phosphorylation of a WRKY Transcription Factor by Two Pathogen-Responsive MAPKs Drives Phytoalexin Biosynthesis in *Arabidopsis*,” *Plant Cell*, vol. 23, no. 4, pp. 1639–1653, 2011.
[127] J. Xu *et al.*, “Pathogen-responsive MPK3 and MPK6 reprogram the biosynthesis of indole glucosinolates and their derivatives in Arabidopsis immunity,” *Plant Cell*, vol. 28, no. 5, pp. 1144–1162, 2016.
[128] Y. Liu and S. Zhang, “Phosphorylation of 1-aminocyclopropane-1-carboxylic acid synthase by MPK6, a stress-responsive mitogen-activated protein kinase, induces ethylene biosynthesis in Arabidopsis,” *Plant Cell*, vol. 16, pp. 3386–3399, 2004.
[129] M. Boudsocq *et al.*, “Differential innate immune signalling via Ca2+ sensor protein kinases,” *Nature*, vol. 464, no. 7287, pp. 418–422, 2010.
[130] X. Gao, K. Cox Jr., and P. He, “Functions of Calcium-Dependent Protein Kinases in Plant Innate Immunity,” *Plants*, vol. 3, no. 1, pp. 160–176, 2014.
[131] C. M. J. Pieterse, A. Leon-Reyes, S. Van der Ent, and S. C. M. Van Wees, “Networking by small-molecule hormones in plant immunity.,” *Nat. Chem. Biol.*, vol. 5, no. 5, pp. 308–316, 2009.
[132] M. J. Pozo, L. C. Van Loon, and C. M. J. Pieterse, “Jasmonates - Signals in plant-microbe interactions,” *J. Plant Growth Regul.*, vol. 23, no. 3, pp. 211–222, 2004.
[133] G. Loake and M. Grant, “Salicylic acid in plant defence—the players and protagonists.,” *Curr. Opin. Plant Biol.*, vol. 10, pp. 466–472, 2007.
[134] B. Asselbergh, D. De Vleesschauwer, and M. Höfte, “Global switches and fine-tuning— ABA modulates plant pathogen defense.,” *Mol. Plant Microbe Interact.*, vol. 21, pp. 709–719, 2008.
[135] L. Navarro *et al.*, “DELLAs control plant immune responses by modulating the balance of jasmonic acid and salicylic acid signaling.,” *Curr. Biol.*, vol. 6, no. 18, pp. 650–655, 2008.
[136] H. Nakashita *et al.*, “Brassinosteroid functions in a broad range of disease resistance in tobacco and rice.,” *Plant J.*, vol. 33, pp. 887–898, 2003.
[137] L. Navarro *et al.*, “A plant miRNA contributes to antibacterial resistance by repressing auxin signaling.,” *Science.*, vol. 312, pp. 436–439, 2006.
[138] C. M. J. Pieterse, D. Van der Does, C. Zamioudis, A. Leon-Reyes, and S. C. M. Van Wees, “Hormonal modulation of plant immunity,” *Annu. Rev. Cell Dev. Biol.*, vol. 28, no. 1, pp. 489–521, 2012.

[139] B. P. H. J. Thomma *et al.*, “Separate jasmonate-dependent and salicylate-dependent defense-response pathways in Arabidopsis are essential for resistance to distinct microbial pathogens,” *Proc. Natl. Acad. Sci. U. S. A.*, vol. 95, pp. 15107–15111, 1998.
[140] X.-F. Xin and S. Y. He, “Pseudomonas syringae pv. tomato DC3000: A Model Pathogen for Probing Disease Susceptibility and Hormone Signaling in Plants,” *Annu. Rev. Phytopathol.*, vol. 51, no. 1, pp. 473–498, 2013.
[141] L. Wang, K. Tsuda, M. Sato, J. D. Cohen, F. Katagiri, and J. Glazebrook, “Arabidopsis CaM binding protein CBP60g contributes to MAMP-induced SA accumulation and is involved in disease resistance against Pseudomonas syringae,” *PLoS Pathog.*, vol. 5, no. 2, 2009.
[142] Y. Zhang *et al.*, “Control of salicylic acid synthesis and systemic acquired resistance by two members of a plant-specific family of transcription factors,” *Proc. Natl. Acad. Sci.*, vol. 107, no. 42, pp. 18220–18225, 2010.
[143] C. Seyfferth and K. Tsuda, “Salicylic acid signal transduction: the initiation of biosynthesis, perception and transcriptional reprogramming,” *Front. Plant Sci.*, vol. 5, no. 697, p. doi: 10.3389/fpls.2014.00697, 2014.
[144] Z. Q. Fu *et al.*, “NPR3 and NPR4 are receptors for the immune signal salicylic acid in plants,” *Nature*, vol. 486, no. 7402, pp. 228–232, 2012.
[145] S. H. Spoel, Z. Mou, Y. Tada, N. W. Spivey, P. Genschik, and X. Dong, “Proteasome-Mediated Turnover of the Transcription Co-Activator NPR1 Plays Dual Roles in Regulating Plant Immunity,” *Cell*, vol. 137, no. 5, pp. 860–872, 2009.
[146] J. M. Zhou *et al.*, “NPR1 differentially interacts with members of the TGA/OBF family of transcription factors that bind an element of the PR-1 gene required for induction by salicylic acid.,” *Mol. Plant. Microbe. Interact.*, vol. 13, no. 2, pp. 191–202, 2000.
[147] D. Wang, N. Amornsiripanitch, and X. Dong, “A genomic approach to identify regulatory nodes in the transcriptional network of systemic acquired resistance in plants,” *PLoS Pathog.*, vol. 2, no. 11, pp. 1042–1050, 2006.
[148] M. Odjakova and C. Hadjiivanova, “The complexity of pathogen defense in plants,” *Bulg. J. Plant Physiol.*, vol. 27, pp. 101–109, 2001.
[149] F. Katagiri, R. Thilmony, and S. Y. He, “The Arabidopsis Thaliana-Pseudomonas Syringae Interaction,” *Arab. B.*, vol. 1, no. e0039, 2002.
[150] S. AbuQamar, K. Moustafa, and L. S. Tran, “Mechanisms and strategies of plant defense against *Botrytis cinerea*,” *Crit. Rev. Biotechnol.*, vol. 37, no. 2, pp. 262–274, 2017.
[151] J. Amselem *et al.*, “Genomic analysis of the necrotrophic fungal pathogens sclerotinia sclerotiorum and botrytis cinerea,” *PLoS Genet.*, vol. 7, no. 8, 2011.
[152] B. J. F. Feys, C. E. Benedetti, C. N. Penfold, and J. G. Turner, “Arabidopsis Mutants Selected for Resistance To the Phytotoxin Coronatine Are Male-Sterile, Insensitive To Methyl Jasmonate, and Resistant To a Bacterial Pathogen,” *Plant Cell*, vol. 6, no. 5, pp. 751–759, 1994.
[153] D.-X. Xie, B. Feys, S. James, M. Nieto-Rostro, and J. TUrner, “COI1: An Arabidopsis Gene Required for Jasmonate-Regulated Defense and Fertility,” *Science.*, vol. 280, no. 5366, pp. 1091–1094, 1998.
[154] A. Chini *et al.*, “The JAZ family of repressors is the missing link in jasmonate signalling,” *Nature*, vol. 448, no. 7154, pp. 666–671, 2007.
[155] Y. Yan *et al.*, “A Downstream Mediator in the Growth Repression Limb of the Jasmonate Pathway,” *Plant Cell*, vol. 19, no. 8, pp. 2470–2483, 2007.
[156] B. Thines *et al.*, “JAZ repressor proteins are targets of the SCFCOI1 complex during jasmonate signalling,” *Nature*, vol. 448, no. 7154, pp. 661–665, 2007.
[157] S. Berger, E. Bell, and J. E. Mullet, “Two Methyl Jasmonate-Insensitive Mutants Show Altered Expression of AtVsp in Response to Methyl Jasmonate and Wounding.,” *Plant Physiol.*, vol. 111, no. 2, pp. 525–531, 1996.
[158] O. Lorenzo, J. M. Chico, J. J. Sánchez-Serrano, and R. Solano, “JASMONATE-INSENSITIVE1 encodes a MYC transcription factor essential to discriminate between different jasmonate-regulated defense responses in Arabidopsis.,” *Plant Cell*, vol. 16, no. 7, pp. 1938–50, 2004.
[159] B. Dombrecht *et al.*, “MYC2 Differentially Modulates Diverse Jasmonate-Dependent Functions in Arabidopsis,” *Plant Cell*, vol. 19, no. July, pp. 2225–2245, 2007.
[160] M. Pre, M. Atallah, A. Champion, M. De Vos, C. M. J. Pieterse, and J. Memelink, “The AP2/ERF Domain Transcription Factor ORA59 Integrates Jasmonic Acid and Ethylene Signals in Plant Defense,” *Plant Physiol.*, vol. 147, no. 3, pp. 1347–1357, 2008.
[161] O. Lorenzo, R. Piqueras, J. J. Sánchez-serrano, and R. Solano, “ETHYLENE RESPONSE FACTOR1 Integrates Signals from Ethylene and Jasmonate Pathways in Plant Defense,” *Plant Cell*, vol. 15, pp. 165–178, 2003.
[162] A. Verhage *et al.*, “Rewiring of the jasmonate signaling pathway in Arabidopsis during insect herbivory,” *Front. Plant Sci.*, vol. 2, no. 47, p. doi: 10.3389/fpls.2011.00047, 2011.
[163] Z. Zhu *et al.*, “Derepression of ethylene-stabilized transcription factors (EIN3/EIL1) mediates jasmonate and ethylene signaling synergy in Arabidopsis,” *Proc. Natl. Acad. Sci.*, vol. 108, no. 30, pp. 12539–12544, 2011.
[164] S. Ferrari, R. Galletti, C. Denoux, G. De Lorenzo, F. M. Ausubel, and J. Dewdney, “Resistance to Botrytis cinerea induced in Arabidopsis by elicitors is independent of salicylic acid, ethylene, or jasmonate signaling but requires PHYTOALEXIN DEFICIENT3.,” *Plant Physiol.*, vol. 144, no. 1, pp. 367–79, 2007.
[165] E. W. Chehab, S. S. S. Kim, T. Savchenko, D. Kliebenstein, K. Dehesh, and J. Braam, “Intronic T-DNA Insertion Renders Arabidopsis opr3 a Conditional Jasmonic Acid-Producing Mutant,” *Plant Physiol.*, vol. 156, no. 2, pp. 770–778, 2011.
[166] M. Berrocal-Lobo, A. Molina, and R. Solano, “Constitutive expression of ETHYLENE-RESPONSE-FACTOR1 in Arabidopsis confers resistance to several necrotrophic fungi,” *Plant J.*, vol. 29, no. 1, pp. 23–32, 2002.
[167] S. Ferrari, J. M. Plotnikova, G. De Lorenzo, and F. M. Ausubel, “Arabidopsis local resistance to Botrytis cinerea involves salicylic acid and camalexin and requires EDS4 and PAD2, but not SID2, EDS5 or PAD4,” *Plant J.*, vol. 35, no. 2, pp. 193–205, 2003.
[168] V. Gupta, M. G. Willits, and J. Glazebrook, “Arabidopsis thaliana EDS4 contributes to salicylic acid (SA)-dependent expression of defense responses: evidence for inhibition of jasmonic acid signaling by SA.,” *Mol. Plant. Microbe. Interact.*, vol. 13, no. 5, pp. 503–511, 2000.
[169] H. Pena-Cortes, T. Albrecht, S. Prat, E. W. Weiler, and L. Willmitzer, “Aspirin prevents would-induced gene expression in tomato leaves by blocking jasmonic acid biosynthesis,” *Planta*, vol. 191, pp. 123–128, 1993.
[170] S. H. Spoel *et al.*, “NPR1 Modulates Cross-Talk between Salicylate- and Jasmonate-Dependent Defense Pathways through

a Novel Function in the Cytosol," *Plant Cell*, vol. 15, no. 3, pp. 760–770, 2003.
[171] S. H. Spoel, J. S. Johnson, and X. Dong, "Regulation of tradeoffs between plant defenses against pathogens with different lifestyles," *Proc. Natl. Acad. Sci.*, vol. 104, no. 47, pp. 18842–18847, 2007.
[172] P. Brodersen *et al.*, "Arabidopsis MAP kinase 4 regulates salicylic acid- and jasmonic acid/ethylene-dependent responses via EDS1 and PAD4," *Plant J.*, vol. 47, no. 4, pp. 532–546, 2006.
[173] L. A. J. Mur, P. Kenton, A. J. Lloyd, H. Ougham, and E. Prats, "The hypersensitive response; The centenary is upon us but how much do we know?," *J. Exp. Bot.*, vol. 59, no. 3, pp. 501–520, 2008.
[174] A. Levine, R. I. Pennell, M. E. Alvarez, R. Palmer, and C. Lamb, "Calcium-mediated apoptosis in a plant hypersensitive disease resistance response," *Curr. Biol.*, vol. 6, no. 4, pp. 427–437, 1996.
[175] H. Xu and M. Heath, "Role of calcium in signal transduction during the hypersensitive response caused by basidiospore-derived infection of the cowpea rust fungus," *Plant Cell*, vol. 10, no. 4, pp. 585–598, 1998.
[176] K. Overmyer, M. Brosché, and J. Kangasjärvi, "Reactive oxygen species and hormonal control of cell death," *Trends Plant Sci.*, vol. 8, no. 7, pp. 335–342, 2003.
[177] M. Delledonne, Y. Xia, R. A. Dixon, and C. Lamb, "Nitric oxide functions as a signal in plant disease resistance.," *Nature*, vol. 394, no. 6693, pp. 585–588, 1998.
[178] J. Dangl, R. Dietrich, and M. Richberg, "Death Don't Have No Mercy: Cell Death Programs in Plant-Microbe Interactions.," *Plant Cell*, vol. 8, no. 10, pp. 1793–1807, 1996.
[179] J. Durner, J. Shah, and F. D. Klessig, "Salicylic acid and disease resistance in plants," *Trends Plant Sci.*, vol. 2, no. 7, pp. 266–274, 1997.
[180] A. Mazel and A. Levine, "Induction of cell death in Arabidopsis by superoxide in combination with salicylic acid or with protein synthesis inhibitors," *Free Radic. Biol. Med.*, vol. 30, no. 1, pp. 98–106, 2001.
[181] S. T. Lund, R. E. Stall, and H. J. Klee, "Ethylene regulates the susceptible response to pathogen infection in tomato.," *Plant Cell*, vol. 10, no. 3, pp. 371–382, 1998.
[182] W. Moeder *et al.*, "Ethylene Synthesis Regulated by Biphasic Induction of 1-Aminocyclopropane-1-Carboxylic Acid Synthase and 1-Aminocyclopropane-1-Carboxylic Acid Oxidase Genes Is Required for Hydrogen Peroxide Accumulation and Cell Death in Ozone-Exposed Tomato," *Plant Physiol.*, vol. 130, no. 4, pp. 1918–1926, 2002.
[183] K. Overmyer *et al.*, "Ozone-sensitive arabidopsis rcd1 mutant reveals opposite roles for ethylene and jasmonate signaling pathways in regulating superoxide-dependent cell death," *Plant Cell*, vol. 12, no. 10, pp. 1849–1862, 2000.
[184] M. Rao, H. Lee, R. Creelman, J. Mullet, and K. Davis, "Jasmonic Acid Signaling Modulates Ozone-Induced Hypersensitive Cell Death," *Plant Cell*, vol. 12, no. 9, pp. 1633–1646, 2000.
[185] G. Aspinall and G. Kessler, "The structure of callose from the grape vine," *Chem. Ind.*, vol. 1296, 1957.
[186] B. Stone and A. Clarke, *Chemistry and biology of (1-3)-beta-glucans*. La Trobe University Press, [Bundoora, Vic.], 1992.
[187] R. Zeyen, W. Kruger, M. Lyngkjaer, and T. Carver, "Differential effects of D-mannose and 2-deoxy-D-glucose on attempted powdery mildew fungal infection of inappropriate and appropriate Graminea," *Physiol. Mol. Plant Pathol.*, vol. 61, pp. 315–323, 2002.
[188] J. García-Andrade, V. Ramírez, V. Flors, and P. Vera, "Arabidopsis ocp3 mutant reveals a mechanism linking ABA and JA to pathogen-induced callose deposition," *Plant J.*, vol. 67, no. 5, pp. 783–794, 2011.
[189] D. Ellinger *et al.*, "Elevated Early Callose Deposition Results in Complete Penetration Resistance to Powdery Mildew in Arabidopsis," *Plant Physiol.*, vol. 161, pp. 1433–1444, 2013.
[190] A. K. Jacobs *et al.*, "An Arabidopsis Callose Synthase, GSL5, Is Required for Wound and Papillary Callose Formation.," *Plant Cell*, vol. 15, no. 11, pp. 2503–13, 2003.
[191] M. Nishimura, M. Stein, B.-H. Hou, J. Vogel, H. Edwards, and S. C. Somerville, "Loss of a Callose Synthase Results in Salicylic Acid-Dependent Disease Resistance," *Science.*, vol. 301, no. 5635, pp. 969–972, 2003.
[192] E. Luna, V. Pastor, J. Robert, V. Flors, B. Mauch-Mani, and J. Ton, "Callose deposition: a multifaceted plant defense response," *Mol. Plant-Microbe Interact.*, vol. 24, no. 2, pp. 183–193, 2011.
[193] N. K. Clay, A. M. Adio, C. Denoux, G. Jander, and F. M. Ausubel, "Glucosinolate Metabolites Required for an Arabidopsis Innate Immune Response," *Science.*, vol. 323, no. 5910, pp. 95–101, 2009.
[194] X. Geng, J. Cheng, A. Gangadharan, and D. Mackey, "The coronatine toxin of Pseudomonas syringae is a multifunctional suppressor of Arabidopsis defense.," *Plant Cell*, vol. 24, no. 11, pp. 4763–74, 2012.
[195] X. Dong *et al.*, "Expression of callose synthase genes and its connection with Npr1 signaling pathway during pathogen infection," *Planta*, vol. 229, no. 1, pp. 87–98, 2008.
[196] Y. Wu *et al.*, "The Arabidopsis NPR1 Protein Is a Receptor for the Plant Defense Hormone Salicylic Acid," *Cell Rep.*, vol. 1, no. 6, pp. 639–647, 2012.
[197] D. Ellinger and C. A. Voigt, "Callose biosynthesis in arabidopsis with a focus on pathogen response: What we have learned within the last decade," *Ann. Bot.*, vol. 114, no. 6, pp. 1349–1358, 2014.
[198] L. Scalschi *et al.*, "Silencing of OPR3 in tomato reveals the role of OPDA in callose deposition during the activation of defense responses against Botrytis cinerea," *Plant J.*, vol. 81, no. 2, pp. 304–315, 2015.
[199] E. E. Rogers, J. Glazebrook, and F. M. Ausubel, "Mode of action of the Arabidopsis thaliana phytoalexin camalexin and its role in Arabidopsis-pathogen interactions.," *Mol. Plant. Microbe. Interact.*, vol. 9, no. 8, pp. 748–757, 1996.
[200] D. J. Kliebenstein, H. C. Rowe, and K. J. Denby, "Secondary metabolites influence Arabidopsis/Botrytis interactions: Variation in host production and pathogen sensitivity," *Plant J.*, vol. 44, no. 1, pp. 25–36, 2005.
[201] A. Sellam, B. Iacomi-Vasilescu, P. Hudhomme, and P. Simoneau, "In vitro antifungal activity of brassinin, camalexin and two isothiocyanates against the crucifer pathogens Alternaria brassicicola and Alternaria brassicae," *Plant Pathol.*, vol. 56, no. 2, pp. 296–301, 2007.
[202] B. P. H. J. Thomma, I. Nelissen, K. Eggermont, and W. F. Broekaert, "Deficiency in phytoalexin production causes enhanced susceptibility of Arabidopsis thaliana to the fungus Alternaria brassicicola," *Plant J.*, vol. 19, no. 2, pp. 163–171, 1999.
[203] A. Joubert *et al.*, "Cell wall integrity and high osmolarity glycerol pathways are required for adaptation of Alternaria brassicicola to cell wall stress caused by brassicaceous indolic phytoalexins," *Cell. Microbiol.*, vol. 13, no. 1, pp. 62–80, 2011.
[204] N. Shlezinger *et al.*, "Anti-apoptotic machinery protects the necrotrophic fungus botrytis cinerea from host-induced apoptotic-like cell death during plant infection," *PLoS Pathog.*, vol. 7, no. 8, 2011.

[205] I. Ahuja, R. Kissen, and A. M. Bones, “Phytoalexins in defense against pathogens.,” *Trends Plant Sci.*, vol. 17, no. 2, pp. 73–90, Feb. 2012.

[206] M. Nafisi *et al.*, “*Arabidopsis* Cytochrome P450 Monooxygenase 71A13 Catalyzes the Conversion of Indole-3-Acetaldoxime in Camalexin Synthesis,” *Plant Cell*, vol. 19, no. 6, pp. 2039–2052, 2007.

[207] P. Van Baarlen, E. J. Woltering, M. Staats, and J. A. L. Van Kan, “Histochemical and genetic analysis of host and non-host interactions of Arabidopsis with three Botrytis species: An important role for cell death control,” *Mol. Plant Pathol.*, vol. 8, no. 1, pp. 41–54, 2007.

[208] K. Schlaeppi, E. Abou-Mansour, A. Buchala, and F. Mauch, “Disease resistance of Arabidopsis to Phytophthora brassicae is established by the sequential action of indole glucosinolates and camalexin,” *Plant J.*, vol. 62, no. 5, pp. 840–851, 2010.

[209] S. P. Pandey, M. Roccaro, M. Schön, E. Logemann, and I. E. Somssich, “Transcriptional reprogramming regulated by WRKY18 and WRKY40 facilitates powdery mildew infection of Arabidopsis,” *Plant J.*, vol. 64, no. 6, pp. 912–923, 2010.

[210] N. Zhou, T. L. Tootle, and J. Glazebrook, “Arabidopsis PAD3, a gene required for camalexin biosynthesis, encodes a putative cytochrome P450 monooxygenase,” *Plant Cell*, vol. 11, no. 12, pp. 2419–2428, 1999.

[211] E. Glawischnig, “Camalexin,” *Phytochemistry*, vol. 68, no. 4, pp. 401–406, 2007.

[212] S. C. M. VanWees *et al.*, “Characterization of the early response of Arabidopsis to Alternaria brassicicola infection using expression profiling.,” *Plant Physiol.*, vol. 132, no. 2, pp. 606–617, 2003.

[213] H. C. Rowe, J. W. Walley, J. Corwin, E. K.-F. Chan, K. Dehesh, and D. J. Kliebenstein, “Deficiencies in Jasmonate-Mediated Plant Defense Reveal Quantitative Variation in Botrytis cinerea Pathogenesis,” *PLoS Pathog.*, vol. 6, no. 4, p. e1000861, 2010.

[214] C. Nawrath and J. P. Métraux, “Salicylic acid induction-deficient mutants of Arabidopsis express PR-2 and PR-5 and accumulate high levels of camalexin after pathogen inoculation.,” *Plant Cell*, vol. 11, no. 8, pp. 1393–404, 1999.

[215] A. Roetschi, A. Si-Ammour, L. Belbahri, F. Mauch, and B. Mauch-Mani, “Characterization of an Arabidopsis-Phytophthora pathosystem: Resistance requires a functional pad2 gene and is independent of salicylic acid, ethylene and jasmonic acid signalling,” *Plant J.*, vol. 28, no. 3, pp. 293–305, 2001.

[216] S. Heck, T. Grau, A. Buchala, J. P. Métraux, and C. Nawrath, “Genetic evidence that expression of NahG modifies defence pathways independent of salicylic acid biosynthesis in the Arabidopsis-Pseudomonas syringae pv. tomato interaction,” *Plant J.*, vol. 36, no. 3, pp. 342–352, 2003.

[217] J. Zhao, C. Williams, and R. Last, “Induction of Arabidopsis tryptophan pathway enzymes and camalexin by amino acid starvation, oxidative stress, and an abiotic elicitor.,” *Plant Cell*, vol. 10, pp. 359–370, 1998.

[218] P. Aranega-Bou, M. de la O Leyva, I. Finiti, P. Garci-a-Agusti-n, and C. Gonzalez-Bosch, “Priming of plant resistance by natural compounds. Hexanoic acid as a model,” *Front. Plant Sci.*, vol. 5, no. 488, p. doi: 10.3389/fpls.2014.00488, 2014.

[219] C. J. Frost, M. C. Mescher, J. E. Carlson, and C. M. De Moraes, “Plant Defense Priming against Herbivores: Getting Ready for a Different Battle,” *Plant Physiol.*, vol. 146, no. 3, pp. 818–824, 2008.

[220] A. Martinez-Medina *et al.*, “Recognizing Plant Defense Priming,” *Trends Plant Sci.*, vol. 21, no. 10, pp. 818–822, 2016.

[221] B. Mauch-Mani, I. Baccelli, E. Luna, and V. Flors, “Defense Priming: An Adaptive Part of Induced Resistance,” *Annu. Rev. Plant Biol.*, vol. 68, no. 1, pp. 485–512, 2017.

[222] U. Conrath, “Molecular aspects of defence priming,” *Trends Plant Sci.*, vol. 16, no. 10, pp. 524–531, 2011.

[223] U. Conrath, G. J. M. Beckers, C. J. G. Langenbach, and M. R. Jaskiewicz, “Priming for Enhanced Defense,” *Annu. Rev. Phytopathol.*, vol. 53, no. 1, pp. 97–119, 2015.

[224] G. J. M. Beckers *et al.*, “Mitogen-Activated Protein Kinases 3 and 6 Are Required for Full Priming of Stress Responses in Arabidopsis thaliana,” *Plant Cell*, vol. 21, no. 3, pp. 944–953, 2009.

[225] C. Tateda, Z. Zhang, J. Shrestha, J. Jelenska, D. Chinchilla, and J. T. Greenberg, “Salicylic Acid Regulates Arabidopsis Microbial Pattern Receptor Kinase Levels and Signaling,” *Plant Cell*, vol. 26, no. 10, pp. 4171–4187, 2014.

[226] W. Strober, “Trypan blue exclusion test of cell viability.,” *Curr. Protoc. Immunol.*, vol. May, p. A3–B, 2001.

[227] M. C. Romero-Puertas *et al.*, “S-Nitrosylation of Peroxiredoxin II E Promotes Peroxynitrite-Mediated Tyrosine Nitration,” *Plant Cell*, vol. 19, no. 12, pp. 4120–4130, 2007.

[228] M. Leitner, E. Vandelle, F. Gaupels, D. Bellin, and M. Delledonne, “NO signals in the haze. Nitric oxide signalling in plant defence,” *Curr. Opin. Plant Biol.*, vol. 12, no. 4, pp. 451–458, 2009.

[229] M. de Pinto, F. Tommasi, and L. D. Gara, “Changes in the antioxidant systems as part of the signaling pathway responsible for the programmed cell death activated by nitric oxide and reactive oxygen species in tobacco Bright-Yellow 2 cells,” *Plant Physiol.*, vol. 130, no. 2, pp. 698–708, 2002.

[230] W. Mevius, “Nitrite,” *Handb. der Pflanzenphysiologie*, vol. 8, pp. 166–175, 1958.

[231] O. L. Oke, “Nitrite Toxicity to Plants,” *Nature*, vol. 212, no. 5061. pp. 528–528, 1966.

[232] T. Berardini *et al.*, “The Arabidopsis information resource: Making and mining the ‘gold standard’ annotated reference plant genome.,” *Genesis*, vol. 53, pp. 474–485, 2015.

[233] E. Miedes, R. Vanholme, W. Boerjan, and A. Molina, “The role of the secondary cell wall in plant resistance to pathogens,” *Front. Plant Sci.*, vol. 5, no. 358, p. doi: 10.3389/fpls.2014.00358, 2014.

[234] N. S. Coll, P. Epple, and J. L. Dangl, “Programmed cell death in the plant immune system,” *Cell Death Differ.*, vol. 18, no. 8, pp. 1247–1256, 2011.

[235] J. Mierziak, K. Kostyn, and A. Kulma, “Flavonoids as important molecules of plant interactions with the environment,” *Molecules*, vol. 19, no. 10, pp. 16240–16265, 2014.

[236] A. Dave and I. A. Graham, “Oxylipin Signaling: A Distinct Role for the Jasmonic Acid Precursor cis-(+)-12-Oxo-Phytodienoic Acid (cis-OPDA).,” *Front. Plant Sci.*, vol. 3, no. 42, p. doi: 10.3389/fpls.2012.00042, 2012.

[237] J. G. Turner, C. Ellis, and A. Devoto, “The jasmonate signal pathway.,” *Plant Cell*, vol. 14 Suppl, pp. S153–S164, 2002.

[238] M. De Vos *et al.*, “Signal Signature and Transcriptome Changes of Arabidopsis During Pathogen and Insect Attack,” *Mol. Plant-Microbe Interact.*, vol. 18, no. 9, pp. 923–937, 2005.

[239] N. Kitaoka *et al.*, “Arabidopsis CYP94B3 encodes jasmonyl-L-isoleucine 12-hydroxylase, a key enzyme in the oxidative catabolism of jasmonate.,” *Plant Cell Physiol.*, vol. 52, pp. 1757–1765, 2011.

[240] A. J. K. Koo, T. F. Cooke, and G. A. Howe, “Cytochrome P450 CYP94B3 mediates catabolism and inactivation of the plant hormone jasmonoyl-L-isoleucine,” *Proc. Natl. Acad. Sci.*, vol. 108, no. 22, pp. 9298–9303, 2011.

[241] T. Heitz *et al.*, “Cytochromes P450 CYP94C1 and CYP94B3 catalyze two successive oxidation steps of plant hormone jasmonoyl-isoleucine for catabolic turnover,” *J. Biol. Chem.*, vol. 287, no. 9, pp. 6296–6306, 2012.

[242] E. Widemann *et al.*, “The amidohydrolases IAR3 and ILL6 contribute to jasmonoyl-isoleucine hormone turnover and generate 12-hydroxyjasmonic acid upon wounding in arabidopsis leaves,” *J. Biol. Chem.*, vol. 288, no. 44, pp. 31701–31714, 2013.
[243] L. Caarls *et al.*, “Arabidopsis JASMONATE-INDUCED OXYGENASES down-regulate plant immunity by hydroxylation and inactivation of the hormone jasmonic acid.,” *Proc. Natl. Acad. Sci. U. S. A.*, vol. 114, no. 24, pp. 6388–6393, 2017.
[244] J. Malamy, J. P. Carr, D. F. Klessig, and I. Raskin, “NoSalicylic Acid: A Likely Endogenous Signal in the Resistance Response of Tobacco to Viral Infection,” *Science.*, vol. 250, no. 4983, pp. 1002–1004, 1990.
[245] M. C. Wildermuth, J. Dewdney, G. Wu, and F. M. Ausubel, “Isochorismate synthase is required to synthesize salicylic acid for plant defence.,” *Nature*, vol. 414, no. 6863, pp. 562–565, 2001.
[246] Z. Chen, Z. Zheng, J. Huang, Z. Lai, and B. Fan, “Biosynthesis of salicylic acid in plants.,” *Plant Signal. Behav.*, vol. 4, no. 6, pp. 493–496, 2009.
[247] J.-L. Coquoz, A. Buchala, and J.-P. Métraux, “The Biosynthesis of Salicylic Acid in Potato Plants1,” *Plant Physiol.*, vol. 117, no. 3, pp. 1095–1101, 1998.
[248] D. M. Ribnicky, V. Shulaev, and I. Raskin, “Intermediates of Salicylic Acid Biosynthesis in Tobacco,” *Plant Physiol.*, vol. 118, pp. 565–572, 1998.
[249] N. Zhou, T. L. Tootle, F. Tsui, D. F. Klessig, and J. Glazebrook, “PAD4 functions upstream from salicylic acid to control defense responses in Arabidopsis.,” *Plant Cell*, vol. 10, no. 6, pp. 1021–30, 1998.
[250] A. Falk, B. J. Feys, L. N. Frost, J. D. Jones, M. J. Daniels, and J. E. Parker, “EDS1, an essential component of R gene-mediated disease resistance in Arabidopsis has homology to eukaryotic lipases.,” *Proc. Natl. Acad. Sci. U. S. A.*, vol. 96, no. 6, pp. 3292–3297, 1999.
[251] B. J. Feys, L. J. Moisan, M. A. Newman, and J. E. Parker, “Direct interaction between the *Arabidopsis* disease resistance signaling proteins, EDS1 and PAD4.,” *EMBO J.*, vol. 20, no. 19, pp. 5400–11, 2001.
[252] M. Serrano *et al.*, “Export of Salicylic Acid from the Chloroplast Requires the Multidrug and Toxin Extrusion-Like Transporter EDS5,” *Plant Physiol.*, vol. 162, no. 4, pp. 1815–1821, 2013.
[253] C. Nawrath, “EDS5, an Essential Component of Salicylic Acid-Dependent Signaling for Disease Resistance in Arabidopsis, Is a Member of the MATE Transporter Family,” *Plant Cell*, vol. 14, no. 1, pp. 275–286, 2002.
[254] J. H. Park, R. Halitschke, H. B. Kim, I. T. Baldwin, K. A. Feldmann, and R. Feyereisen, “A knock-out mutation in allene oxide synthase results in male sterility and defective wound signal transduction in Arabidopsis due to a block in jasmonic acid biosynthesis,” *Plant J.*, vol. 31, no. 1, pp. 1–12, 2002.
[255] A. Stintzi and J. Browse, “The Arabidopsis male-sterile mutant, opr3, lacks the 12-oxophytodienoic acid reductase required for jasmonate synthesis,” *Proc. Natl. Acad. Sci. U. S. A.*, vol. 97, no. 19, pp. 10625–10630, 2000.
[256] T. P. Delaney *et al.*, “A Central Role of Salicylic Acid in Plant Disease Resistance,” *Science.*, vol. 266, pp. 1247–1250, 1994.
[257] K. Lawton, K. Weymann, L. Friedrich, B. Vernooij, S. Uknes, and J. Ryals, “Systemic Acquired Resistance in Arabidopsis Requires Salicylic Acid but not Ethylene,” *Am. Phytopathol. Soc.*, vol. 8, no. 6, pp. 863–870, 1995.
[258] H. Cao, S. A. Bowling, and A. S. Gordon, “Characterization of an Arabidopsis Mutant That 1 s Nonresponsive to Inducers of Systemic Acquired Resistance,” *Plant Cell*, vol. 6, pp. 1583–1592, 1994.
[259] K. F. Tierens *et al.*, “Study of the role of antimicrobial glucosinolate-derived isothiocyanates in resistance of Arabidopsis to microbial pathogens.,” *Plant Physiol.*, vol. 125, no. 4, pp. 1688–1699, 2001.
[260] N. Yalpani, P. Silverman, M. A. Wilson, D. A. Kleier, and I. Raskin, “Salicylic Acid Is a Systemic Signal and an Inducer of Pathogenesis-Related Proteins in Virus-Infected Tobacco,” *Plant Cell*, vol. 3, no. 8, pp. 809–818, 1991.
[261] A. Stintzi *et al.*, “Plant ‘pathogenesis-related’ proteins and their role in defense against pathogens,” *Biochimie*, vol. 75, no. 8, pp. 687–706, 1993.
[262] J. M. Manners *et al.*, “The promoter of the plant defensin gene PDF1.2 from Arabidopsis is systemically activated by fungal pathogens and responds to methyl jasmonate but not to salicylic acid,” *Plant Mol. Biol.*, vol. 38, no. 6, pp. 1071–1080, 1998.
[263] I. A. Penninckx *et al.*, “Pathogen-induced systemic activation of a plant defensin gene in Arabidopsis follows a salicylic acid-independent pathway.,” *Plant Cell*, vol. 8, no. 12, pp. 2309–23, 1996.
[264] J. Tsuji, E. P. Jackson, D. a Gage, R. Hammerschmidt, and S. C. Somerville, “Phytoalexin Accumulation in Arabidopsis thaliana during the Hypersensitive Reaction to Pseudomonas syringae pv. syringae,” *Plant Physiol.*, vol. 98, no. 4, pp. 1304–1309, 1992.
[265] J. Glazebrook and F. M. Ausubel, “Isolation of phytoalexin-deficient mutants of Arabidopsis thaliana and characterization of their interactions with bacterial pathogens.,” *Proc. Natl. Acad. Sci. U. S. A.*, vol. 91, no. 19, pp. 8955–8959, 1994.
[266] A. K. Hull, R. Vij, and J. L. Celenza, “Arabidopsis cytochrome P450s that catalyze the first step of tryptophan-dependent indole-3-acetic acid biosynthesis,” *Proc. Natl. Acad. Sci.*, vol. 97, no. 5, pp. 2379–2384, 2000.
[267] M. D. Mikkelsen, C. H. Hansen, U. Wittstock, and B. A. Halkier, “Cytochrome P450 CYP79B2 from Arabidopsis catalyzes the conversion of tryptophan to indole-3-acetaldoxime, a precursor of indole glucosinolates and indole-3-acetic acid,” *J. Biol. Chem.*, vol. 275, no. 43, pp. 33712–33717, 2000.
[268] E. Glawischnig, B. G. Hansen, C. E. Olsen, and B. A. Halkier, “Camalexin is synthesized from indole-3-acetaldoxime, a key branching point between primary and secondary metabolism in Arabidopsis.,” *Proc. Natl. Acad. Sci. U. S. A.*, vol. 101, no. 21, pp. 8245–50, 2004.
[269] H. Frerigmann, E. Glawischnig, and T. Gigolashvili, “The role of MYB34, MYB51 and MYB122 in the regulation of camalexin biosynthesis in Arabidopsis thaliana,” *Front. Plant Sci.*, vol. 6, no. 654, p. doi: 10.3389/fpls.2015.00654, 2015.
[270] T. M. Müller *et al.*, “TRANSCRIPTION ACTIVATOR-LIKE EFFECTOR NUCLEASE-Mediated Generation and Metabolic Analysis of Camalexin-Deficient *cyp71a12 cyp71a13* Double Knockout Lines,” *Plant Physiol.*, vol. 168, no. 3, pp. 849–858, 2015.
[271] V. Parisy, B. Poinssot, L. Owsianowski, A. Buchala, J. Glazebrook, and F. Mauch, “Identification of PAD2 as a γ-glutamylcysteine synthetase highlights the importance of glutathione in disease resistance of Arabidopsis,” *Plant J.*, vol. 49, no. 1, pp. 159–172, 2007.
[272] C. Bottcher, L. Westphal, C. Schmotz, E. Prade, D. Scheel, and E. Glawischnig, “The Multifunctional Enzyme CYP71B15 (PHYTOALEXIN DEFICIENT3) Converts Cysteine-Indole-3-Acetonitrile to Camalexin in the Indole-3-Acetonitrile Metabolic Network of Arabidopsis thaliana,” *Plant Cell*, vol. 21, no. 6, pp. 1830–1845, 2009.
[273] T. Su *et al.*, “Glutathione-indole-3-acetonitrile is required for camalexin biosynthesis in Arabidopsis thaliana.,” *Plant Cell*, vol.

23, no. 1, pp. 364–80, 2011.
[274] F. Geu-Flores, M. E. Møldrup, C. Böttcher, C. E. Olsen, D. Scheel, and B. A. Halkier, “Cytosolic γ-Glutamyl Peptidases Process Glutathione Conjugates in the Biosynthesis of Glucosinolates and Camalexin in *Arabidopsis*,” *Plant Cell*, vol. 23, no. 6, pp. 2456–2469, 2011.
[275] R. Schuhegger *et al.*, “CYP71B15 (PAD3) catalyzes the final step in camalexin biosynthesis,” *Plant Physiol.*, vol. 141, pp. 1248–1254, 2006.
[276] R. P. Birkenbihl, C. Diezel, and I. E. Somssich, “Arabidopsis WRKY33 is a key transcriptional regulator of hormonal and metabolic responses toward Botrytis cinerea infection.,” *Plant Physiol.*, vol. 159, no. 1, pp. 266–85, 2012.
[277] M. T. Nishimura, M. Stein, B.-H. Hou, J. P. Vogel, H. Edwards, and S. C. Somerville, “Loss of a Callose Synthase Results in Salicylic Acid – Dependent Disease resitance,” *Science.*, vol. 301, no. 15, pp. 969–972, 2003.
[278] J. Ton and B. Mauch-Mani, “Beta-amino-butyric acid-induced resistance against necrotrophic pathogens is based on ABA-dependent priming for callose,” *Plant J.*, vol. 38, no. 1, pp. 119–130, 2004.
[279] V. Flors *et al.*, “Absence of the endo-β-1,4-glucanases Cel1 and Cel2 reduces susceptibility to Botrytis cinerea in tomato,” *Plant J.*, vol. 52, no. 6, pp. 1027–1040, 2007.
[280] B. Vicedo *et al.*, “Hexanoic Acid-Induced Resistance Against Botrytis cinerea in Tomato Plants Begonya,” *Am. Phytopathol. Soc.*, vol. 22, no. 11, pp. 1455–1465, 2009.
[281] C. J. Bayles, M. S. Ghemawat, and J. R. Aist, “Inhibition by 2-deoxy-D-glucose of callose formation, papilla deposition, and resistance to powdery mildew in an ml-o barley mutant,” *Physiol. Mol. Plant Pathol.*, vol. 36, no. 1, pp. 63–72, 1990.
[282] B. R. Datema and R. T. Schwarz, “Interference with Glycosylation of Glycoproteins,” *Biochem J*, vol. 184, pp. 113–123, 1979.
[283] L. G. Baker, C. A. Specht, M. J. Donlin, and J. K. Lodge, “Chitosan, the deacetylated form of chitin, is necessary for cell wall integrity in Cryptococcus neoformans,” *Eukaryot. Cell*, vol. 6, no. 5, pp. 855–867, 2007.
[284] R. Pearce and J. Ride, “Chitin and related compounds as elicitors of lignification response in wounded wheat leaves.,” *Physiol Plant Pathol*, vol. 20, pp. 119–123, 1982.
[285] G. Povero *et al.*, “Transcript profiling of chitosan-treated Arabidopsis seedlings,” *J. Plant Res.*, vol. 124, no. 5, pp. 619–629, 2011.
[286] H. Köhle, W. Jeblick, F. Poten, W. Blaschek, and H. Kauss, “Chitosan-Elicited Callose Synthesis in Soybean Cells as a Ca2+-dependent Process,” *Plant Physiol.*, vol. 77, no. 3, pp. 544–551, 1985.
[287] T. E. Mishina and J. Zeier, “Pathogen-associated molecular pattern recognition rather than development of tissue necrosis contributes to bacterial induction of systemic acquired resistance in Arabidopsis,” *Plant J.*, vol. 50, no. 3, pp. 500–513, 2007.
[288] L. Gómez-Gómez, G. Felix, and T. Boller, “A single locus determines sensitivity to bacterial flagellin in Arabidopsis thaliana,” *Plant J.*, vol. 18, no. 3, pp. 277–284, 1999.
[289] K. Tsuda, M. Sato, J. Glazebrook, J. D. Cohen, and F. Katagiri, “Interplay between MAMP-triggered and SA-mediated defense responses,” *Plant J.*, vol. 53, no. 5, pp. 763–775, 2008.
[290] A. Levine, R. Tenhaken, R. Dixon, and C. Lamb, “H2O2 from the oxidative burst orchestrates the plant hypersensitive disease resistance response,” *Cell*, vol. 79, no. 4, pp. 583–593, 1994.
[291] A. J. Zeevaart, “Induction of nitrate reductase by NO2,” *Acta hot. need.*, vol. 23, pp. 346–346, 1974.
[292] I. Berber and H. Önlü, “The levels of nitrite and nitrate, proline and protein profiles in tomato plants infected with Pseudomonas syringae,” *Pakistan J. Bot.*, vol. 44, no. 5, pp. 1521–1526, 2012.
[293] G. Noctor and C. H. Foyer, “Ascorbate and glutathione: keeping active oxygen under control,” *Annu. Rev. Plant Biol.*, vol. 49, no. 1, pp. 249–279, 1998.
[294] R. Mittler, “Oxidative stress, antioxidants and stress tolerance,” *Trends Plant Sci.*, vol. 7, no. 9, pp. 405–410, 2002.
[295] E. H. Lee and J. H. Bennett, “Speroxide Dismutase - a possible protective enzyme against ozone injury in Snap Beans (Phaseolus Vulgaris L.),” *Plant Physiol.*, vol. 69, pp. 1444–1449, 1982.
[296] P. Sharma, A. B. Jha, R. S. Dubey, and M. Pessarakli, “Reactive Oxygen Species, Oxidative Damage, and Antioxidative Defense Mechanism in Plants under Stressful Conditions,” *J. Bot.*, vol. 2012, pp. 1–26, 2012.
[297] M. A. Torres and J. L. Dangl, “Functions of the respiratory burst oxidase in biotic interactions, abiotic stress and development,” *Curr. Opin. Plant Biol.*, vol. 8, no. 4, pp. 397–403, 2005.
[298] S. Gilroy *et al.*, “A tidal wave of signals: Calcium and ROS at the forefront of rapid systemic signaling,” *Trends Plant Sci.*, vol. 19, no. 10, pp. 623–630, 2014.
[299] L. Mignolet-Spruyt *et al.*, “Spreading the news: subcellular and organellar reactive oxygen species production and signalling.,” *J. Exp. Bot.*, vol. 67, no. 13, pp. 3831–3844, 2016.
[300] M. Grant, I. Brown, S. Adams, M. Knight, A. Ainslie, and J. Mansfield, “The RPM1 plant disease resistance gene facilitates a rapid and sustained increase in cytosolic calcium that is necessary for the oxidative burst and hypersensitive cell death,” *Plant J.*, vol. 23, no. 4, pp. 441–450, 2000.
[301] G. Bolwell *et al.*, “The apoplastic oxidative burst in response to biotic stress in plants: a three-component system,” *J. Exp. Bot.*, vol. 53, no. 372, pp. 1367–1376, 2002.
[302] J. Frohlich, A., and Durner, “The hunt for plant nitric oxide synthase (NOS): is one really needed?,” *Plant Sci.*, vol. 181, pp. 401–404, 2011.
[303] D. D. D. Thomas *et al.*, “The chemical biology of nitric oxide: Implications in cellular signaling,” *Free Radic. Biol. Med.*, vol. 45, no. 1, pp. 18–31, 2008.
[304] W. Prütz, H. Mönig, J. Butler, and E. Land, “Reactions of nitrogen dioxide in aqueous model systems: oxidation of tyrosine units in peptides and proteins.,” *Arch Biochem Biophys*, vol. 243, no. 1, pp. 125–134, 1985.
[305] J. M. Souza *et al.*, “Proteolytic degradation of tyrosine nitrated proteins.,” *Arch. Biochem. bBophysics*, vol. 380, no. 2, pp. 360–366, 2000.
[306] D. Clark, J. Durner, D. a Navarre, and D. F. Klessig, “Nitric oxide inhibition of tobacco catalase and ascorbate peroxidase.,” *Mol. Plant. Microbe. Interact.*, vol. 13, no. 12, pp. 1380–1384, 2000.
[307] C. Holzmeister *et al.*, “Differential inhibition of Arabidopsis superoxide dismutases by peroxynitrite-mediated tyrosine nitration,” *J. Exp. Bot.*, vol. 66, no. 3, pp. 989–999, 2015.
[308] J. C. Begara-Morales *et al.*, “Dual regulation of cytosolic ascorbate peroxidase (APX) by tyrosine nitration and S-nitrosylation,” *J. Exp. Bot.*, vol. 65, no. 2, pp. 527–538, 2014.

[309] J. C. Begara-Morales *et al.*, “Differential molecular response of monodehydroascorbate reductase and glutathione reductase by nitration and S-nitrosylation,” *J. Exp. Bot.*, vol. 66, no. 19, pp. 5983–5996, 2015.
[310] D. Camejo *et al.*, “Functional and structural changes in plant mitochondrial PrxII F caused by NO,” *J. Proteomics*, vol. 119, pp. 112–125, 2015.
[311] A. P. Ortega-Galisteo, M. Rodríguez-Serrano, D. M. Pazmiño, D. K. Gupta, L. M. Sandalio, and M. C. Romero-Puertas, “S-Nitrosylated proteins in pea (Pisum sativum L.) leaf peroxisomes: Changes under abiotic stress,” *J. Exp. Bot.*, vol. 63, no. 5, pp. 2089–2103, 2012.
[312] M. C. de Pinto *et al.*, “S-Nitrosylation of Ascorbate Peroxidase Is Part of Programmed Cell Death Signaling in Tobacco Bright Yellow-2 Cells,” *Plant Physiol.*, vol. 163, no. 4, pp. 1766–1775, 2013.
[313] H. Yang *et al.*, “*S* -Nitrosylation Positively Regulates Ascorbate Peroxidase Activity during Plant Stress Responses,” *Plant Physiol.*, vol. 167, no. 4, pp. 1604–1615, 2015.
[314] L. C. Van Loon, B. P. J. Geraats, and H. J. M. Linthorst, “Ethylene as a modulator of disease resistance in plants.,” *Trends Plant Sci.*, vol. 11, no. 4, pp. 184–191, 2006.
[315] S. Vanneste and J. Friml, “Auxin: A Trigger for Change in Plant Development,” *Cell*, vol. 136, no. 6, pp. 1005–1016, 2009.
[316] D. E. Richards, K. E. King, T. Ait-ali, and N. P. Harberd, “How Gibberellin regulates plant growth and development: A Molecular Genetic Analysis of Gibberellin Signaling,” *Annu. Rev. Plant Physiol. Plant Mol. Biol.*, vol. 52, pp. 67–88, 2001.
[317] T. L. Karasov, E. Chae, J. J. Herman, and J. Bergelson, “Mechanisms to Mitigate the Trade-Off between Growth and Defense,” *Plant Cell*, vol. 29, no. 4, pp. 666–680, 2017.
[318] M. Naseem, M. Kaltdorf, and T. Dandekar, “The nexus between growth and defence signalling: Auxin and cytokinin modulate plant immune response pathways,” *J. Exp. Bot.*, vol. 66, no. 16, pp. 4885–4896, 2015.
[319] L. A. Lewis *et al.*, “Transcriptional Dynamics Driving MAMP-Triggered Immunity and Pathogen Effector-Mediated Immunosuppression in Arabidopsis Leaves Following Infection with Pseudomonas syringae pv tomato DC3000,” *Plant Cell*, vol. 27, no. 11, pp. 3038–3064, 2015.
[320] K. Ramonell *et al.*, “Loss-of-Function Mutations in Chitin Responsive Genes Show Increased Susceptibility to the Powdery Mildew Pathogen Erysiphe cichoracearum,” *Plant Physiol.*, vol. 138, no. 2, pp. 1027–1036, 2005.
[321] C. Zipfel *et al.*, “Bacterial disease resistance in Arabidopsis through flagellin perception.,” *Nature*, vol. 428, no. 6984, pp. 764–767, 2004.
[322] E. Georgii *et al.*, “Relationships between drought, heat and air humidity responses revealed by transcriptome-metabolome co-analysis,” *BMC Plant Biol.*, vol. 17, no. 1, p. 120, 2017.
[323] A. Stintzi, H. Weber, P. Reymond, J. Browse, and E. E. Farmer, “Plant defense in the absence of jasmonic acid: the role of cyclopentenones.,” *Proc. Natl. Acad. Sci.*, vol. 98, no. 22, pp. 12837–42, 2001.
[324] A. Dave *et al.*, “12-Oxo-Phytodienoic Acid Accumulation during Seed Development Represses Seed Germination in *Arabidopsis*,” *Plant Cell*, vol. 23, no. 2, pp. 583–599, 2011.
[325] S. Goetz *et al.*, “Role of cis-12-Oxo-Phytodienoic Acid in Tomato Embryo Development,” *Plant Physiol.*, vol. 158, no. 4, pp. 1715–1727, 2012.
[326] N. Taki *et al.*, “12-Oxo-Phytodienoic Acid Triggers Expression of a Distinct Set of Genes and Plays a Role in Wound-Induced Gene Expression in Arabidopsis,” *Plant Physiol.*, vol. 139, no. 3, pp. 1268–1283, 2005.
[327] A. J. Koo *et al.*, “Endoplasmic reticulum-associated inactivation of the hormone jasmonoyl-L-isoleucine by multiple members of the cytochrome P450 94 family in Arabidopsis,” *J. Biol. Chem.*, vol. 289, no. 43, pp. 29728–29738, 2014.
[328] E. Smirnova *et al.*, “Jasmonic Acid Oxidase 2 Hydroxylates Jasmonic Acid and Represses Basal Defense and Resistance Responses against Botrytis cinerea Infection,” *Mol. Plant*, vol. 10, no. 9, pp. 1159–1173, 2017.
[329] L. Caarls, C. M. J. Pieterse, and S. C. M. Van Wees, “How salicylic acid takes transcriptional control over jasmonic acid signaling.,” *Front. Plant Sci.*, vol. 6, no. March, p. 170, 2015.
[330] A. Leon-Reyes *et al.*, “Salicylate-mediated suppression of jasmonate-responsive gene expression in arabidopsis is targeted downstream of the jasmonate biosynthesis pathway,” *Planta*, vol. 232, no. 6, pp. 1423–1432, 2010.
[331] A. J. Koo, “Metabolism of the plant hormone jasmonate: a sentinel for tissue damage and master regulator of stress response,” *Phytochem. Rev.*, pp. 1–30, 2017.
[332] S. La Camera *et al.*, “The glutaredoxin ATGRXS13 is required to facilitate Botrytis cinerea infection of Arabidopsis thaliana plants,” *Plant J.*, vol. 68, no. 3, pp. 507–519, 2011.
[333] I. Ndamukong *et al.*, “SA-inducible Arabidopsis glutaredoxin interacts with TGA factors and suppresses JA-responsive PDF1.2 transcription,” *Plant J.*, vol. 50, no. 1, pp. 128–139, 2007.
[334] P. Schweizer, A. Buchala, P. Silverman, M. Seskar, I. Raskin, and J.-P. Métraux, “Jasmonate-inducible genes are activated in rice by pathogen attack without a concomitant increase in endogenous jasmonic acid levels.,” *Plant Physiol.*, vol. 114, pp. 79–88, 1997.
[335] K. Kazan and J. M. Manners, “MYC2: The master in action,” *Mol. Plant*, vol. 6, no. 3, pp. 686–703, 2013.
[336] C. M. J. Pieterse *et al.*, “A Novel Signaling Pathway Controlling Induced Systemic Resistance in Arabidopsis,” *Plant Cell*, vol. 10, no. 9, pp. 1571–1580, 1998.
[337] P. Nie, X. Li, S. Wang, J. Guo, H. Zhao, and D. Niu, “Induced Systemic Resistance against Botrytis cinerea by Bacillus cereus AR156 through a JA/ET- and NPR1-Dependent Signaling Pathway and Activates PAMP-Triggered Immunity in Arabidopsis,” *Front. Plant Sci.*, vol. 8, no. 238, p. doi: 10.3389/fpls.2017.00238, 2017.
[338] D.-D. Niu *et al.*, “The plant growth-promoting Rhizobacterium Bacillus cereus AR156 induces systemic resistance in arabidopsis thaliana by simultaneously activating salicylate- and jasmonate/ethylene-dependent signaling pathways.,” *Mol. Plant. Microbe. Interact.*, vol. 24, no. 5, pp. 533–542, 2011.
[339] T. Boller and G. Felix, “A renaissance of elicitors: perception of microbe-associated molecular patterns and danger signals by pattern-recognition receptors,” *Annu. Rev. Plant Biol.*, vol. 60, no. 1, pp. 379–406, 2009.
[340] D. Chinchilla *et al.*, “A flagellin-induced complex of the receptor FLS2 and BAK1 initiates plant defence,” *Nature*, vol. 448, no. 7152, pp. 497–500, 2007.
[341] P. Singh *et al.*, “The Lectin Receptor Kinase-VI.2 Is Required for Priming and Positively Regulates Arabidopsis Pattern-Triggered Immunity,” *Plant Cell*, vol. 24, no. 3, pp. 1256–1270, 2012.
[342] S. Sreekanta *et al.*, “The receptor-like cytoplasmic kinase PCRK1 contributes to pattern-triggered immunity against Pseudomonas syringae in Arabidopsis thaliana,” *New Phytol.*, vol. 207, no. 1, pp. 78–90, 2015.
[343] M. W. Rasmussen, M. Roux, M. Petersen, and J. Mundy, “MAP Kinase Cascades in Arabidopsis Innate Immunity,” *Front.*

Plant Sci., vol. 3, no. 169, p. doi: 10.3389/fpls.2012.00169, 2012.
[344] K. Ichimura *et al.*, "Mitogen-activated protein kinase cascades in plants: a new nomenclature," *Trends Plant Sci.*, vol. 7, no. 7, pp. 301–308, 2002.
[345] M. Boudsocq and J. Sheen, "CDPKs in immune and stress signaling," *Trends Plant Sci.*, vol. 18, no. 1, pp. 30–40, 2013.
[346] A. Brutus, F. Sicilia, A. Macone, F. Cervone, and G. De Lorenzo, "A domain swap approach reveals a role of the plant wall-associated kinase 1 (WAK1) as a receptor of oligogalacturonides," *Proc. Natl. Acad. Sci.*, vol. 107, no. 20, pp. 9452–9457, 2010.
[347] W. . Pryor *et al.*, "Free radical biology and medicine: it's a gas, man!," *Am. J. Physiol. Integr. Comp. Physiol.*, vol. 291, pp. R491–R511, 2006.
[348] S. Ferrari, D. Savatin, F. Sicilia, G. Gramegna, F. Cervone, and G. Lorenzo, "Oligogalacturonides: plant damage-associated molecular patterns and regulators of growth and development," *Front. Plant Sci.*, vol. 4, no. 49, p. doi: 10.3389/fpls.2013.00049, 2013.
[349] H. . An *et al.*, "Determination of pathogen-related enzyme action by mass spectrometry analysis of pectin breakdown products of plant cell walls," *Anal. Biochem.*, vol. 338, pp. 71–82, 2005.
[350] S. Y. Yi, K. Shirasu, J. S. Moon, S. G. Lee, and S. Y. Kwon, "The activated SA and JA signaling pathways have an influence on flg22-triggered oxidative burst and callose deposition," *PLoS One*, vol. 9, no. 2, 2014.
[351] K. Buxdorf, H. Yaffe, O. Barda, and M. Levy, "The Effects of Glucosinolates and Their Breakdown Products on Necrotrophic Fungi," *PLoS One*, vol. 8, no. 8, 2013.
[352] N. Agerbirk, M. De Vos, J. H. Kim, and G. Jander, "Indole glucosinolate breakdown and its biological effects," *Phytochem. Rev.*, vol. 8, no. 1, pp. 101–120, 2009.
[353] H. Heggestad, "Origin of Bel-W3, Bel-C and Bel-B Tobacco Varieties and their use as Indicators of Ozone," *Environ. Pollut.*, vol. 74, pp. 264–291, 1991.
[354] M. Schraudner *et al.*, "Ozone-induced oxidative burst in the ozone biomonitor plant, tobacco Bel W3," *Plant J.*, vol. 16, no. 2, pp. 235–245, 1998.
[355] G. T. Kuruthukulangarakoola *et al.*, "Nitric oxide-fixation by non-symbiotic haemoglobin proteins in Arabidopsis thaliana under N-limited conditions," *Plant Cell Environ.*, vol. 40, no. 1, pp. 36–50, 2017.
[356] J. Vogel and S. Somerville, "Isolation and characterization of powdery mildew-resistant Arabidopsis mutants.," *Proc. Natl. Acad. Sci. U. S. A.*, vol. 97, no. 4, pp. 1897–1902, 2000.
[357] E. Xu, L. Vaahtera, and M. Brosche, "Roles of defense hormones in the regulation of ozone-induced changes in gene expression and cell death," *Mol. Plant*, vol. 8, no. 12, pp. 1776–1794, 2015.
[358] M. Koornneeff, L. W. M. Dellaert, and J. H. van der Veen, "EMS- and relation-induced mutation frequencies at individual loci in Arabidopsis thaliana (L.) Heynh," *Mutat. Res. Mol. Mech. Mutagen.*, vol. 93, no. 1, pp. 109–123, 1982.
[359] S. Zhao and R. D. Fernald, "Comprehensive Algorithm for Quantitative Real-Time Polymerase Chain Reaction," *J. Comput. Biol.*, vol. 12, no. 8, pp. 1047–1064, 2005.
[360] S. Arvidsson, M. Kwasniewski, D. M. Riaño-Pachón, and B. Mueller-Roeber, "QuantPrime-a flexible tool for reliable high-throughput primer design for quantitative PCR.," *BMC Bioinformatics*, vol. 9, p. 465, 2008.
[361] J. Vandesompele *et al.*, "Accurate normalization of real-time quantitative RT-PCR data by geometric averaging of multiple internal control genes," *Genome Biol.*, vol. 3, no. 711, pp. 34–1, 2002.
[362] E. Huala *et al.*, "The Arabidopsis Information Resource (TAIR): a comprehensive database and web-based information retrieval, analysis, and visualization system for a model plant," *Nucleic Acids Res.*, vol. 29, no. 1, pp. 102–105, 2001.
[363] H. Mi *et al.*, "PANTHER version 11: Expanded annotation data from Gene Ontology and Reactome pathways, and data analysis tool enhancements," *Nucleic Acids Res.*, vol. 45, pp. D183–D189, 2016.
[364] F. Supek, M. Bošnjak, N. Škunca, and T. Šmuc, "Revigo summarizes and visualizes long lists of gene ontology terms," *PLoS One*, vol. 6, no. 7, 2011.
[365] P. Bardou, J. Mariette, F. Escudié, C. Djemiel, and C. Klopp, "jvenn: an interactive Venn diagram viewer.," *BMC Bioinformatics*, vol. 15, p. 293, 2014.
[366] N. Kolesnikov *et al.*, "ArrayExpress update - simplifying data submissions," *Nucleic Acids Res.*, vol. 43, no. Database Issue, pp. D1113–D1116, 2015.
[367] J. H. Joo, S. Wang, J. G. Chen, A. M. Jones, and N. V Fedoroff, "Different signaling and cell death roles of heterotrimeric G protein alpha and beta subunits in the Arabidopsis oxidative stress response to ozone," *Plant Cell*, vol. 17, pp. 957–970, 2005.
[368] M. M. Bradford, "A rapid and sensitive method for the quantiWcation of microgram quantities of protein utilizing the principle of protein– dye binding," *Anal. Biochem.*, vol. 72, pp. 248–254, 1976.
[369] J. Vadassery, M. Reichelt, B. Hause, J. Gershenzon, W. Boland, and A. Mithöfer, "CML42-mediated calcium signaling coordinates responses to Spodoptera herbivory and abiotic stresses in Arabidopsis," *Plant Physiol.*, vol. 159, no. 3, pp. 1159–1175, 2012.
[370] H. Kojima *et al.*, "Development of a fluorescent indicator for nitric oxide based on the fluorescein chromophore.," *Chem. Pharm. Bull. (Tokyo).*, vol. 46, no. 2, pp. 373–375, 1998.
[371] H. Kojima *et al.*, "Detection and Imaging of Nitric Oxide with Novel Fluorescent Indicators: Diaminofluorescins," *Anal. Chem.*, vol. 70, no. 13, pp. 2446–2453, 1998.
[372] H. Kojima, Y. Urano, K. Kikuchi, T. Higuchi, Y. Hirata, and T. Nagano, "Fluorescent Indicators for Imaging Nitric Oxide Production," *Angew Chem Int Ed Engl*, vol. 38, no. 21, pp. 3209–3212, 1999.
[373] A. Daudi and J. A. O'Brien, "Detection of Hydrogen Peroxide by DAB Staining in Arabidopsis Leaves," *Bio-protocol*, vol. 2, no. 18, pp. 1–5, 2012.
[374] F. Ramel, C. Sulmon, M. Bogard, I. Couée, and G. Gouesbet, "Differential patterns of reactive oxygen species and antioxidative mechanisms during atrazine injury and sucrose-induced tolerance in Arabidopsis thaliana plantlets.," *BMC Plant Biol.*, vol. 9, no. January 2017, p. 28, 2009.
[375] G. Smyth, "Limma: linear models for microarray data. In: Bioinformatics and Computational Biology Solutions using R and Bioconductor, R. Gentleman, V. Carey, S. Dudoit, R. Irizarry, W. Huber (eds.)," *Springer, New York*, pp. 397–420, 2005.
[376] G. Smyth, "Linear models and empirical bayes methods for assessing differential expression in microarray experiments.," *Stat Appl Genet Mol Biol.*, vol. 3, no. Article3, 2004.
[377] M. Ritchie *et al.*, "limma powers differential expression analyses for RNA-sequencing and microarray studies.," *Nucleic*

Acids Res., vol. 43, no. e47, 2015.
[378] R. Cho and M. Campbell, “Transcription, genomes, function,” *Trends Genet.*, vol. 16, no. 9, pp. 409–415, 2000.
[379] J. Wobbrock, L. Findlater, D. Gergle, and J. Higgins, “The Aligned Rank Transform for Nonparametric Factorial Analyses Using Only ANOVA Procedures,” *Proc. CHI’11. New York ACM Press*, pp. 143–146, 2011.
[380] D. Kasten, J. Durner, and F. Gaupels, “Gas Alert : The NO2 Pitfall during NO Fumigation of Plants,” *Front. Plant Sci.*, vol. 8, no. 2, pp. 8–11, 2017.

8 Supplement

Supplemental Figures

Supplemental Tables

8.1 Supplementary Figures

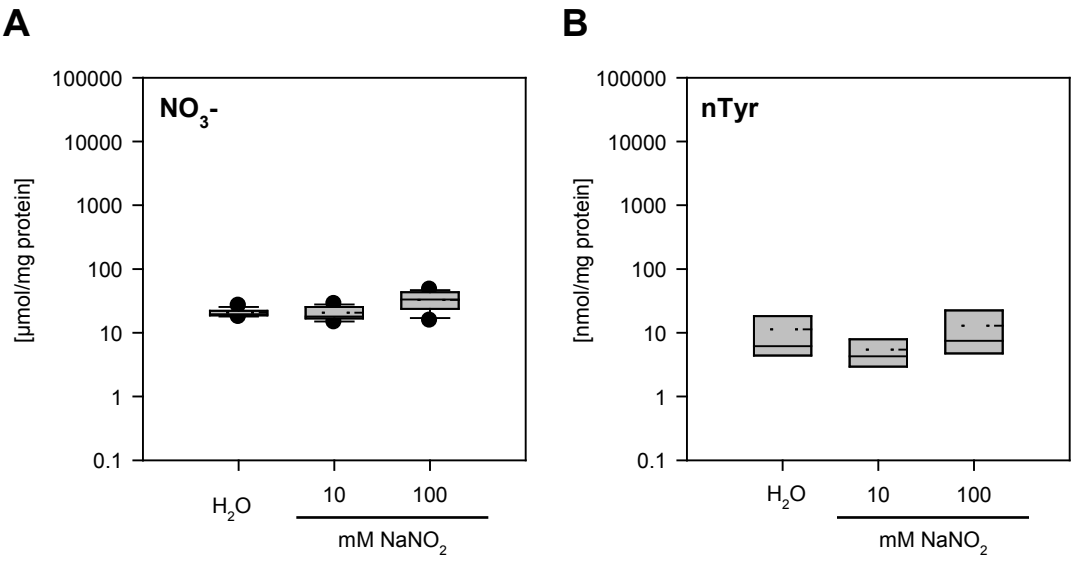

Supplemental Figure 1: Nitrite injection does not influence nitrate levels and nitrated proteins
Leaves were infiltrated with H_2O (control), 10 mM, or 100 mM $NaNO_2$. All measurements were performed 3 h after infiltration. A Nitric Oxide Analyzer was used to quantify **A)** nitrate (NO_3^-). **B)** Tyrosine-nitrated protein levels (nTyr) were measured by an enzyme-linked immunoassay. **A, B)** Box plots represent median (solid line), mean (dashed line), and 25th/75th percentiles (grey box) from 2 independent experiments; n = 7 (A), 3-4 (B). Whiskers represent 5th and 95th percentiles (only when n > 3), black dots are outliers.

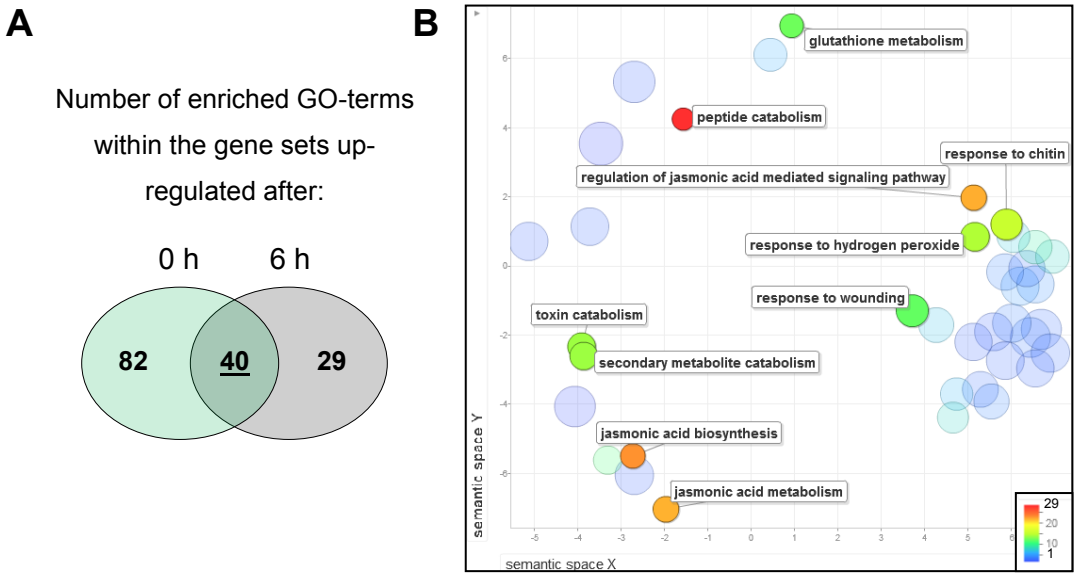

Supplemental Figure 2: GO-term enrichment analysis of genes up-regulated by 10 ppm NO_2 directly and 6 h after fumigation

A) Venn Diagram illustrating the number of enriched GO-terms within the gene sets that were up-regulated at 0 h and 6h after fumigation with 10 ppm NO_2. Right: GO-terms of genes exclusively up-regulated 0 h after fumigation, left: GO-terms of genes exclusively up-regulated 6 h after fumigation, middle: GO-terms of genes mutually up-regulated at both time points. **B)** GO-terms significantly enriched ($p < 0.05$) within the up-regulated gene sets of both time points were identified using the PANTHER 11.0 overrepresentation test and visualized in a scatter plot using the REVIGO tool. Each circle represents a GO-term, whereat the number of genes it encompasses is represented by the circle size. The color code depicts the fold enrichment of the respective GO-term within the data set compared to the PANTHER *Arabidopsis thaliana* reference list. Circles are clustered according to the distance of the respective GO-terms within the GO hierarchical tree. Axes have no intrinsic meaning. Highly enriched or interesting GO terms are labeled.

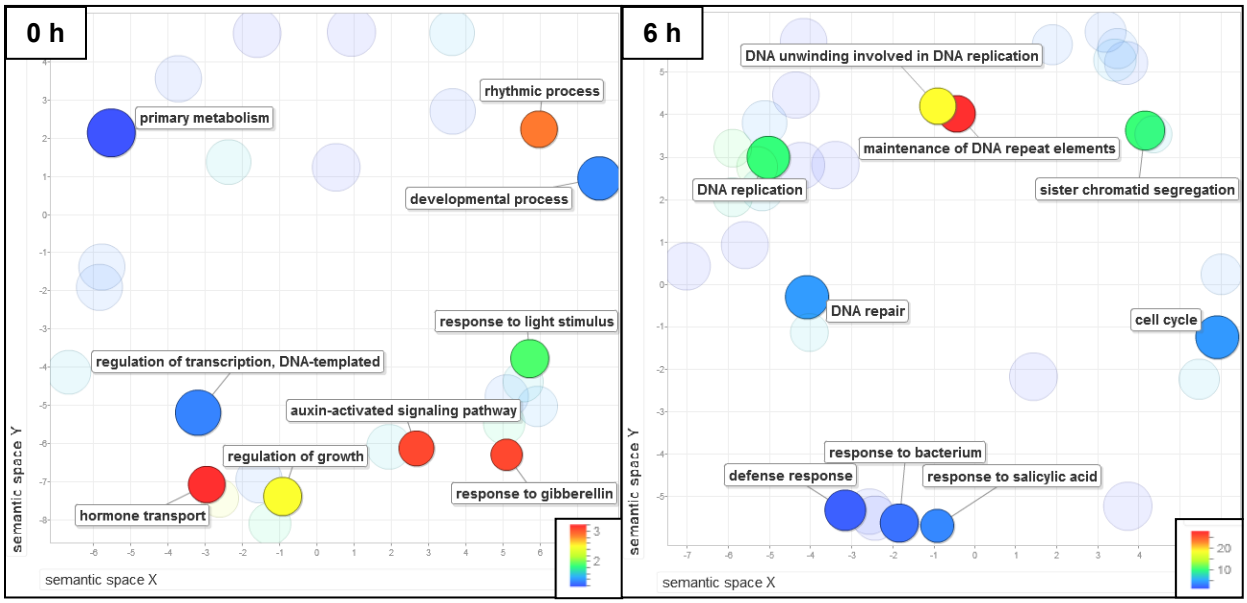

Supplemental Figure 3: GO-term enrichment analysis of genes down-regulated by 10 ppm NO_2
Enriched GO-terms ($p < 0.05$) were identified using the PANTHER 11.0 overrepresentation test and visualized in scatter plots using the REVIGO tool. Each circle represents a GO-term, whereat the number of genes it encompasses is represented by the circle size. The color code depicts the fold enrichment of the respective GO-term within the data set compared to the PANTHER *Arabidopsis thaliana* reference list. Circles are clustered according to the distance of the respective GO-terms within the GO hierarchical tree. Axes have no intrinsic meaning. Highly enriched or interesting GO-terms are labeled. GO-term enrichment of genes down-regulated directly (0 h) (left) or 6 h (right) after fumigation.

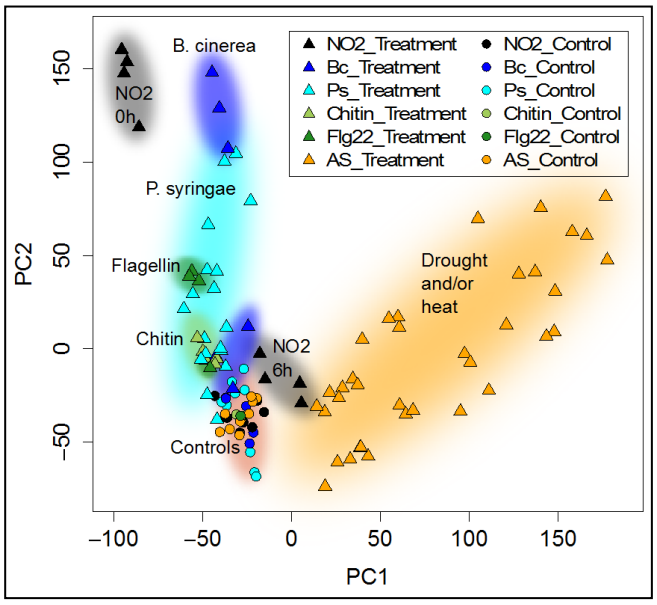

Supplemental Figure 4: NO_2–induced genes are related to pathogen defense
Meta-analysis of Col-0 *Arabidopsis thaliana* gene expression responses to NO_2 fumigation, biotic stress, and abiotic stress. Microarray measurements from the NO_2 fumigation were combined with previously published microarray data representing different biotic and abiotic stresses (ArrayExpress accession numbers, E-GEOD-6176, E-GEOD-17382 and E-MTAB-4867), yielding 115 samples in total. Gene expression levels were centered for each experiment relative to the mean of its controls, to focus on treatment responses. The overall expression similarities between samples of the combined dataset are visualized using the top two principal components, capturing 22% and 14% of the total variation, respectively. NO2, NO_2 fumigation; Bc = *Botrytis cinerea* infection, ArrayExpress accession numbers E-GEOD-5684; Ps = *Pseudomonas syringae* infection, E-GEOD-6176; Chitin = Chitin treatment, E-GEOD-2538; flg22 = flagellin epitope 22 treatment, E-GEOD-17382; AS = abiotic stress treatment study, E-MTAB-4867; for each study, treated samples are marked by triangles and controls by circles. Analysis and graphical representation was kindly performed by Dr. Elisabeth Georgii.

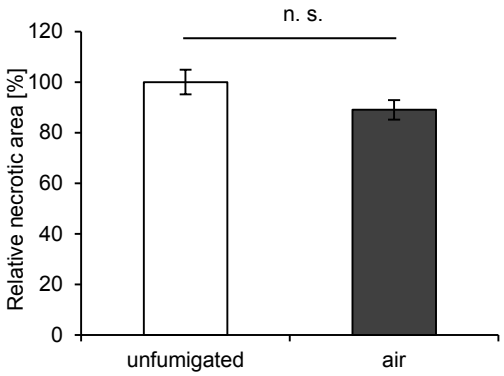

Supplemental Figure 5: *Botrytis cinerea*-induced necrotic lesions on air and unfumigated plants
Col-0 plants were fumigated with air for 1 h (or unfumigated) followed by droplet-infection of detached leaves with approx. 1000 spores of *B. cinerea* 6 h after fumigation. Evaluation of necrotic lesion development occurred 3 days after infection by measuring the necrotic area via ImageJ. The necrotic areas formed on fumigated leaves were normalized to the mean necrotic area of unfumigated leaves (= 100 %). Columns represent means ± SEM; n_{leaves} = 81-89. Mann Whitney Rank Sum Test showed no significant differences (n. s.).

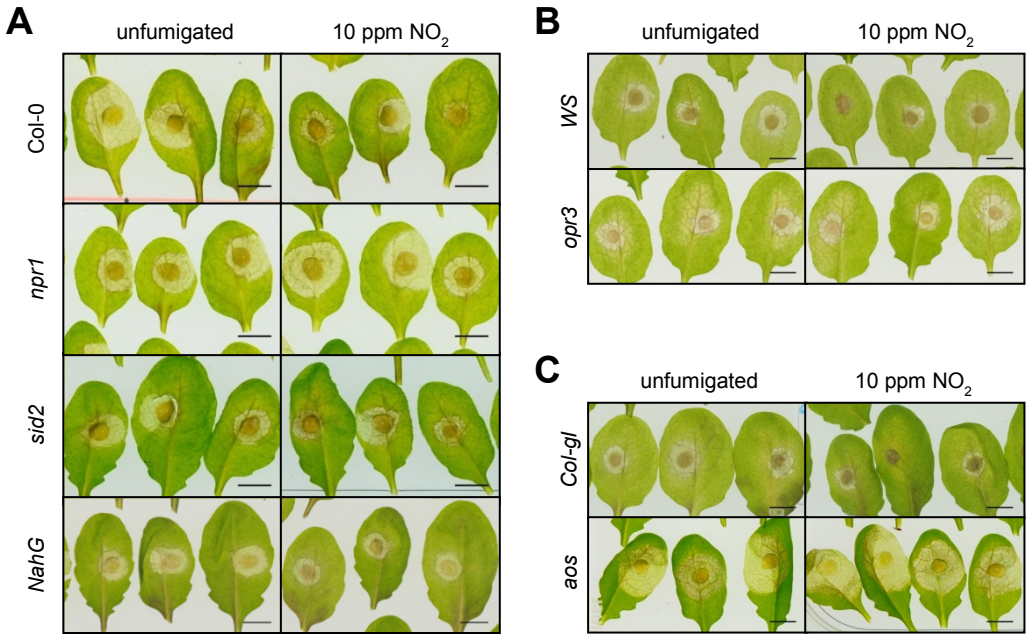

Supplemental Figure 6: Representative necrotic lesions formed on NO_2-fumigated mutants
Mutants were fumigated with 10 ppm NO_2 for 1 h (or unfumigated) followed by droplet-infection of detached leaves with approx. 1000 spores of *B. cinerea* 6 h after fumigation. The necrotic lesions developed 3 days after infection were documented for further evaluation of the relative necrotic area. Representative pictures of necrotic lesion formation are shown. **A)** Mutants impaired in SA-accumulation (*sid2, NahG)* and SA-signaling (*npr1*) alongside their Col-0 WT control. **B)** JA-deficient *opr3* and its parental line WS **C)** A-deficient *aos* and its parental line *Col-gl*. Scale = 5 mm.

B. cinerea-induced hormone accumulation is not altered by NO_2-pretreatment

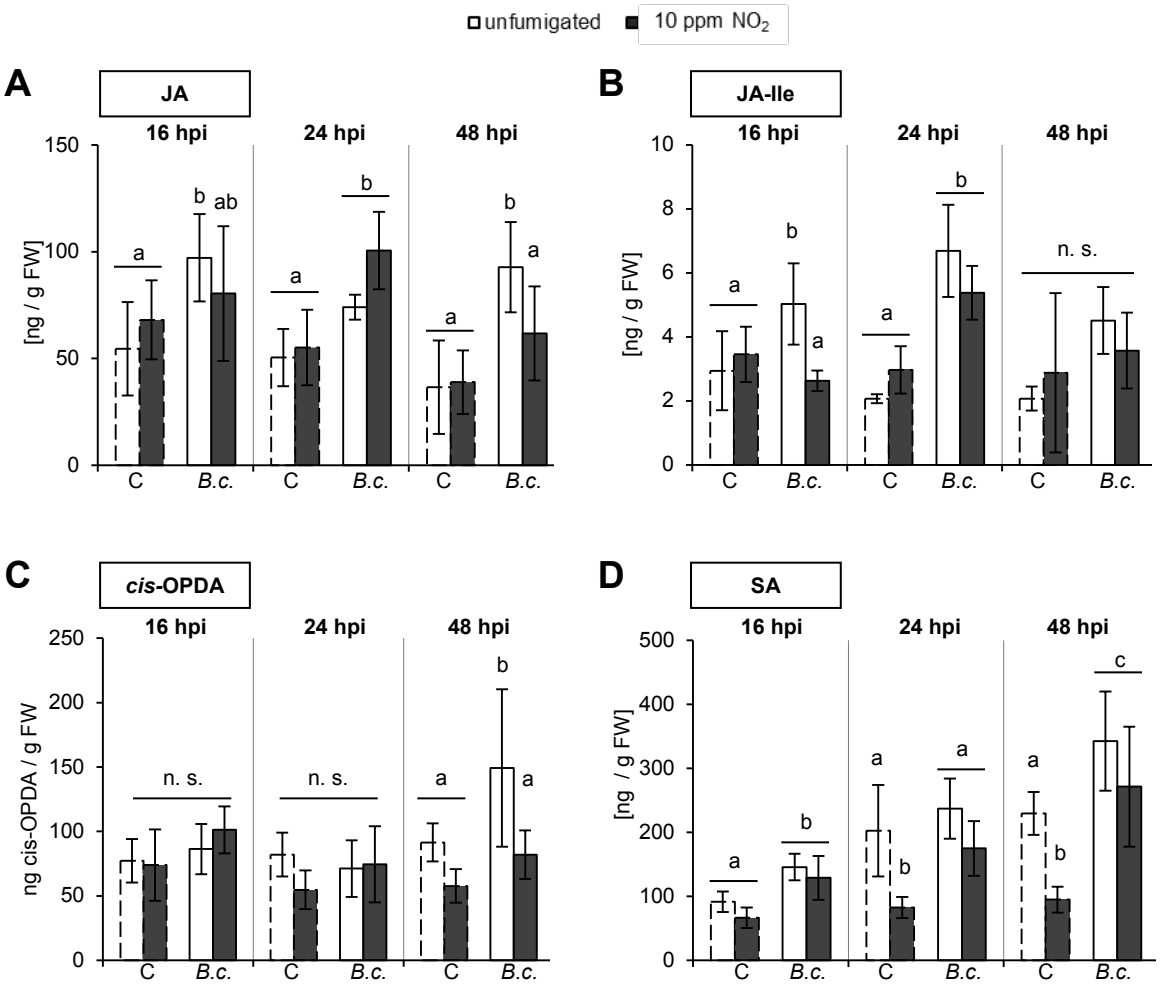

Supplemental Figure 7: *B. cinerea*-induced jasmonate and SA accumulation is not altered by NO_2
Col-0 plants were spray-infected with 2 x 10^5 *B. cinerea* spores 6 h after fumigation with air or 10 ppm NO_2 for 1 h. Leaf material was harvested for LC-MS/MS analysis at the indicated time points. The levels of **A)** jasmonic acid (JA), **B)** jasmonoyl-isoleucine (JA-Ile), **C)** *cis*-(+)-12-oxophytodienoic acid (*cis*-OPDA), and **D)** salicylic acid (SA) were normalizied to the sample's fresh weight (FW). Columns represent means ± SD; n = 4-5. **A, B, C, D)** Letters indicate significant differences of all pairwise comparisons within the time points via Two Way ANOVA + Holm-Sidak post-hoc Test ($p < 0.05$). Two Way ANOVA revealed that changes in hormone levels were significantly dependent on the type of infection for all hormones and time points ($p < 0.05$). The infection-induced changes were not dependent on the type of fumigation. Dashed-lined columns distinguish infection controls. C = half-strength grape juice as infection control, *B.c.* = *B. cinerea*, n. s. = not significant, hpi = hours post infection.

The previous results suggested that the NO_2-induced synthesis of JA and, at least in part, SA are crucial processes during the observed induced resistance against *B. cinerea* (see section 2.4) . This is further supported by the necessity of functional JA- and SA-mediated signaling pathways during the NO_2-induced resistance development. To investigate, whether the observed resistance was

conveyed by an enhanced or temporally advanced production of these phytohormones, their levels were quantified in NO_2- and air-fumigated Col-0 plants at various time points after spray-infection with *B. cinerea*.

The LC-MS/MS measurements revealed a significant increase of JA in air fumigated plants at all analyzed time points after *B. cinerea* infection. However, in NO_2-fumigated samples JA increased significantly only at 24 h after infection (Supplemental Figure 7 A). Multi-factorial analysis via Two Way ANOVA demonstrated that changes in the JA content was significantly dependent on the type of infection (control *vs. B. cinerea*) but not on the type of fumigation (air *vs.* NO_2). Similar results were obtained after measuring the JA-Ile and *cis*-OPDA content (Supplemental Figure 7 B, C). In contrast to JA, SA levels were gradually increasing significantly over time upon *B. cinerea* infection in both NO_2- and air- fumigated plants (Three Way ANOVA, $p < 0.001$). However, the SA content in NO_2-fumigated plants was consistently lower than the levels measured in plants exposed to air prior to infection (Supplemental Figure 7 D). This was reflected by the multi-factorial analysis via Two Way ANOVA that determined a significant difference in SA levels due to fumigation at 24 and 48 h after infection ($p < 0.006$).

In summary, these results indicated that the *B. cinerea*-induced jasmonate accumulation was not altered by NO_2 pretreatment. Moreover, it was demonstrated that *B. cinerea* infection generally induced a gradual increase in SA, which however was less pronounced in NO_2-fumigated plants. Therefore, it can be concluded that the NO_2-induced resistance against *B. cinerea* was not mediated by a temporally advanced or enhanced accumulation of the above mentioned phytohormones.

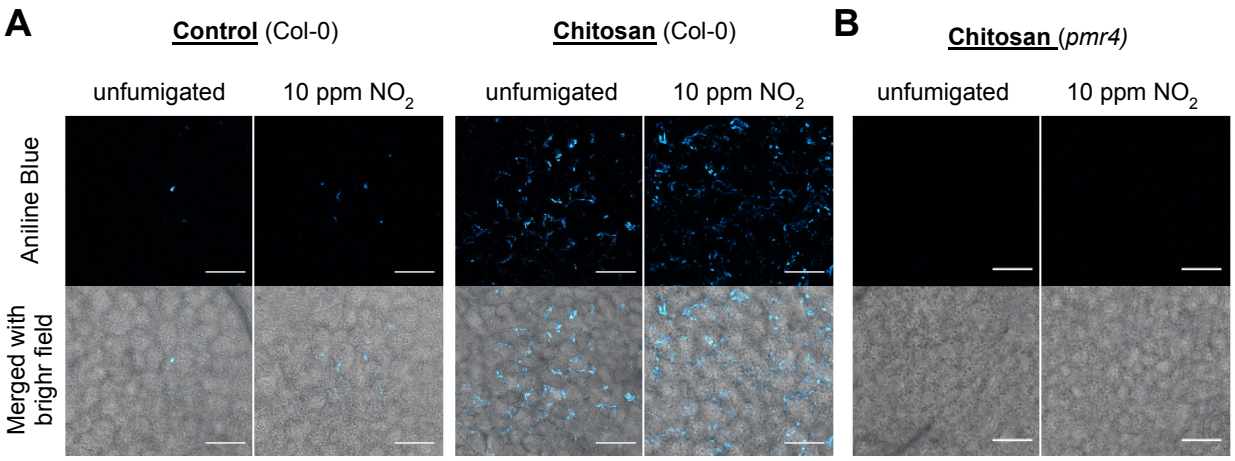

Supplemental Figure 8: Callose detection via Aniline Blue 16 h after chitosan elicitation
Plants were fumigated with 10 ppm NO_2 for 1 h (unfumigated as control) and infiltrated with 500 µg/ml chitosan (0.04 % acetic acid as control) 4 h after fumigation. Leaf discs were obtained 16 h after chitosan treatment and stained with Aniline Blue. Fluorescence was detected with the TCS SP8 X confocal laser scanning microscope (Leica). Excitation with Diode Laser UV 405 nm (0.1 % intensity), Emission at 480 – 500 nm. Bright field pictures were taken at gain 400 using the Transmission PMT. Channels were merged using the ImageJ software. Representative pictures of the Aniline Blue fluorescence were taken of NO_2-fumigated or unfumigated **A)** Col-0 leaves 16 h after treatment with chitosan or control or **B)** of *pmr4* leaves 16 h after treatment with chitosan. **A, B)** 3 different areas of 3 independent leaf discs were examined with similar results. Scale = 100 µm.

Stomatal conductance of utilized mutants

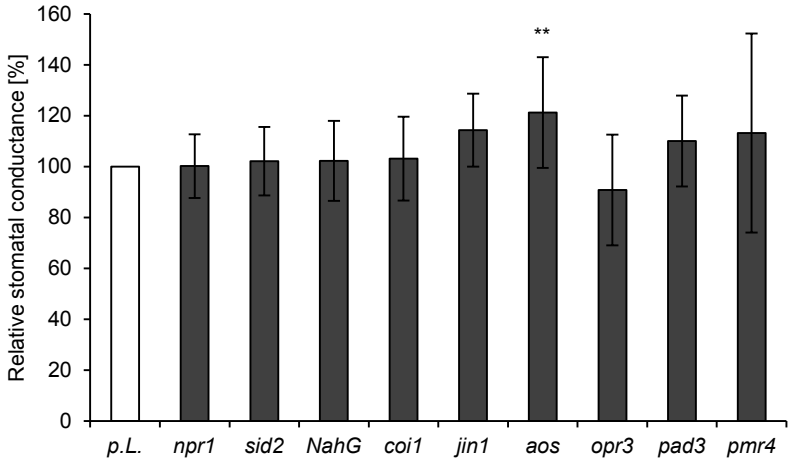

Supplemental Figure 9: Basal stomatal conductance of utilized mutants.
Stomatal conductance was measured using a leaf porometer. Conductance of mutants was normalized to their respective parental line (= 100 %). Columns represent mean ± SD; n = 13-16, except n = 35 for *pmr4*. p.L. = parental line (Col-0 for *npr1, sid2*, NahG, *coi1, jin1, pad3, pmr4*; WS for *opr3*; *Col-gl* for *aos*) Asterisks indicate significant differences from respective parental line via One Way ANOVA + Holm-Sidak Test (**p < 0.01).

The stomatal conductance measurements to water vapor (mmol/m^2s) were done using a SC-1 Leaf Porometer (Decagon Devices Inc) to determine the plants capability to take up the applied NO_2. Stomata conductance measurements of four-week-old Col-0 plants directly after fumigation with various concentrations of NO_2 were performed in the course of the publication of Kasten *et al*., 2016. Here, it was shown that the fumigation with 10 ppm NO_2 did not induce stomatal closure. However,

20 ppm NO_2 caused a 20 % reduction of the stomatal conductance, whereas exposure to 30 ppm NO_2 led to a 75 % increase in stomatal conductance which was linked to the rapid wilting. As a e control, untreated Col-0 plants were transferred to the dark for 2.5 h to obtain a conductance reference of closed stomata [39]. Moreover, the basal stomatal conductance of the mutants utilized in this work was analyzed to ensure comparable NO_2 uptake through the stomata throughout the used genotypes.

As shown in Supplemental Figure 9, the stomatal conductance of the utilized mutants was similar to the parental lines, indicating that the mutations did not influence the stomatal aperture. Therefore, it can be concluded, that the mutants were taking up similar amounts of NO_2 during the fumigation period. The only exception was the *aos* mutant which displayed a significantly elevated stomatal conductance when compared to the respective Col-gl parental line.

B. cinerea susceptibility of the utilized mutants

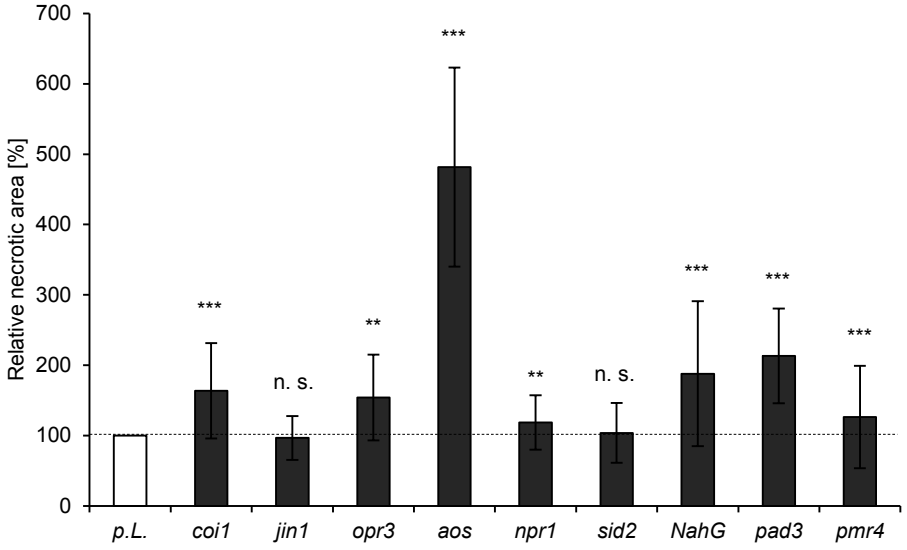

Supplemental Figure 10: B. *cinerea* susceptibility of the utilized mutants
Detached leaves of unfumigated plants were droplet-infected with approx. 1000 spores of *B. cinerea.* Evaluation of necrotic lesion development occurred 3 days after infection by measuring the necrotic area via ImageJ. The necrotic areas formed on leaves of untreated plants were normalized to the mean necrotic area formed on leaves of their respective untreated parental line (= 100 %). Columns represent means ± SD; n_{leaves} = *coi1*: 99 (p.L: 91); *jin1*: 95 (p.L: 37); *opr3*: 21 (p.L: 18); *aos*: 125 (p.L: 66); *npr1*: 95 (p.L: 37); *sid2*: 154 (p.L: 68); *NahG*: 223 (p.L: 263); *pad3*: 98 (p.L: 91); *pmr4*: 206 (p.L: 197). p.L. = parental line (Col-0 for *npr1, sid2*, NahG, *coi1, jin1, pad3, pmr4*; WS for *opr3, Col-gl* for *aos*) Asterisks indicate significant differences to the corresponding parental line via Mann-Whitney Rank Sum Test (**p < 0.01, ***p < 0.001). n. s. = not significant.

The general susceptibility of the utilized mutants towards B. cinerea infection was analyzed in parallel to the B. cinerea infection assay of NO_2-fumigated plants, since untreated mutants and their

respective parental lines were infected alongside the NO_2 treated ones (see 6.3.2 for detailed method). The obtained necrotic areas formed on leaves of untreated mutants were normalized to the mean necrotic area formed on leaves of their respective untreated parental line (= 100 %). Supplemental Figure 10 depicts the determined necrotic area formed on the investigated mutants three days after infection relative to their respective parental lines.

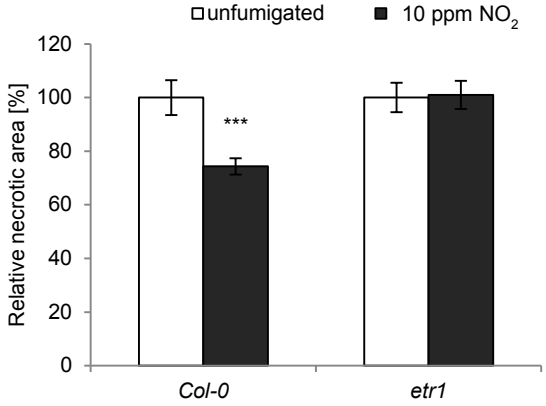

Supplemental Figure 11: The *etr1* mutant lacks the NO2-induced resistance against *B. cinerea*
etr1 and Col-0 plants were subjected to *B. cinerea* droplet-infection 6 h after fumigation with 10 ppm NO_2 for 1 h (unfumigated as control). Necrotic areas formed on fumigated leaves after 2 days were normalized to the mean necrotic area of the respective unfumigated leaves (= 100 %). Columns represent means of 2 independent experiments ± SEM; n_{leaves} = 57 (Col-0), 30-35 (*etr1*). Asterisks indicate significant differences of all pairwise comparisons via Kruskal Wallis Test + Dunn's post-hoc Test (***p < 0.001). The displayed results are preliminary.

8.2 Supplementary Tables

Supplemental Table 1: List of significantly enriched GO-terms of genes up-regulated directly after NO_2 fumigation

A = number of genes in the reference list mapping to the GO-term. B = number of genes in the sample list mapping to the GO-term. C = number of genes from the sample list that is expected to map to the GO-term based on the reference list (reference genes $_{total}$ / A) * samples genes $_{total}$). FE = Fold enrichment of genes in sample list over the expected number (B/C; FE > 1 = overrepresented GO-term). Blue: Selection of GO-terms associated with stress and defense responses against pathogens. Yellow: GO-terms highlighted in the corresponding REVIGO scatterplot.

GO biological process	GO-term ID	A	B	C	FE	p-value
camalexin metabolic process	GO:0052317	9	7	0.79	8.88	4.11E-02
camalexin biosynthetic process	GO:0010120	9	7	0.79	8.88	4.11E-02
cellular response to hypoxia	GO:0071456	23	16	2.01	7.94	1.12E-06
response to chitin	GO:0010200	109	75	9.55	7.85	9.17E-38
cellular response to oxygen levels	GO:0071453	26	16	2.28	7.03	6.24E-06
cellular response to decreased oxygen levels	GO:0036294	26	16	2.28	7.03	6.24E-06
response to organonitrogen compound	GO:0010243	136	83	11.91	6.97	3.07E-38

GO biological process	GO-term ID	A	B	C	FE	p-value
regulation of jasmonic acid mediated signaling pathway	GO:2000022	23	12	2.01	5.96	3.15E-03
response to molecule of bacterial origin	GO:0002237	20	10	1.75	5.71	3.33E-02
jasmonic acid biosynthetic process	GO:0009695	22	11	1.93	5.71	1.27E-02
jasmonic acid metabolic process	GO:0009694	27	13	2.37	5.5	2.81E-03
response to oomycetes	GO:0002239	35	16	3.07	5.22	3.49E-04
defense response to oomycetes	GO:0002229	29	13	2.54	5.12	6.05E-03
toxin metabolic process	GO:0009404	54	24	4.73	5.07	5.59E-07
induced systemic resistance	GO:0009682	29	12	2.54	4.72	3.16E-02
response to nitrogen compound	GO:1901698	211	87	18.48	4.71	7.45E-28
response to hypoxia	GO:0001666	59	24	5.17	4.64	3.10E-06
response to wounding	GO:0009611	184	74	16.12	4.59	9.15E-23
regulation of response to biotic stimulus	GO:0002831	50	20	4.38	4.57	9.11E-05
toxin catabolic process	GO:0009407	43	17	3.77	4.51	1.07E-03
secondary metabolite catabolic process	GO:0090487	43	17	3.77	4.51	1.07E-03
regulation of response to external stimulus	GO:0032101	54	21	4.73	4.44	6.77E-05
plant-type hypersensitive response	GO:0009626	68	26	5.96	4.36	2.34E-06
glutathione metabolic process	GO:0006749	55	21	4.82	4.36	9.16E-05
response to decreased oxygen levels	GO:0036293	66	25	5.78	4.32	5.82E-06
host programmed cell death induced by symbiont	GO:0034050	69	26	6.04	4.3	3.15E-06
defense response to bacterium, incompatible interaction	GO:0009816	40	15	3.5	4.28	9.20E-03
response to oxygen levels	GO:0070482	67	25	5.87	4.26	7.80E-06
regulation of immune system process	GO:0002682	91	31	7.97	3.89	9.69E-07
programmed cell death	GO:0012501	94	31	8.23	3.76	2.06E-06
regulation of immune response	GO:0050776	82	27	7.18	3.76	2.49E-05
indole-containing compound metabolic process	GO:0042430	65	21	5.69	3.69	1.35E-03
response to hydrogen peroxide	GO:0042542	53	17	4.64	3.66	1.66E-02
regulation of innate immune response	GO:0045088	80	25	7.01	3.57	2.24E-04
response to bacterium	GO:0009617	354	110	31.01	3.55	2.01E-25
defense response to bacterium	GO:0042742	282	87	24.7	3.52	1.75E-19
innate immune response	GO:0045087	241	74	21.11	3.51	3.58E-16
flavonoid glucuronidation	GO:0052696	62	19	5.43	3.5	9.50E-03
cellular glucuronidation	GO:0052695	62	19	5.43	3.5	9.50E-03

GO biological process	GO-term ID	A	B	C	FE	p-value
glucuronate metabolic process	GO:0019585	62	19	5.43	3.5	9.50E-03
immune response	GO:0006955	246	74	21.55	3.43	1.07E-15
immune system process	GO:0002376	277	83	24.26	3.42	9.78E-18
uronic acid metabolic process	GO:0006063	64	19	5.61	3.39	1.48E-02
cell death	GO:0008219	125	37	10.95	3.38	9.74E-07
regulation of defense response	GO:0031347	182	53	15.94	3.32	3.53E-10
defense response, incompatible interaction	GO:0009814	132	38	11.56	3.29	1.21E-06
response to jasmonic acid	GO:0009753	178	51	15.59	3.27	1.80E-09
aging	GO:0007568	114	31	9.99	3.1	1.55E-04
response to salicylic acid	GO:0009751	171	45	14.98	3	5.51E-07
regulation of response to stress	GO:0080134	233	61	20.41	2.99	4.93E-10
response to toxic substance	GO:0009636	96	25	8.41	2.97	5.73E-03
ethylene-activated signaling pathway	GO:0009873	135	35	11.83	2.96	7.26E-05
response to reactive oxygen species	GO:0000302	138	35	12.09	2.9	1.22E-04
protein autophosphorylation	GO:0046777	115	29	10.07	2.88	1.79E-03
cellular modified amino acid metabolic process	GO:0006575	106	26	9.29	2.8	1.04E-02
cellular response to ethylene stimulus	GO:0071369	151	36	13.23	2.72	3.47E-04
response to oxygen-containing compound	GO:1901700	1168	274	102.32	2.68	2.57E-44
positive regulation of response to stimulus	GO:0048584	143	33	12.53	2.63	2.22E-03
flavonoid biosynthetic process	GO:0009813	113	26	9.9	2.63	3.09E-02
response to oxidative stress	GO:0006979	364	83	31.89	2.6	4.57E-11
defense response	GO:0006952	1302	293	114.05	2.57	2.84E-44
response to acid chemical	GO:0001101	907	197	79.45	2.48	1.15E-26
response to ethylene	GO:0009723	235	51	20.59	2.48	2.15E-05
phosphorelay signal transduction system	GO:0000160	167	36	14.63	2.46	3.44E-03
response to heat	GO:0009408	161	34	14.1	2.41	1.01E-02
response to water deprivation	GO:0009414	237	50	20.76	2.41	7.05E-05
response to water	GO:0009415	243	51	21.29	2.4	6.06E-05
response to abscisic acid	GO:0009737	416	86	36.44	2.36	2.71E-09
abscisic acid-activated signaling pathway	GO:0009738	161	33	14.1	2.34	2.50E-02
response to alcohol	GO:0097305	420	86	36.79	2.34	4.41E-09
cellular response to abscisic acid stimulus	GO:0071215	173	35	15.15	2.31	1.82E-02
cellular response to alcohol	GO:0097306	173	35	15.15	2.31	1.82E-02
response to other organism	GO:0051707	1016	204	89	2.29	1.67E-23
response to external biotic	GO:0043207	1017	204	89.09	2.29	1.88E-23

GO biological process	GO-term ID	A	B	C	FE	p-value
stimulus						
response to organic cyclic compound	GO:0014070	288	57	25.23	2.26	6.83E-05
protein phosphorylation	GO:0006468	755	148	66.14	2.24	1.81E-15
response to biotic stimulus	GO:0009607	1058	206	92.68	2.22	3.70E-22
response to endogenous stimulus	GO:0009719	1309	250	114.67	2.18	2.39E-26
defense response to other organism	GO:0098542	784	149	68.68	2.17	1.88E-14
response to organic substance	GO:0010033	1496	284	131.05	2.17	5.27E-30
cellular response to acid chemical	GO:0071229	354	66	31.01	2.13	5.35E-05
regulation of response to stimulus	GO:0048583	426	79	37.32	2.12	2.96E-06
response to stress	GO:0006950	2769	505	242.56	2.08	6.01E-53
response to chemical	GO:0042221	2100	382	183.96	2.08	5.60E-38
response to temperature stimulus	GO:0009266	416	75	36.44	2.06	2.40E-05
response to external stimulus	GO:0009605	1294	229	113.35	2.02	1.12E-19
response to lipid	GO:0033993	567	100	49.67	2.01	2.89E-07
sulfur compound metabolic process	GO:0006790	303	52	26.54	1.96	1.53E-02
response to osmotic stress	GO:0006970	461	79	40.38	1.96	7.97E-05
response to salt stress	GO:0009651	418	71	36.62	1.94	5.27E-04
cellular response to oxygen-containing compound	GO:1901701	454	77	39.77	1.94	1.77E-04
signal transduction	GO:0007165	1477	248	129.38	1.92	1.33E-18
response to inorganic substance	GO:0010035	693	116	60.71	1.91	2.12E-07
phosphorylation	GO:0016310	1084	181	94.96	1.91	1.21E-12
single organism signaling	GO:0044700	1505	249	131.84	1.89	6.98E-18
signaling	GO:0023052	1506	249	131.92	1.89	7.58E-18
cellular response to chemical stimulus	GO:0070887	864	142	75.69	1.88	5.84E-09
cell communication	GO:0007154	1662	269	145.59	1.85	2.73E-18
cellular response to endogenous stimulus	GO:0071495	653	105	57.2	1.84	1.28E-05
response to hormone	GO:0009725	1226	195	107.4	1.82	8.51E-12
cellular response to hormone stimulus	GO:0032870	646	102	56.59	1.8	5.08E-05
cellular response to organic substance	GO:0071310	755	119	66.14	1.8	3.83E-06
intracellular signal transduction	GO:0035556	488	76	42.75	1.78	4.89E-03
response to abiotic stimulus	GO:0009628	1507	233	132.01	1.77	3.07E-13
response to stimulus	GO:0050896	4768	736	417.67	1.76	1.80E-53
hormone-mediated signaling pathway	GO:0009755	605	93	53	1.75	6.59E-04
cellular response to stimulus	GO:0051716	2138	324	187.29	1.73	2.66E-18

GO biological process	GO-term ID	A	B	C	FE	p-value
response to fungus	GO:0009620	503	75	44.06	1.7	2.46E-02
phosphate-containing compound metabolic process	GO:0006796	1476	215	129.3	1.66	1.54E-09
phosphorus metabolic process	GO:0006793	1532	223	134.2	1.66	5.90E-10
protein modification process	GO:0036211	1693	238	148.3	1.6	2.75E-09
cellular protein modification process	GO:0006464	1693	238	148.3	1.6	2.75E-09
positive regulation of biological process	GO:0048518	648	91	56.76	1.6	2.97E-02
macromolecule modification	GO:0043412	1904	244	166.79	1.46	7.22E-06
regulation of cellular process	GO:0050794	3772	450	330.42	1.36	1.57E-08
regulation of biological process	GO:0050789	4093	485	358.54	1.35	5.00E-09
single-organism process	GO:0044699	7081	795	620.29	1.28	2.72E-12
biological regulation	GO:0065007	4745	521	415.66	1.25	4.31E-05
cellular process	GO:0009987	9015	965	789.7	1.22	8.33E-11
cellular metabolic process	GO:0044237	6708	699	587.61	1.19	2.59E-04
metabolic process	GO:0008152	8335	841	730.14	1.15	1.43E-03
organic substance metabolic process	GO:0071704	7223	728	632.73	1.15	1.62E-02

Supplemental Table 2: List of significantly enriched GO-terms of genes up-regulated 6 h after NO_2 fumigation

A = number of genes in the reference list mapping to the GO-term. B = number of genes in the sample list mapping to the GO-term. C = number of genes from the sample list that is expected to map to the GO-term based on the reference list (reference genes $_{total}$ / A) * samples genes $_{total}$). FE = Fold enrichment of genes in sample list over the expected number (B/C; FE > 1 = overrepresented GO-term). Bold: GO-Terms specifically enriched 6 h after fumigation (remaining GO terms also enriched 0 h after fumigation). Yellow: GO-terms highlighted in the corresponding REVIGO scatterplot.

GO biological process	GO-term ID	A	B	C	FE	p-value
cellular water homeostasis	**GO:0009992**	**10**	**5**	**0.3**	**16.4**	**3.69E-02**
jasmonic acid metabolic process	GO:0009694	27	9	0.82	10.93	4.83E-04
regulation of jasmonic acid mediated signaling pathway	GO:2000022	23	7	0.7	9.98	1.92E-02
response to hydrogen peroxide	GO:0042542	53	14	1.62	8.66	4.24E-06
toxin catabolic process	GO:0009407	43	9	1.31	6.86	2.07E-02
secondary metabolite catabolic process	GO:0090487	43	9	1.31	6.86	2.07E-02
xyloglucan metabolic process	**GO:0010411**	**50**	**10**	**1.52**	**6.56**	**9.91E-03**
response to wounding	GO:0009611	184	35	5.61	6.24	8.99E-14
response to chitin	GO:0010200	109	20	3.32	6.02	8.84E-07

GO biological process	GO-term ID	A	B	C	FE	p-value
glutathione metabolic process	GO:0006749	55	10	1.68	5.96	2.24E-02
response to organonitrogen compound	GO:0010243	136	23	4.15	5.55	2.12E-07
response to toxic substance	GO:0009636	96	15	2.93	5.12	9.98E-04
response to jasmonic acid	GO:0009753	178	27	5.43	4.97	5.67E-08
cell wall polysaccharide metabolic process	**GO:0010383**	**93**	**13**	**2.84**	**4.58**	**1.86E-02**
response to reactive oxygen species	GO:0000302	138	19	4.21	4.52	2.14E-04
cellular response to nutrient levels	**GO:0031669**	**105**	**14**	**3.2**	**4.37**	**1.44E-02**
cellular response to starvation	**GO:0009267**	**98**	**13**	**2.99**	**4.35**	**3.20E-02**
response to light intensity	**GO:0009642**	**107**	**14**	**3.26**	**4.29**	**1.77E-02**
cellular response to extracellular stimulus	**GO:0031668**	**130**	**17**	**3.96**	**4.29**	**1.99E-03**
response to nutrient levels	**GO:0031667**	**124**	**16**	**3.78**	**4.23**	**4.89E-03**
cellular response to external stimulus	**GO:0071496**	**134**	**17**	**4.09**	**4.16**	**2.98E-03**
response to extracellular stimulus	**GO:0009991**	**150**	**19**	**4.57**	**4.15**	**7.45E-04**
response to nitrogen compound	GO:1901698	211	26	6.43	4.04	9.53E-06
organonitrogen compound catabolic process	**GO:1901565**	**167**	**20**	**5.09**	**3.93**	**8.76E-04**
response to water deprivation	GO:0009414	237	28	7.23	3.87	6.02E-06
response to oxidative stress	GO:0006979	364	42	11.1	3.78	1.42E-09
response to water	GO:0009415	243	28	7.41	3.78	1.02E-05
response to heat	GO:0009408	161	18	4.91	3.67	8.39E-03
defense response to fungus	**GO:0050832**	**438**	**43**	**13.36**	**3.22**	**1.22E-07**
response to fungus	GO:0009620	503	49	15.34	3.19	7.15E-09
response to acid chemical	GO:0001101	907	88	27.66	3.18	1.26E-17
response to oxygen-containing compound	GO:1901700	1168	113	35.61	3.17	2.23E-23
cellular carbohydrate metabolic process	**GO:0044262**	**287**	**25**	**8.75**	**2.86**	**1.02E-02**
response to inorganic substance	GO:0010035	693	60	21.13	2.84	3.27E-09
single-organism catabolic process	GO:0044712	498	43	15.18	2.83	5.52E-06
chemical homeostasis	**GO:0048878**	**270**	**23**	**8.23**	**2.79**	**3.40E-02**
response to temperature stimulus	GO:0009266	416	35	12.68	2.76	3.07E-04
response to salt stress	GO:0009651	418	33	12.75	2.59	2.72E-03
response to osmotic stress	GO:0006970	461	36	14.06	2.56	1.16E-03
monocarboxylic acid metabolic process	**GO:0032787**	**452**	**35**	**13.78**	**2.54**	**2.01E-03**
cellular catabolic process	**GO:0044248**	**821**	**63**	**25.03**	**2.52**	**1.26E-07**
response to external stimulus	GO:0009605	1294	98	39.46	2.48	8.19E-13

GO biological process	GO-term ID	A	B	C	FE	p-value
defense response to other organism	GO:0098542	784	59	23.91	2.47	1.08E-06
response to endogenous stimulus	GO:0009719	1309	98	39.91	2.46	1.67E-12
response to other organism	GO:0051707	1016	76	30.98	2.45	3.97E-09
response to external biotic stimulus	GO:0043207	1017	76	31.01	2.45	4.16E-09
response to chemical	GO:0042221	2100	154	64.03	2.41	1.23E-20
response to biotic stimulus	GO:0009607	1058	77	32.26	2.39	1.04E-08
response to organic substance	GO:0010033	1496	108	45.62	2.37	5.36E-13
response to abscisic acid	GO:0009737	416	30	12.68	2.37	4.47E-02
response to abiotic stimulus	GO:0009628	1507	105	45.95	2.29	1.43E-11
response to hormone	GO:0009725	1226	84	37.38	2.25	2.17E-08
response to stress	GO:0006950	2769	188	84.43	2.23	2.67E-22
response to lipid	GO:0033993	567	38	17.29	2.2	1.92E-02
catabolic process	**GO:0009056**	**1157**	**77**	**35.28**	**2.18**	**6.22E-07**
response to light stimulus	**GO:0009416**	**562**	**37**	**17.14**	**2.16**	**3.65E-02**
oxoacid metabolic process	**GO:0043436**	**963**	**63**	**29.36**	**2.15**	**5.20E-05**
organic acid metabolic process	**GO:0006082**	**965**	**63**	**29.42**	**2.14**	**5.60E-05**
response to radiation	**GO:0009314**	**583**	**38**	**17.78**	**2.14**	**3.50E-02**
defense response	GO:0006952	1302	81	39.7	2.04	4.44E-06
carboxylic acid metabolic process	**GO:0019752**	**852**	**53**	**25.98**	**2.04**	**3.04E-03**
carbohydrate metabolic process	**GO:0005975**	**882**	**54**	**26.89**	**2.01**	**3.83E-03**
oxidation-reduction process	GO:0055114	1294	79	39.46	2	1.59E-05
small molecule metabolic process	**GO:0044281**	**1316**	**78**	**40.13**	**1.94**	**6.78E-05**
regulation of biological quality	**GO:0065008**	**1047**	**59**	**31.92**	**1.85**	**1.57E-02**
response to stimulus	GO:0050896	4768	267	145.38	1.84	2.70E-21
organic substance catabolic process	**GO:1901575**	**1010**	**56**	**30.8**	**1.82**	**4.20E-02**
single-organism metabolic process	**GO:0044710**	**3137**	**156**	**95.65**	**1.63**	**1.61E-06**
single-organism process	GO:0044699	7081	281	215.91	1.3	7.34E-04

Supplemental Table 3: List of significantly enriched GO-terms of genes down-regulated directly (0 h) after NO_2 fumigation

A = number of genes in the reference list mapping to the GO-term. B = number of genes in the sample list mapping to the GO-term. C = number of genes from the sample list that is expected to map to the GO-term based on the reference list (reference genes $_{total}$ / A) * samples genes $_{total}$). FE = Fold enrichment of genes in sample list over the expected number (B/C; FE > 1 = overrepresented GO-term). Yellow: GO-terms highlighted in the corresponding REVIGO scatterplot.

GO biological process	GO-term ID	A	B	C	FE	p-value
regulation of organ growth	GO:004662	17	9	1.29	6.98	1.86E-02
hormone transport	GO:0009914	86	21	6.53	3.22	1.08E-02
auxin transport	GO:0060918	84	20	6.38	3.14	2.57E-02
response to gibberellin	GO:0009739	123	29	9.34	3.11	3.91E-04
auxin-activated signaling pathway	GO:0009734	165	39	12.52	3.11	3.10E-06
cellular response to auxin stimulus	GO:0071365	176	39	13.36	2.92	1.73E-05
rhythmic process	GO:0048511	100	22	7.59	2.9	3.21E-02
regulation of growth	GO:0040008	204	39	15.48	2.52	7.27E-04
response to red or far red light	GO:0009639	173	31	13.13	2.36	3.80E-02
regulation of hormone levels	GO:0010817	232	41	17.61	2.33	2.61E-03
response to auxin	GO:0009733	296	49	22.47	2.18	1.60E-03
hormone-mediated signaling pathway	GO:0009755	605	98	45.92	2.13	1.88E-08
cellular response to hormone stimulus	GO:0032870	646	100	49.03	2.04	1.34E-07
cellular response to endogenous stimulus	GO:0071495	653	100	49.56	2.02	2.37E-07
response to light stimulus	GO:0009416	562	82	42.66	1.92	8.65E-05
response to radiation	GO:0009314	583	83	44.25	1.88	1.97E-04
cellular response to organic substance	GO:0071310	755	108	57.3	1.88	1.80E-06
cellular response to chemical stimulus	GO:0070887	864	117	65.58	1.78	7.57E-06
regulation of developmental process	GO:0050793	484	65	36.74	1.77	2.87E-02
response to lipid	GO:0033993	567	75	43.03	1.74	1.09E-02
response to hormone	GO:0009725	1226	159	93.05	1.71	2.37E-07
anatomical structure morphogenesis	GO:0009653	631	79	47.89	1.65	4.08E-02
signaling	GO:0023052	1506	184	114.3	1.61	7.90E-07
response to endogenous stimulus	GO:0009719	1309	160	99.35	1.61	1.16E-05
single organism signaling	GO:0044700	1505	184	114.23	1.61	7.51E-07
signal transduction	GO:0007165	1477	181	112.1	1.61	8.90E-07
protein phosphorylation	GO:0006468	755	91	57.3	1.59	4.02E-02
response to organic substance	GO:0010033	1496	176	113.55	1.55	2.74E-05
cell communication	GO:0007154	1662	196	126.14	1.55	3.18E-06
response to abiotic stimulus	GO:0009628	1507	168	114.38	1.47	1.66E-03

GO biological process	GO-term ID	A	B	C	FE	p-value
RNA biosynthetic process	GO:0032774	1534	166	116.43	1.43	1.03E-02
nucleic acid-templated transcription	GO:0097659	1532	166	116.28	1.43	9.60E-03
transcription, DNA-templated	GO:0006351	1532	166	116.28	1.43	9.60E-03
cellular response to stimulus	GO:0051716	2138	224	162.27	1.38	2.04E-03
heterocycle biosynthetic process	GO:0018130	1883	196	142.92	1.37	1.52E-02
developmental process	GO:0032502	2342	244	177.76	1.37	9.60E-04
single-organism developmental process	GO:0044767	2292	239	173.96	1.37	1.20E-03
response to chemical	GO:0042221	2100	219	159.39	1.37	3.73E-03
regulation of nucleobase-containing compound metabolic process	GO:0019219	2052	212	155.75	1.36	1.01E-02
anatomical structure development	GO:0048856	2186	226	165.92	1.36	4.54E-03
regulation of cellular process	GO:0050794	3772	390	286.29	1.36	3.48E-07
single-multicellular organism process	GO:0044707	2012	206	152.71	1.35	2.41E-02
regulation of RNA biosynthetic process	GO:2001141	1992	204	151.19	1.35	2.62E-02
regulation of transcription, DNA-templated	GO:0006355	1992	204	151.19	1.35	2.62E-02
regulation of nucleic acid-templated transcription	GO:1903506	1992	204	151.19	1.35	2.62E-02
organic cyclic compound biosynthetic process	GO:1901362	2085	212	158.25	1.34	2.72E-02
multicellular organism development	GO:0007275	1962	200	148.91	1.34	4.20E-02
regulation of RNA metabolic process	GO:0051252	2011	205	152.63	1.34	3.28E-02
regulation of cellular biosynthetic process	GO:0031326	2175	219	165.08	1.33	3.54E-02
regulation of macromolecule biosynthetic process	GO:0010556	2134	215	161.97	1.33	4.10E-02
regulation of biological process	GO:0050789	4093	408	310.66	1.31	1.03E-05
response to stimulus	GO:0050896	4768	450	361.89	1.24	9.03E-04
biological regulation	GO:0065007	4745	448	360.14	1.24	9.28E-04
primary metabolic process	GO:0044238	6726	600	510.5	1.18	9.01E-03
single-organism process	GO:0044699	7081	631	537.44	1.17	4.93E-03
metabolic process	GO:0008152	8335	732	632.62	1.16	3.54E-03

Supplemental Table 4: List of significantly enriched GO-terms of genes down-regulated 6 h after NO_2 fumigation

A = number of genes in the reference list mapping to the GO-term. B = number of genes in the sample list mapping to the GO-term. C = number of genes from the sample list that is expected to map to the GO-term based on the reference list (reference genes $_{total}$ / A) * samples genes $_{total}$). FE = Fold enrichment of genes in sample list over the expected number (B/C; FE > 1 = overrepresented GO-term). Yellow: GO-terms highlighted in the corresponding REVIGO scatterplot.

GO biological process	GO-term ID	A	B	C	FE	p-value
maintenance of DNA repeat elements	GO:0043570	5	4	0.14	27.77	3.47E-02
DNA unwinding involved in DNA replication	GO:0006268	11	6	0.32	18.93	2.30E-03
DNA replication initiation	GO:0006270	19	10	0.55	18.27	8.41E-07
mismatch repair	GO:0006298	19	7	0.55	12.79	3.87E-03
DNA-dependent DNA replication	GO:0006261	66	22	1.9	11.57	3.41E-13
regulation of DNA replication	GO:0006275	22	7	0.63	11.04	1.00E-02
sister chromatid segregation	GO:0000819	30	9	0.86	10.41	7.19E-04
DNA replication	GO:0006260	105	31	3.03	10.25	6.99E-18
sister chromatid cohesion	GO:0007062	24	7	0.69	10.12	1.76E-02
regulation of DNA metabolic process	GO:0051052	62	15	1.79	8.4	1.71E-06
double-strand break repair	GO:0006302	65	13	1.87	6.94	2.01E-04
recombinational repair	GO:0000725	45	9	1.3	6.94	1.89E-02
double-strand break repair via homologous recombination	GO:0000724	45	9	1.3	6.94	1.89E-02
meiosis I	GO:0007127	50	10	1.44	6.94	6.04E-03
nuclear chromosome segregation	GO:0098813	56	11	1.61	6.82	2.30E-03
DNA conformation change	GO:0071103	77	15	2.22	6.76	2.96E-05
DNA recombination	GO:0006310	104	20	3	6.68	1.49E-07
chromosome segregation	GO:0007059	74	14	2.13	6.57	1.27E-04
chromosome organization	GO:0051276	160	28	4.61	6.07	2.31E-10
nuclear division	GO:0000280	140	20	4.03	4.96	2.18E-05
DNA metabolic process	GO:0006259	407	57	11.73	4.86	1.27E-18
DNA repair	GO:0006281	238	33	6.86	4.81	8.42E-10
cellular response to DNA damage stimulus	GO:0006974	251	34	7.23	4.7	7.01E-10
cell cycle	GO:0007049	336	45	9.68	4.65	1.51E-13
mitotic cell cycle	GO:0000278	159	20	4.58	4.37	1.68E-04
cell cycle process	GO:0022402	257	32	7.4	4.32	2.96E-08
mitotic cell cycle process	GO:1903047	155	19	4.47	4.25	5.19E-04
organelle fission	GO:0048285	171	20	4.93	4.06	5.23E-04
regulation of cell cycle	GO:0051726	123	14	3.54	3.95	4.35E-02
response to salicylic acid	GO:0009751	171	19	4.93	3.86	2.19E-03
covalent chromatin modification	GO:0016569	184	19	5.3	3.58	6.26E-03

GO biological process	GO-term ID	A	B	C	FE	p-value
chromatin organization	GO:0006325	266	25	7.66	3.26	9.98E-04
response to bacterium	GO:0009617	354	29	10.2	2.84	1.96E-03
defense response to bacterium	GO:0042742	282	23	8.12	2.83	2.75E-02
macromolecular complex subunit organization	GO:0043933	569	36	16.39	2.2	3.29E-02
cellular response to stress	GO:0033554	641	39	18.47	2.11	3.49E-02
defense response	GO:0006952	1302	76	37.51	2.03	1.82E-05
cellular response to stimulus	GO:0051716	2138	107	61.59	1.74	5.13E-05
nucleic acid metabolic process	GO:0090304	2342	112	67.47	1.66	2.38E-04
response to stress	GO:0006950	2769	125	79.77	1.57	8.52E-04
cellular macromolecule biosynthetic process	GO:0034645	2322	103	66.9	1.54	2.18E-02
macromolecule biosynthetic process	GO:0009059	2365	103	68.13	1.51	4.57E-02
nucleobase-containing compound metabolic process	GO:0006139	2668	114	76.86	1.48	3.58E-02
cellular macromolecule metabolic process	GO:0044260	4640	195	133.68	1.46	4.32E-05
cellular nitrogen compound metabolic process	GO:0034641	3391	141	97.69	1.44	1.21E-02
macromolecule metabolic process	GO:0043170	5102	202	146.99	1.37	1.81E-03
cellular process	GO:0009987	9015	319	259.72	1.23	1.27E-02

Supplemental Table 5: Expression levels of genes involved in SA synthesis and signaling after NO_2 fumigation

Gene identifier	Gene name	Log_2(FC) 0 h after fumigation	Adjusted p-value (0 h)	Log_2(FC) 6 h after fumigation	Adjusted p-value (6 h)
Salicylic acid biosynthesis					
AT1G74710	*SID2*	2.3053534	1.37E-07	-0.31670839	0.27809226
AT4G39030	*EDS5*	3.4845846	1.67E-08	-0.27153089	0.477030564
AT3G52430	*PAD4*	1.4214768	2.48E-05	-0.64033254	0.027362497
AT3G48090	*EDS1*	1.43692611	6.85E-07	-0.93948064	0.000237996
AT5G13320	*PBS3*	3.77980444	9.09E-09	-0.10520734	0.808827945
AT5G67160	*EPS1*	0.58619695	0.011819885	1.32496964	5.96E-05
AT2G37040	*PAL1*	1.74224789	9.93E-10	0.01219666	0.948353146
AT3G53260	*PAL2*	1.1927456	8.51E-09	0.86416786	2.11E-06

Gene identifier	Gene name	Log_2(FC) 0 h after fumigation	Adjusted p-value (0 h)	Log_2(FC) 6 h after fumigation	Adjusted p-value (6 h)
AT5G04230	*PAL3*	0.07396231	0.674201616	0.27061899	0.127486251
AT3G10340	*PAL4*	0.2601411	0.193130629	0.14511412	0.53277289
Salicylic acid signaling					
AT1G64280	*NPR1*	1.13147433	6.94E-09	-0.61358311	2.87E-05
AT5G45110	*NPR3*	2.98459189	1.06E-10	-0.6097793	0.004280587
AT4G19660	*NPR4*	1.36710295	1.65E-08	-1.47053007	7.19E-08
AT2G14610	*PR1*	0.48457067	0.713171685	0.45859077	0.757733057
AT3G57260	*PR2*	1.38537964	0.012745562	-0.59005243	0.327840235
AT1G75040	*PR5*	-0.23199291	0.644028905	-0.41090322	0.440667848
SA/JA antagonism					
AT1G28480	*GRX480*	4.954707006	3.88E-11	0.362616221	0.249993984
AT1G03850	*GRXS13*	2.366637283	2.25E-07	-0.276725041	0.396429606
AT3G56400	*WRKY70*	1.649574763	2.54E-06	-1.273249496	0.000130928

Supplemental Table 6: Expression levels of genes involved in JA metabolism and signaling after NO_2 fumigation

Gene identifier	Gene name	Log_2(FC) 0 h after fumigation	Adjusted p-value (0 h)	Log_2(FC) 6 h after fumigation	Adjusted p-value (6 h)
Jasmonic acid biosynthesis					
AT3G45140	*LOX2*	0.29936586	0.20539973	0.09023726	0.758535601
AT5G42650	*AOS*	1.06884717	2.88E-07	0.47674915	0.002347514
AT3G25760	*AOC1*	3.74756795	4.30E-08	2.09437071	0.000103818
AT3G25770	*AOC2*	2.00832712	2.13E-05	1.00521972	0.014251216
AT3G25780	*AOC3*	5.89378452	8.86E-09	1.4277827	0.008198394
AT2G06050	*OPR3*	4.55497977	1.49E-09	0.96858217	0.01487426
AT1G20510	*OPCL1*	3.29065124	2.51E-11	0.03284445	0.886476281
AT4G16760	*ACX1*	2.04941269	8.24E-10	1.02350605	1.09E-05
AT1G19640	*JMT*	1.772145	3.62E-07	0.569341	0.022749138

Gene identifier	Gene name	Log_2(FC) 0 h after fumigation	Adjusted p-value (0 h)	Log_2(FC) 6 h after fumigation	Adjusted p-value (6 h)
AT2G46370	*JAR1*	0.84270923	0.003031519	0.42470691	0.176340243
Jasmonate degradation					
AT3G48520	*CYP94B3*	5.027700359	7.85E-06	-	-
AT2G27690	*CYP94C1*	7.369592824	8.40E-12	2.309638659	1.79E-05
AT1G51760	*IAR3*	4.319788841	1.45E-09	1.22380636	0.002273903
AT1G44350	*ILL6*	3.338781836	4.76E-08	1.206166754	0.003448252
AT3G11180	*JOX1*	-0.227574086	0.704935835	0.604919743	0.423333559
AT5G05600	*JOX2*	4.642255982	2.75E-07	3.869310863	1.01E-05
AT3G55970	*JOX3*	1.338194284	0.063009528	5.485827802	0.000337485
AT2G38240	*JOX4*	6.629138728	1.90E-09	7.774977258	4.44E-08
Jasmonic acid signaling					
AT2G39940	*Coi1*	-0.35855322	0.002834311	0.13641258	0.268753124
AT1G32640	*Jin1*	2.99256481	4.25E-09	0.82382461	0.005260595
AT5G24770	*VSP2*	0.438796	0.53128334	0.844486	0.253393582
AT1G06160	*ORA59*	2.10652946	9.33E-05	1.60891672	0.002366441
AT3G23240	*ERF1*	3.342387	9.57E-10	-1.235135	0.000599824
AT5G44420	*PDF1.2a*	-1.64941911	0.00059253	1.65231951	0.001414071
AT3G12500	*PR3/ CHI-B*	0.15154295	0.320426581	0.45500831	0.010220648
AT3G04720	*PR4/ HEL*	-1.10776727	5.76E-05	0.47459554	0.050739575

Supplemental Table 7: Expression levels of genes involved in camalexin and IG biosynthesis and regulation after NO_2 fumigation

Gene identifier	Gene name	Log_2(FC) 0 h after fumigation	Adjusted p-value (0 h)	Log_2(FC) 6 h after fumigation	Adjusted p-value (6 h)
Camalexin and indole glucosinolate biosynthesis					
AT4G39950	*CYP79B2*	1.5942638	1.47E-05	0.15002735	0.651132865
AT2G22330	*CYP79B3*	0.657435	3.92E-05	0.234207	0.089628303
AT1G74080	*MYB122*	3.15432391	0.005689325	-	-
AT1G18570	*MYB51*	2.89400572	1.97E-11	-0.8458643	5.55E-05
AT5G60890	*MYB34*	-1.17378227	8.69E-07	0.2335127	0.177074107

Gene identifier	Gene name	Log_2(FC) 0 h after fumigation	Adjusted p-value (0 h)	Log_2(FC) 6 h after fumigation	Adjusted p-value (6 h)
AT3G23250	*MYB15*	6.950444311	6.02E-12	1.70474003	6.53E-05
Camalexin biosynthesis					
AT2G30750	*CYP71A12*	1.78825	0.000271105	-0.364713	0.399877932
AT2G30770	*CYP71A13*	4.01893268	1.24E-06	0.88673599	0.17518124
AT2G38470	*WRKY33*	4.18155	3.57E-11	-0.479832	0.054996766
AT1G02930	*GSTF6/GST1*	3.11845959	4.26E-07	1.05326363	0.017426827
AT4G30530	*GGP1*	2.02688605	1.69E-08	0.54477288	0.013020945
AT3G26830	*PAD3*	5.54423567	5.94E-10	-0.00566199	0.992435407
Indole glucosinolate biosynthesis					
AT4G31500	*SUR2*	1.26942088	2.56E-05	-0.16312868	0.547924355
AT1G74100	*ST5A*	2.40142849	4.48E-09	0.20806597	0.364102054
AT5G57220	*CYP81F2*	3.32760805	2.11E-09	-2.11173085	2.40E-06

Supplemental Table 8: Expression levels of genes involved in PTI signaling after NO_2 fumigation

Gene identifier	Gene name	Log_2(FC) 0 h after fumigation	Adjusted p-value (0 h)	Log_2(FC) 6 h after fumigation	Adjusted p-value (6 h)
Pattern recognition receptors and receptor kinases					
AT5G46330	*FLS2*	2.477331855	4.92E-11	-0.238748242	0.117538282
AT5G20480	*EFR*	3.771551511	3.18E-12	-0.117755052	0.515795596
AT1G73080	*PEPR1*	4.120852467	1.17E-11	0.508838978	0.02274284
AT1G17750	*PEPR2*	3.955601202	9.14E-12	0.57961727	0.007297789
AT4G33430	*BAK1*	1.116936477	5.79E-08	-0.164699479	0.222964589
AT2G13790	*BKK1*	3.02960254	4.03E-12	-0.499414173	0.001551624
AT2G33580	*LYK5*	2.25391379	5.07E-10	-0.94912091	3.60E-05
AT2G23770	*LYK4*	2.875943463	5.91E-10	-0.795346924	0.001509231
AT3G21630	*CERK1*	0.745213821	1.50E-05	-0.805176556	2.66E-05
AT2G32680	*RLP23*	2.160953709	9.18E-05	-1.123777282	0.025555714
AT2G31880	*SOBIR1*	1.640076212	1.31E-06	-1.136025163	0.000200735
AT3G59700	*LecRL-VI.2*	3.141663212	8.05E-11	0.062771907	0.803796841
AT1G21250	*WAK1*	0.076996692	0.854144616	-1.931174806	0.000111168

Gene identifier	Gene name	Log_2(FC) 0 h after fumigation	Adjusted p-value (0 h)	Log_2(FC) 6 h after fumigation	Adjusted p-value (6 h)
Receptor-like cytoplasmic kinases (RLCKs)					
AT4G35230	*BSK1*	0.044561305	0.656935677	0.003341069	0.979985825
AT3G09830	*PCRK1*	2.70921087	3.23E-12	-0.644516276	5.71E-05
AT2G39660	*BIK1*	3.634331265	6.51E-11	0.325397528	0.157625644
MAP kinase kinase kinases (MEKKs)					
AT4G08500	*MEKK1*	2.009116819	5.00E-11	-0.130891369	0.298110129
AT4G08480	*MEKK2*	0.069838028	0.636188162	-0.601898895	0.000588096
AT4G08470	*MEKK3*	0.070979674	0.617301043	-0.571901047	0.000672963
AT4G12020	*MEKK4*	0.451596151	0.000389128	0.008906519	0.957148535
MAP kinase kinases (MEKs)					
At4g26070	*MKK1*	0.575988102	6.51E-05	-1.775317697	4.01E-09
AT4G29810	*MKK2*	0.493302809	0.065234191	-0.477493511	0.10428203
AT1G51660	*MKK4*	3.049221543	2.08E-10	-0.529980276	0.017271867
AT3G21220	*MKK5*	2.306362326	8.48E-10	-0.547756158	0.005513085
AT5G56580	*MKK6*	1.931544114	3.84E-08	-0.150962394	0.508985968
AT1G73500	*MKK9*	2.738896055	2.29E-11	-0.339005692	0.031850921
MAP kinases (MPKs)					
AT3G45640	*MPK3*	2.635972207	6.42E-12	-0.626840703	0.000121204
AT4G01370	*MPK4*	0.862073329	5.63E-05	-0.480309983	0.013306768
AT4G11330	*MPK5*	1.425609226	2.90E-09	0.212999981	0.095805978
AT2G43790	*MPK6*	0.341417379	0.002334733	0.040493942	0.75098806
AT1G01560	*MPK11*	5.703046812	2.38E-11	-0.715179763	0.030775879
AT2G01450	*MPK17*	2.255883102	4.46E-10	0.449895309	0.011594938
Ca^{2+}-dependent protein kinases (CPKs)					
AT5G04870	*CPK1*	1.804845119	1.75E-09	-0.26940905	0.082343909
AT3G10660	*CPK2*	1.427466374	1.40E-08	-0.090684336	0.562516545
AT4G23650	*CPK3*	0.461996149	0.001028162	-0.279159081	0.030172701
AT4G09570	*CPK4*	2.524332616	2.55E-12	-0.539859815	8.74E-05
AT2G17290	*CPK6*	1.789589439	9.99E-10	0.522978667	0.001405313
AT5G12480	*CPK7*	1.489326265	1.79E-08	-0.349937464	0.027879828
AT3G20410	*CPK9*	1.640635399	9.08E-09	-0.364096212	0.027532029

Gene identifier	Gene name	Log_2(FC) 0 h after fumigation	Adjusted p-value (0 h)	Log_2(FC) 6 h after fumigation	Adjusted p-value (6 h)
AT1G18890	*CPK10*	2.125274405	2.59E-08	-0.269580356	0.246656109
AT1G35670	*CPK11*	1.423269492	2.20E-08	0.501233994	0.002593215
AT2G41860	*CPK14*	-1.059475199	0.175969588	-0.511183888	0.73312425
AT4G21940	*CPK15*	0.714779209	3.76E-05	-0.092429475	0.56186187
AT4G04740	*CPK23*	0.988034405	6.40E-05	-0.336776738	0.121328043
AT5G66210	*CPK28*	4.358471374	2.69E-13	-0.251194166	0.079626589
AT1G76040	*CPK29*	2.64395474	5.06E-09	-0.333866077	0.190305817
AT1G74740	*CPK30*	1.277947686	1.77E-08	0.20094548	0.133336925
AT4G04695	*CPK31*	0.979199227	4.28E-06	-1.736402068	6.31E-08
AT3G57530	*CPK32*	3.501399242	3.62E-12	0.14948961	0.368232792
		WRKY transcription factors			
AT1G62300	*WRKY6*	4.077917071	9.99E-11	0.115095912	0.711260987
AT5G46350	*WRKY8*	2.040451284	1.90E-08	0.317326093	0.140302811
AT4G31550	*WRKY11*	2.189308072	1.42E-11	-0.627206062	4.94E-05
AT2G23320	*WRKY15*	2.874086746	4.53E-11	-0.522785183	0.00511854
AT4G31800	*WRKY18*	3.01017454	9.45E-11	-0.071076129	0.750560984
AT4G01250	*WRKY22*	4.2778598	1.31E-10	1.355499138	0.000216219
AT5G07100	*WRKY26*	2.576262524	3.94E-08	0.474069165	0.101465146
AT4G18170	*WRKY28*	4.449973058	1.04E-09	2.569515658	1.30E-05
AT5G24110	*WRKY30*	3.651716874	3.67E-11	-0.698252502	0.028992386
AT2G38470	*WRKY33*	4.181549838	3.57E-11	-0.479832282	0.054996766
AT5G22570	*WRKY38*	2.016822922	0.000154773	-3.653812537	1.75E-06
AT3G04670	*WRKY39*	1.283942258	1.62E-07	0.265716494	0.118368375
AT1G80840	*WRKY40*	7.060795372	5.00E-11	1.762008578	0.000533941
AT2G46400	*WRKY46*	3.489935514	3.83E-09	0.169986703	0.624236928
AT5G49520	*WRKY48*	5.324693137	8.18E-10	1.797994595	0.000687954
AT5G26170	*WRKY50*	1.758786671	0.001389325	-1.292401537	0.020651216
AT5G64810	*WRKY51*	3.588365052	2.57E-08	-1.526927017	0.000675467
AT4G23810	*WRKY53*	3.114489521	1.10E-09	-1.256090574	0.00010193
AT2G40750	*WRKY54*	1.669092458	1.29E-06	-2.682848199	5.73E-08
AT2G40740	*WRKY55*	3.03082701	2.32E-08	-0.41869877	0.252065738
AT5G01900	*WRKY62*	3.490965249	8.19E-06	-0.053538495	0.922088843

Gene identifier	Gene name	Log_2(FC) 0 h after fumigation	Adjusted p-value (0 h)	Log_2(FC) 6 h after fumigation	Adjusted p-value (6 h)
AT1G66600	*WRKY63*	2.801526358	1.13E-08	0.09100254	0.786691071
AT3G56400	*WRKY70*	1.649574763	2.54E-06	-1.273249496	0.000130928
AT5G28650	*WRKY74*	1.242829873	2.87E-09	0.310506291	0.007968568
AT5G13080	*WRKY75*	4.368888622	6.86E-06	1.720546864	0.008598336

9 Acknowledgments

First, I would like to express my gratitude to Prof. Dr. Jörg Durner for giving me the opportunity to work at the BIOP. The fruitful discussions, his support of integrating my personal ideas into this thesis, and his encouragement to attend several international conferences jointly provided input which significantly shaped the outcome of this thesis and promoted my capabilities and confidence to conduct independent research.

Secondly, I would like to thank PD Dr. Farhah Assaad-Gerbert for participating in my thesis committee. Her expertise and viewpoints were very helpful in order to identify inconclusive weak points and often put new perspectives on my work. In addition, I would like to thank Prof. Dr. Erwin Grill for being willing to chair my defense.

I further want to express my gratitude to Dr. Axel Mithöfer and his team for performing the hormone measurements, as well as to Prof. Dr. Erich Glawischnig for detecting camalexin. These experiments provided crucial findings which tied up loose ends and facilitated the progress of this project**.**

Moreover, I would like to thank Dr. Elisabeth Georgii for her analytical and statistical support throughout my thesis, especially during the evaluation of the microarray data. Similarly, I want to thank Marion Wenig and Claudia Knappe for providing guidance in pathogen handling and infection.

Special thanks go to my (former) coworkers Dr. Felicitas Mengel, Dr. Katharina Kempkens, Jessica Lehnert, Alexandra Ageeva-Kieferle and Dr. Alexander Mengel. You guys made my days at work, no matter the scientific results. You comforted me in hard times and joined me in laughing during the good ones. I am happy and honored to consider you my friends and miss our awesome coffee breaks.

Most of all I want to thank Dr. Frank Gaupels. Thank you for inviting me in to participate in your exciting field of research and for your constant support, advice, critical thinking, and motivation. I really enjoyed working with you as a team that turned out to be highly productive. Your unshakable optimism with that little splash of sarcasm kept me going through numerous setbacks and taught me that even a winding road can reach its destination.

An meine Familie, vielen Dank, dass ihr mich auf all meinen Wegen und in all meinen Entscheidungen bedingungslos unterstützt habt. Mutti, ihr habt mir mein Leben lang immer Rückhalt gegeben, mich in allem gefördert und mir damit ermöglicht alle Türen zu öffnen, die mich hierhin gebracht haben, dafür kann ich euch nicht genug danken und schätzen. Papa, ich weiß, das Ergebnis all eurer Mühen hätte dich sicher stolz gemacht. Du fehlst.

To my husband Jeremy, I can’t even put into words how grateful I am for your endless patience and support throughout the entire time. You always endured the full brunt of it all and picked me up when I was down and were my voice of reason when I needed it. Thank you for being my partner through this roller-coasting experience. You are my rock.

10 Eidesstattliche Erklärung

Ich erkläre an Eides statt, dass ich die bei der promotionsführenden Einrichtung

Wissenschaftszentrum Weihenstephan für Ernährung, Landnutzung und Umwelt (WZW)

Lehrstuhl für Biochemische Pflanzenpathologie

Der TUM zur Promotionsprüfung vorgelegt Arbeit mit dem Titel:

"Nitrogen dioxide (NO_2) - induced signaling in *Arabidopsis thaliana*:
NO_2 provides basal pathogen resistance or induces a hypersensitive response-like cell death"

unter der Anleitung und Betreuung durch Prof. Dr. Jörg Durner ohne sonstige Hilfe erstellt und bei der Abfassung nur die gemäß § 6 Abs. 6 und 7 Satz 2 angegebenen Hilfsmittel benutzt habe.

Ich habe keine Organisation eingeschaltet, die gegen Entgelt Betreuerinnen und Betreuer für die Anfertigung von Dissertationen sucht, oder die mir obliegenden Pflichten hinsichtlich der Prüfungsleistungen für mich ganz oder teilweise erledigt.

Ich habe die Dissertation in dieser oder ähnlicher Form in keinem anderen Prüfungsverfahren vorgelegt.

Ich habe den angestrebten Doktorgrad noch nicht erworben und bin nicht in einem früheren Promotionsverfahren für den angestrebten Doktorgrad endgültig gescheitert.

Die öffentlich zugängliche Promotionsordnung der TUM ist mir bekannt, insbesondere habe ich die Bedeutung von § 28 (Nichtigkeit der Promotion) und § 29 (Entzug des Doktorgrades) zur Kenntnis genommen. Ich bin mir der Konsequenzen einer falschen Eidesstaatlichen Erklärung bewusst.

Mit der Aufnahme meiner personenbezogenen Daten in die Alumni-Datei bei der TUM bin ich einverstanden.

München, den 29.04.2018

Dörte Mayer